Faculty of Engineering
Department of Mechanical Engineering

6th INTERNATIONAL SCIENTIFIC CONFERENCE ON ADVANCES IN MECHANICAL ENGINEERING (ISCAME 2018)
11-13 October, 2018 Debrecen, Hungary

CONFERENCE PROCEEDINGS
(BOOK OF EXTENDED ABSTRACTS)

organized by
Department of Mechanical Engineering
Faculty of Engineering, University of Debrecen
and
Working Commission in Mechanical Engineering
Specialized Committee in Engineering
Regional Committee in Debrecen, Hungarian Academy of Science

Edited by **Tamás MANKOVITS PhD**

Technical editor **Szandra SITKU**

Publisher: **Department of Mechanical Engineering**
Faculty of Engineering
University of Debrecen
2-4 Ótemető str. Debrecen, Hungary
Phone: +36 52 512 900
Web page: https://mecheng.unideb.hu/

ISBN 978-963-490-051-1

CONFERENCE PROCEEDINGS
(BOOK OF EXTENDED ABSTRACTS)

6th INTERNATIONAL SCIENTIFIC CONFERENCE ON ADVANCES IN MECHANICAL ENGINEERING (ISCAME 2018)

11-13 October, 2018

Debrecen, Hungary

Chair of ISCAME 2018

Tamás MANKOVITS, University of Debrecen, Hungary

Scientific Program Committee of ISCAME 2018

Ágnes BATTÁNÉ GINDERT-KELE, University of Debrecen, Hungary
Sándor BODZÁS, University of Debrecen, Hungary
Gábor BOHÁCS, Budapest University of Technology and Economics, Hungary
István BUDAI, University of Debrecen, Hungary
Levente CZÉGÉ, University of Debrecen, Hungary
Igor DRSTVENSEK, University of Maribor, Slovenia
János Péter ERDÉLYI, University of Miskolc, Hungary
Lajos FAZEKAS, University of Debrecen, Hungary
Csaba GYENGE, Technical University of Cluj-Napoca, Romania
Sándor HAJDU, University of Debrecen, Hungary
György JUHÁSZ, University of Debrecen, Hungary
Gábor KALÁCSKA, Szent István University, Hungary
Ferenc KALMÁR, University of Debrecen, Hungary
Imre KOCSIS, University of Debrecen, Hungary
Ákos LAKATOS, University of Debrecen, Hungary
Daniel LATES, Petru Maior University of Targu Mures, Romania
Stanislav LEGUTKO, Poznan University of Technology, Poland
Zoltán MAJOR, Johannes Kepler University Linz, Austria
József MENYHÁRT, University of Debrecen, Hungary
Ljubica MILOVIC, University of Belgrade, Serbia
Imre Norbert ORBULOV, Budapest University of Technology and Economics, Hungary
Sándor PÁLINKÁS, University of Debrecen, Hungary
Tibor POÓS, Budapest University of Technology and Economics, Hungary
Milan RACKOV, University of Novi Sad, Serbia
Istvánné RÁTHY, Óbuda University, Hungary
Tamás SZABÓ, University of Miskolc, Hungary
Ferenc SZODRAI, University of Debrecen, Hungary
Edit SZŰCS, University of Debrecen, Hungary
György THALMAIER, Technical University of Cluj-Napoca, Romania
Zsolt TIBA, University of Debrecen, Hungary
László TÓTH, University of Debrecen, Hungary
Matej VESENJAK, University of Maribor, Slovenia
László ZSIDAI, Szent István University, Hungary

Technical Assistance

Szandra SITKU, University of Debrecen, Hungary
Lilla CSONKÁNÉ DÓRÓ, University of Debrecen, Hungary

CONTENTS

NVH CHARACTERISTICS CHANGE OF FRP COMPOSITE PARTS THROUGH VISIBLE AND NON VISIBLE DAMAGES

ALSARAYEFI Saad, JÁLICS Károly PhD
István Sályi Doctoral School of Mechanical Engineering Sciences, University of Miskolc
E-mail: Saad.alsreefi @gmail.com, machijk@uni-miskolc.hu

Keywords: Composite, Crack, Vibration, Modal analysis.

Composite materials, e.g. fiber reinforced polymers (FRP), are more and more utilized in the vehicle and machine industry. FRP components can show damages that are not visible after impact or crash. A component that is damaged (even not visibly) loses its load capacity, its original energy absorption capacity and its NVH behavior can change significantly. Current paper will present the investigation of the Noise, Vibration and Harshness (NVH) behavior of damaged and not damaged fiber reinforced polymer FRP test probes with simple geometry. For that purpose, artificial defect/failure generation procedure for the test probes is developed and applied. Afterwards some NVH measures, e.g. natural frequencies, modal damping and mode shapes is evaluated. The results show on the one hand the sensitivity of the measurement method for damages and on the other hand the change of the NVH characteristics of the probes through damages. The modal analysis method was used in this investigation. The method delivers the modal frequencies, mode shapes and modal damping where the parameters can be more or less responsible for the NVH behavior of a vehicle. If the excitation meets a modal frequency, and the mode shape at that modal frequency has a good radiation efficiency or the path of vibration transfer from that part to another in the vehicle is sufficient, this method will be applied for the investigations. After getting the results of the modal test, they are analyzed, and the change of the modal behavior between undamaged and damaged specimen is explained. At the end the eligibility, respectively the sensitivity of the modal analysis method for crack detection at FRP should be verified. For this investigations, a glass reinforced plastic plate with the material type of MF GC 201 (melamin resin laminate) is selected due to the simple accessibility, also, such materials are often used by vehicles. The specimen had a simple rectangular shape with the dimensions of 500x200x3 mm (Figure 1).

Figure 1 The rectangular FRP test specimen (with the marks of the measurement points)

By using an air gun, type type Diana 300R cal.177, which has the maximum kinetic energy of Ekin = 7.5 J at the muzzle, a crack is produced with a length of 70 mm (Figure 2 left and right). So, that cracked specimen was used for the further investigations.

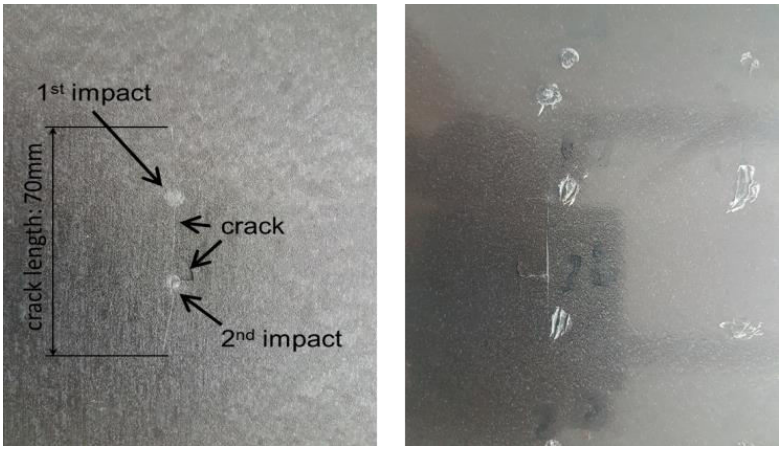

Figure 2 Damage of the specimen (left: side of the impact; right: back side)

In order to perform the test, 30 measurement points on the plate were defined to be able to represent the mode shapes. The distance between points was 50 mm along the long side, and 75 mm along the short side of the plate (visible on Figure 1.). Measurement point Nr. 30 was also the excitation point. For the measurements, test equipment B&K Pulse frontend, B&K Pulse Labshop, B&K 4397 uniaxial accelerometer, and Endevco 2202-10 impact hammer were used.

At first sight on the average of the transfer functions (Figure 3), no significant difference can be seen in the overall characteristics of the FRFs. From 550 Hz, there is some difference, but this is rather due to the poor excitation level, and the high damping of the material. Beyond that frequency, no more distinct resonances can be found in the FRFs.

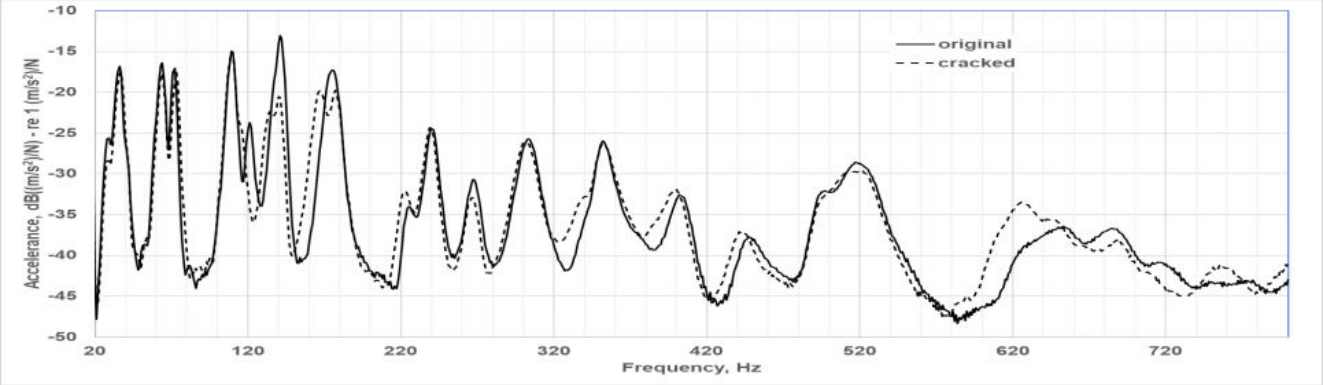

Figure 3 The average of the measured FRFs for the uncracked and for the cracked specimen.

If we take a look at the individual resonances (roughly 20 pieces up to 500 Hz) in the range from 110 to 190 Hz (Figure 4), differences in level of the peaks, and missing resp. new peaks can be found in the averaged FRF of the cracked plate compared to the uncracked one. It can be stated, that an existing crack in the material causes the appear and the disappear of certain resonances. Presumably the modes are not appearing/disappearing, they are always there, but due to the crack they will be simply better or worse excited, depending on the frequency, mode shape and damping.

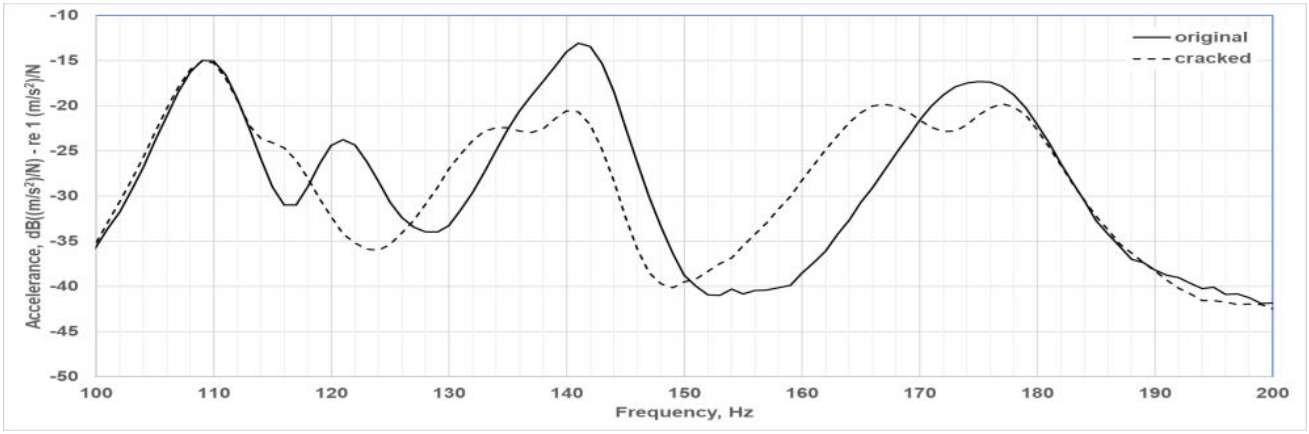

Figure 4 The average of the measured FRFs for the uncracked and for the cracked specimen from 100 to 200 Hz.

The modal analysis can help in certain ideal conditions to detect a crack in FRP material. The method can only work in the low frequency range due to the poor excitation with impact hammers over 800 Hz. With an excitation with a light shaker this limit can be raised, but due to the gradually growing modal density the investigation of single resonances and modes will be difficult. In this case we know about the crack, so we were waiting some change in the modal behavior of the specimen (the previous mentioned ideal condition). In real cases by a relatively complex shaped vehicle component other effects have to be considered, even a not optimal support of the component by the test can cause some change in the modal behavior. The modal analysis still has to be more investigated for the purpose of crack detection in FRP, but also in general for other types of material. At the time of writing this paper only a single test is existing, so the test has to be repeated several times, in order to obtain the sensitivity of the method for external influences and for the crack generation. More promising acoustic method for crack detection is e.g. the acoustic emission which will be also utilized later.

STIFFNESS OF DOKA FORMWORK BEAMS REINFORCED WITH CFRP

[1]ANDOR Krisztián PhD, [2]LENGYEL András PhD, [1]KARÁCSONYI Zsolt PhD, [1]BELLOVICS Bertalan
[1]Institute for Applied Mechanics and Structures, University of Sopron
E-mail: andor.krisztian@uni-sopron.hu, karacsonyi.zsolt@uni-sopron.hu, bellovics.bertalan@phd.uni-sopron.hu
[2]Budapest University of Technology and Economics
E-mail: lengyel.andras@epito.bme.hu

Keywords: Timber framework, reinforcement, CFRP, modulus of elasticity, bending test.

The application of glass fibre reinforced plastics (GFRP) or carbon fibre reinforced plastics (CFRP) for the improvement of structural behaviour has several decades of history, that also includes research on timber structures. Similarly to structural elements made of reinforced concrete, the application of fibre reinforced plastics for timber has been proven feasible and usually effective. It can be applied to sawn beams, glued-laminated structural elements, as well as to reinforce existing structures like bridges or historical buildings. The reinforcement is mostly applied in form of sheets, fabrics, or rods in parts of the structural elements under tension, either fitted to the outer surface or embedded in grooves or between layers. The bond is usually provided by synthetic resin.
A special case of usage of this reinforcement is to apply it to formwork beams in construction, see. Figure 1. Such beams serve as supports for slabs or other structural system and are designed to shearing and bending. The flanges are solid sawn timber planks connected by a web of compressed particle board. The understanding of the structural behaviour of formwork beams reinforced with FRP materials, experimental and numerical analyses are required.

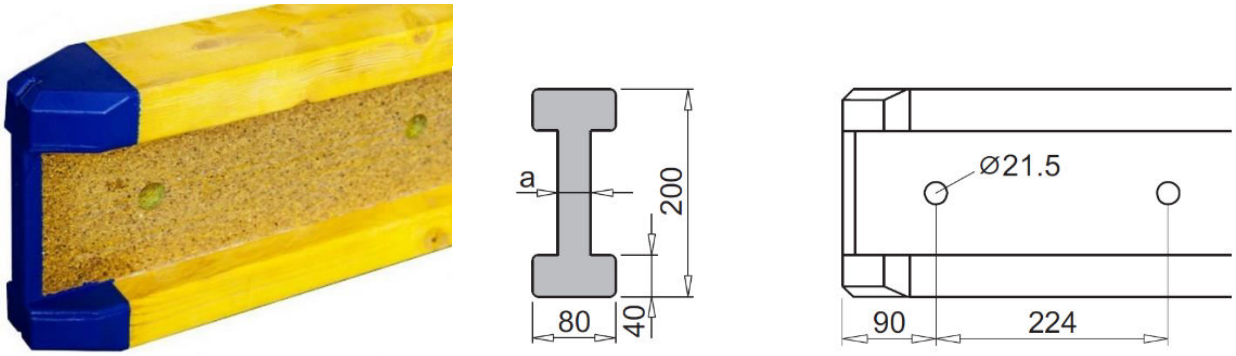

Figure 1 Formwork beam and specifications

In the Structural Laboratory at University of Sopron experiments have been conducted since 2013 on bending of real size spruce beams regarding reinforcement CFRP [1]. Several problems arose during the modelling of the reinforced beams because of difficulties in FE simulations, during which the modulus of elasticity has been assumed constant while the latest investigations have shown that it varies significantly during the loading process [2]. Analysis of the modulus of elasticity during the loading provides answers to several questions enabling the analysis to be profoundly optimized and yield more accurate estimates. Analysis has been extended to load-modulus functions of previous investigations. Specimens without reinforcement were also included in the investigations, in order to eliminate anomalies of previous measurements and to get easier comparison. In this study formwork beams are analysed from this aspect. A series of bending experiments has been carried out on formwork beams provided by Magyar Doka Zsalutechnika Kft. Carbon fibre material and epoxy were provided by Sika Hungária Kft. Specimens were prepared in three groups: without any reinforcement, CFRP sheet applied at half width of the bottom flange at full length, and sheet applied at full width at full length. All beams were tested with three-point bending, continuously measuring load and mid-span deflection. The data sets enable the calculation of an equivalent modulus representing the stiffness of the beam, which includes the contribution of the fibres as well in the case of reinforcement. In addition to the load-deflection curves, the variation of the equivalent modulus provides further information on the behaviour. The modulus can be plotted either against the mid-span deflection or against the load. The diagrams in the case of full reinforcement are shown in Figure 2.

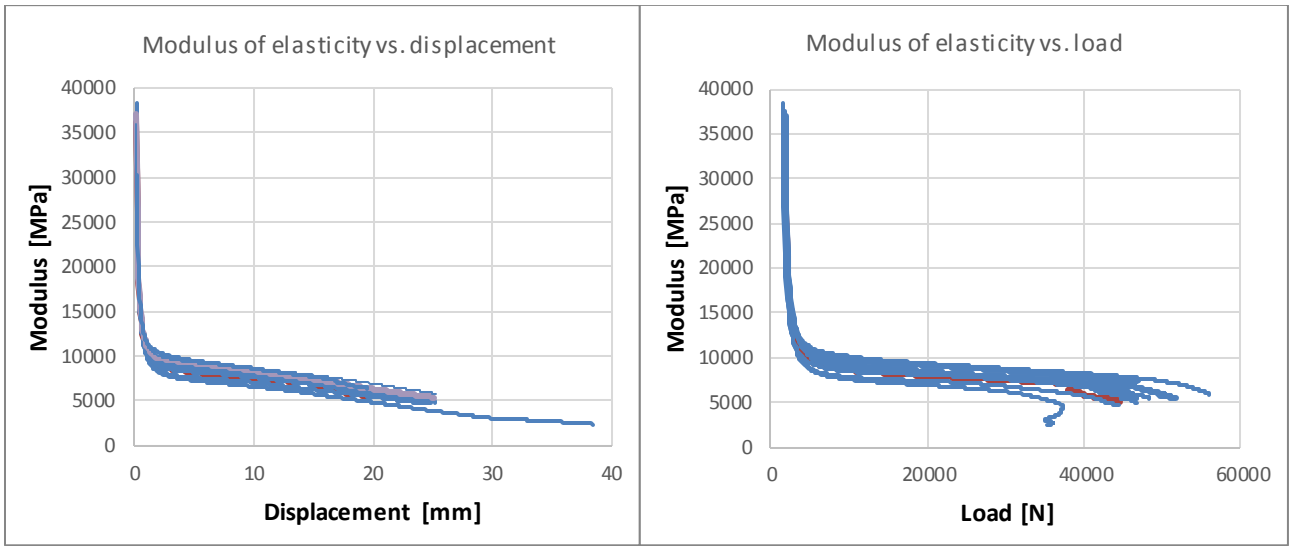

Figure 2 Modulus of elasticity of reinforced beams vs. mid-span displacement and load

After a short initial phase of fluctuation, the diagrams show a steady slow decrease of stiffness, which implies that the modulus is not constant during the loading. Data sets created during the measurements enabled the evaluation of the modulus in every 0.5 seconds, therefore it can be plotted in detail against any variable, e.g. mid-span deflection and load. The two diagrams revealed that while in the case of the modulus plotted against the displacement no significant change occurred until failure, in the case of plotting against the load the end of the curve showed a small fold indicating the approach of the failure in 90% of the cases. The above investigation has revealed that the modulus cannot be regarded constant during the loading and that the failure may be predicted by the analysis of the curves.
It was observed for both sets of functions that the reinforcement with carbon fibre not only resulted in higher load-bearing capacity but also reduced the scattering of the functions, that is the curves nearly coincided. The difference between the cases of reinforcement at half width and that at full width is not so significant as in the case of non-reinforced specimens.
These phenomena predetermine further investigations for the prediction of failure, and indicating that during design the consideration of constant modulus may be unsafe as assumed by the decreasing trend of the modulus.

ACKNOWLEDGMENTS
The described work was carried out as part of the "Roadmap for Structural Changes of the University of Sopron" - nr. 32388-2/2017 INTFIN. The Ministry of Human Capacities of the Hungarian Government supported the realization of this project. The authors are grateful to Magyar Doka Zsalutechnika Kft. for providing test specimens and technical data. The authors are grateful to Sika Hungária Kft. for providing raw material for the experiments.

REFERENCES
[1] K. Andor, A. Lengyel, R. Polgár, T. Fodor, Z. Karácsonyi: *Experimental and statistical analysis of spruce timber beams reinforced with CFRP fabric*, Construction and Building Materials, 2015.
[2] B. Bellovics: *Szénszálas erősítésű fatartók vizsgálata VEM analízissel*, MSc degree work, (In Hungarian) University of West Hungary, 2016.

EFFECT OF NATURAL AND ARTIFICIAL DRYING ON THE ESSENTIAL OIL COMPOSITION OF BASIL

[1]ANTAL Tamás PhD, [2]NYÁRÁDI Imre István PhD, [1]SIKOLYA László PhD
[1]Institute of Engineering and Agricultural Sciences, University of Nyíregyháza
E-mail: antal.tamas@nye.hu, sikolya.laszlo@nye.hu
[2]Faculty of Technical and Human Sciences Targu Mures, Sapientia Hungarian University of Transylvania
E-mail: nyaradi@ms.sapientia.ro

Keywords: Basil leaves, artificial and natural air drying, essential oil content, gas chromatography.

High weather dependence and pollution from the air are the greatest hazards of natural air drying. The most common method of artificial dehydration is drying with hot-air. The color of the hot-air dried material changes, the product is shrinking, difficult to rehydrate and loss of essential oil content occurs. Injurious processes can be avoided by using modern drying techniques such as vacuum drying.
This article presents the results pertaining to the drying behaviour of basil leaves (*Ocimum basilicum* L.) in natural air drying (~25-30°C, 2 days), hot air drying (50°C, 6h, 1m/s), and vacuum drying (50°C, 8kPa, 7h) conditions. About 50 g of basil leaves were dried using an air-, hot-air- and vacuum drying methods. The SPME (Solid Phase Micro Extraction) sample preparation was made with manual tool. The GC-MS measurements were executed on a 5890 Series II – 5971 mass spectrometer system. The components were identified with Wiley and NIST databases and retention indices from different manuals. The moisture content before and after drying of the leaves was determined by the gravimetric method (105°C for 4 h) in triplicate. The aim of the research is examine the natural and artificial drying methods influence on the amount of the main components in the herb in comparison with the raw material.
In terms of product quality, twelve (eucalyptol, linalool, camphor, estragole, beta-elemene, beta-caryophyllene, alpha-guaiene, alpha-humulene, germacrene-d, delta-guaiene, alpha-cadinene and delta-cadinene) major constituents of basil leaves essential oil were quantified by gas chromatography–mass spectrometry (GC-MS). A total of 36 essential oil components were identified (Fig. 1).

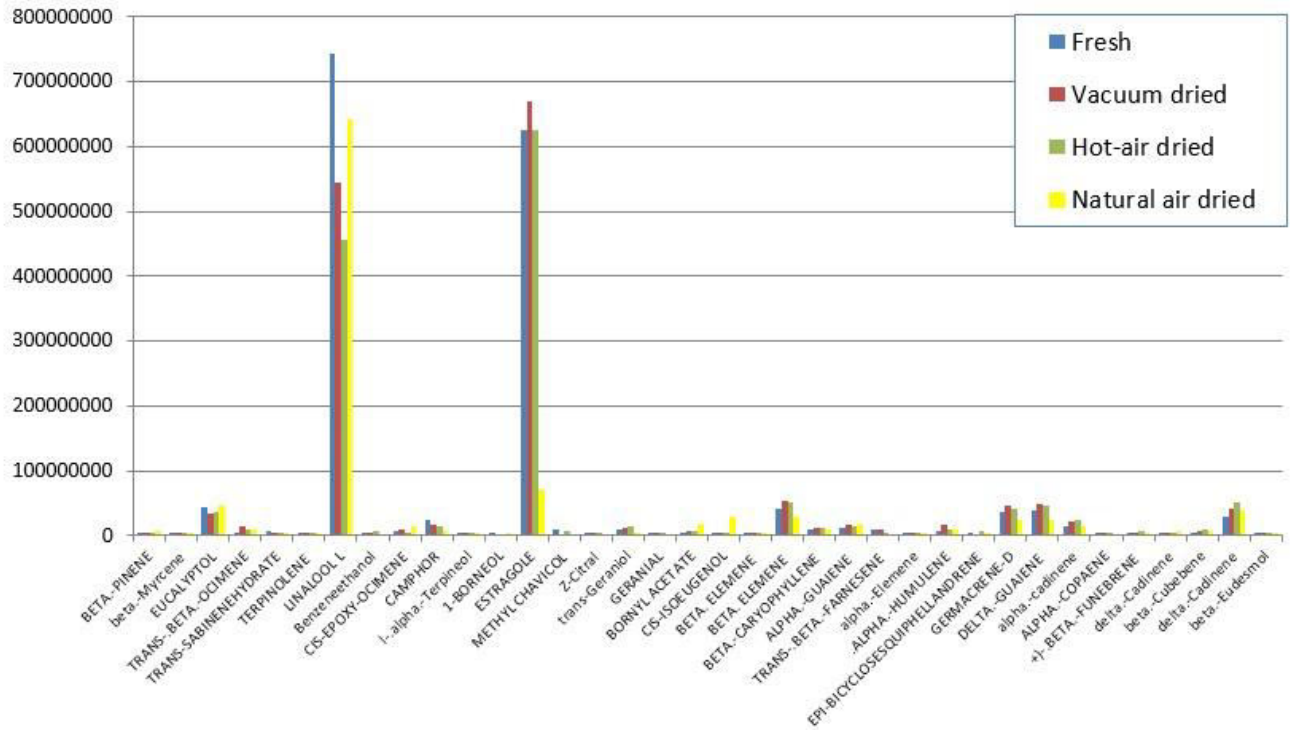

Figure 1 Comparison of basil based on the area value of total ion chromatograms

Remark: The values in the chromatogram obtained with the GC-MS of basil refer to fresh plant matter.
Politeo et al. (2007) identified by GC-MS 33 essential oil components from basil leaves, most of which are consistent with those in this scientific work.

The initial moisture content of the basil leaves was found to be 66,7% (wet basis: w.b.). The basil were dried by different drying methods until the final moisture content (0,8-1,4%, wet basis: w.b.).
The concentration of the main constituents of basil leaves oil extracted from fresh and dehydrated samples are presented in Table 1.

Table 1 Concentration of the main essential oil components in basil

Components	Fresh (area)	Natural air drying (NAD)	Hot-air drying (HAD)	Vacuum drying (VD)
eucalyptol	43775484	+4,76% [1]	-19,46% [2]	-22,08% [3]
linalool	742065773	-13,46% [1]	-38,48% [3]	-26,58% [2]
camphor	24425461	-68,76% [3]	-43,01% [2]	-32,03% [1]
estragole	625315818	-88,56% [3]	+0,07 [2]	+7,08% [1]
beta-elemene	41861493	-33,39% [3]	+23,28% [2]	+26,55% [1]
beta-caryophyllene	9555398	-6,24% [3]	+15,47% [2]	+18,05% [1]
alpha-guaiene	12984727	+35,67% [1]	+10,99% [3]	+28,39% [2]
alpha-humulene	7166493	+29,85% [3]	+31,92% [2]	+136,66% [1]
germacrene-d	36272278	-32,05% [3]	+16,55% [2]	+25,94% [1]
delta-guaiene	37820670	-35,86% [3]	+25,11% [2]	+28,54% [1]
alpha-cadinene	15254299	+0,25% [3]	+51,06% [1]	+35,56% [2]
delta-cadinene	27993928	+36,72% [3]	+81% [1]	+48,3% [2]
Ranking	-	III.	II.	I.

Areas defined by the mass spectrum of essential oil components identified from the raw and dried basil leaves serve as a basis for ranking the drying methods. The area of the 12 main constituents found in the raw plant material was the control and the deviation – the effect of drying methods – was expressed as percentile form in Table 1. Differences due to drying were marked with a positive and negative sign in relation to the crude basil. In the brackets, we indicate the rank based on the values.

CONCLUSIONS

This study focused on the chemical composition characteristics of essential oils extracted from fresh and different dried basil leaves. The results showed that drying methods had a significant effect on essential oil content and composition of basil leaves. The volatile oil found in herbs is very sensitive to some drying parameters (e.g. pressure, temperature, weather, non-uniform drying, etc.).
The quality of the vacuum dried (1) product was assessed – from a twelve major constituents (eucalyptol, linalool, camphor, estragole, beta-elemene, beta-caryophyllene, alpha-guaiene, alpha-humulene, germacrene-d, delta-guaiene, alpha-cadinene and delta-cadinene) – as being higher than that of a hot-air dried (2) and natural air dried (3) products. Losses in the content of essential oil in vacuum dried samples can also be observed. The amount oil losses is dependent on the pressure of vacuum drier (VD). The applied vacuum (8000 Pa) at the VD probably split open the outer (exogenous) essential oil containers of the leaf.
A comparison between the vacuum drying and hot air-drying methods showed a difference in the quality of the dried basil leaves because hot air drying uses relatively high temperatures and intensive ventilation, which causes undesirable alteration of the volatile compounds in the finished product.
In the case of natural air drying, non-uniform drying and rewetting by the weather caused a loss of quality in plant material.
Taking into account all these considerations we recommend the drying of basil leaves by vacuum drying.

REFERENCES

[1] O. Politeo, M. Jukic, M. Milos: *Chemical composition and antioxidant capacity of free volatile aglycones from basil (Ocimum basilicum L.) compared with its essential oil.* Food Chemistry, 101, 379-385. 2007.

EXAMINATION OF A TYPICAL HIGH VOLTAGE PHASE CONDUCTOR UNDER VARIOUS OPERATING AND LOAD CONDITIONS

BAGI Tamás Zoltán PhD
Department of Safety Science, Óbuda University (AD&TE Research Group)
E-mail: bagi.tamas@elinor.hu

Keywords: Phase Conductor, Warming, Load, Short Circuit, Models

Abstract
There are many Hungarian and International Standards valid relating to safe load, wire structures, warming, and examination of phase conductors, and ground wires. There are significant differences between practical experiences, results of calculation, and modeling according to standards. These differences have various causes: different material quality, newer or modern materials, different manufacturing processes, and even different theoretical considerations. The necessary information and data for the verification can be obtained in several ways. The first way is the Measuring, and Data collecting, but it's a very expensive way. The other way is computer simulating and modeling. In this article, I would like to present a program that I have developed.

INTRODUCTION

From above, it can be stated that Hungarian Standards largely follow the IEC standards for the structure of wires and main mechanical and electrical properties. The MSZ and DIN standards contain different calculation models to determine the warming of wiring in case of short circuit. The problem is further enhanced by the fact that domestic standards also give different results. The above mentioned shows that there is a high uncertainty in the calculation method according to regulation. There are very strict restriction to determine the safe load by measurement, which cannot be avoided on the current level of measurement technology. The original structure of wiring must be disrupted to mount the thermal sensors, thus making the measurement unreliable. On the other hand computer aided modeling and simulation gives an opportunity to examine the wiring by calculation, where the precision depends only on the applied model (and the available computation capacity).

ELECTRIC MODEL

The electrical model is a multilayer, cylinder-symmetrical model in conformity with the twisted structure. Every layer contains a heat flow generator, accordingly, all heating by electrical origin should be determined by layer. To determine the heat developing in each layer, current in the given layer and the resistance should be calculated. When calculating the resistance of the wires for each layer, the resistance values given in standard MSZ 149/1 must be assumed.

ALTERNATING CURRENT RESISTANCE

The efficient cross-section narrows, because of the skin effect and the alternating-current resistance (R_{AC}) increases compared to the direct-current resistance (R_{DC}). The value of the δ skin-depth in the case of aluminum is δ_{Al}=12.03 mm, in case of transformer sheet (μ=500) is 1.01 mm and in case of a steel thread with smaller relative permeability ($\mu \approx 100$) is δ_{St}=2.26 mm, if the frequency of current is 50 Hz. With the exception of the steel core wire, the individual layers can be approximated by a ring cylinder, where the wall thickness of the cylinder is equal to the diameter of the elemental thread, the wall thickness being the same as that of the primary thread. The alternating current resistance of the steel core wire (Z_{real0}) can be calculated from the previous case with d=r substitution. Literature as a guide we can say that between the current distribution of steel and aluminium (Al-St) approx. 99% -1%, if it is thicker and if it is thinner 98% - 2% . When the distribution of the current inside the wiring is calculated, we take two layers into consideration: the steel layer and the aluminum layer, because the distribution between these two layers can quite simply be expressed. This requires calculation with complex numbers, where both the absolute value and the phase-angle, or the real and the imaginary parts of the result are needed. There is a demonstrable phase shift between the steel and the aluminum layer. Naturally, if the wiring has a different structure, the current of the inner aluminum layer has to be determined first with the given expression and material-properties, then the current in the steel can be obtained with a simple subtraction. It should be noted that this relationship of flow distribution was originally defined as a two-layered half space. A much more complicated, Bessel function solution for the cylinder would give a more accurate value. The approximate error is not significant to aluminum, around the center, so that the steel core wire is larger than approx. 10-20%, but luckily due to the impact and the material characteristics, only small currents are taking place here. Furthermore, the model does not take into account that concentric cylinders of thickness "d" are not compact, but comprise elementary fibers of circular cross-section. This latter fact can only be taken into consideration in the system by the DC or AC resistors.

EDDY CURRENT AND HYSTERESIS LOSS

In addition to the heat developing at resistive resistance, the eddy currents in the steel core also develop heat. Similarly, heat is produced in steel by the transient magnetization of the alternating current period. For eddy currents, the model should be constructed so that for the steel core wire only the layer 1 (steel) current is taken into account, and for the steel layer 1 only all the aluminum layers surrounding it. This can be done because each steel layer shields each other relatively well. The eddy current loss is only accounted for by the steel, because in the case of aluminum it is 2-3 orders of magnitude smaller than the steel and the hysteresis loss in the case of aluminum does not actually exist.

THERMAL MODEL

The thermal model, similarly to the electrical model, describes the behavior of the wiring as a system of concentric cylinders. However, at the same time it differs from that, because all the elements having significant heat capacity, heat resistance etc. independently from their electrical behavior have to be taken into consideration. According to this the model takes into account the irregular stratum between the elementary threads with a concentric air cylinder. Because of the air layers and because of the fact, that all layers (steel, aluminum, air) have to have the same thermal behavior as the real part of the wiring, there is a necessary difference between the thickness and the number of the layers of the electrical and the thermal model. The model handles the layers as homogenous, so inside the given layer the temperature, the material properties (specific heat, density, heat resistance…) are constant. The heat exchange is conductive. The heat conduction between any two neighboring layers is determined by taking into account the half of the thickness of the given layers. Heat source is primarily the heat production of ohmic resistors, in the secondary iron losses of steel wires, as well as the sun and heat transfer on the surface of the wire.

IMPLEMENTATION OF THE MODEL, AND RESULTS

A simulation framework, which was developed in LabVIEW was used to solve the problem. The framework is able to manage any kinds of models given by differential equations, and various control tasks. The fundamental properties of LabVIEW are the following: graphical programming language and the ability to develop high speed, time-critical applications.

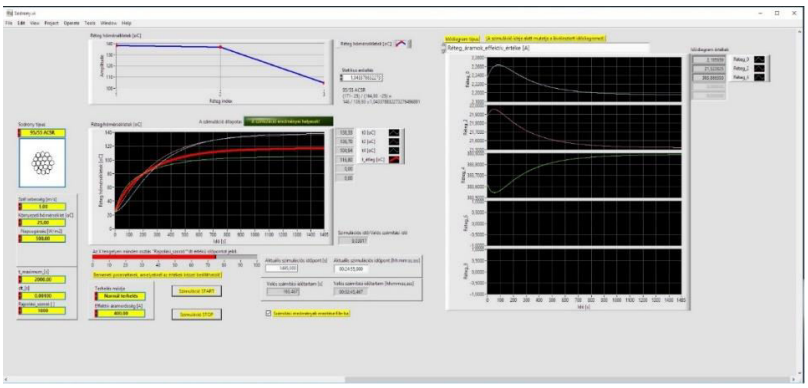

Figure 1 User Interface

ACKNOWLEDGMENTS

Hereby we would like to say thank you to Mr György Lipovszki Dr. who provided great support with his expertise and useful remarks /advise to develop the simulation program.

REFERENCES

[2] MSZ 149 *Heavy current stranded conductors.*
[3] MSZ-05-33.7551 - *Steel stranded grounding conductors and aluminum coated steel wire strand for protection and anchoring*
[4] MSZ-09-00.0315 -*Testing methods determining the common parameters of stranded conductors and armatures*
[5] MSZ-09-00.0316 - *Permissible thermal stresses for stranded aluminum conductor overhead lines*
[6] DIN 57103 - *Mechanical and Thermal Short Circuit Strength of Electrical Power Installations*
[7] T. Bagi:*A method presented by measurements to prevent harmful effects of icing forming on ground wires of high-voltage transmission lines*, 34th Danubia-Adria Symposium on Advances in Experimental Mechanics, Trieste, 2017, pp. 1-3

NUMERICAL SIMULATIONS ON BASIC MODELS OF LOW-SPEED AXIAL FAN BLADE SECTIONS

BALLA Esztella
Department of Fluid Mechanics, Budapest University of Technology and Economics
E-mail: balla@ara.bme.hu

Keywords: computational fluid dynamics (CFD), low Reynolds number, axial fan

Abstract *In this study two- and three-dimensional numerical simulations are compared for basic models of low-speed axial fan blade sections. The basis of comparison is the lift-to-drag ratio. The two-dimensional and the three-dimensional simulations were carried out with the same settings. The geometry of the three-dimensional case was set in accordance with previous wind tunnel measurements. By comparing the cases it was found that the two-dimensional simulations are in good agreement with literature data, however further studies are needed to obtain better fitting between the three-dimensional simulations and the measurements.*

INTRODUCTION

The aim of the present study is to establish a connection between force measurements carried out on blades in a finite wind tunnel, and the forces acting on blades with infinite span. Two blade geometries are in the focus: a cambered plate with 8% relative camber, and a RAF6-E profile. Both geometries are used in axial fan blade design. The investigated chord based Reynolds number (Re) range is from $0.6 \cdot 10^5$ to $1.4 \cdot 10^5$. This range corresponds to the operation of low-speed axial fans, e.g. computer processor cooling fans, refrigerator fans etc. The investigated angles of attack (0°, 2°, 4°, 6°) correspond to the range including the maxima of the lift-to-drag ratio (LDR) of both blade sections. The long-term goal of the author is to decrease the noise emission of these low-speed axial fans. In order to achieve this goal first the aerodynamics at this low Re has to be understood. It has already been stated in the literature that the LDR of profiled blade sections starts to deteriorate below a certain Re value ($\sim 10^5$) [1]. This phenomenon implies that a simpler, cambered blading can be superior to profiled blading for low-speed axial fans from the efficiency point of view. Besides, manufacturing costs are also lower for simpler geometries. The above confirm the importance of the investigation of the aerodynamic behavior of such bladings.

Wind tunnel measurements have already been carried out at the Department of Fluid Mechanics at three Reynolds numbers: $0.6 \cdot 10^5$, 10^5 and $1.4 \cdot 10^5$[2]. The lift and drag force measurements confirmed that the drag coefficient of the RAF6-E profile increases significantly as the Re is lowered to $0.6 \cdot 10^5$. The numerical simulation presented herein were carried out in order to better understand the underlying aerodynamic phenomena. In the literature, data on profiles with infinite span are presented mostly. To be able to determine the relationship between results on finite and infinite profiles, both two-and three-dimensional simulations are desirable.

NUMERICAL SETUP

For the two-dimensional simulation an O-grid mesh was made in ICEM CFD, which is presented in [3]. The diameter of the domain was 61 chord, enabling an uninterrupted flow around the profiles. For the three-dimensional simulation the test section of the wind tunnel was modelled. The mesh contained two parts. The inner part contained only the vicinity of the profile, and the rest of the model was included in the outer part. Different angles of attack (α) were set by rotating the inner part of the mesh. The simulations were carried out in ANSYS Fluent 19.0 [4]. In accordance with [5] the transitional k-ω SST turbulence model was used. At the inlet of the domain a velocity boundary condition was set. For the two-dimensional case a homogeneous velocity distribution was used, while for the three-dimensional case a velocity profile, measured at the inlet of the test section. The turbulence intensity was set to 0.8% for both cases, which is in accordance with the measured turbulence intensity in the wind tunnel. During the simulations the lift (C_L) and drag (C_D) coefficients were monitored in order to determine convergence.

RESULTS

First, the two-dimensional simulations were compared with simulation results in the literature on very similar geometries, which have already been validated with measurement results. By this comparison it was determined that the results of the present simulations are in accordance with literature data. The used turbulence model proved to be capable of demonstrating the Re dependence of the LDR. As for two-dimensional cases the model proved to be appropriate, three-dimensional simulations were also conducted. Results are shown in Figure 1. The expected Re dependence was moderate in the three-dimensional cases. Also a significant decrease in the LDR can be observed. This is caused mainly by the decrease of the lift coefficient. There is a significant difference between the LDR of the RAF6-E and the cambered plate in the two-dimensional cases. However, this cannot be observed for the three-dimensional cases: the lift-to-drag ratios are in the same range.

To determine the validity of the results of the three-dimensional simulations, they are compared with own measurement data. For the RAF6-E profile the simulations generally over predict the LDR. For the cambered plate the LDR is over predicted for lower angles of attack, while the trend changes for higher angles. In the measurement results the Re dependence is more pronounced, compared to the three-dimensional simulations.

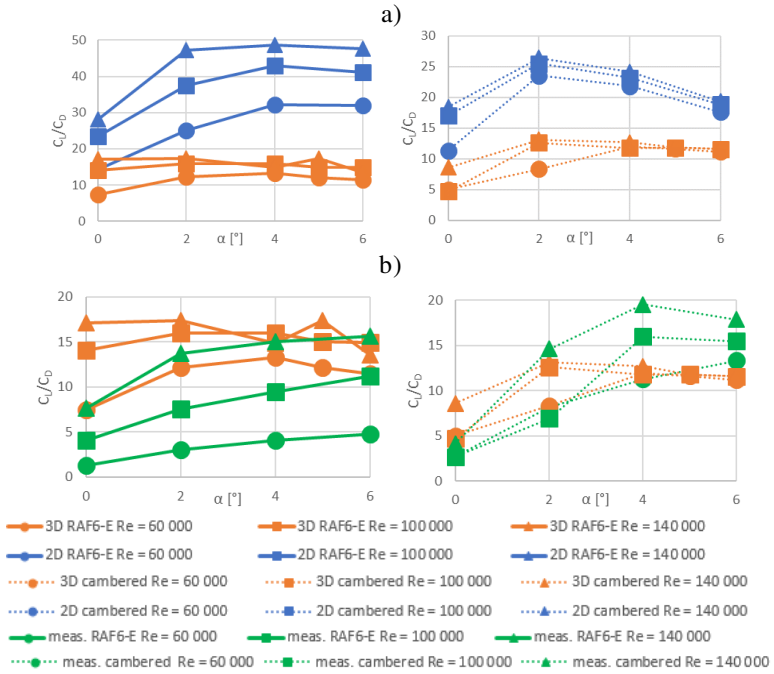

Figure 1 LDR results for a) Two- and three dimensional simulations and for b) Measurements and three-dimensional simulations

CONCLUSION AND FUTURE REMARKS

The two-dimensional simulations are in good agreement with the expectations, they can be suitable for further aerodynamic investigations, and aeroacoustic simulations. Further studies are needed to obtain better fitting between the three-dimensional simulations and the measurements. The change in the parameters of the turbulence model and/or transient simulations offer a possibility for improvement.

ACKNOWLEDGMENTS

This work has been supported by the Hungarian National Research, Development and Innovation Centre under contract No. K 119943 and by the ÚNKP-18-3-I New National Excellence Program of the Hungarian Ministry of Human Capacities. The research reported in this paper was supported by the Higher Education Excellence Program of the Ministry of Human Capacities in the frame of Water science & Disaster Prevention research area of Budapest University of Technology and Economics (BME FIKP-VÍZ).

REFERENCES

[1] TJ. Mueller: *Aerodynamic measurements at low Reynolds numbers for fixed wing micro-air vehicles. In: RTO AVT/VKI special course on development and operation of UAVs for military and civil applications,* Belgium: Von Karman Institute for Fluid Dynamics, 13–17 September 1999.

[2] E. Balla, J. Vad: *Lift and drag force measurements on basic models of low-speed axial fan blade sections, Proceedings of the Institution of Mechanical Engineers*, Part A: Journal of Power and Energy, DOI: 10.1177/0957650918781906, 2018.

[3] E. Balla: *Lapátmetszetek körüli áramlás által keltett zaj szimulációs vizsgálata,* Tavaszi Szél Konferencia, Győr, 2018.

[4] ANSYS® *Academic Research Fluent, Release 19*, Help System, User's Guide, ANSYS, Inc.

[5] J. Winslow, H. Otsuka, B. Govindarajan, I. Chopra: *Basic Understanding of Airfoil Characteristics at Low Reynolds Numbers* (10 4–10 5). *Journal of Aircraft,* 55(3), 1050-1061.

SEAWATER RESISTANCE TESTING AND EQUIPMENT DESIGN

BALOGH Gábor
Department of Mechanical Engineering, University of Debrecen
E-mail: balogh.gabor@eng.unideb.hu

Keywords: seawater test, seawater resistance, seawater resistance of structural steel, stainless steel, and coated layers, material testing methods, seawater resistance test equipment

INTRODUCTION

Nowadays in industrial life, especially the energetic sectors and oil and gas stations and oil refineries the seawater resistance of the structural materials became in point of the engineers view because of the several damages that the seawater cause on the surface of the material. Parallel with that the basic phenomena cause several failures of the structures. That was the reason of development different wear test and corrosion resistance test methods and equipment, to describe the corrosion by time. This kind of tests has to be aggressively restructure the surface to get results in relatively short time. By this point of view and by the results of different type of test, or results of the combination of different test the engineers are able to describe the remaining lifetime of the structure or other words the resistance of the material opposite to the corrosion.

BASIC CONCEPTS OF THE TEST POSSIBILITIES

MARTENSITIC STAINLESS STEELS

[1] Martensitic stainless steels have been used in components operating under wear, corrosion and wear–corrosion conditions found in distillation towers, slurry pumps and mixers of chemical products [3,4]. These materials show high mechanical properties and moderate corrosion resistance, but when under erosion action by the presence of hard particles in aqueous solutions their performance is reduced due to a synergistic effect between wear and corrosion mechanisms [5–7]. Much information concerning the relationship between surface properties and slurry erosion behavior is available in literature for a number of materials, austenitic and martensitic stainless steels. These results have been acquired as a function of pH, solid content and temperature of solution [6,8–10], as well as hardness and morphology of abrasive particles [11,12]. Peterson et al. [13] and ZumGahr [14] reported the erosion wear mechanisms in steels to the microstructure of the eroded surfaces, showing that the brittle or ductile nature of phases present can determine the wear behavior of the tribosystem. Wang–Xu [9] classified a wide variety of alloys as a function of their mass loss under erosion in silica–water slurry, establishing a consistent relationship between hardness and wear resistance. On the other hand, Aiming et al. [5] reported the existence of a 'breakaway' impingement velocity, which marks the transition from moderate to severe erosive wear conditions. Generally speaking, wear of ductile materials under slurry erosion can differ from that under dry erosion conditions [15]. Maximum wear rates of ductile metals submitted to solid particle impingement are commonly observed for impingement angles up to 30°. Conversely, under slurry wear conditions, the maximum erosion rate can be reached at normal incidence, even for ductile materials [5,16]. Spalling of second phase particles and the existence of passive layers may explain this behavior in high-alloyed steels and, in particular, stainless steels [9,10]. Nitrogen can improve the surface properties of industrial steel components. Rogers et al. [17] showed that sub-critical nitriding of 2.25–1Mo steels increases the resistance to corrosion–erosion of heat exchanger tubing for bubbling fluidized bed combustors, and Berns et al. [18] improved the slurry erosion resistance of stainless steels used in petrochemical applications by solution nitriding of stainless steels at high temperature (1423 K). In addition, a number of laboratory tests and theoretical models have been proposed to explain the beneficial effects of nitrogen in corrosion. [19–21] and erosion resistance [22,23] of stainless steels inaqueous solutions. Some of the most important mechanisms used to explain the enhancement of corrosion resistance due to nitrogen alloying are: (a) formation of ammonia or nitrate ions near the surface, leading to corrosion inhibition through localized increase of surrounding environment pH and inhibition of pit growth; (b) retardation of nucleation and/or growth of Cr-rich carbides; (c) strengthening of passive film layer by nitrogen-induced segregation of Cr and Mo. On the other hand, solid solution strengthening and inhibition of second phase particles precipitation are pointed out as the main factors of erosion resistance improvement.

PLASMA SPRAYED CERAMIC AND METALLIC LAYERS

[2] Nowadays, the carbon steels have been applied extensively due to their high mechanical properties and machine-ability at a low price. However, poor corrosion resistance greatly restricts their further application, especially in aggressive environments (e.g. seawater). Various methods such as cathodic protection, corrosion inhibitor technique and covering the steels with coatings or films are employed to protect the steels against the corrosion [24]. One of the most common routes to decrease the corrosion rate of steel is to deposit a protective coating onto the steel surface [25,26]. The protective

coating could be prepared by some kinds of techniques like chemical vapor deposition (CVD), physical vapor deposition (PVD), sol–gel, plasma electrolytic oxidation (PEO) and plasma spray [27–29]. Among these techniques, plasma spraying is one of the most popular methods because it does not cause deterioration of the substrate, and thick coatings (up to hundreds of microns) can be formed at a low cost and high deposition rate [30–32]. Plasma sprayed metallic coating can protect carbon steels against the corrosion [33–35]. The ceramic coatings can work in the environments where both wear and corrosion resistances are required, especially at an elevated temperature; other coatings, such as organic and metallic coatings, cannot compare [36–38]. For example, alumina and zirconia coatings are increasingly and widely used for a range of industrial applications to provide wear and erosion resistance, corrosion protection and thermal insulation [39,40]. Despite of the fact that the coating materials themselves are highly corrosion resistant, existing defects in plasma sprayed ceramic coatings are detrimental to the corrosion resistance of such coated systems [41–43]. Through-coating defects (e.g. pores) are particularly deleterious as they provide direct paths for corrosive electrolytes to reach the coating/substrate interface [44,45]. Electrochemical impedance spectroscopy (EIS) is a powerful analysis technique and has shown its usefulness to study the localized corrosion of coating/steel systems [46,47]. However, there are few instances of research work on plasma sprayed ceramic coatings in saline solution by EIS technique at present. In this paper, the corrosion process of plasma sprayed coatings during long time immersion was investigated by EIS technique. In addition, the corrosion resistance of carbon steel Q235, samples covered with plasma sprayed ceramic coatings (Al2O3 and ZrO2) as well as the metallic coatings (Ni60, for comparison) in simulated seawater were evaluated using the corrosion potential–time curve (Ecorr™) and potentiodynamic polarization, complemented by scanning electron microscopy (SEM).

DESIGN OF TEST EQUIPMENT

The task to build up a real simulator for the sweater resistance test for different kind of tests looks a heavy task and it is. At first we have to solve the total separation of the equipment from the surrounding environment. These test are really corrosive for the sample and also for the structure of the testing chamber, so we have to select the best materials for the complete task. At the moment the equipment is in design state and later we will build the first prototype.

CONCLUSION

Basically this article is an overview of the available publication of seawater resistance test methods, beside that we want to create a testing equipment for wide range of different potential failure modes. During the development of the concept of a test equipment for seawater resistance tests we found different problems which are still not solved and we try to give one kind of solution for those question. Our future view is positive and I'm sure that there will be more publication of this topic to show the result of the developed testing equipment at our university.

ACKNOWLEDGMENTS

The work/publication is supported by the EFOP-3.6.1-16-2016-00022 project. The project is financed by the European Union and the European Social Fund.

REFERENCES

[1] A. Toro , A. Sinatora , D.K. Tanaka , A.P. Tschiptschin: *Corrosion–erosion of nitrogen bearing martensitic stainless steels in seawater–quartz slurry,* Wear 251 1257–1264. 2001.

[2] Zhe Liu, Yanchun Dong, Zhenhua Chu, Yong Yang, Yingzhen Li, Dianran Yan, *Corrosion behavior of plasma sprayed ceramic and metallic coatings on carbon steel in simulated seawater*, Materials and Design 52 630–637. 2013.

[3] ***References from [3] to [47] available at full text article.

SENSOR SYSTEMS AND DATA PROCESSING

BARKÓ György PhD, KALÁCSKA Gábor DSc, MUHANDES Hasan
Institute for Mechanical Engineering Technology, Szent István University
E-mail: suestados@freemail.hu, kalacska.gabor@gek.szie.hu, hasanmuhandes@gmail.com

Keywords: Wear of plastics, factor analysis, patter recognition, neural network

Wear of different structural plastic materials were analyzed by measuring relevant features during abrasion tests (time, force, abrasion rate). Experimental equipment has been utilized to trace the wear of plastic materials under the same conditions. Abrasion rate has been recorded, together with pressure (force) applied on the sample. Length (duration) of the experiments have been standardized by taking identical experimental runtime. Simple apparatus assembled (Figure 1) and sensors were connected to a computer data collecting interface. The interface was converting the sensor signals into digital values and provided the data to a computer that was recording the values.

Figure 1 Experimental setup

Computer based data processing techniques were investigated starting from simple methods (like factor analysis [1]) up to state of the arts (artificial neural network [2] – patter recognition [3]) to classify plastic materials based on the wear measured.
Several mathematical methods are known for the multivariate data handling, like factor analysis, principal component analysis (PCA) and cluster analysis. The factor analysis algorithm is a part of the general commercial data processing software, since the data evaluation can be produced easier and faster with this program. The sensor signals can successfully be evaluated when more sensor types measuring different features are used for the investigation of different plastic samples. The measurement results can be processed also by PCA and characteristic factors shall be obtained. The factor values can be drawn in a plane or in space. Generally, the aim of the visualization is simple: data are separated from each other in feature space. The sensor signals are arranged in a data matrix for the analysis. The aim of the PCA is to calculate factors which can describe the original variables. If the number of the sensors is n, x factors are appropriate to transform the signal matrixes, and x<n. The factors are calculated and the results are plotted in two- or three-dimensional space. The similarity of the investigated structural plastic materials can be drawn with the co-ordinates or factors of the calculated values.
Sensor signals can be expressed as the linear combination of eigenvectors. The r^{th} principal component X_r, is a sum of the sensor responses, S:

$$X_r = \sum_{i=1}^{n} \alpha_{i,r} \cdot S_i$$

where $a_{i,r}$ is an eigenvector
The eigenvectors can be used to characterize the variance. The original vectors in the primary matrix are illustrated by the 100 % variance. The variance is related to the quantity of the information which is supplied by the component. The fewer the vectors, the less information on the variance can be obtained. The variance could be characterized properly between 94-99 % using the first two or three eigenvectors.

Factor analysis and principal component analysis were performed to characterize the features, influencing the abrasion of the plastic samples. After the PCA mathematical analysis of the matrix had been completed, the first eigenvector was calculated for characterization of the variance at 68.6 %, the second one at 25.5, % and finally the third one at 3.2 %. Plastic structural materials can be classified based on the wear observed (Figure 2). Unknown plastics can also be assigned to the material group and wear behavior can be predicted.

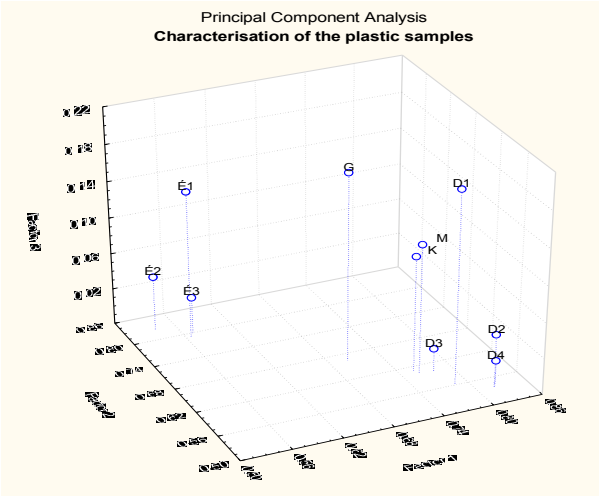

Figure 2 Classification of plastic samples based on wear

Pattern recognition / artificial neural networks (ANN) can be applied also, for the classification of samples by evaluation of the signals of different sensors. The ANN based on the "back propagation of error" method. Multilayer systems using back propagation method is part of the parallel distributed processing [2]. In these cases, the processing unit is a so-called neuron. Two neurons are linked by a connection. Every connection has a weight factor (W), the input values Ij(t) correcting by the weight factor are summarized.

$$I_j(t) = \sum_i W_{i,j}(t) O_i(t)$$

The i and j neurons are connected by W(i,j). All the results, collected from the measurements were analyzed also to identify similarities of group of plastic materials from wear out standpoint. The above-mentioned ANN algorithm can be applied to predict mechanical property, wear of unknown plastic parts. The optimum values of primary weight factors, learning rate (η =0,15), momentum term (μ =0,9) and the sigmoidal parameter (β =1) were already determined. Generally, the higher the learning rate the faster the adaptation of the model. After the teaching process of the ANN, the network will be able to identify the taught plastics. There is opportunity for improvement for the ANN method proving robust and reliable way to identify new structural plastics and plastic parts.

REFERENCES

[1] C. Chatfield and A. J. Collins, *Introduction to Multivariate Analysis*, Routledge, New York
[2] R. Beale and T. Jackson, *Neural Computing: An Introduction*, IOP Publishing Ltd Bristol, England
[3] G. Barkó and J. Hlavay, *Talanta*, Volume 44, Issue 12, Pages 2237-2245

ANALYTICAL AND DISCRETIZED CALCULATIONS FOR THE DIFFUSION BONDED SPECIMENS ON A GLEEBLE 3800 THERMOMECHANICAL SIMULATOR

[1]BAROSS Tétény, [2]JÁNOSI László PhD, [1]VERES Gábor PhD,
[1]WIGNER RCP, RMI, PO Box 49, H-1525 Budapest, Hungary
E-mail: baross.teteny@wigner.mta.hu
[2]Department of Mechatronics, Szent István University, Hungary
E-mail: janosi.laszlo@gek.szie.hu

Keywords: Diffusion bonding, thermal distribution, Gleeble 3800, contact surface

Diffusion bonding methods as a candidate solution for Plasma Facing Components in fusion reactors involved significant investigations over the last decades. The Gleeble 3800 thermomechanical simulator at University of Dunaújváros is a general-purpose servo-hydraulic thermomechanical testing device, which provides suitable environment for the diffusion bonding processes. The heating is carried out by Joule heating with 50 Hz alternating current passed through the specimens griped by special jaws at the ends. It applies direct resistance heating up to 10,000°C/second and apply maximum static pressure 20 t [Uniduna, 2016] under mid 10-5 Torr range. Diffusion welding is a slower process with a relatively low applied stress 10-100 MPa that is well within the Gleeble's capacity, furthermore the digital feedback loops are able for precise control of the process. The system can monitor and control the temperature by four thermoelements. Figure 1. shows a schematic view of the Gleeble jaws with specimens.

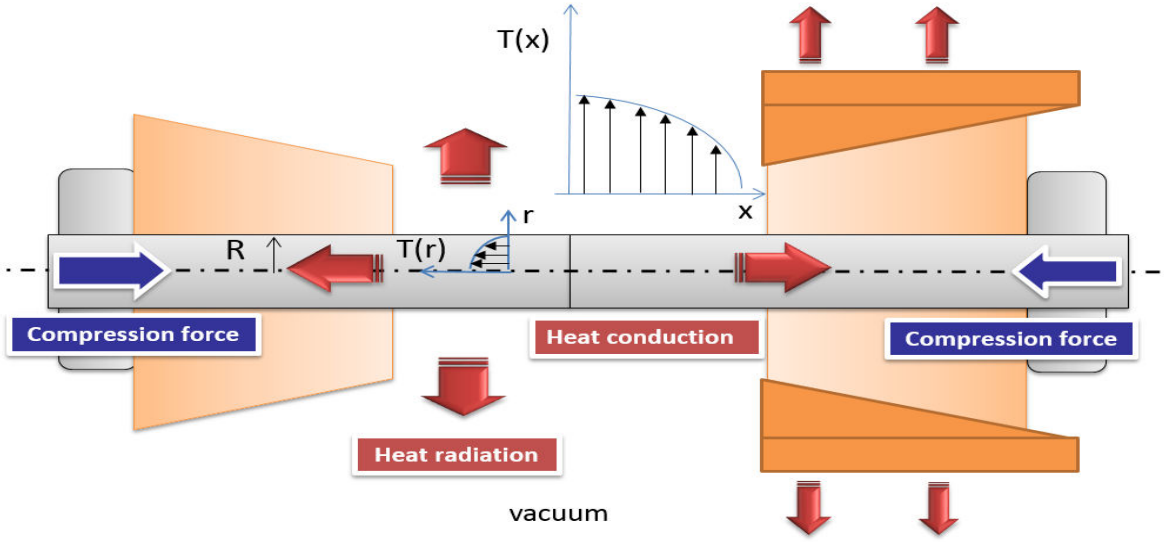

Figure 1 Schematic view of specimens with copper jaws for temperature distribution

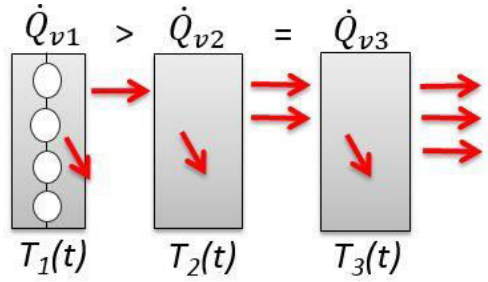

Figure 2 Discretized elements closed to the mated surface for 1D calculation

The present calculations engage with thermal aspects of the mating surfaces during diffusion bonding. Heat generation rate at contact asperities may melt the material during the first term of diffusion welding. A discretized 1D model was built for investigation of thermal distribution, see Figure 2. The results are shown in Figure 3. However the heat generation rate is

in fact significantly larger at contact asperities - that may need special care during heat up process - the heat conduction at a so small range is several order of magnitude larger too. This effect helps to avoid melting the joining surface.

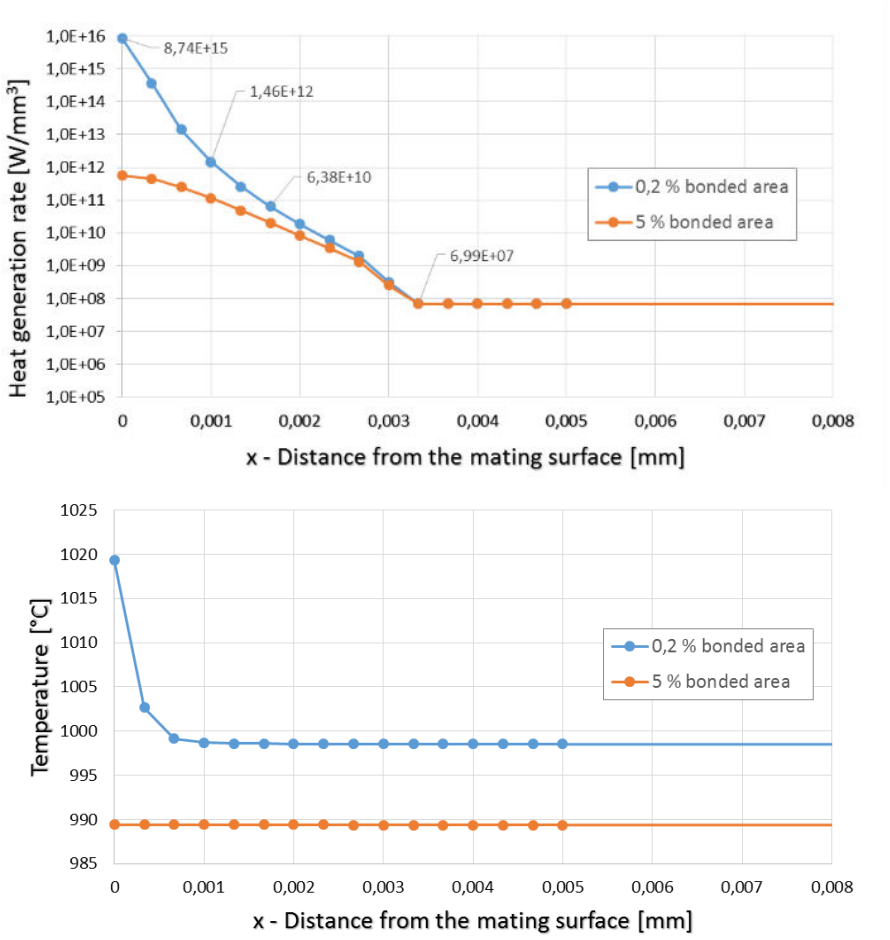

Figure 3 Heat generation rate and temperature distribution in specimen near to the joining surface in contact asperities in steady state

Since the joined surface with different percent of bonded area has presumable varying thermal conductance as well, the advance of diffusion bonding process shall to be observed by thermal or electrical resistance, as a non-destructive method. The transient thermal distributions of welded specimens was investigated also using different grips, jaw models with different heat conduction for validation of the measurements presented in the Gleeble Users Training book.

SUMMARY

The presented work is an outline of temperature distributions closed to the mating surfaces in steady state condition during welding processes. The goal of this work is to prepare the Gleeble physical simulations for the newly developed fusion material as ODS steels, which weldability is a key issue at fusion reactor first walls.

ACKNOWLEDGMENTS

This calculation was prepared in the frame of SZIE PhD school, in this way many thanks the leaders of IPMP (International PhD Mentor Programm) Dr. Gábor Kalácska. Special thanks to Dr. Péter Bereczki, who demonstrated me the Gleeble 3800 Thermomechanical Simulator at University of Dunaújváros.

This work is supported by the ÚNKP-18-3 IV New National Excellence Program of The Ministry of Human Capacities.

COOPERATING ROBOTS USING ARTIFICIAL INTELLIGENCE

[1]BENOTSMANE Rabab, [1]DUDÁS László PhD, [2]KOVÁCS György PhD
[1]Institute of Information Science and Technology, University of Miskolc
E-mail: benrabab1@gmail.com, iitdl@uni-miskolc.hu
[2]Institute of Logistics, University of Miskolc
E-mail: altkovac@uni-miskolc.hu

Keywords: Collaborating robots; Multi agent systems; Artificial intelligence.

The emergence of new technologies such as multi agent systems has an important effect on improving and creating a smart factory. Typically, multi agent systems integrate autonomous systems which are endowed by artificial intelligence (AI), this concept aims to apply intelligent machines collaborating together to build a flexible environment. This article will discuss two parts; the first part describes the terms of cooperating robots and artificial intelligence technics, while the second part presents a real example of cooperation between two robots putting into evidence the advantages of the use of artificial intelligence techniques within the handled industrial problem.

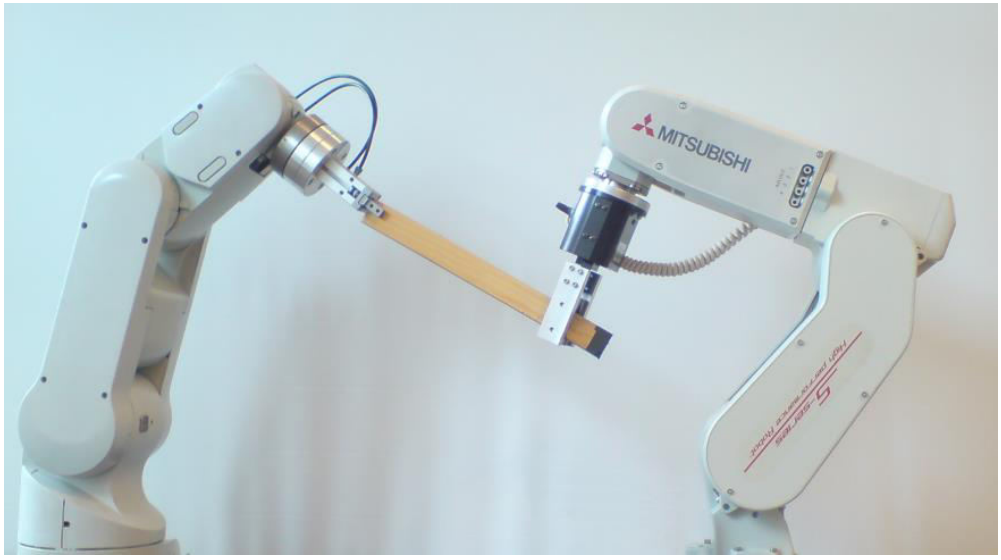

Figure 1 Cooperating robots in industry

The essential goal of our research is creating a virtual simulation model of an assembly line that includes a few robot manipulators equipped with sensors and intelligent controllers. These robots as members of a multi-agent system can help each other and cooperate to finalize the tasks defined in this line, if some malfunction or another problem occurs in the production line, the robots can reconfigure themselves and reorganize and redistribute the steps of the same task. Our process is presented in two scenarios:

Table 1 Possible scenarios of our process

Scenarios	The model
I Scenario	Presents the static model of process including tasks and executed steps of each robots. In this scenario the focus is on the optimal scheduling for the tasks and we intend to apply AI methods for planning parallel work of the robots.
II Scenario	Presents the disturbed process including some problems, random happenings, errors, etc. In this scenario the abnormalities and malfunctions will be created in the process using probability algorithms and the mentioned AI methods will be used for the re-planning of the process.

The model and the working scenarios will be implemented in a 3D simulation software. The working of the model based on the I Scenario applies the well-known simulation methods for the visualisation of the parallel activities. To find an optimal scheduling of assembly steps the next AI methods of planning are considered:

- Classic search methods
- Tabu search
- Situation calculus

In case of the II Scenario the working of the model has to create new solution that takes into account the situation caused by the malfunction and to analyse the possible solutions for the continuance of the assembly process. Practically this is a similar task like was the original planning of the working steps, but the resources, so the inputs of the planning task are modified. In hard situations may happen that there is no possibility for continuance of the process. The main difference in the realisation of the two scenarios is the modelling of the malfunctions or abnormalities. For this, random generator functions, that can actuate changing of process parameters using different types of partitions of the process input or internal variable values, will be used. So the list of the applied methods has to be enlarged with the malfunction generator algorithms that mainly use probability variables. To provide realistic behaviour of the model right probability functions has to be used. To achieve the real behaviour concrete situations, have to be collected, analysed and inbuilt in the model.
The process will be designed in AutoMOD 3D Process Simulation Software, this software has different probability function types which can be used for generating a malfunction and abnormalities such us:

- Logarithmic function,
- Gaussian function,
- Triangular function,
- Continuous function.

To get some experience with real robots we created a real process which two Mitsubishi robots, these two robots collaborate together to realize two different applications:

- First application: The task is providing some building elements (“cards”), the two robots have to build up a house of cards. This task needs the cooperation trivially if there is no some sort of supporting element, because to build an A shape from the two cards needs two hands.
- Second application: The task is solving a 3D packaging job in the case of two co-operating robots, that is to put the bricks in a 3D work space (on one another) into a larger rectangular space.

The main goal of this paper is based on the field of multi agent systems collaborating together to realize some tasks defined by us, in this paper we present three different applications, the first one presents the general objective which is creating a virtual simulation model of an assembly line then the second application is providing some building elements (“cards”) to build an A shape from the two cards needs two hands and the third one is solving a 3D packaging job in the case of two co-operating robots, that is to put the bricks in a 3D work space (on one another) into a larger rectangular space, the scenarios of these tasks will be programmed using artificial intelligence techniques such as Tabu-search. (to find optimal solution).

ACKNOWLEDGMENTS
This research was partially carried out in the framework of the Center of Excellence of Mechatronics and Logistics at the University of Miskolc. The described study additionally was carried out as part of the EFOP-3.6.1-16-00011 “Younger and Renewing University – Innovative Knowledge City – institutional development of the University of Miskolc aiming at intelligent specialization” project implemented in the framework of the Széchenyi 2020 program. The realization of this project is supported by the European Union, co-financed by the European Social Fund. The financial support is acknowledged.

MICROMECHANICAL MODEL OF DRY FRICTION HYBRID POLYMER COMPOSITE CLUTCH FACINGS

BICZÓ Roland, KALÁCSKA Gábor DSc
Doctoral School of Engineering Science, Szent István University
E-mail: rolbicz@gmail.com, kalacska.gabor@gek.szie.hu

Keywords: clutch facing, hybrid polymer composite, micromechanical model, scatter-wound facing, ROM

Modeling the complex coupled thermomechanical and tribological contact of a dry friction clutch system between cast iron flywheel and scatter-wound hybrid composite clutch facing requires a thought through investigation of the friction material properties and behavior. Challenges of the creation of a mechanical stiffness matrix for such a complex material are described in this paper along with simplification ideas and solutions.
Requirements of composite friction materials derive from the operating characteristics of their applications. A clutch transfers the kinetic energy of a rotating crankshaft – coupled to a power source – to the transmission and wheels. Slippage results in the generation of heat, which is absorbed and eventually dissipated to the atmosphere by the clutch. [2] To fulfill these requirements typical components of polymer composite friction materials for clutches can be classified in the following groups: reinforcements, binders, friction modifiers, and fillers. Since there are more than two components such composites are called hybrid composites. The manufacturing steps for the investigated fiber reinforced woven clutch facings are wire preforming, dry mixing of fillers and modifiers, molding of mix around strand or wire preforms (coating), weaving according to a specified pattern, then hot pressing, curing and grinding.

Figure 1 From left to right: Parts of a dry clutch system, dry clutch plate, products of phases of dry friction material production [1]

Determing the material properties of such materials isn't always possible through standard methods especially when some components are industrial secrets. In our case the hybrid composite can be derived into two main component groups. The first group is long fibre reinforcement that consists of glass fibre, copper, aramid and poly-acryl-nitrile. The second group is the so called matrix, that is also a hybrid composite itself with short fibre reinforcement, fillers, sulfur, phenol and melamine resin etc. in it. The two groups then united by coating. Taking the secret properties and the special orientation due to wreath-waving production method into consideration the idea is to determine the mechanical properties of these two component groups separately and then utilize a rule of mixture to create a mechanical stiffness matrix.
Such rule of mixtures (ROMs) are utilized in micromechanical models like Chamis's [3] semi empiric model for unidirectional composites, Halpin-Tsai [4] equations also for unidirectional composite materials or Tsai-Pagano [5] model for randomly oriented fibrous composites. All of these deal separately with fiber and matrix properties then unites them to evaluate mechanical properties of the whole composite. The Tsai-Pagano equations are:

$$E_{11}^{*} = E_m * V_m + E_f * V_f$$

$$E_{22}^{*} = \frac{E_f * E_m}{E_f - \sqrt{V_f}(E_f - E_m)}$$

$$E = \frac{3}{8}E_{11}^{*} + \frac{5}{8}E_{22}^{*}$$

$$G = \frac{1}{8}E_{11}^{*} + \frac{1}{4}E_{22}^{*}$$

$$\nu = \frac{E}{2G} - 1$$

where:

E11* - fictive elastic modulus in the direction of load,
E22* - fictive elastic modulus perpendicular to the direction of load,
E – effective elastic modulus,
G – effective shear modulus,
υ – effective Poisson's ratio.

To evaluate the properties of the 'matrix component group' facings made only of coating matrix were produced without fibre reinforcement. Via abrasive water jet cutting test specimen were created from these facings. Tensile test according to DIN 53455, two directional strain measurement and Iosipescu shear test were carried out to determine the tensile strength, elastic modulus, Poisson's ratio and shear modulus of the matrix. For evaluating the mechanical properties of long fibre reinforcement standard tests of Schaeffler Savaria Ltd. were utilized and the lowest fibre Poisson ratio was taken into account. The measured properties are the following:

Table 1 Mechanical properties of the matrix component group

E_m	[MPa]	4122
ν_m	[-]	0,38
G_m	[MPa]	1326

Table 2 Mechanical properties of the long fibre reinforcement group

E_f	[MPa]	4122
ν_f	[-]	0,38
G_f	[MPa]	1326

Utilising the rule of mixtures and taking into consideration the sinusoidal running of the coated fibre in the wraith, that the facing is created from, through vulcanization steps the missing mechanical material properties in a helical coordinate system [r,φ,z] for the facing are:

Table 3 Mechanical properties of the fibre reinforced woven dry friction clutch facing

E_{rr}	[GPa]	12,3
E_{22}	[GPa]	12,3
ν_{12}	[-]	0,46
G_{12}	[GPa]	7,6

With the material being identified mechanically, further investigations can be initiated regarding it's behavior.

REFERENCES

[1] LuK symposia 1986 – 2006.
[2] M. G. Jacko, S. K. Rhee: *Brake Linings and Clutch Facings*. Kirk-Othmer Encyclopedia of Chemical Technology, 144-154, 2000.
[3] C. C. Chamis: *Mechanics of composite materials: past, present, and future*. J Compos 9 Technol Res ASTM, 11:3–14. 1989.
[4] J. C. Halpin, J. L. Kardos: *The Halpin-Tsai equations: A review*. Polymer Engineering and 7 Science, Vol. 16, No. 5. 1976.
[5] S. W. Tsai, N. J. Pagano: *Invariant properties of composite materials*. In: S. W. Tsai, J. C. Halpin, N. J. Pagano, *Composite materials workshop*, St. Louis, Missouri, 1967. Technomic Publishing Company; p. 233–53. 1968.

ANALYSIS OF THE EFFECT OF THE ADDENDUM MODIFICATION COEFFICIENT FOR CONTACT SURFACES OF SPUR GEARS

BODZÁS Sándor PhD
Department of Mechanical Engineering, University of Debrecen
E-mail: bodzassandor@eng.unideb.hu

Keywords: addendum modification coefficient, normal stress, deformation, elastic strain, spur gear

The analyzing of the mechanical parameters of the connecting gear pairs for given load and boundary conditions is the aim of the TCA (Tooth Contact Analysis) analysis.
We have worked out a computer program with which the parameters and the profiles of the gears could be determinable. Application of this program all parameters of the gears could be modified. This program is helped to create the CAD (Computer Aided Design) models of the connecting gears. We have designed five types of spur gear pairs where the addendum modification coefficients are different. All of other parameters have not been changed.
After the setting of the finite element mesh, the load and boundary conditions the normal stress, the normal elastic strain and the normal deformation have been analyzed in the function of the changing of the addendum modification coefficient.

Figure 1 Designing of the spur gears having different addendum modification coefficients

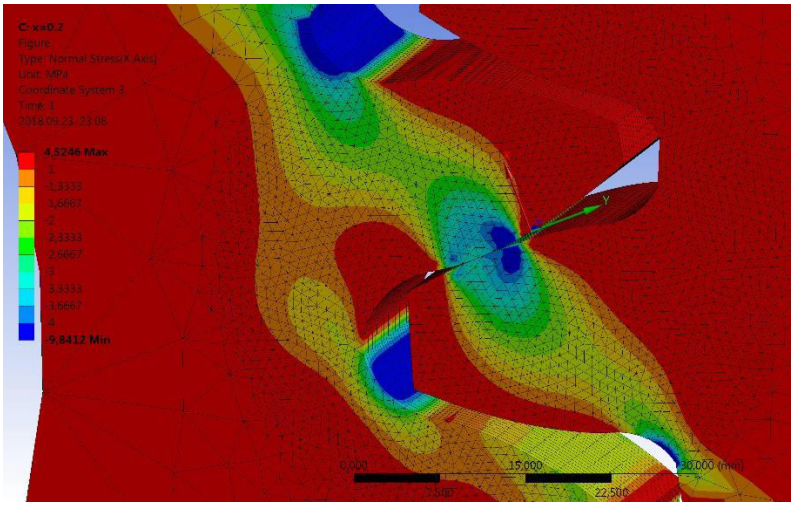

a) The distribution of the normal stress on the connecting surfaces

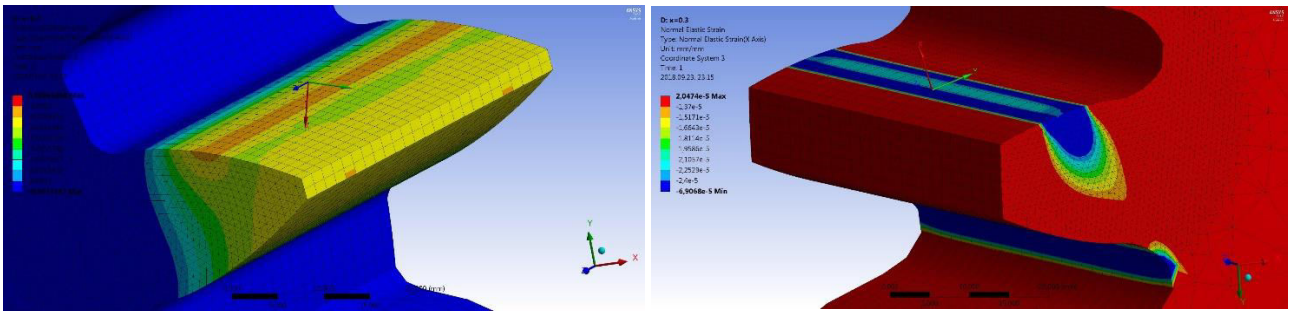

b) normal deformation of the driving gear c) normal elastic strain of the driven gear

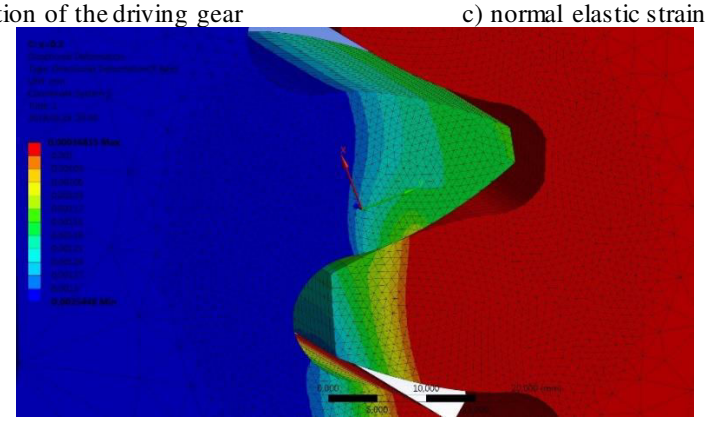

d) The distribution of the normal deformation on the connecting surfaces

Figure 2 TCA results

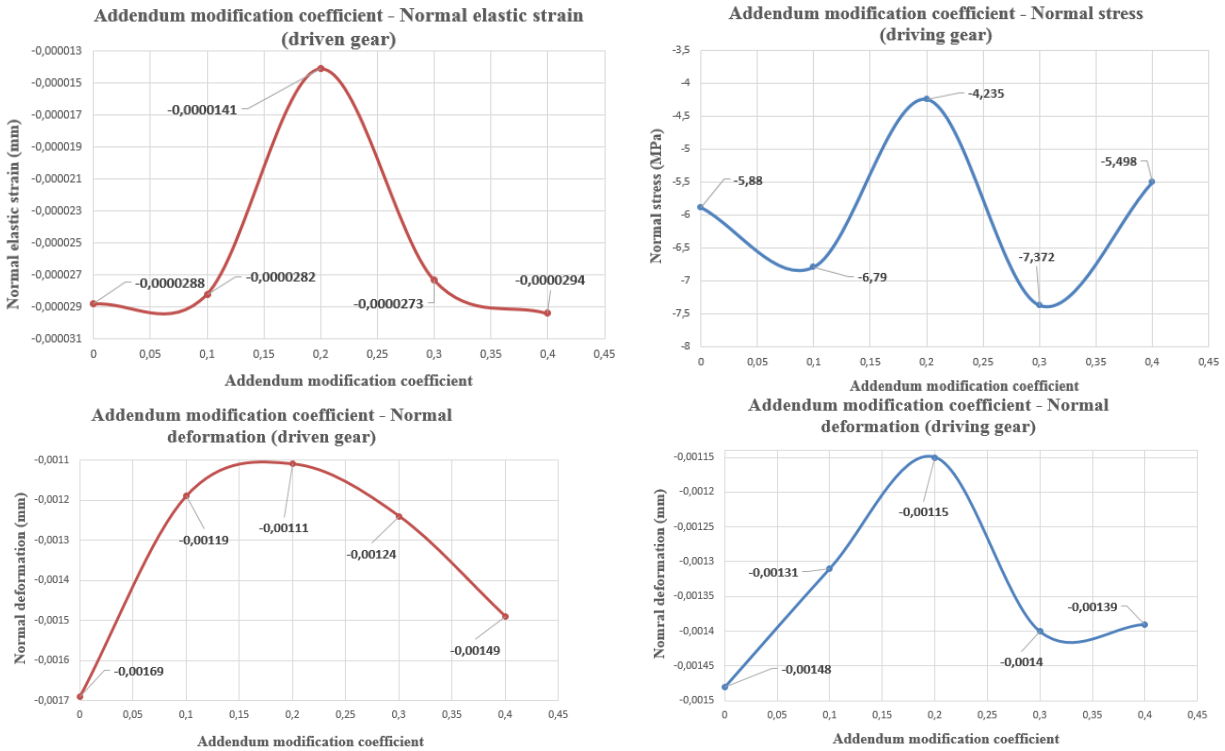

Figure 3 The analysed TCA parameters in the function of the addendum modification coefficient

ACKNOWLEDGMENTS

„Supported BY the ÚNKP-18-4 New National Excellence Program of the Ministry of Human Capacities”

SIMULATION MODELLING IN THE SIZING OF CITY LOGISTICS SYSTEMS – A STUDY FOR CONCENTRATED DELIVERY POINTS

BÓNA Krisztián PhD, SÁRDI Dávid Lajos
Department of Material Handling and Logistics Systems, Budapest University of Technology and Economics
E-mail: krisztian.bona@logisztika.bme.hu, David.sardi@logisztika.bme.hu

Keywords: logistics, simulation, modelling, city logistics, cost model

Nowadays, urban freight traffic is causing significant noise and air pollution, so it is in the focus of green logistics developments, both in technology and system organization. Based on experiences within city logistics, significant problems are caused by the so-called concentrated delivery points. Since the summer of 2015, we collected lots of data about stores of concentrated delivery points to help the modelling and the simulation of the new green solutions for the examined logistics systems. In the viewpoint of our project, there are two main groups of delivery points. There are single delivery points and the concentrated delivery points, they include more single delivery points according to some aspects. Concentrated delivery points have two main groups: there are concentrated delivery points, organized by opened or closed infrastructure. Closed infrastructure means that the concentrated delivery point is marked by a building (like in the case of shopping malls, hypermarkets, markets of duty-free areas of airports). In the case of opened infrastructure there is no building, so the concentrated delivery point is bound by roads or by a square (like a shopping area or an outdoor market). On figure 1, we can see the concentrated delivery points of Budapest.

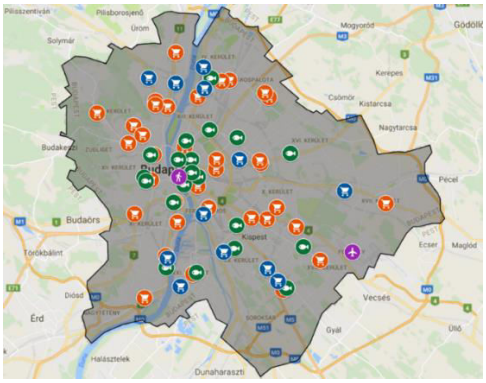

Figure 1 Concentrated delivery points in Budapest on Google Maps

According to our earlier assumptions, these concentrated delivery points are causing significant traffic flows and also noise and air pollution; while their logistics systems are badly constructed - there are no innovative technologies used and their processes are not handled by a city logistics provider in a common system. Some European projects (for example in Bristol or Padova) show us that the innovative multistage city logistics systems can reduce performances and emissions significantly. In case of Bristol, where they deliver to 63 stores in a two-stage system, they reduced mileage by 196.000 km and CO_2 emissions by 22,5 t between 2006 and 2009.
First, in 2015 we developed a research methodology which makes it possible to examine the logistics characteristics of concentrated delivery points in a standard way. It has two parts: an exploratory research and a questionnaire with questions about all important logistics fields which must be filled in by the shops in the examined area. By using this methodology, we examined 3 shopping malls and a shopping area in Budapest and collected data about nearly 500 shops inside them. The collected data shows us that the expected problems are real, they deliver with high frequency, mostly in smaller lorries in the rush hour, mostly only small packages to the shops of the concentrated delivery points.
For the simulation runs, we used the data of 178 stores from shopping malls after developing the simulation model in MS Excel and also the mathematical model of the physical processes of the system. In this project, we modelled and examined the current system and a new two-stage system, where we inserted a consolidation center between the suppliers and the concentrated delivery points and converted the logistics areas of the malls into cross docks. In the modelled new system, a city logistics provider operates the deliveries. The main purpose of the simulations was to compare performances and emissions (of the supplies and the inverse transactions) in the current and in the new system, so for first, we modelled only the physical processes. The simulation model which examines the processes of 178 shops, works with random generators for which parameters are calculated from the statistics of the collected data. The first component of the simulation model

models the operation of the current system, the second works with the new system. The components are similar: first, they generate when we need to deliver and generates the amount of goods to be delivered and the distance to be covered. From these parameters it calculates the performances, the consumption and the emissions, and it models also the stocking points of the system. In the new system, the model needs to calculate the number of concentrated deliveries too (which must be handled by the city logistics provider), and in both cases it generates the number of empties to be handled and the home deliveries too, and it calculates the performances that belong to these transactions. Before the simulations, we validated and verified the model.

Based on the results of the experiments, in the current system we have 3.397 monthly deliveries (standard deviation 16,5). In the new system, between the suppliers and the consolidation center there are 1.339 monthly merged deliveries (st. dev. 16,7), between the center and the malls there are 269 monthly consolidated deliveries (st. dev. 6). This is a significant reduction of transactions (in every case, we need to handle approximately 1.350 tons goods/month). The sum mileage (with empty handling) in the current system is monthly 635.385 km, in the new system we can reduce it to 316.109 km (which is more than a 50% reduction). This means also a significant reduction of consumption and emission too, for example we reduce the monthly CO_2 emissions from 7,1 tons to 3,5 tons. The only parameter which is increasing (by 14%) is the delivery performance, because of the new point in the system (the consolidation center). In the current system it is 152.852 tkm/month, in the new system it is 174.983 tkm/month, but in the city, we have a 38% performance reduction. In the home deliveries we need to handle monthly approximately 50 tons goods, this means monthly 4.097 transactions in the current and 991 consolidated transactions in the new system which means a monthly approximate 3.000 km mileage-reduction.

After developing the mathematical and the simulation model of the physical processes, we created also the mathematical model of the cost structure. We modelled the logistics costs in three dimensions and we could adopt it easily to the existing system architecture. The three dimensions are the cost centers (e.g. suppliers sites), the companies of the systems (e.g. store owners, logistics providers) and the processes of the system (e.g. loading, administration). The given cells of this three-dimensional matrix give as the logistics costs of the given company in the given process at the given cost center. For the simulations, we collected specific cost data from former projects and tenders. Based on the simulation runs, the sum of monthly logistics costs in the current system (for 178 shops) is approximately 288.000 Euros. In the new system, we can reduce it to 216.000 Euros (see on Figure 2) which means a cost reduction of 25%, because of the significant reduction of number of deliver transaction and with that the reduction of delivery costs. We also examined the effects of parameter changes on the sum cost. We can say that the increasing of number of deliveries and the increasing of specific delivery costs has the most significant effect on the reduction of logistics costs.

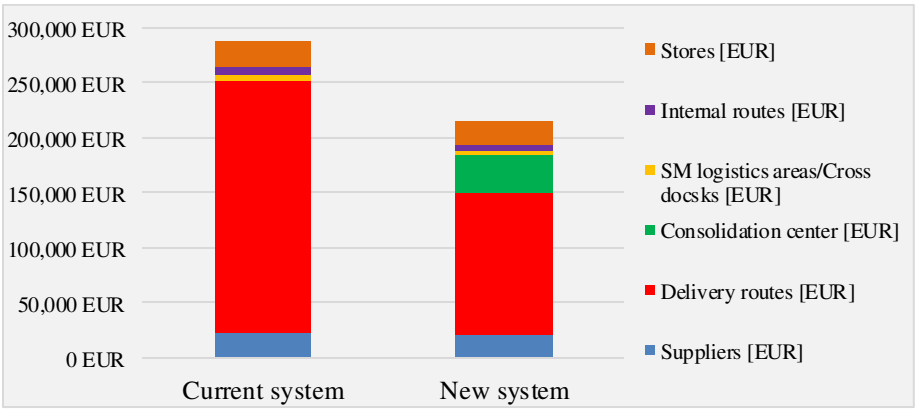

Figure 2 Comparison of monthly logistics costs

Of course, the investment costs of the new city logistics system are not negligible, but about this we don't have exact data yet. For the new system, new infrastructure needs to be planned, we need to invest in new vehicles (maybe with some special technologies too, e.g. cargo trams or cargo boats) and a new IT system is needed too, but on the operational side in case of only 178 shops we are going to have significant operation cost reduction based on our experiments (and by use of this data, later we can also examine the returns in the system). However, it can be deservedly assumed, that the use of innovative and modern technologies could even more reduce the emissions and costs. Now, we can say, that we can expect significant cost reduction on the operational side by use of the new, two-stage logistics system.

ACKNOWLEDGMENTS
Supported by the ÚNKP-17-2 New National Excellence Program of The Ministry of Human Capacities.

ENHANCING PERFORMANCES OF CEMENT BONDED WOOD-BASED PRODUCTS

BRAHMIA Fatima Zohra PhD, ALPÁR Tibor PhD, HORVÁTH Péter György PhD
Simonyi Károly Faculty of Engineering, University of Sopron
E-mail: fatima.zohra.brahmia@phd.uni-sopron.hu, alpar.tibor@uni-sopron.hu, horvath.peter.gyorgy@uni-sopron.hu

Keywords: scots pine, curing agent additives, fire retardants, cement hydration.

The cement wood composites are one of the favourable building materials, because it has both advantages of two materials wood and concrete. It has good strength, fire resistance, durability, lightweight and better dimensional stability. The known cement wood composites products are cement fibreboard, cement bonded particleboard (CPB) wood-wool cement boards (WWCB) and building blocks [1]. Most of previous products used as structural and construction material or for insulation purposes. The problem in cement wood composites is the cement wood bonding because the wood compounds like sugars and lignin effect on the cement curing, it make the cement curing time lager [2]. The solution was using curing agent additives like water glass (Na_2SiO_2), calcium chloride ($CaCl_2$), aluminium silicate ($Al_2(So_4)_3$) and magnesium chloride ($MgCl_2$) to accelerate the hydration process of cement [3]. In addition choosing the wood pieces has big effect on producing the cement wood composites, even the ratio of wood cement and ratio of cement water has effect on cement wood bonding [4]. The aim of this research is Enhancing performances of cement bonded wood-based products by increasing its Fire resistance. For enhancing the performance of the cement bonded wood-based product, it must focus on relations between wood and cement. Moreover, studying the effect of additives and its concentration on hydration of cement. In addition the effect of additives on the fire resistance of wood. In this experiment for wood, scots pine (*Pinus sylvestris*) was used with dimension *Table 1* and with different surface roughness. For additives Disodium-tetra borate ($Na_2B_4O_7$), Disodium-hydrogen phosphate (Na_2HPO_4), Diammonuim-hydrogen phosphate ($(NH_2)_4HPO_4$) and polyethylene glycol 400 (PEG400) were used as fire retardants with different concentrations. The investigations were made by Linder test as a fire test and the hydration test for cement. For preparation to the Linder test, the wood samples were saved on room climate under the temperature of 20°C and humidity of 65% for 7 days. The surface modification done by painting 5g of each additives by brush on the surface of wood. After that it were let to dry for one day and next day were put back to room climate under the same condition for that same period. Portland cement CEM I 42.5. Water glass, mixing water, Fire retardants were used in hydration test. The test is about measuring the temperature changing in 24 hours during the cement curing. After investigations results showed that for Linder test *Figure 1*. The fire retardant were effective on the fire retardation of scots pine but the concentration of fire retardants has big effect on the performance of fire retardation higher concentration higher protection and also the surface roughness of wood had no significant effect on the fire resistance and on the fire retardants. For hydration test, *Figure 2* all samples treated with fire retardants cured in 24 hours the best result was with borax because the curve of temperature changing during the cement curing similar to the untreated cement mixture. For the other fire retardants the smallest concentration had also the same behavior as the opposite of the high concentration that have high temperature peak in the beginning cement curing this is why it may needs longer pressing time. Polyethylene glycol has no good results on all tests specially the hydration test. It prevent the cement from curing.

Table 1 Data for the investigated samples.

Geometry for Linder test		surface types	Ra	Rz	Rmax
Height (H)	100*mm*	*sawn*	*6,2 µm*	*42,6 µm*	*64,2 µm*
Length (L)	100*mm*	*sanded*	*5,4 µm*	*39,9 µm*	*46,3 µm*
Width (W)	10*mm*	*planed*	*5,6 µm*	*46,2 µm*	*67,2 µm*

Note: Ra: Average surface roughness. Rz: Roughness depth. Rmax: maximum roughness.

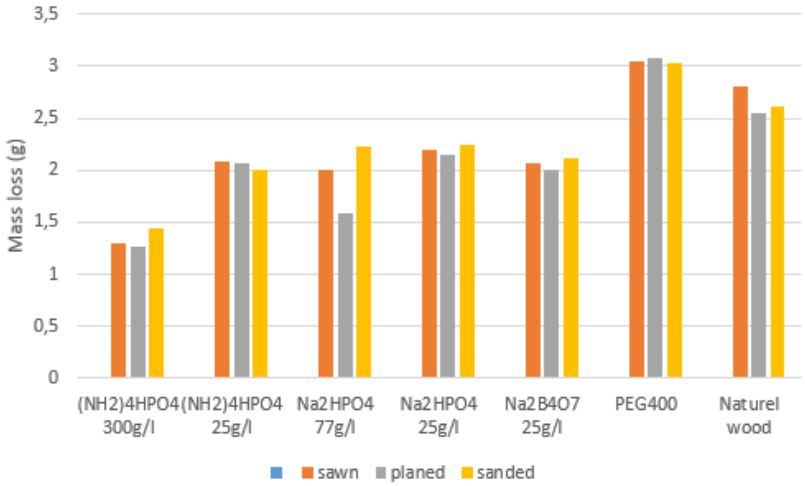

Figure 1 Linder test.

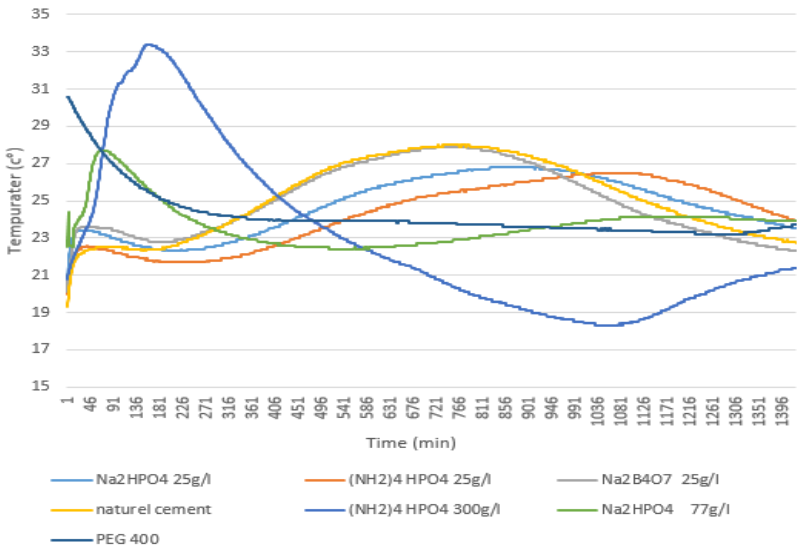

Figure 2 Hydration test.

ACKNOWLEDGMENTS

This article made in frame of the „EFOP-3.6.1-16-2016-00018 – Improving the role of research+ development+ innovation in the higher education through institutional developments assisting intelligent specialization in Sopron and Szombathely".

REFERENCES

[1] G. Vaickellionis, R. Vaickellionis: *Cement Hydration in the Presence of Wood Extractives and Pozzolan Mineral Additives,* Ceramics-Silikáty, 50 (2), 115-122; 2006.

[2] S. Frybort, R. Maurtiz, A. Teischinger, U. Müller: *Cement Bonded composites-A Mechanical review*, Bio Resource, 3 (2), 602-626; 2008.

[3] T. Alpar, A. Pavlekovics, L. Csoka, L. Horvath: *Wood Wool Cement Boards Produced with Nano Minerals*, International Scientific Conference on Hardwood Processing (ISCHP2011), 75-82; 2011.

[4] Y. M. Wei, Y. G. Zhou, B. Tomita: *Hydration behavior of wood cement-based composite I: evaluation of wood species effects on compatibility and strength with ordinary portland cement*, Journal of Wood Science 46, 296 -302; 2000.

THE EFFECT OF THE EXCESS TITANIUM CONTENT ON THE MICROSTRUCTURE OF ALUMINIUM-SILICON FOUNDRY ALLOYS

BUBENKÓ Marianna, FEGYVERNEKI György PhD, TOKÁR Mónika, MOLNÁR Dániel PhD
Faculty of Material Science and Engineering, University of Miskolc
E-mail: ontbm@uni-miskolc.hu, gyorgy.fegyverneki@nemak.com, monika.tokar@uni-miskolc.hu, daniel.molnar@uni-miskolc.hu

Keywords: Hypoeutectic Al-Si alloys, microstructure refining, AlTi5B1 master alloy, grain refining

For providing the uniaxial dendritic structure for cast alloys, fine–grained cast state is necessary. Thus, the regulation of the nucleus formation of the melt via grain refinement is an essential step to achieve the required quality and mechanical properties. [1-3] Grain refining is one of the strengthening mechanisms which provide higher mechanical properties to an alloy. Grain refinement would increase the number of grains and their boundaries *(Figure 1.)* and therefore, increases the yield strength of the material. [4] The addition of grain refiner increases the number of nucleation sites, thus, promoting equiaxed grain growth rather than columnar. Large grains of α–Al in the microstructure are responsible for a number of defects, like disperse porosity, microcracks, decrement of mechanical properties, etc.

Figure 1 The Barker colour etched micrographs: (a) 3rd alloy before grain refinement, (b) after the addition of AlTi5B1 grain refining master alloy

The three examined foundry alloys were: ***AlSi7MgCu0.5 (1st alloy); AlSi9Cu1 (2nd alloy); AlSi9Cu3Fe0.5 (3rd alloy)***. These melts were alloyed with AlTi5B1 master alloy during the rotary degassing process, with nitrogen inert gas. The initial titanium contents were between 900–1200 ppm. Based on the recommendation of the alloy manufacturer, 750 g AlTi5B1 master alloy was added to 1000 kg melt, which is 37.5 ppm titanium content in function of total amount. The effect of additional titanium content on the nucleus formation properties of the aluminium melt was examined. The titanium was added in the form of AlTi5B1 master alloy.
An optical emission analyzer technique was used to determine the chemical compositions of the alloys and the amount of the beneficial master alloy. Thermal analysis was carried out to examine the degree of grain refinement. The thermal analysis specimens were casted into preheated (200°C) steel crucible.
The titanium concentration before and after AlTi5B1 addition and the difference of the minimal liquidus temperature before and after AlTi5B1 addition are shown in Table 2.

Table 1 The differences of the starting temperature of nucleation before and after AlTi5B1 addition

Alloy	Titanium concentration before AlTi5B1 addition (ppm)	Titanium concentration after AlTi5B1 addition (ppm)	ΔT_{Lmin} (°C)
AlSi7MgCu0.5	1193,5	1229.4	3.03
AlSi9Cu1	1076,6	1088.5	4.87
AlSi9Cu3Fe0.5	891,1	928.6	0.17

The addition of extra 750 g master alloy had a positive effect, mainly in case of 1st and 2nd alloys, on the nucleus formation and increased the ΔT_{Lmin}, cause the starting temperatures of the nucleation were increased.
For the examination of the mechanical properties, Diez–test bars were casted after melt treatment into a steel die, according to the German standard. [5] Tensile test specimens (cylindrical shaped, 5 mm diameter, 50 mm length) were machined out from the test bars according to the industrial standard.

The Diez–test bars are technological test specimens which were used to examine the grain refining effect of master alloy. The test bars were heat treated (1st alloy-T5, 2nd alloy-T6, 3rd alloy-was not heat treated) to examine the effect of heat treatment on the mechanical properties. The Diez–test die and the locations of the tensile specimens can be seen in *Figure 2*.
The average standard deviation of the elongation values was rather high. In order to determine the reason for the low strength values, the fracture surfaces of the tensile specimens were examined.
In case of all the examined alloys, the fracture surfaces of all specimens were examined with a stereo microscope. The stereo microscopic image of a chosen test bar with an Al_2O_3 oxide inclusion can be seen in *Figure 3*.

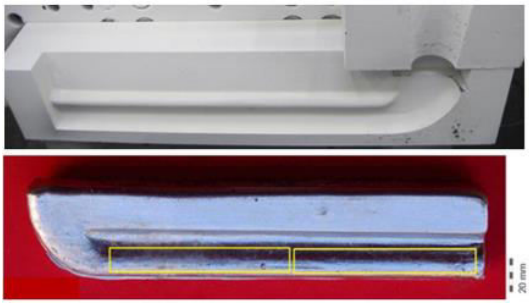

Figure 2 Diez–test die and the locations of the tensile specimens

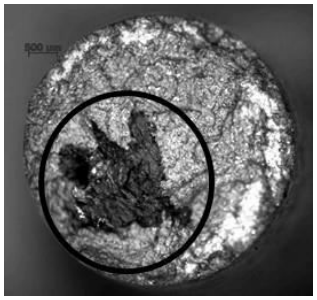

Figure 3 The stereo microscopic image of a chosen test bar

Based on the evaluation of the experimental test bars and the prepared diagrams, it can be concluded that the extra 750 g master alloy addition to all Al–Si melts had a positive effect on the nucleus formation and increased the starting temperature of the crystallization.
The additional titanium concentration resulted in increased average grain number. The grain number was 2.8 times higher of the thermal test bars after AlTi5B1 addition, in case of when the ΔT_{Lmin} was higher (3.03°C and 4.87°C).
The effect of the additional 750 g master alloy on the mechanical properties could be observed on the Diez–test bars. A correlation can be observed between the average tensile strength, yield strength and grain number of the series and the test bars with higher titanium concentration: the increased grain number resulted in higher tensile strength and yield strength values. However, the elongation values were greatly affected by the inclusion content of the melt. The parameters influencing melt quality (e.g. the efficiency of the melt cleaning) should be reviewed, as the decreased mechanical properties cannot be attributed to the addition of AlTi5B1 master alloy, but the inclusion content of the melt.

ACKNOWLEDGMENTS
The authors are grateful to Árpád Kovács for carrying out the tests with scanning electron microscope, to Zoltán Márkus for her help with the sample preparation. The authors are grateful to Mária Ambrus for her advice.

REFERENCES
[1] Y Birol: *Performance of AlTi5B1*, AlTi3B3 and AlB3 master alloys in refining grain structure of aluminium foundry alloys - Materials Science and Technology – 28:4, pp. 481-486., 2012.
[2] K. T. Kashyap, T. Chandrashekar: *Effects and mechanism of grain refinement in Al alloys* – Indian Academy of Science – Vol. 24., No. 4., pp. 345 – 353., Aug. 2001.
[3] P.S. Mohanty, J. E. Gruzleski: *Mechanism of grain refinement in Al, Department of Mining & Metal Engineering, Acta Metallurgical Material,* Vol. 43., No. 5., pp. 2001 – 2012., 1995.
[4] M. Deni Ferdian: *Effect de la vitesse de refroidissement sur la tailla des grains, la modification eutectique et la precipitation d´intermetalliques riches en fer dans des alliages Al-Si hypoeutectiques,* pp. 10, PhD Thesis, 2014.
[5] H. W. Rockenschaub, R. Gschwandter: *Eigenschaftsprofil und Wärmebehandlung der kokillengusslegierung AlSi12 cunimg (EN1706 AC–48000)* – Österreichisches Gießerei Institut, Leoben, 2008.

LOCAL ANNEALING OF COLD ROLLED ALUMINIUM SHEETS BY LASER TREATMENT

[1]BUBONYI Tamás, [1]BÁNÓCZY Zsuzsanna, [1]BARKÓCZY Péter PhD, [2]BUZA Gábor PhD
[1]Institute of Physical Metallurgy, University of Miskolc
[2]Department of Automotive Technologies, Budapest University of Technology and Economics
E-mail: fembubo@uni-miskolc.hu

Keywords: LASER treatment, aluminium alloys, recrystallization, microstructure, metallography

LASER treatment is frequently used in surface treatment of different kind of metals. It is an easy way to projects high energy to the surface, so it is an excellent method in surface hardening remelting, welding, cutting etc. This technique is widely used in the case of aluminum alloys, despite of the aluminum reflects more than 90% of the LASER intensity naturally. The modification of the layer, ex. carbon coverage, solve this problem. With modern automation the movement of the LASER dot is easy on the targeted surface, so where the energy density of the LASER beam is enough, it is an ideal solution. The LASER has a high energy density, so the heating rate of the surface is high. If the material has enough weight, the focused energy can heat up a small volume on the surface, so the cooling rate also will be large. This behavior of the LASER treatment means a limit in the applications.
It is possible to apply low energy density treatment also. The main question of the current study, what happens during the treatment of cold rolled aluminium sheets. It is well known that deformation energy stored in the deformed metals in its dislocation structure, and during heating this energy releases due to the recovery and recrystallization. Both processes cause the decrease of the hardness of metals, but during the recrystallization new grains formed and a new grain structure can be seen during the metallographic inspection. As large the heating rate and the temperature of the objects, as fine grain structure will form.
Different aluminium alloys (high silicon and high iron content) were produced as slabs. The slabs hot rolled in the range of 400-500°C. After hot rolling the sheets are cold rolled in a different extent, which mans different thickness of the sheets. The recrystallization behaviour of the alloys studied by isothermal heat treatments. This series of experiments reveals the mechanical properties of the alloys too. Samples were prepared for LASER heat treatment.

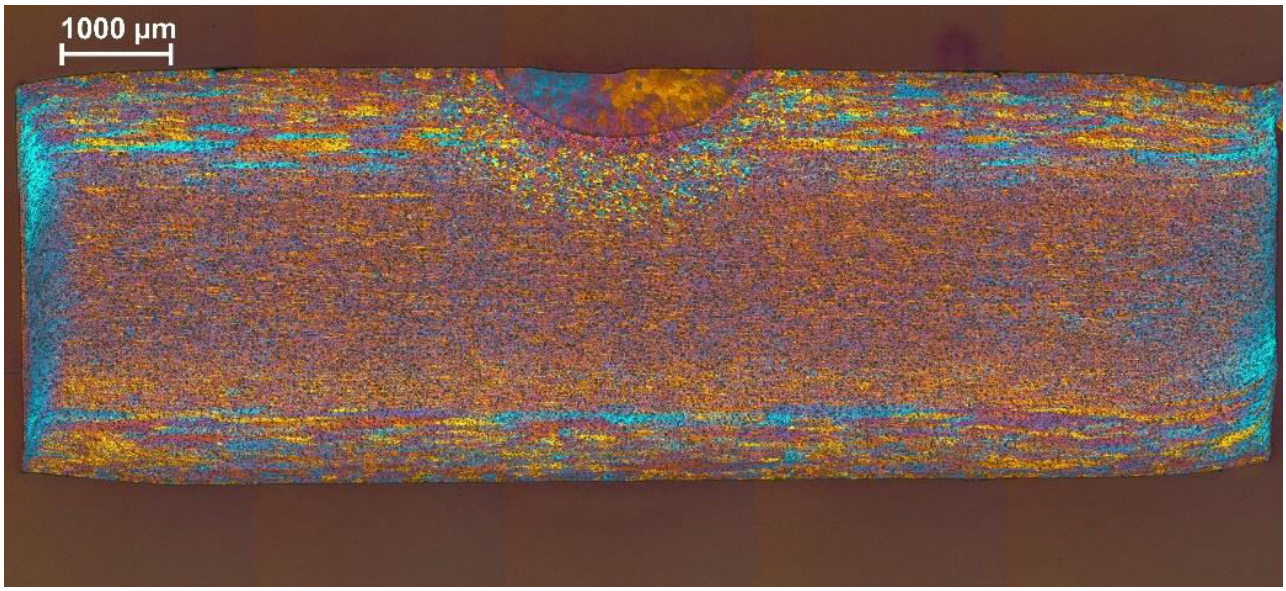

Figure 1 Microstructure of the LASER treated aluminium sheet.

The surface of the samples covered by carbon spray. This black surface can effectively heat up by LASER. The sample sheets were fixed between copper slabs for a good heat conduction to avoid the accumulation of the heat in the samples. The power of the LASER is continuously decreased by 1000W to determine the suitable LASER power. The melting of the surface is observed by naked eye. Where the effect of the melting was not visible, that power lever was used. The prepared samples treated with the same way.
The microstructures of the samples are studied after metallographic preparation. Samples cut perpendicular to the direction of the LASER treatment. The samples prepared mechanically (grinding and polishing) then etched by Barker's reagent electrochemically. Mosaic images were taken from the microstructure where the effect of the treatment could be studied.

A remelted zone was observed in all case. But the dimensions of this zones are small. Under the remelted zones a recrystallized and then partially recrystallized zones were observed. The dimension of this zones, and the typical grain size were measured and compared between the different samples. The presentation shows the detailed results and the comparison by the different alloys and different extent of deformation.

ACKNOWLEDGMENTS


„ Supported BY the ÚNKP-18-2 New National Excellence Program of the Ministry of Human Capacities”

The described work was carried out as part of a project supported by the National Research, Development and Innovation Office – NKFIH, K119566.

DATA HOUSE OF POLYURETHANE A COMBINED THEORETICAL AND EXPERIMENTAL METHODS

CHEIKH Wafaa, FEJES Zsolt PhD, VISKOLCZ Béla PhD
Institute of Chemistry, University of Miskolc
E-mail: cheikhwafaa.92@gmail.com, zsolt.fejes@gmail.com, bela.viskolcz@uni-miskolc.hu

Keywords: Polymers; Polyurethanes; Foams; Isocyanates; Polyols.

Polymers, commonly called plastics, are among the chemicals with the most industrial applications. These macromolecules are long-chain molecules with a very high molecular weight, which are obtained by the combination of a large number of functional groups and linked together by covalent bonds. Polyurethane foams are among the most important class of polymers (*Figure 1*) produced by reacting a diisocyanate with a polyol in the presence of water, the latter serving as the blowing agent generating carbon dioxide for the foam formation. Besides altering the two main components (diisocyanate and polyol) of the foam, with the addition of different modification agents, there are many possibilities to tune the final physical properties of the polymer.

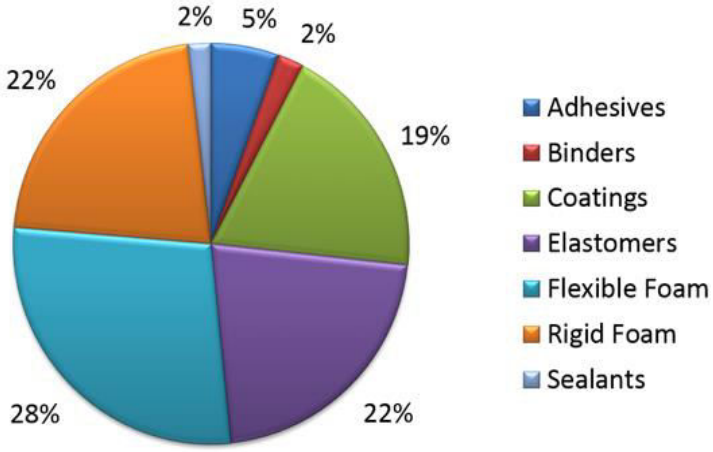

Figure 1 Global production of polyurethane in 2012, source: IAL Consultants

Several studies have been carried out and research continue to date in order to better understand the diversity of the chemical structures and physical forms of polyurethanes that depend on the specific constitution of polyols and isocyanates, therefore in our study, the effect of each basic components used and/or added on the foam properties have been examined.

Figure 2 Basic experiments of polyurethane foam

In order to improve our understanding of modern polyurethane, we would like to perform a computation investigation of one of the basic components which is the isocyanate. The polyurethane industry is mainly based on the reactions of isocyanates with different type of polyols. Besides toluene diisocyanate, methylene diphenyl diisocyanate (MDI) is the major isocyanate used to make polyurethanes Since MDI is mainly produced from methylene dianiline (MDA) by

phosgenation, the side products of the phosgenation reaction can debase the MDI as well as the quality of the polyurethane produced. However, although the reaction mechanism for the phosgenation of MDA is relatively well-established, possible competing reaction channels have never been discussed in the literature.
The aim of the current work is to explore the energetics of these competing phosgenation reactions using computational chemical approaches. These reaction mechanisms were computed using the B3LPY/6-31G(d) level of theory as well as the more accurate and robust G3MP2B3 chemistry model. The obtained energy profile was compared with that of MDI production from MDA. All calculations were carried out using the Gaussian09 program package.

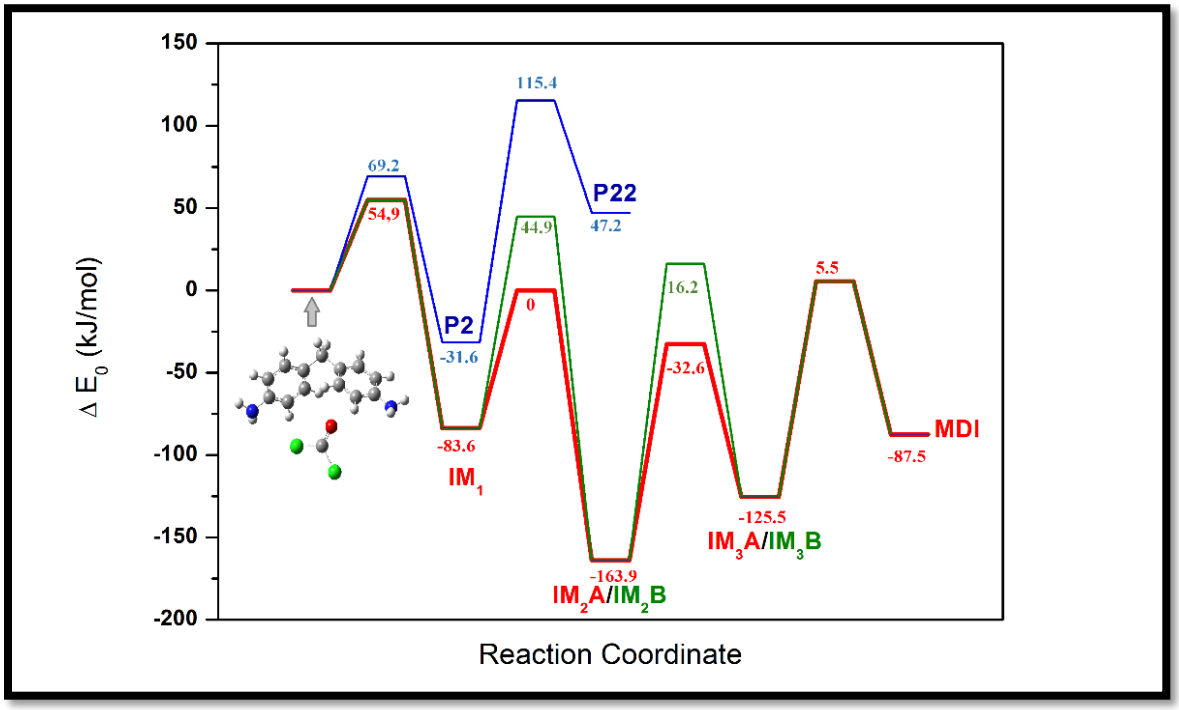

Figure 3 Potential energy surface of the low-lying reaction channels

ACKNOWLEDGMENTS
The research was supported by the European Union and the Hungarian State, co-financed by the European Regional Development Fund in the framework of the GINOP-2.3.4-15-2016-00004 project, aimed to promote the cooperation between the higher education and the industry.

DESIGN ISSUES OF STEAM TURBINES

CZÉGÉ Levente PhD, MENYHÁRT József PhD, DEÁK Krisztián
Department of Mechanical Engineering, University of Debrecen
E-mail: czege.levente@eng.unideb.hu, menyhart.jozsef@eng.unideb.hu, deak.krisztian@eng.unideb.hu

Keywords: steam turbine, systematic design process, design principles of division of task, principle of balanced forces

The development of steam turbines dates back far in history. It was a long journey from Heron's aeolipile through Parson's turbines, through the developments of Laval and other engineers to the high-performance modern power plant turbines operating with ultra-supercritical steam. The development of steam turbines was influenced by the new results of material science, aerodynamics, production technology and the introduction of computer-assisted engineering applications, as well as the spread of mechanical and aerodynamical analyzes and simulations. One might think that today steam turbine technology is a highly sophisticated, "improved to the extreme" technology that does not have much development opportunities. The fact is, however, that due to the increasing user requirements, and the changing market environment the development did not stop. The latest developments include optimization of blade profile, modular system design, development of labyrinth seals, reduction of flow and gap losses, etc. The most important requirements for today's modern turbines are efficiency, low operational costs through the lifecycle, high reliability, availability and operational flexibility. It is a general trend that, as with other products, engineers in this area also face the reduced available development time. As a result, some of the developments focus on the design process to be able to fulfil the changing customer requirements as quickly and efficiently as possible: modular elements, modular design of components, standardized elements, efficient computer aided design, etc.

The mentioned requirements pose new challenges to the development and design process: it must be plannable, not relying on finding solutions by chance, must support the management of teamwork in an integrated process, foster inventiveness, etc. There have been systematic design processes worked out, which offer a strategy for the designer to meet the goals. They usually divide the process into phases such as Planning and Task Clarification, Conceptual Design, Embodiment Design, and Detail Design. In the design and development of the turbines, the embodiment design phase is emphasized, since the basic concept is typically not modified, the physical principle, the geometric and material characteristics rarely change. In the embodiment phase the form, shape and size, materials, manufacturing concepts and the auxiliary functions are determined on the basis of the technical-economic aspects. For this phase a strictly determined sequence of steps can be hardly prescribed, the methodology offers only theoretical sequence of principle activities, emphasising the iterative feature of the process. In addition to the description of the process, the methodology sets out basic rules, principles, and guidelines that provide basic and essential guidance for design. The basic rules are clarity, simplicity, and safety. The principles defined to help to find the best solution include: Principles of Force Transmission, Principle of the Division of Tasks, Principle of Self-Help, Principles of Stability and Bi-Stability, Principles for Fault-Free Design.

In this paper we present some examples of how these fundamentals, design principles and guidelines apply to the design of steam turbines.

For steam turbines, one of the main source of design problems is related to the high operating temperature and the significant variation in temperature during the start and stop process. Such problems include expansion due to the temperature changes, relative expansion of component, internal stresses due to expansion, maintaining constant clearances, etc.

The casing of a turbine has two fundamental roles: to ensure sealing in all operating conditions and pressures, and to ensure secure anchorage for the fixed blades of the stages. The position of the blades is of significant importance, because the clearance between the blade tips and the rotor must be maintained during operation to keep the leakage loss on the minimum. It is easy to recognize, how the principle of division of task was applied to solve this complex task: the high- and medium-pressure turbine cylinders are typically made with double casing (*Figure 1*), that is the blades are fastened in the inner casing, which is supported in the outer casing in such a way that the difference in thermal expansion does not cause extra stress in the structure (*Figure 2*). The design of the inner case can also be based on the principle of division of task: in certain turbine designs, the two halves of the inner case are joined together by shrink rings. Due to this solution the task of joining is separated from that of the sealing and holding the blades. Shrink rings are a good example of principle of self-help as well. The shrink rings are cooled by the relatively cold exhaust steam, so by increasing steam flow, the increased temperature of the inner case causes its higher relative expansion, which results in an increased joining force.

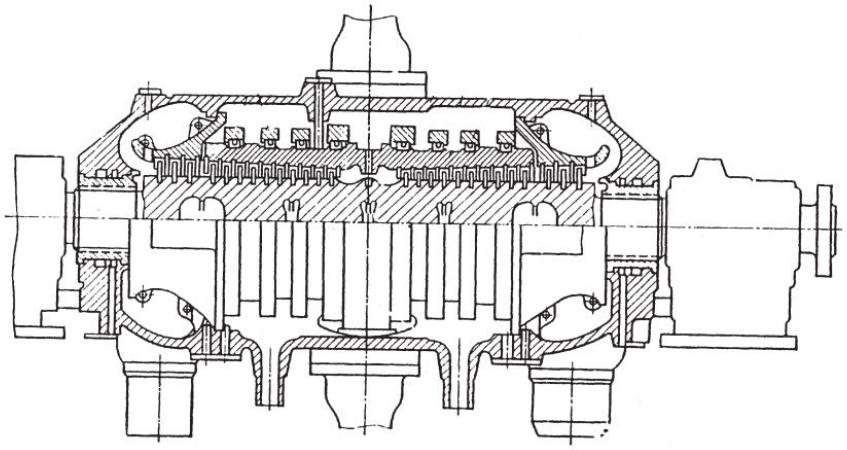

Figure 1 Longitudinal section of a high-pressure cylinder with double casing and shrink rings for the inner case

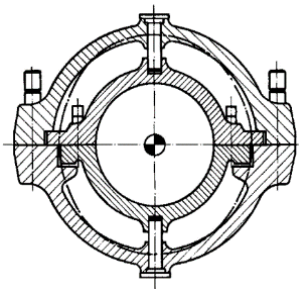

Figure 2 The connection between casings allows different thermal expansions for the outer and inner casing

The Principles of Force Transmission includes the Principle of Balanced Forces, which means the balancing of the associated forces acting in addition to the functionally determined main forces. In order to reduce the negative effects of the associated forces (e.g.: extra load for bearing, heavier construction) these should be balanced at their place of origin. In axial-flow turbines the functionally determined main force is the tangential force caused by the steam on the blades. The axial component of the force acting on the blade can be regarded as the associated force. To balance this force there are various solutions existing depending on the turbine type. In case of high-pressure steam turbines this force is balanced with a balancing element. The steam exhaust chamber of the turbine is connected to the inlet end of the rotor through a balancing pipe, where the pressure acts on a balancing drum, thus resulting in a counter-directional axial force on the rotor to balance the associated force. For low-pressure turbines the force is balanced due the symmetrical design of the rotor. Low-pressure turbines in general have a double-flow structure, that is, the incoming steam is divided into two paths, in which the flows have an opposite direction. In this design the associated axial forces generated on the blades are of equal magnitude and opposite direction, thus balancing each other.

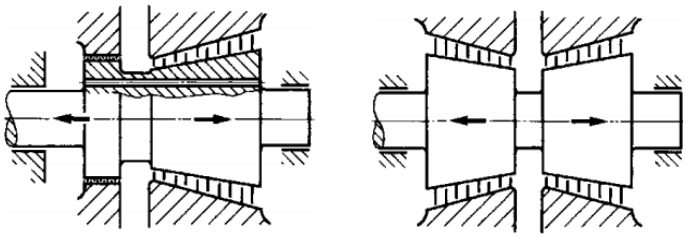

a.) *b.)*

Figure 3 Balancing of the axial forces with *a.)* dummy-disc and with *b.)* double-flow structure

DESIGN OR TECHNOLOGY: THE ANTIQUE RÖMER GLASS

DARABOS Anita DLA, SZALAI Judit
Budapest University of Technology and Economics
E-mail:darabos.anita@gt3.bme.hu, szalai.judit@gt3.bme.hu

Keywords: glass technology, römer-glass, green forest glass, design, human body

Abstract. *In this paper, the Römer-glass are assessed as indicator of the technology and design by using a comparative method. We divide the glass into different groups: Prunted beakers (Waldglas, forest glass), beakers and cups. Very common vessels are prunted Roemer beakers. They come in different sizes, with two, three and even four rows of prunted knobs. [1]*

Figure 1 Representation of a Medieval Forest Glass hut.

We identifed their designing technology methods and associated them with manufacturing centres. All of them made from green forest glass and produced in northwestern and central Europe from around 1000-1700 AD. The Römer glass present dining traditions and habits in the middle ages, furthermore like a personal belongings can be associated with the presentation of social status or individual expression.

Figure 2 A selection of prunted beakers Roemer, Germany [2]

The examination of the surface tactile sensation of glass cups, cups and cups points out that during the marking loading of the fingerprints, partial overlaps on the glass surface without the use of partial surface grooves occur at the periphery of the finger-to-eye contact before the hand is completely sliced out. [3-10]

Assumed, these results show that full and partial surface texture patterns of the exposed period are important to the slip recognition of the hand and support the assumption that the central nervous system is relied upon when it is used to attach the force of the subject when using the object.

ACKNOWLEDGMENTS

The research reported in this paper was supported by the Higher Education Excellence Program of the Ministry of Human Capacities in the frame of Artificial intelligence research area of Budapest University of Technology and Economics (BME FIKP-MI).

REFERENCES

[1] Catherine Hess, Timothy Husband: *European Glass in the J. Paul Getty Museum*: Catalogue of the Collections.
[2] Michel Hulst, J. Jerzy, Kunicki-Goldfinger*: The golden age of Amsterdam glass. A chemical and typological approach to recognize Amsterdam 17th century glass production,* p. 550., AIHV Annales du 20e Congrès 2015.
[3] The Corning Museum of Glass, https://www.cmog.org/glass-dictionary/maigelein
[4] Rijkmuseum, Amsterdam, Netherlands www.rijkmuseum.nl
[5] Catherine Hess, Timothy Husband: *European Glass in the J. Paul Getty Museum*: Catalogue of the Collections, p. 33-35.
[6] http://www.britishmuseum.org
[7] Historisches Museum Basel, http://www.hmb.ch
[8] Museum Boijmans Van Beuningen, Rotterdam, https://www.boijmans.nl
[9] The Museum of Fine Arts, Houston https://www.mfah.org
[10] Museum für Kunst und Gewerbe, Hamburg
[11] https://www.mkg-hamburg.de

THE OBSERVATION OF NATURAL ANALOGIES AND THEIR USE IN DESIGN

DARABOS Anita DLA
Budapest University of Technology and Economics
E-mail: darabos.anita@gt3.bme.hu

Keywords: Natural analogy, design

Abstract. *In an age of mass production when everything must be planned and designed, design has become the most powerful tool with which man shapes his tools and environments (and, by extension, society and himself). This demands high social and moral responsibility from the designer. It also demands greater understanding of the people by those who practise design and more insight into the design process by the public. [1,2]*

Humans have always looked to nature for inspiration to solve problems. Nature success is achieved by the patient and long term process of evolution. [3,4] Sometimes we are inspired by nature and sometimes that inspiration can come from the most unexpected places. [5] According to, Thomas Heatherwick, who was an English architecture, 'The biggest object is a building'.[6] Nature has phenomenal problem solving skills – 'nature knows it better'.

Figure 1 Steps of mud dauper's nest construction

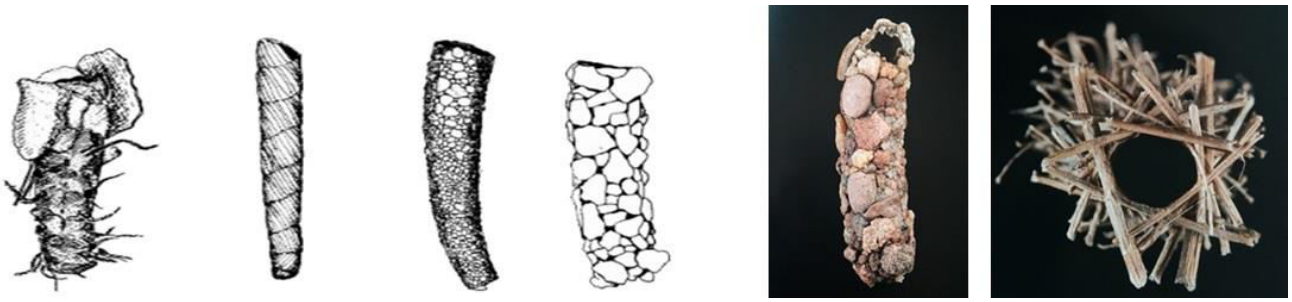

Figure 1 Caddish-fly use the original materials in construction

Construction behaviour occurs across the entire spectrum of the animal kingdom and affects the survival of both builders. This research provides an overview of the analogies of animal and human building. It represents broad categories of built structure: nests, huts, tombs. Even though some of these structures are complex and very large the materials of buildings helps to building, and self-organizing effects help create complexity.[7] (*Figure 1,2)*
The complexity of the shape and colours are inevitable in the case of the product. The design determines marketability. But this depends on harmony. Our opinions depend on strong, subjective elements and the decision making will happen in our unconscious. We were born with the harmony of nature and we still live in harmony with nature against our social environment. We can see the beauty of something when it suggests the phenomenon of nature. Designers should pay attention to the phenomenon of nature and we should also look for the colours, forms and combinations to create a new style. (*Figure 3)*

Our understanding of the modern world is largely based on an ever increasing volume of scientific knowledge. Engineering designers have at their disposal a vast array of relationships for materials, mechanisms and control, and these laws have been painstakingly assembled by observation of nature.[8]

Figure 3 Franz Josef glaciers and the design of Zaha Hadid's super yacht.

The main goal of this study is to understand and use the knowledge and the information that naturally aggregated over millions of years.

ACKNOWLEDGMENTS

The described work was carried out as part of a project supported by the National Research, Development and Innovation Office – NKFIH, K123456.

REFERENCES

[1] Benjamin De Brie Taylor: *Design Lessons from Nature,* Watson-Guptill Publications, 1974.
[2] *Design for the Real World, Human Ecology and Social Change by Victor Papanek* . 1984
[3] David Wan: Biologic: *Environmental protection by design,* Johnson Books, 1990.
[4] David Wann: *Deep Design: Pathways To A Livable Future*, Island Press, 1996.
[5] Nick Baker:*What part of nature is our inspiration for the built environment*, University of Cambridge, https://www.researchgate.net/ What part of natureis our inspiration for the built environment 2015.
[6] Thomas Heatherwick, Maisie Rowe: *Making, Thames & Hudson*, 328.
[7] Mike Hansell: *Animal Architecture,* Oxford Scholarship, 2007
[8] Ed M. W. Collins: *Nature and Design*, WIT Press, 2004.

WAVELET DESIGN FOR DIAGNOSIS OF TAPERED ROLLER BEARING MANUFACTURING DEFECTS

DEÁK Krisztián, KOCSIS Imre PhD
Department of Mechanical Engineering, University of Debrecen
E-mail:deak.krisztian@eng.unideb.hu, kocsisi@eng.unideb.hu

Keywords: wavelet, diagnosis, bearing, fault, manufacturing

The research focus on revealing manufacturing defects that occur in production of tapered roller bearings. For effective fault detection it is critical to find a proper wavelet that matches well with the shape of the signal at a specific scale and location. Low transform value is obtained if the signal and the wavelet do not correlate well. Visual observation of contour plots is not appropriate for adequate wavelet selection. Thus, a more sophisticated method for wavelet selection is used in this experiment. Real valued wavelet is compared to complex Morlet wavelet according to the Energy-to-Shannon-Entropy ratio criteria to determine which is the most efficient for detecting the manufacturing fault. Complex Morlet wavelet is a kind of band-pass filter which has a good capacity for noise reduction and bearing fault frequency detection. The center frequency and bandwidth of complex Morlet wavelet is adjustable, thus, it has more flexibility for feature extraction. To determine the efficiency of the designed wavelet and compare to the other wavelets, a test-rig was constructed equipped with high-precision sensors and devices. The designed wavelet is found to be the most effective to detect the manufacturing fault that can be expressed in this form:

$$DWT_s(j,k) = \frac{1}{\sqrt{2^j}} \int_{-\infty}^{\infty} s(t) \cdot \psi^* \left(\frac{t - 2^j k}{2^j} \right) dt$$

For the experiment, a bearing test-rig was planned and constructed equipped with high-precision measurement devices and sensors The shaft is driven by an alternating current motor, the power of 0.75 kW, frequency of 50 Hz and nominal speed of 2770 rpm which is reduced to 1800 rpm with variable speed drive device. By Schneider ATV32HU22M2 variable speed drive device the rpm can be adjusted.

Figure 1 Outer ring (OR2) of the tapered roller bearing with grinding defect of 1.2492 mm (left) and its 50x enlarged image by Garant MM1-200 video microscope

Constant spanning force during the measurements is measured by strain gauges in Wheatstone-bride mode on the basis of difference in voltage measurement. NI 9234 DAQ is used in the experiment that delivers 102 dB of dynamic range with sampling rates up to 51.2 kHz per channel with built-in anti-aliasing filters. 32 bit AMD Athlon II X2 M300 2.0 GHz processor is used for data processing. PCB IMI 603C01 vibration transducer is applied with low noise level, high sensitivity of 100 mV/g, frequency range up to 10 kHz with top exit 2-pin connector. The accelerometer is placed on the ground smooth surface (Ra=1.6 µm) of the top of the bearing house with screw that perpendicular to the axis of the rotation of the shaft. Thin layer couple fluid is applied between the bearing house and the transducer. Garant MM1-200 video microscope is used to produce magnified image about the fault and to measure its geometrical width parameter.

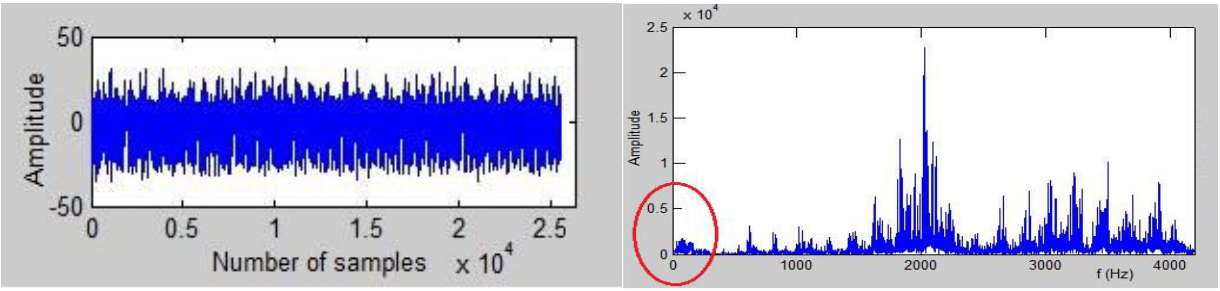

Figure 2 Outer ring (OR2) of the tapered roller bearing with grinding defect of 1.2492 mm (left) and its 50x enlarged image by Garant MM1-200 video microscope

The shaft in the test rig is supported by two tapered roller bearings. One of the bearing is a "Type 30205" tapered roller bearing which is examined in the experiments. Four tapered roller bearings with different manufacturing defect width on the outer race were measured.

Table 1 Geometrical parameters of grinding defects of outer rings

Type	Width (mm)	Depth (μm)
OR1 defect	0.6311	6.5
OR2 defect	1.2492	33.6
OR3 defect	1.4751	42.3
OR4 defect	1.6236	51.4

The fault width measurement procedure was executed with the other nine wavelets for the purpose to compare them to the optimized wavelet. By analyzing the spectrogram with Sobel edge detection and local maxima peak detection of the wavelet coefficients, the entry point and the exit points were exactly determined where the roller entered into and exited from the defect. Results were verified by optical measurement with high resolution Garant MM1-200 video microscope.

Table 2 Geometrical parameters of grinding defects of outer rings

Wavelet	Calculated width	Width deviation
Sym2	1.277	2.24
Sym5	1.269	1.56
Sym8	1.2713	1.77
Cmor	1.2640	1.19

The deviation from the optically measured width was only 1.19 % in case of the optimized complex Morlet wavelet. The measurements proved its capability for industrial bearing fault diagnosis in manufacturing.

NUMERICAL INVESTIGATIONS OF FLOW AROUND A FREELY VIBRATING CYLINDER: NATURAL FREQUENCY RATIO EFFECTS

DOROGI Dániel, BARANYI László PhD
Department of Fluid and Heat Engineering, University of Miskolc
E-mail: aramdd@uni-miskolc.hu, arambl@uni-miskolc.hu

Keywords: distorted figure-eight motion, natural frequency ratio, vortex-induced vibration

INTRODUCTION

Flow around a freely vibrating circular cylinder has been thoroughly investigated in the past few decades. In reality the body is allowed to move in two-degree-of-freedom (both streamwise and transverse directions). In this case the natural frequencies fNx and fNy can be different in the two directions. Sarpkaya [1] investigated experimentally the range of fNx/fNy = 1–2 and showed that the oscillation amplitude for fNx/fNy = 1 is increased by 19% compared with that obtained from transverse-only vibrations. Dahl et al. [2] found that the maximum vibration amplitude shifts to higher reduced velocity $U^* = U\infty/(fNyD)$ values with increasing fNx/fNy, where $U\infty$ is the free stream velocity and D is the cylinder diameter. Due to the high computational cost numerical studies are mostly carried out at low Reynolds numbers $Re = U\infty D/\nu$, where ν is the kinematic viscosity of the fluid. Bao et al. [3] and Han et al. [4] investigated numerically the effects of natural frequency ratio at Re= 150 and 200, respectively. Their results showed that the cylinder follows a distorted figure-eight path in all investigated cases. Prasanth and Mittal [5] carried out computations for fNx/fNy=1, finding that in the lock-in domain (where the cylinder motion synchronizes with the vortex shedding) the oscillation amplitudes in both streamwise and transverse directions slightly decrease.

COMPUTATIONAL METHOD, RESULTS AND DISCUSSION

In this study two-dimensional, incompressible, Newtonian, constant property fluid flow around an elastically supported cylinder is investigated numerically. The governing equations for the fluid flow are the two components of the Navier-Stokes equations, continuity and pressure Poisson equations. The instantaneous cylinder displacements and components of velocity and of acceleration are obtained from two structural equations. Dirichlet and Neumann-types of boundary conditions (BCs) are applied for velocity and pressure both on the cylinder surface and in the far field. In order to impose these BCs accurately, boundary-fitted coordinates are used. The transformed equations with the transformed BCs are solved using finite difference method [6].

In this paper two-degree-of-freedom free vibration of a circular cylinder is investigated at constant Reynolds number (Re=150) and mass ratio ($m^*=8/\pi$) (the same values used in [3]). The structural damping coefficient is set to zero in order to obtain large amplitude vibrations. The aim of this study is to investigate the effect of natural frequency ratio FR = fNx/fNy at U^*St = 0.9, 1 and 1.1, where St is the dimensionless vortex shedding frequency for a stationary cylinder.

Figures 1a and b show the root-mean-square (rms) values of streamwise and transverse vibration components $x0_{rms}$ and $y0_{rms}$ against FR for the investigated U^*St values. At around FR = 2 the cylinder motion and the flow show chaotic behavior and in these cases $x0_{rms}$ and $y0_{rms}$ cannot be computed. This is the reason why some of the computational points are missing from the curves. It can be seen in Figs. 1a and b that the cylinder response completely changes at FR = 2. For FR < 2 $x0_{rms}$ and $y0_{rms}$ increase steeply with FR and the data sets belonging to different U^*St values shift upwards with increasing U^*St. Prasanth and Mittal [5] carried out numerical simulations for FR = 1. They found that in the lock-in domain $x0_{rms}$ and $y0_{rms}$ slightly decrease with U^*St. The current results (Figs. 1a and b) are in agreement with their findings. However, for FR > 2 there are no data in the literature for comparison. In this range the oscillation amplitudes in the two directions decrease and the curves shift downward with U^*St.

In Fig. 2 the paths of the cylinder are shown at FR = 1, 1.5, 2 and 2.5 for U^*St=0.9. It can be seen that the cylinder follows a distorted figure-eight path in the entire FR domain. This finding agrees well with data in [3] and [4]. It can be seen that the shape of the path changes significantly with FR.

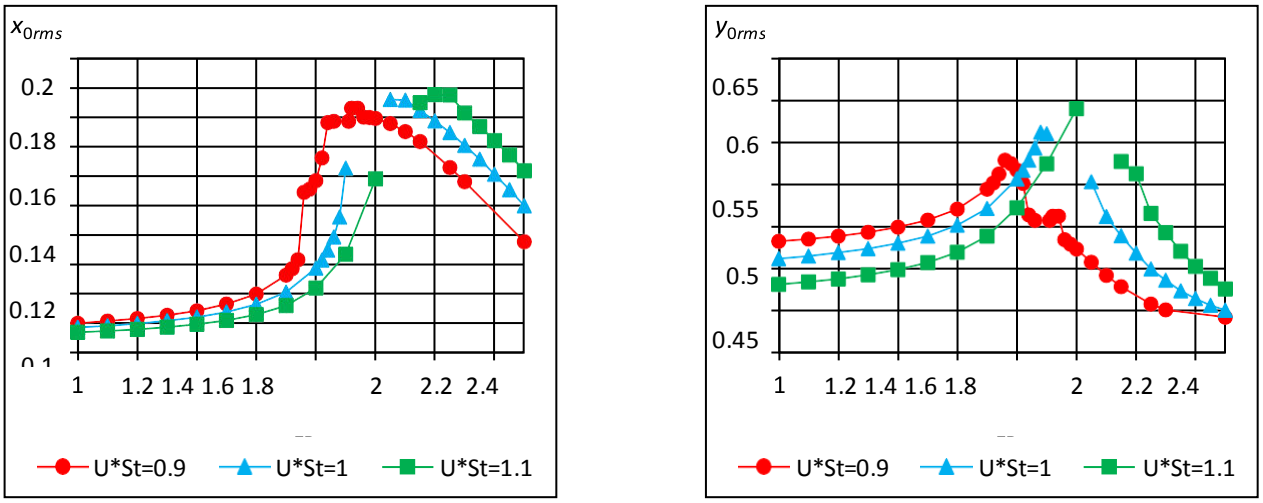

(a) (b)

Figure 1 Root-mean-square values of streamwise (a) and transverse (b) vibration components against FR for different

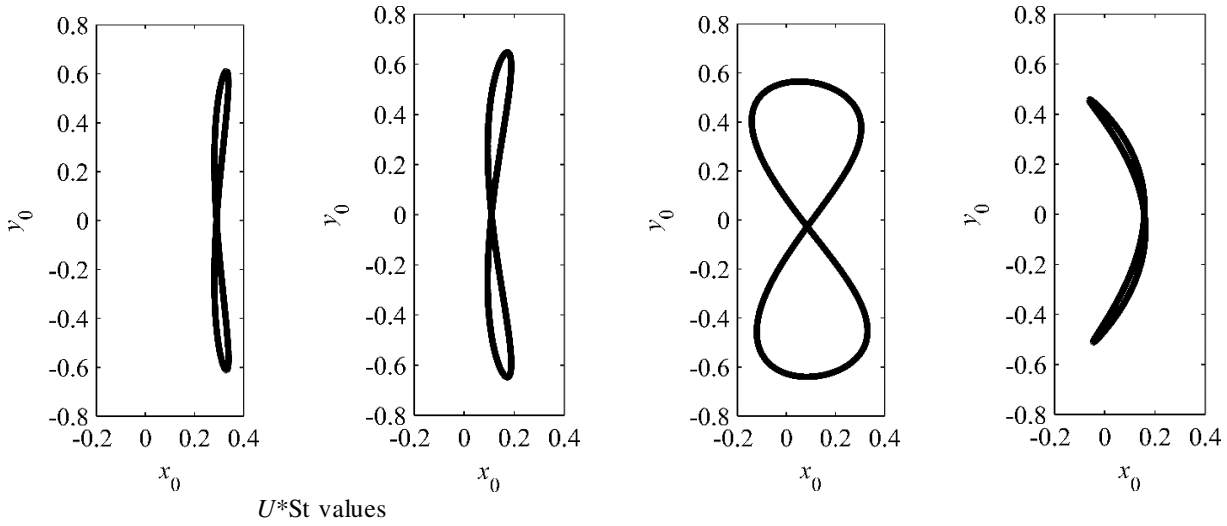

(a) (b) (c) (d)

Figure 2 Cylinder path at FR=1 (a), 1.5 (b), 2.0 (c) and 2.5 (d) for *U*St = 0.9

CONCLUSIONS

In this numerical study flow around a circular cylinder elastically supported in two-degree-of-freedom is investigated. The Reynolds number and the mass ratio are kept at Re=150 and $m^*=8/\pi$, respectively, and the structural damping coefficient is set to zero. The effect of natural frequency ratio FR = f_{Nx}/f_{Ny} ranging from FR=1 to 2.5 is analyzed at *U*St=0.9, 1.0 and 1.1. For FR < 2.0 the oscillation amplitudes in the two directions increase and the data sets belonging to different *U*St shift upwards. Above FR ≅ 2 the oscillation amplitude decreases with FR and the curves shift downwards for increasing *U*St values. Distorted figure-eight paths are identified in all cases investigated.

REFERENCES

[1] T. Sarpkaya: *J Offshore Mech Arct* 117, 232–238. 1995.
[2] J. M. Dahl, F. S. Hover, M. S. Triantafyllou: *J Fluid Struct* 22, 807–818. 2006.
[3] Y. Bao, C. Huang, D. Zhou, J. Tu, Z. Han: *J Fluid Struct* 35, 50–75. 2012.
[4] X. Han, W. Lin, Y. Tang, C. Zhao, K. Sammut: *Comput Fluids* 110, 62–76. 2015.
[5] T. K. Prasanth, S. Mittal: *J Fluid Mech* 594, 463–491. 2008.
[6] L. Baranyi: *J Fluid Struct* 24, 883–906. 2008.

MASS RATIO EFFECT ON FLOW AROUND A TRANSVERSELY OSCILLATING CIRCULAR CYLINDER

DOROGI Dániel, BARANYI László PhD
Department of Fluid and Heat Engineering, University of Miskolc
E-mail: aramdd@uni-miskolc.hu, arambl@uni-miskolc.hu

Keywords: circular cylinder, mass ratio, vortex structure, wake mode map

INTRODUCTION

Vortex-induced vibration (VIV) of a circular cylinder has been thoroughly investigated due to its practical importance. The most important parameters characterizing the problem are the cylinder diameter D, mass m, natural frequency of the cylinder f_N, freestream velocity U_∞ and kinematic viscosity ν. Although in reality the cylinder moves in both streamwise and transverse directions, the motion of the body is often modeled with transverse-only vibration. Khalak and Williamson
[1] identified initial, upper and lower branches using experimental approach, where the maximum oscillation amplitude was observed at the upper branch. Govardhan and Williamson [2] showed that the vortex structure changes between 2S (two single vortices are shed from the body in a period) and 2P modes (two vortex pairs are shed) at the range of transition between initial and upper branches. Due to the high computational cost, most numerical simulations are carried out for low Reynolds numbers $\mathrm{Re} = U_\infty D/\nu$. Singh and Mittal [3] investigated two-degrees-of-freedom VIV numerically. They found 2S and C(2S) vortex structures for low and fairly high oscillation amplitudes, respectively. Here C refers to positive and negative vortices coalescing in the cylinder wake. In addition, [3] also found P+S vortex structure for $\mathrm{Re} \geq 300$, which is a very rare wake mode in vortex-induced vibrations.

VIV is often modeled with forced cylinder vibrations where the body oscillates with a given amplitude and frequency. In the wake mode map created by Williamson and Roshko [4] 2P vortex structure can be seen at the fundamental lock-in domain (where the vibration frequency coincides with the natural frequency of the cylinder). This observation is in agreement with the results of [2]. Leontini et al. [5], using a numerical approach, created wake mode maps for Re=100 and 300. In both cases they found only 2S and P+S modes (and no 2P mode) which is in agreement with results of [3].

COMPUTATIONAL METHOD, RESULTS AND DISCUSSION

The governing equations for the two-dimensional, incompressible, Newtonian, constant property fluid flow around a freely vibrating circular cylinder are the two components of the Navier-Stokes equations, the continuity and pressure Poisson equations. Two structural equations are used to compute the temporal cylinder displacements, the velocity and acceleration components. In order to satisfy the boundary conditions (BCs) accurately, boundary-fitted coordinates are used. The transformed equations with the transformed BCs are solved using finite difference method [6]. Potential flow is used as the initial condition of the computations.

In this study undamped, transverse-only vortex-induced vibration of a circular cylinder is investigated at Re=300 (the same value used by [5]). The effects of reduced velocity $U^* = U_\infty/(f_N D)$ is investigated at the mass ratios (ratio of mass of the cylinder and that of the displaced fluid) of m^*=5, 10, 50 and 100. The obtained free vibration data is compared with the forced vibration results of Leontini et al. [5].

Figure 1a shows the dimensionless oscillation amplitude A^* against reduced velocity for different mass ratio values. As expected, an initial branch with small oscillation amplitudes and a lower branch with relatively high cylinder displacements are observed. In the transition range between these two branches (at around $U^* \cong 3.5$–4.5) the oscillation amplitude cannot be computed due to the cylinder motion and because the flow is chaotic. This is the reason that some computations points are missing in this range. It can also be seen that the width of the lower branch depends highly on the mass ratio; increasing m^* the width of the high-amplitude domain diminishes. A small jump can be observed in the oscillation amplitude at around U^*=4.8. In Figs. 1b and c vorticity contours are shown at time t=800 before and after the jump in A^* (see Fig. 1a). As can be seen in Figs. 1b and c, P+S and C(2S) modes are found in the pre- and post-jump cases, respectively. Leontini et al. [5], using a forced vibration model, also found these two types of vortex structures, which provides a good opportunity for the comparison. Figure 2 shows the comparison between the currently applied free vibration data with the forced vibration results of [5]. Here f is the vibration frequency and f_{St} is the vortex shedding frequency for a stationary cylinder. The filled markers represent P+S mode and the empty markers refer to 2S or C(2S) vortex structures. Good agreement can be seen; these two types of vortex structures occurs in the same location for free and forced vibration models. These findings are practically independent of the mass ratio values.

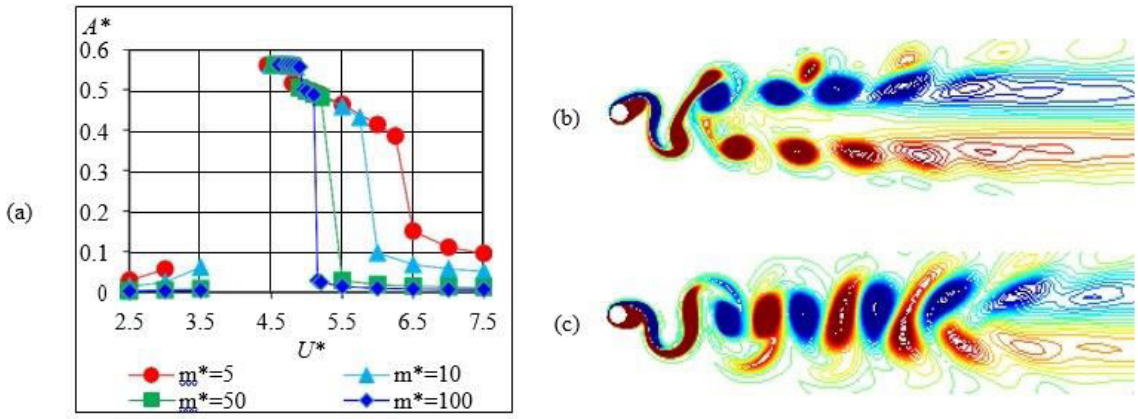

Figure 1 Dimensionless oscillation amplitude vs. reduced velocity (a) and vortex structures at U*=4.79 (b) and U*=4.80 (c) at t=800 for m*=5

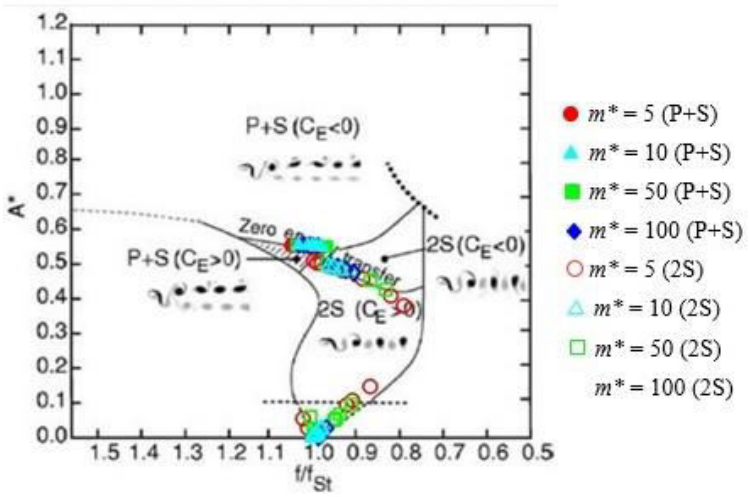

Figure 2 Free vibration points imposed on wake mode map for forced vibration data of Leontini et al [5]

CONCLUSIONS

In this study transverse-only vortex-induced vibration of a circular cylinder is investigated at the Reynolds number of Re=300 and varying reduced velocity U^*. Mass ratio values of $m^* = 5$, 10, 50 and 100 are considered. Initial and lower branches with low and relatively high vibration amplitudes are found. It is shown that the width of the lower branch diminishes as mass ratio is increased. A small jump is identified in the oscillation amplitude at $U^* \cong 4.8$ which is explained by the sudden change in the vortex structure between P+S and 2S modes. The comparison between the currently obtained free vibration data and the forced vibration results of Leontini et al. [5] shows good agreement. This provides further evidence that the forced vibration model can be used to predict VIV.

REFERENCES

[1] A. Khalak, C. H. K. Williamson: *J Fluid Struct* 13, 813–851. 1999.
[2] R. Govardhan, C. H. K. Williamson: *J Fluid Mech* 420, 85–130. 2000.
[3] S. P. Singh, S. Mittal: *J Fluid Struct* 20, 1085–1104. 2005.
[4] C. H. K. Williamson, A. Roshko: *J Fluid Struct* 2, 355–381. 1988.
[5] J. S. Leontini, B. E. Stewart, M. C. Thompson, K. Hourigan: *Phys Fluids* 18, Paper No. 067101, 9 pages, 2006.
[6] L. Baranyi: *J Fluid Struct* 24, 883–906. 2008.

DIGITALIZATION OF ANCIENT SCULPTING MODELS AND 3D DESIGN USING PHOTOGRAMMETRY METHODOLOGY

DOVRAMADJIEV Tihomir PhD
Dept. Industrial Design, Technical University of Varna
E-mail: dr.tihomir.dovramadjiev@gmail.com

Keywords: photogrammetry, 3D, re-design, reconstruction, sculpting

The digitization of ancient sculptures is particularly relevant and necessary in relation to the preservation of the cultural heritage. And the studied ancient models have their unique identity in terms of their visual and functional qualities. In parallel, the study aims to optimize the technological process related to photogrammetric measurements and calculations, technological tools and specialized software applications such as Autodesk ReCap, Blender and MeshMixer. The used models in the article are for re-presentation of popular ancient models & artifacts from city of Varna (by the ancient name Odessos). By using a 3D print device, one of the resulting digitized models of an ancient angel will materialize by applying specific techniques to redesign its geometry. The completed 3D printed item of re-designed model of ancient stone angel is only for personal and non-comercial use. One of the main point in the article is to show advanced computer techniques for teaching and studying. The information in this article has been built for helping other specialist working in digital field regarding photogrammetry. Also the material can be useful for designers, engineers, archaeologists and others in their work for the publicity of ancient treasures.

Figure 1 Photogrammetry final result: re-designed ancient angel with textures

Research purposes:
- Exploring and optimizing photogrammetric capabilities and calculations by modern technical means;
- Optimizing the interaction between different software systems and file formats;
- Creating a quality 3D geometry of the received computer models;
- Systematizing the methodology for the transfer of information data which is applicable to the three-dimensional printing;
- Developing a re-design of an exemplary artifact for educational and non-commercial purposes; - Digitalizing in 3D and preserving sample objects - artifacts with educational purpose.

Table 1 An useful, popular & effective software – Autodesk ReCAP, Blender & Autodesk MeshMixer

Software	License
Autodesk ReCAP	Trial /paid
Blender	Free
Autodesk MeshMixer	Free

ACKNOWLEDGMENTS
The described work was carried out as part of the research "Advanced technologies in design"

MODEL BASED OPTIMIZATION OF PORK FETTENERS

ERDÉLYI Viktor, JÁNOSI László PhD
Mechatronics Department, Szent István University
E-mail: erdely.viktor@gmail.com, janosi.laszlo@gek.szie.hu

Keywords: black-box, white-box, grey-box model, pig farm

INTRODUCTION

The relevance of this topic is the question of the sustainability of welfare society. In our current society it is usual, or even expected, to get cheap, high quality meat every day, so it is important to produce it quickly and at a low cost in large-scale farms. The biggest challenge is the growing demand for population growth (Boserup, 2005) and climate change (Zhang et al., 2017). To meet the growing food demand, automation plays an increasingly important role in animal husbandry. However, it is important to know whether a certain degree of automation is sustainable and, if so, how short is its payback time. To answer this question, I started to create a model describing pig fatteners, in this paper the current state of my work will be presented.

Pork is one of the most popular sources of protein in Europe. The swine is extremely sensitive to environmental parameters, such as air quality and most importantly, temperature (Cross et al., 2018), therefore, it's important to know what production parameters and what technologies we need to use for the most efficient production. Experimenting with real-world circumstances would be a lengthy and costly procedure, so it is worth to set up a digital copy of both the technology and the product, and then we can examine our experimental setups.

MATERIALS AND METHODS

With the help of our models, we can carry out our experiments using a fraction of the time and material requirements of real-life tests, which can be advantageous not just for creating new fatteners but also for setting up running ones. The model of the technological side of the production is based on well-known physical laws, so therefore, it uses a white-box model.

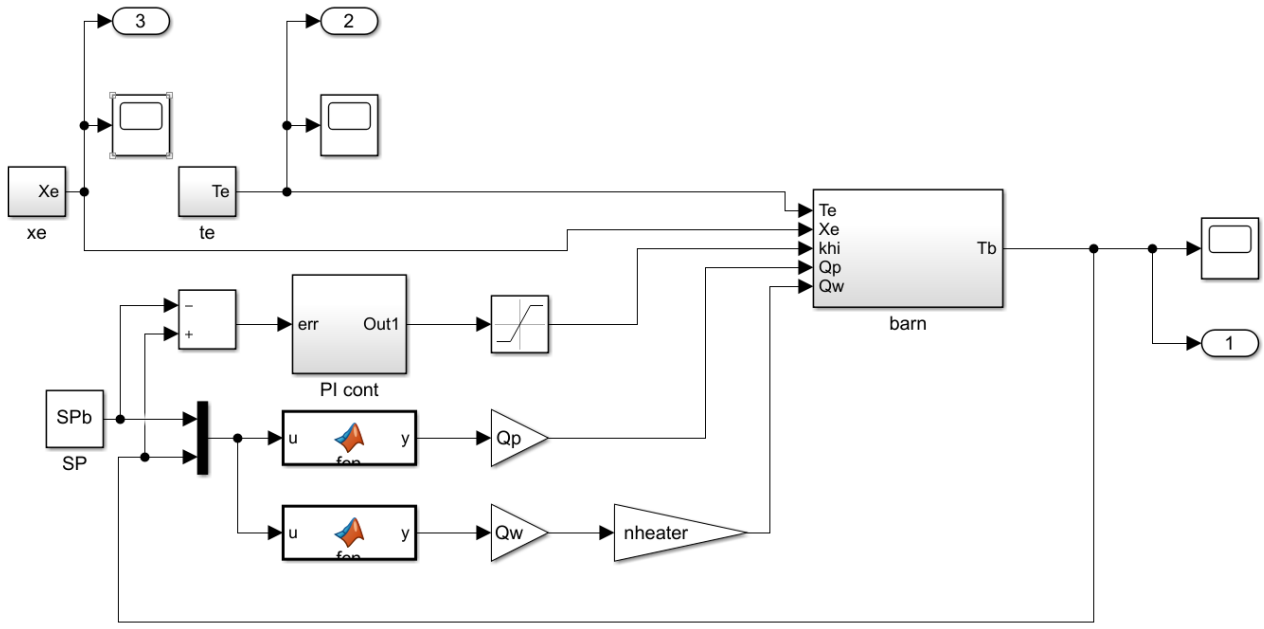

Figure 1 Main model

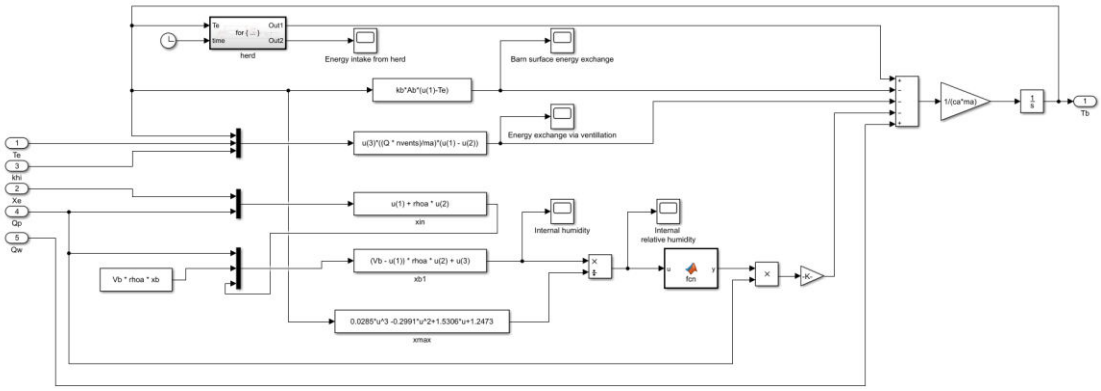

Figure 2 Barn model

Since I can rely on the statistical data available in the literature (Fenyvesi et al.,2004.) it is important that all of my models gives us average values. Since the production characteristics of each pig is different, therefore it is important to introduce the "uncertainty factor", which simulates virtually the deviations from the average, based on normal distribution. The models, which are describing the production parameters of the porks are too copmlicated, therefore, I built the models as black-box models based on the literature. In this case, the standard deviance is occuring as a multiplication factor of the production curves, therefore, I've used the normal distribution random generator in MATLAB-Simulink. The mean value of the distribution is 1 (which represents the statistical average value of the production), the standard deviation is 0.2.

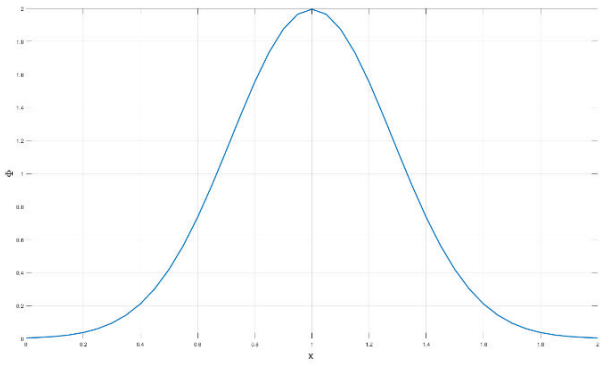

Figure 3 Normal distribution random

SUMMARY

The models presented in this article are based on data found in literature using white- or black-box models. This model is suitable for describing the operation of the stall, but it is not yet suitable to carry out experiments. The models are still in development, and all models need to be validated. In the future it is expected that this complex model will allow us to select the equipment that will help to achieve the best possible production parameters and, at the same time, result in an optimal return of investment.

REFERENCES

[1] E. Boserup: *The Conditions of Agricultural Growth.* New York: Routledge. 2005.

[2] P. Zhang, J. Zhang, M. Chen: *Economic impacts of climate change on agriculture: The importance of additional climatic variables other than temperature and precipitation.* Journal of Environmental Economics and Management, 83, pp. 8-31. 2017.

[3] Amanda J. Cross, Brittney N. Keel, Tami M. Brown-Brandl, Joseph P. Cassady, Gary A. Rohrer: *Genome-wide association of changes in swine feeding behaviour due to heat stress Genetics Selection Evolution*, Volume 50, Number 1, p. 1 2018.

[4] L. Fenyvesi, L. Mátyás, I. Pazsiczki: *Technologies of pig husbandry*, Hungarian Institute of Agricultural Engineering, Gödöllő, ISBN 963-611-426-9, pp. 10-11. 2004.

FACTORS AFFECTING THE DYNAMIC STABILTY OF CONIFERS AND BROAD-LEAVED IN DIFFERENT CONDITION

[1]FATHI Shadabeh, [1]BEJÓ László PhD, [2]DIVÓS Ferenc PhD
[1]Institute of Wood Based Products and Technologies, University of Sopron
E-mail: shadabe.fathi@gmail.com, laszlo.bejo@skk.nyme.hu
[2]Institute of Physics and Electronics, University of Sopron
E-mail: divos@fakopp.hu

Keywords: Inclinometer, Anemometer, Dynaroot system, Safety factor, Root system, Dynamic stability

Until recently, pulling tests have been used during research in tree stability as a means to determine the resistance of trees against rupture and uprooting. A simpler assessment method is required in order to identify hazard trees quickly and efficiently. Pulling test is the static method for measuring stability of tree roots. In this method, the main force is mechanical; it is slow and cumbersome, and may in some situations damage the tree. However, in this research the static loading is replaced by actual wind loads In this study, The DynaRoot system has made this possible. DynaRoot system is a dynamic method for measuring the stability of tree roots. It has three main parts: anemometer, inclinometer and evaluation software. The purpose of this study is to show differences in tree root behavior in different seasons. The An anemometer measured wind velocity at or near the tree to be evaluated and wind data was recorded in an SD card. An inclinometer was affixed to the root collar and measured the inclination of trunk in two different directions also recording the data in an SD card. Then both sets of data were imported into an evaluation software. Safety factor (SF) is calculated for a given wind velocity value of the area. In Hungary V_{Wind} = 33m/s and ρ_{air}=1.2kg/m3. (2)

$$P_{wind} = \frac{\rho_{air}}{2} V_{wind}^2$$

$$SF = \frac{P_{crit}}{P_{wind}}$$

The interpretation of the safety factor (SF) is straightforward. A SF below one means that a wind velocity corresponding to P_{Wind} is likely to uproot the tree. Trees with SF above 1.5 are considered safe, and in-between these two values there is a region of uncertainty. Also, the evaluation software calculates some more information about critical wind pressure, correlation coefficient, wind direction, tangential relationship between wind pressure and inclination of tree. In this study Spruce and Poplar (i.e. one conifer and one broad-leaved) were measured. Table 1 shows the results obtained from analysis data. In Poplar, the safety factor in spring is less than the safety factor in winter. This could be because, broad leaved trees lose their leaves in the winter, and the trunk and branches exerted lower pressure on the roots. In snowy weather, the safety factor was close to spring season, which means that the snow covering the branches imposes heavy load on the roots (figure 1). The wind direction in spring was SE, winter SW and in snowy condition NW direction. This means that

Table 1 The result obtained from valuation software

Species	***condition***	***SF***	***C.C %***	***CWP Pa***	***AVE-DIR Degree***
Poplar	*SPRING*	*4.62*	*77*	*3487*	*152*
	WINTER	*4.77*	*87*	*3879*	*228*
	WINTER SNOWY	*4.14*	*73*	*3293*	*319*
Spruce	Autumn	6.44	67	5162	149
	Spring	4.14	82	3063	43
*SF= Safety Factor, C.C= Correlation Coefficient, CWP=Critical Wind Pressure AVE-DIR= Wind Direction					

crown surface area is more influential than wind direction. Conifers don't lose their leaves in different seasons, but, as seen in table 1, spruce SF was higher in autumn than in spring. This could be because of the difference in wind direction, or the higher Drag factor, which is a dimensionless quantity that is used to quantify the drag or resistance of an object in a fluid environment, such as air or water.

Figure 1 Poplar (Populus alba) in different season (left: winter, snowy; right: spring)

The drag coefficient is always associated with a particular surface area (3). M_{wind} (the torque on the root collar) depends on the drag factor and crown surface. The latter is lower in autumn than in spring, while Drag factor in winter is approximately 0.7 but in autumn is 0.2-0.3 and it is lowest in spring. This means that the surface area and drag factor changes counteract one another, and their effect more or less cancels out.

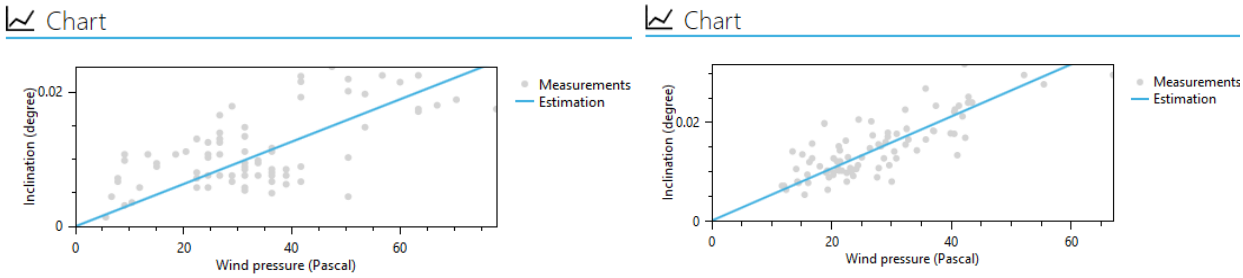

Figure 2 Tangent function Spruce (Picea abies) in 2 seasons (left-autumn, right-spring)

As shown in table-1 wind direction in autumn was in the SE direction while in spring it was from the NE. For this reason, as seen in figure 2, the tangent function in autumn is more diffuse than in the spring. The basic structural stability of a tree can be determined if the individual factors of structural stability are weighted at first without considering any possible damage. As shown in the results, many factors influence the root collar inclination due to wind load. determining factors of basic structural stability like soil humidity, tree trunk diameter, with attention paid to the macroscopic properties of the species, crown surface, crown base, shape of crown, crown height, root crown trunk base, root stock. Extended biological and physical data can help us undrestandig the behavior of trees in various conditions, and also keeping the trees healthy.

REFERENCES

[1] Fakopp Ltd., *DynaRoot Dynamic Root Evaluation System, User's manual* http://fakopp.com/docs/products/dynaroot/UserManualDynaRoot.pdf

[2] L. Bejó, F. Divós, S. Fathi: *Dynamic root stability assessment – basics and practical examples. In: Proc. 20th International Nondestructive Testing and Evaluation of Wood Symposium.* Madison (WI), USA,09.12-15. 7pp. 2017.

[3] McCormick, Barnes W, *AERODYNAMICS AERONAUTICS AND FLIGHT MECHANICS*. Science - 652 pages, 1979.

TRIBOLOGY TESTING OF SUPERHARD MULTILAYERED DLC COATINGS ON TOOL STEELS

FÜLÖP Fruzsina, MAROSNÉ BERKES Mária PhD
Institute of Materials Science and Technology University of Miskolc
E-mail: fulop.fruzsina@uni-miskolc.hu, maria.maros@uni-miskolc.hu

Keywords: DLC coating, PACVD, wear resistance, friction coefficient, tribology testing

INTRODUCTION

Nowadays the automobile industry is one of the most dynamically developing industries. The requirements, relating both mechanical loadability, informatics, aesthetic and convenience services are continuously increasing with the demand of reduced material, fuel consumption, and more and more stringent environmental protection. These changes initiated using higher strength materials for the components, consequently tools with increased loadability and lifetime. However, if we use stronger bulk materials, which have at the same time appropriate toughness, and wear resistance, the costs will be significantly increased. It is much favourable to improve only the surface layer properties of the tools – that is put to the most critical loads – using heat treatment or coating technologies. For metal forming tools superhard ceramic coatings are widely applied, among which DLC (Diamond Like Carbon) are so called self-lubricating coatings and stand out with their great hardness (1500-3200 HV) and very good wear resistance. The most common method of characterizing the tribological behaviour of these coatings are the standardized wear tests, and scratch tests.

OBJECTIVE AND EXPERIMENTAL PROCEDURE

The basic objective of the research work was to compare the friction and wear behaviour of DLC coatings produced by PACVD process on a substrate material made of a widely used cold work tool steel. The applied test methods were pin-on-disc wear test and scratch test. The thickness and operational suitability of the coatings was characterized by Calotest and Mercedes test. During the research work we compared two different types of coatings. One of them was a DLC coating on a Si-underlayer (henceforth SiCH/DLC coatings), the other one was a multi-layered coating system consisting of Cr+CrN+WC layers under the top DLC layer (henceforth Cr+CrN+WC/DLC). The substrate material was a high alloy, precipitation hardened Böhler K110 steel, (1.2379; X153CrMoV12). Test samples were disc shaped specimens with diameter of d=20.8 mm, and heights of h=5 mm. Surface preparation involved grinding before the bulk heat treatment, and two different finishing procedures – i.e. glass bead blasting (GBB) and polishing (P) – after heat treatment prior to coating. The examined coating systems were prepared by PACVD (Plasma-Assisted Chemical Vapor Deposition) process which combines the advantages of PVD (Plasma-Vapor-Deposition) and CVD (Chemical-Vapor-Deposition). [1]

During Calotest we applied steel ball of ϕ30 mm in diameter, and two different test times, since the two kinds of coatings had very different behaviour: the SiCH/DLC coatings were tested for 4 minutes, while the Cr+CrN+WC/DLC coating needed 10 minutes to see the coating thickness properly. The average layer thickness for the SiCH/DLC coating was 2.194 µm and 4.248 µm for the multilayer coating. It is supposed that in case of the Cr+CrN+WC/DLC multilayer coating, the combination of the ceramic underlayers provides a stronger support for the DLC upper layer.

To evaluate the tribological performance of the coating systems pin-on-disc tests were accomplished by an UNMT-1 (CETR) multifunctional modular surface tester. The applied test parameters were as follows: normal load F= 5, 10, and 30 N; sliding rate v= 10 and 30 mm/s; frictional counterpart was a SiC ball, diameter of ϕ6 mm; the tests were executed at room temperature in unlubricated sliding conditions. Altogether 24 tribo-systems were studied, and 3 measurements for each system were accomplished.

TEST RESULTS AND EVALUATION

Analysing the friction coefficient diagrams obtained for the different tribo-systems representing one-one combination of the normal load, sliding rates and surface finish, the following establishments can be made. In case of the uncoated samples the friction coefficient showed mostly an increasing character almost during the whole test and reached a value close to 0.6, while for the coated systems the friction coefficient value stabilized already at 50-70 m sliding distance, getting extremely low value close to 0.02. This friction coefficient is generally characteristic for the DLC coatings at low loadings. Figure 1. illustrates an example of the obtained friction coefficient diagrams for an uncoated and SiCH/DLC coated sample having GBB surface finish below the DLC top layer.

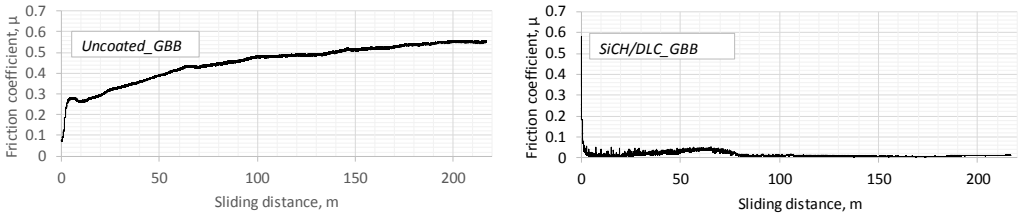

Figure 1 Characteristic friction coefficient vs. sliding distance diagrams recorded during the pin-on-disc test

To compare the friction behaviour of the different tribo-systems we defined the steady state friction coefficients (μ_{SS}) as the average of those obtained at the last 20% of the total sliding distance. The characteristic values are illustrated in Figure 2., based on which we can make the following observations:

- In case of the uncoated and glass bead blasted samples (Uncoated_GBB in Figure 2/a), the friction coefficient value decreased with the increase of the sliding rate. An explanation for this can be that the tribochemical reactions and the formation of the Fe_2O_3 oxid layer, which can serve as a lubricating film, are more enhanced at the higher sliding rates, that results in higher friction heat. The increasing normal load results also in the decrease of the steady state friction coefficient, and a gradually decreasing time up to the stabilization of the μ_{SS} values for these samples (the latter one is not illustrated here).
- For the specimens with multilayer coating and glass bead blasted surface (Cr+CrN+WC/DLC_GBB in Figure 2/b) the μ_{SS} values were systematically lower by one order than those obtained for the Uncoated_GBB samples at the same loading conditions. In Figure 2/b it can be observed that with increasing sliding rate and normal load, the steady state friction coefficient values are increasing, that is an opposite behaviour compared to the Uncoated_GBB materials.
- Comparing the friction behaviour of the samples having SiH/DLC coating and GBB surface finish (SiCH/DLC_GBB in Figure 2/c), with their multilayered counterparts (Cr+CrN+WC/DLC_GBB in Figure 2/b) similar effect of the increasing loading parameters have been observed, and the fluctuation of the friction coefficient values diminished with the increase of the normal load for both sliding rates, i.e. for v=10 and 30 mm/s, in case of both types of the coating systems. It is assumed that due to the higher normal loads the wear debris particles are chopped more intensively, and the finer grains will result in weaker abrasive wear, responsible for the variation of the friction coefficient.
- Friction coefficient for samples with polished surface below the top DLC layer were characteristically lower by 30-50% (Figure 2/d) than those measured for DLC coatings deposited in the same way on substrates having GBB finished surface (Figure 2/b).

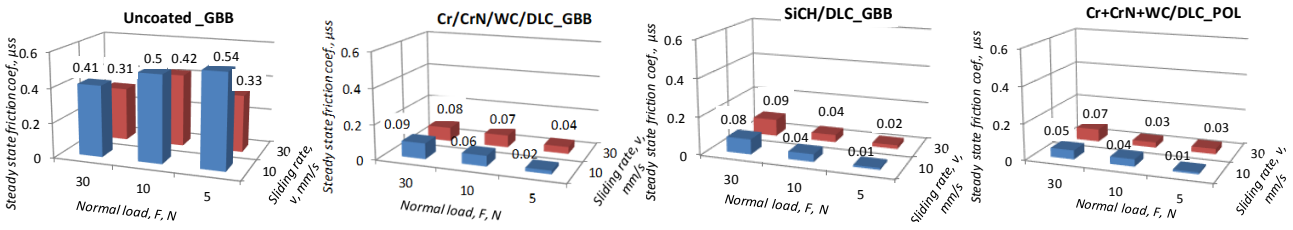

a) *b)* *c)* *d)*

Figure 2. The steady state friction coefficient values for the reference material and the investigated coatings

SUMMARY

Based on the executed tribological study our most important findings can be summarized as follows. Application of DLC coating on the K110 tool steel reduced the friction coefficient significantly – from 0.6 to 0.01 –, comparing to the uncoated state of the tool. Friction coefficients determined during pin-on-disc tests were systematically lower if the underlayer below the DLC coating was made of SiCH, as compared to that of Cr+CrN+WC. Surface finish prior to the PACVD coating may have considerable effect on the friction behaviour of the coating system.

REFERENCES

[1] Fülöp Fruzsina: *Lemezalakító szerszámok korszerű multirétegeс kopásálló bevonatainak vizsgálata,* TDK dolgozat pp.1- 49. TDK Konferencia, Miskolci Egyetem, Anyagszerkezettani és Anyagtudományi Szekció, 2017.

DEVELOPMENT AND CHARACTERIZATION OF SISAL FIBER REINFORCED POLYPROPYLENE COMPOSITE MATERIALS FOR CAR DOOR INTERIOR TRIM PANEL

[1]GEREZGIHER Alula Gebresas PhD, [2]BSRAT Halefom Aregay, [1]SIMON Andrea PhD, [1]SZABÓ Tamás PhD
[1]*Institute of Ceramic and Polymer Engineering, University of Miskolc*
E-mail: gebresas@gmail.com, femandi@uni-miskolc.hu, polsztam@uni-miskolc.hu
[2]*Adi-Grat University*
E-mail: halefom.aregay@yahoo.com

Keywords: Sisal fibre, Polypropylene, compressive moulding, flammability, chemical resistance

There has been a growing interest in utilizing natural fibers as reinforcement in polymer composite for making low cost construction, packaging, automobile parts, biomedical and electronic materials in recent years. This is happening due to the fact that synthetic fibers are not environmentally friendly and are costly when compared with natural fibres. For instance, hemp and flax polymer composite are successfully used as packaging material, interior panels in vehicles and building components among others. Natural fibers like banana, sisal, jute, coconut, bamboo, sponges, wood dusts and oil palm have also attracted scientists and technologists for applications in consumer goods, low-cost housing and other civil structures. A number of investigations have also been conducted on several types of natural fibers to study the effect on the physical, chemical and mechanical properties of polymer composite materials. So many researches have proved natural fibers to be effective reinforcement in thermoplastic and thermo setting matrix composites for automotive sectors. Fiber reinforced polymer composite materials have been widely used in various transportation vehicle structures because of their high specific strength, modulus and high damping capability. If composite materials are applied to vehicles, it is expected that not only the weight of the vehicle is decreased but also that noise and vibration are reduced.

The main purpose of this research is to develop composite material from natural fibre (sisal fiber) reinforced with recycled plastic waste (polypropylene) for interior automobile accessories specifically for internal door trim panel application. This research examines effect of fiber length, fiber loading and chemical treatment of fiber on the physical and chemical properties of the composite material. Experimental investigation of the chemical resistance and flammability on sisal fiber reinforced polypropylene composite was dealt to the detail. In most of the developing countries, plastic polypropylene is not fully recycled and converted in-to use after it is once used. Sisal fiber is also widely available in different developing countries like Ethiopia. Adding this two materials and developing automotive interior part was taken as a primary motive for it reduces cost and is environmentally friendly.

For this research work, sisal plant leaves was collected from Northern region of Ethiopia. After the leaves are cut at their base from the harvest; the fibers are extracted through hand extraction method with knife. Initially the leaves are trimmed in longitudinal direction into strips for ease of fiber extraction. The peel is clamped between the wood plank and knife and hand-pulled in longitudinal direction gently, removing the external cellulosic part, then the extracted fiber was washed with pure water in order to remove the remaining attachments between the fibers. The extracted fibers are sun-dried to reduce their moisture content and are made ready for fabrication.

The recycled PP used as matrix material was collected from broken chairs and tables in near-bye cafes, lounges and hotels with print information "*Polypropylene grade-5*" pasted on them.

While treating the sisal fiber, it was immersed in a 4% NaOH solution for 2 hours. The fiber was then washed with tap water and dried at room temperature. The fiber was cut into ~ 3mm, 6mm, 9mm, and 12 mm using a pair of scissors and prepared for mixing. Washed recycled polypropylene grade-5 was crushed and filled into stainless steel container and inserted into induction furnace at 160 ^{0}C to melt. The waste polypropylene and the treated and untreated sisal fiber with different length and weight ratio (fiber/matrix ratio of 5/95, 15/85, and 25/75) were mixed using portable drill stirrer at a speed of 30 rpm, for 15 min in order to uniformly distribute the fiber with in the matrix. After mixture is allowed to cure for 10 min., compression pressure of 37 MPa was applied on the mould, having the uniformly stirred mixture inside. Air gaps formed between the fibers during the processing were gently squeezed out by hydraulic press. Finally the composites were allowed to dry in air at room temp and get ready for testing.

Flammability and chemical resistance are among the main properties critical for internal door trim panel. Flammability of sisal fiber reinforced Polypropylene (SFRPP) composites material was examined by a horizontal burning test according to ASTM D635. For the burning rate evaluation, a total of 72 samples (2 parameters for treated and untreated ×3 parameters for fiber to PP ratio×4 parameters for fiber length ×3 trial tests) were tested. The average burning rate result for the three trial tests are shown below.

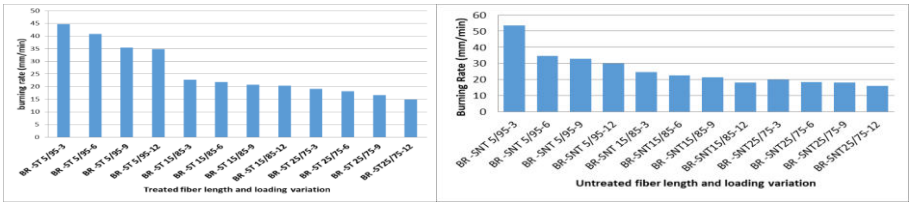

Figure 1 Effect of treatment, fiber length and fiber loading on burning rate of SFRPP composite

As can be shown in Figure 1, the result indicates that burning rate decreases from 3mm fiber length up to 12mm fiber length. This is due to strong bonding formed between fiber and matrix as the length increases.
It is also indicated in figure 1 that treated fiber has lower burning rate (14.89mm/min) than untreated fiber (16.12mm/min). This is because alkali treated SFRPP composite required more oxygen than untreated SFRPP composite to burn and adding flame retardants (4%NaOH) in to SFRPP composite reduced the burning rate. Generally, adding flame retardants (alkali group) into sisal/PP composites reduces burning rate due to an increase in thermal stability of the composites.
Effect of fiber/matrix ratio on the flammability in the above figure shows that burning rate decreases as the ratio of fiber to propylene increase from 5% up to 25%. This might be because as the ratio of fiber to PP increases, strong bond is formed, good interfacial modification created, and high interfacial shear stress between sisal fiber and matrix is maintained.
The chemical resistance of the sisal fibre reinforced PP composites were studied using ASTM D 543 testing method.
For the chemical resistance evaluation, 72 sample specimens were prepared and tested under chemical reagents such as 30% sulphuric acid solution, distilled water and base (30% NaOH solution) and average chemical resistance testing result for the three trial tests are shown below.

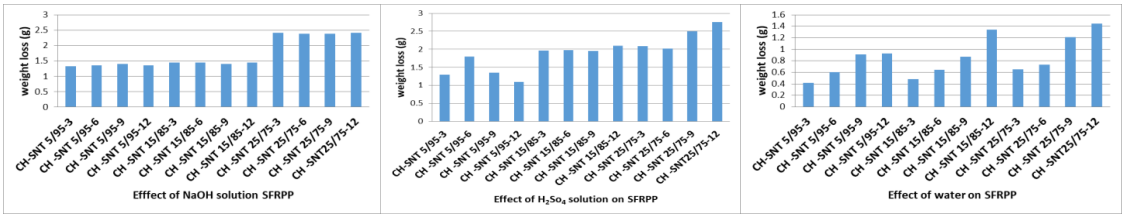

Figure 2 Effect of fiber length and fiber loading on chemical resistance of untreated SFRPP

As shown in Figure 2, the chemical resistance of SFRPP composite, maximum chemical resistance to water (minimum weight loss) was 0.33g followed by 0.36g, 0.68g and 0.84g for treated fiber to Polypropylene ratio of 5/95 (5% fiber & 95% PP) and 3mm, 6mm, 9mm, and 12mm fiber lengths respectively. This result indicates that chemical resistance property is better at fiber length of 3mm than 6mm, 9mm and 12mm. This is because shorter fiber is capable to resist diffusion of water molecules than longer one. In addition, short fiber has less pace of water capillary transport in to the gap and flaws at interface between the fiber and matrix than longer fiber. It can be concluded here that composite with a lowest weight loss have low moisture absorption potential.
Tested with the same method, treated fibre has shown better chemical resistance to water (minimum weight loss, 0.33g) than untreated fiber (0.42g). This is because alkali treatment improves strength of the surface of the composite and creates strong adhesion which hinders the hydrophilic behaviour of sisal fiber and reduces water up take behaviour.
Effect of fiber loading on the chemical resistance for SFRPP composite as shown in Figure 2, indicates that maximum chemical resistance to water (minimum weight loss) is found 0.33g at 5/95 fiber to PP ratio followed by 0.56g and 0.75g for 15/85 and 25/75 fiber to PP ratio respectively for 3mm fiber length. This result implies that chemical resistance for fiber to polypropylene ratio of 5/95 (5% fiber & 95% PP) is better than fiber to PP ratio of 15/85 (15% fiber & 85% PP), and 25/75 (25% fiber & 75% PP). This is because, as the fiber content increases the amount of water uptake by the fiber is increased and this leads to reduced resistance to chemicals. Similarly, the chemical resistance of SFRPP to NaOH and H_2SO_4 is indicated in figure 2.
SFRPP composite is found to have better resistance to water than NaOH and H_2SO_4 and treating the fiber has brought considerable improvement on chemical resistance of the composite. Fiber loading and fiber length has positive and negative effect on the flammability of the SFRPP composite respectively.

COMBUSTORS WITH LOW EMISSION LEVELS FOR AERO GAS TURBINE ENGINES

GUELLOUH Noureddine, SZAMOSI Zoltán PhD, SIMÉNFALVI Zoltán PhD
Faculty of Mechanical Engineering and Informatics, University of Miskolc
E-mail: noureddine.guellouh94@gmail.com, vegyszam@uni-miskolc.hu, simenfalvi@uni-miskolc.hu

Keywords: Combustion, technology, low emissions, rich burn, lean burn

The aircrafts are responsible for emitting several types of pollutants, especially the pollutants in the form of Nitrogen Oxides NO_X (comprising NO and NO_2), Carbon dioxide CO_2 and Carbon Monoxide CO, Unburned Hydrocarbons UHC, Sulfur oxides SO_X and Particulate Matter PM (smoke/soot). The impact of aviation emissions on the global is well known, where these emissions modify the chemical and microphysical properties of the atmosphere resulting in changes of earth's climate system, which can ultimate in critical changes in our planet fragile ecosystem, also the pollutants produced by aircraft engines cause many health problems.
The International Civil Aviation Organisation (ICAO) is seriously seeking to control the emission levels by issuing new standards during the successive meetings of the Committee on Aviation Environmental Protection CAEP (CAEP/01 in 1986, CAEP/2, CAEP/4, CAEP/6, CAEP/8...). The new regulations include more stringent standards aimed to reduce emission levels, this led to increased interest in low emission technologies.
New low emission technologies have been created and developed, where the demand for new improved designs with ultra-low pollutant emissions is rapidly moving to the forefront of combustor development. In this paper, a comprehensive review of low emissions combustion technologies for modern aero gas turbines is represented. The current low emission technologies include the high Technologies Readiness Level (TRL) including Rich-Burn Quick-quench Lean-burn (RQL), Twin Annular Premixing Swirler combustors (TAPS), Double Annular Combustor (DAC), Lean Direct Injection (LDI). Also, there are advanced technologies at lower TRL including Lean Premixed Prevaporised (LPP), Axially Staged Combustors (ASC) and Variable Geometry Combustors (VGC).
The combustion in RQL technology is initiated by a fuel-rich mixture in the primary zone with equivalence ratio normally 1.2–1.8. The rich-burn condition in this zone has a special advantage where it enhances the stability of the combustion reaction by producing and sustaining a high concentration of energetic hydrogen and hydrocarbon radical species, also the production of NO_X is less in case of rich-burn conditions due to the relative low temperatures and low population of oxygen containing intermediate species. In the quick-quench stage, a large amount of air is introduced to mix quickly to complete the rapid transition from rich to lean burn, so as to prevent the area with large NO_X production near the stoichiometric ratio, also this second process is very important because it leads to oxidise CO, hydrogen and hydrocarbon intermediates, where the resulting gas from the first region (rich-burn) contains a high amount of CO, UHC and smoke that cannot be exhausted without further processing. Finally, the Lean-burn region (typical equivalence ratio is in the range of 0.5-0.8), which is very important because it helps to achieve more CO and UHC consumption also for lower NO_X.
A technology of reducing the combustion temperature of various fuels that has gained popularity in the past few decades is to mix fuel and air in fuel lean proportions before the combustible mixture reaches the combustion zone. In LPP technology, the fuel is vaporised and then mixed with the air flow to create a lean, homogeneous mixture before entering the combustion zone and burning at a low equivalence ratio that is close to the lean blowout limit, and due to the low flame temperature and the elimination of hot spots from the combustion zone a significant reduction in emission levels of nitrogen oxides. Basically, LPP combustor consists of three main sections, where the first is for fuel injection, vaporisation, and fuel-air mixing such that completed fuel evaporation and fuel-air mixing can be achieved, the second is for combustion where the flame is stabilised in the recirculation zones and the third may comprise a conventional dilution zone. In the development of LPP combustors, the success of the LPP combustion process mainly depends on the flow field, evaporation characteristics of fuel spray and the fuel/air mixing in the combustion zone. Combustor designs of this kind are very complex because they require sophisticated harde-ware for proper staging of the combustion process.
Generally speaking, the original intent of DAC was to get 50% NO_X reduction over state of-the-art combustors introduced in the early 1970's, where the concept of this technology was first conceived by Bahr and Gleason. These combustors are based on a radially staging strategy. The combustion stoichiometry and hence temperature is controlled through the use of fuel injection in multiple combustion locations. At low power settings, part of combustion zones operates and refers to the pilot zone to raise the equivalence ratio (around 0.8) so as to increase the combustion efficiency and reduce CO and UHC. The DAC technology provides many advantages, where the lean combustion is

operated at high power providing the potential to reduce the NO_X emissions, also the commonly shared feed arm enables the pilot fuel to cool the main fuel, lowering the risks for fuel coking.

The TAPS combustor evolved based on lessons learned with fuel staging of the DAC, and also benefitted from extensive experience with Dry Low Emissions lean premixing combustors in aero-derivative industrial gas turbines. It is a premixing main swirler built concentrically around the well-proven swirl cup mixer, and hence the use of the word twin. The TAPS combustor concept is a lean burn system where each fuel injector contains a center pilot and concentric outer main. The central pilot tip is a rich burn configuration similar to traditional combustors. At starting and low power operation fuel is 100% in the pilot. At higher power fuel is split between the pilot and main. The main injection is a set of radial jets that enter a larger main air swirler. The main is a large effective area swirler to burn fuel lean. At high power most of the fuel is injected through the main. This makes both the pilot and main mixers fuel lean with approximately 70% of combustor total air flow through those 2 mixers.

ASC concept was conceived roughly in the same timeframe as DAC in the 1970s. It was developed by Pratt & Whitney in the NASA Experimental Clean Combustor Program ECCP. The working principle of ASC combustors is similar to the DAC, but fuel staging is achieved through the fuel injection zones placed in the axial direction. The main stage is placed downstream of the combustor, and the pilot zone is placed at the upstream. Axial staging does have certain advantages over radial staging. Since the main stage is downstream of the pilot stage, ignition of the main stage directly from the pilot is both rapid and reliable. Also, the hot gas flow from the pilot into the main combustion zone ensures high combustion efficiency from the main stage, even at low equivalence ratios. The P&W team chose the Axially Controlled Stoichiometry (ACS) as a term in the current development to express the ASC technology. The arrangement of the separation of the pilot and the main provides for efficiency and stability at low power, and stability at all operating conditions. Mixing of the pilot and main is controllable according to PW experience. P&W has experience in the design and manufacture of ASC systems due to the V2500 design. The ASC distributes the heat release axially, reducing susceptibility to acoustics. One of the main advantages of this technology is the lower level of NO_X at high power that can be achieved for reduced residence time since the main stage can burn efficiently.

Variable geometry combustor (VGC) is an unconventional method of reducing engine emissions and increasing combustion efficiency based on the active distribution of air among the individual combustor zones. This technology provides the flexibility to control the airflow distribution inside a combustor and therefore has the ability to reduce the emissions on both high and low operating conditions without losing combustor performance. It also has a great potential to improve combustion efficiency at low power operating conditions, and facilitate engine relight at altitude.

In VGC, The air flow splitter is driven by a hydraulic system and is allowed translational movement (moves forward and backwards) to vary the cross-sectional area and hence the air flow ratio into the primary zone. At lower power conditions, the degree of opening of the splitter increases the quantity of air diverted backwards to create a high primary Fuel Air Ratio FAR and a reducing flow velocity for high combustion efficiency and improved stability, as well as good light-up capability. As power is increased, the splitter opens, introducing more air into the primary zone to achieve low FAR such that lean combustion is achieved for the purpose of NO_X and smoke reduction.

Lean combustion in gas turbine combustors is fast becoming the norm due to environmental and efficiency concerns. A promising design is the lean direct injection (LDI). It has been of active interest due to its potential for low emissions under operational (high-temperature, high pressure) conditions. In this technology, the liquid fuel is injected from a venturi directly into the incoming swirling airstream, and the swirling airflow is used both for atomizing the injected liquid and for fuel-air mixing. Autoignition and/or flashback are minimized since the fuel neither premixed nor prevaporized.

ACKNOWLEDGMENTS

The described article was carried out as part of the EFOP-3.6.1-16-2016-00011 “Younger and Renewing University – Innovative Knowledge City – institutional development of the University of Miskolc aiming at intelligent specialization” project implemented in the framework of the Széchenyi 2020 program. The realization of this project is supported by the European Union, co-financed by the European Social Fund.

THE EFFECT OF FLUXES ON THE MELT QUALITY OF AlSi7MgCu ALLOY

[1]GYARMATI Gábor, [1]FEGYVERNEKI György PhD, [2]MENDE Tamás PhD, [1]TOKÁR Mónika
[1]Foundry Institute, University of Miskolc
E-mail: gygabor007@gmail.com, gyorgy.fegyverneki@nemak.com, monika.tokar@uni-miskolc.hu
[2]Institute of Physical Metallurgy, Metalforming and Nanotechnology, University of Miskolc
E-mail: tamas.mende@uni-miskolc.hu

Keywords: Aluminum alloy, Inclusions, Fluxes, Melt treatment, Melt quality

Inclusions are discontinuities of the material which are non-metallic or sometimes intermetallic phases embedded in a metallic matrix. The most common inclusions in aluminum alloys are non-metallic compounds: oxides, nitrides, carbides, and borides which can occur in the form of solid particles, films or liquid droplets in the molten alloys. Inclusions reduce mechanical properties by detracting from the effective cross-sectional area when stress is applied and because of the concentration of stresses at the inclusion interface. Properties such as elongation, yield strength and ultimate tensile strength have been observed to decrease with the increased inclusion content in the metallic matrix. Inclusions in the melt can negatively influence melt fluidity and can prevent interdendritic feeding.
Nowadays, solid fluxes are widely used in foundries in order to reduce the inclusion content of aluminum melts. The effect of fluxes is determined by their chemical composition, morphology, added quantity, as well as the temperature of the melt and the method of flux addition. It is important that the compounds in the fluxes should be able to form low-melting high-fluidity mixtures at working temperature. Modern melt treatment stations can automatically add flux blends to the melt during the first stages of the rotary degassing process.

In this study, the effect of four different flux on the inclusion content of an aluminum alloy melt was compared. In order to find the reason for differences in melt cleaning efficiency, the chemical composition and thermal properties of the flux blends were investigated. Melt treatments consisting of rotary degassing with flux addition were executed on an Al-7%Si-0.4%Mg-0.5%Cu alloy melt. The stages of melt preparation process can be seen in Figure 1.

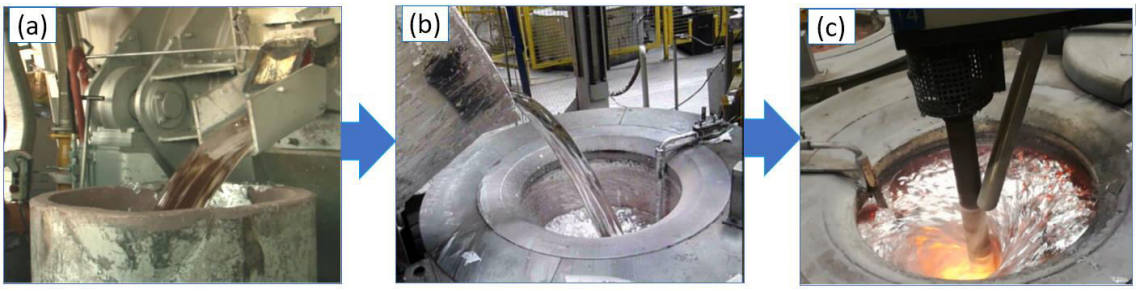

Figure 1 The stages of melt preparation: a) pouring from melting furnace, b) melt transport to holding furnace, and c) melt processing

The inclusion content of the melts treated with different fluxes was investigated by the evaluation of K-mold samples. The fracture surface of K-mold samples was inspected with stereomicroscope at a magnification of 25X. Based on the number of inclusions found on the fracture surfaces, a K-value can be determined which can be used for the quantitative characterization of the melt purity.

$$K = \frac{S}{n}$$

where K is the K-mold value, n is the number of examined samples, and S is the total number of inclusions found in n pieces. The effect of different fluxes on the melt purity was evaluated using the comparison of the K-values determined before and after the melt treatments. The percentage of change in K-values (ΔK [%]) was calculated using the following equation:

$$\Delta K = \frac{K_2 - K_1}{K_1} \cdot 100$$

where K_1 is the K-value determined before the melt treatment and K_2 is the K-value determined after the melt treatment. The inclusions found on the fracture surfaces were examined with scanning electron microscope (SEM) combined with energy dispersive X-ray spectroscopy (EDS analysis).
The elemental composition of the fluxes was examined with EDS analysis. The thermal properties of the fluxes were investigated with derivatographic measurements. The derivatograph is capable of performing differential thermal analysis (DTA) and thermogravimetric (TG) measurements on the same sample at the same time. With the aid of derivatographic measurements, the melting temperature of fluxes can be determined, which is an important property that significantly influences the melt cleaning efficiency. The melting temperature values of the fluxes were compared with the average change in K-values (ΔK) in order to find a relationship between the melt cleaning efficiency and the melting temperatures of the fluxes. The results can be seen in Figure 2.

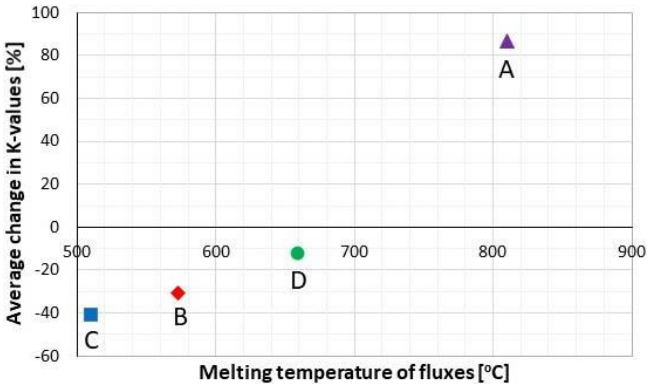

Figure 2 The comparison of melt cleaning efficiency and the melting temperature of fluxes

Based on Figure 2, it can be stated that in the case of the four fluxes investigated, the fluxes with lower melting temperature were more efficient regarding inclusion removal. The reason for the described results is the following: since the viscosity of molten fluxes is temperature dependent, at a constant temperature the viscosity of molten fluxes with lower melting temperature is lower and their fluidity is better. During melt treatment, the molten fluxes with better fluidity can be dispersed more evenly in the molten metal which results in better melt cleaning efficiency. Flux A has the highest melting temperature which is actually higher than the maintained melt temperature (740-750 °C), therefore the grains of flux A could not melt during melt processing. Since the flux grains were in solid state after addition, they were not capable of exposing any inclusion removing action, moreover, they contributed to the degradation of the melt quality via the entrainment of the surface oxide film of the melt during flux addition, which resulted in higher K-values. By the comparison of the measured K-values and the elemental composition of fluxes measured with EDS analysis, it can be concluded that the more effective fluxes (B and C) contain reactive components (like oxidizing compounds) at higher concentration values and their grains have consistent chemical composition. The grains of flux D have significantly different composition values, which is a common attribute of powder fluxes according to the literature. The inhomogeneity of the chemical composition of flux D could be the main reason for the lower ΔK values and thus the lower efficiency of melt cleaning.

From the results of the present study, it can be concluded that the melt cleaning efficiency of different fluxes is highly dependent on their chemical composition, morphology and melting temperature. Based on the results of K-mold tests, flux C was the most effective in inclusion removal. The more effective fluxes (like B and C) are granular, contain oxidizing compounds and fluorides at higher concentration values, their grains have a consistent chemical composition and they have significantly lower melting temperature than the temperature of the treated molten alloy.

ACKNOWLEDGMENTS

SUPPORTED BY THE ÚNKP-18-2-I. NEW NATIONAL EXCELLENCE PROGRAM OF THE MINISTRY OF HUMAN CAPACITIES

ACCURACY ANALYSIS OF TWO PARALLEL MANIPULATORS

HAJDU Sándor PhD, BODNÁR Dávid
Department of Mechanical Engineering, University of Debrecen
E-mail: hajdusandor@eng.unideb.hu, bodnar.david2@gmail.com

Keywords: Parallel manipulators, Stewart platform, Rotary Stewart platform, accuracy, MATLAB.

Parallel manipulators are getting used more and more in industry and medical applications [1, 2]. The most common type is the Stewart platform, which has six actuators connected parallel from a base to a moving platform. It has six degrees of freedom. There is also the rotary type of Stewart platform, where the connection lengths are fixed between the base and the platform, but the attachment points can be moved along the perimeter of the base. This study analyses the theoretical accuracy for these two manipulator if one of the actuators fails to reach its wanted position. The calculations are done in MATLAB, based on previous work from the authors [3] about the kinematic calculations and workspaces of these types of Stewart platforms.

Figure 1 Commercially available versions: General type [4] (left), and rotary type [5] (right)

The aim of the study is to develop a parallel manipulator for patient positioning. Regular and rotary types were investigated, to be able to choose the more suited version for the task. The objective of the work is to have a visual reference for the accuracy, which is useful to compare the manipulators, and also serves the purpose of checking if the kinematics calculations are stable for the reachable workspace.
The calculations started with obtaining scatters of points in a fixed height of the workspace, essentially it is a slice of the workspace. The points were evenly distributed with 1 [mm] distance between them. That distance was chosen because it already resulted in around ten thousand pairs of points, which was adequate for the task. These values were used to calculate the required actuator lengths and positions. After that came the position accuracy analysis.
The accuracy analysis assumes that only one actuator has an error between the required and actual position, but that error is the maximum specified value for the actuator. The control value was the one calculated without any added errors. The error was then added to one of the actuators, forward kinematic calculation was done, saved, and the next actuator got the error value added. When every calculation was done with positive error values the same calculation was done, but with the error value subtracted from the actuator position. This resulted in 144 positions in various distances from the control point. Every points distance were calculated from the control position, and the highest value was saved. That value is the worst case scenario for that position. A more detailed analysis could be made assuming that more than one actuator has errors, which is more likely in practice, but the time required for the MATLAB code to run the analysis already reached more than 8 hours for these set of calculations.
The results of the calculations were instructive. The general type Stewart platform maximum positional error for 0.05 [mm] actuator error was 0.045 [mm]. The rotary type maximum positional error for 0.18 [mm] actuator error was 0.15 [mm].

The visualisation for the results was also done in MATLAB. The accuracy analysis script's output was the same as the points scatter script output, but with one extra value added for each row of points – the highest error. To be able to get a visual reference for the points not included in the analysed points shading was needed. This was done by making a mesh from the obtained points using 2-D Delaunay triangulation, which ensures that the circumcircle associated with each triangle contains no other point in its interior. With that mesh the authors were able get an approximation for the accuracy of every point inside the examined slice of the workspace, which was at zero height. The dispersion of the error is as expected, very low in the centre of the workspace, and gradually increases towards the end of the workspace. The general type shows a large area with high error, which needs further investigation.

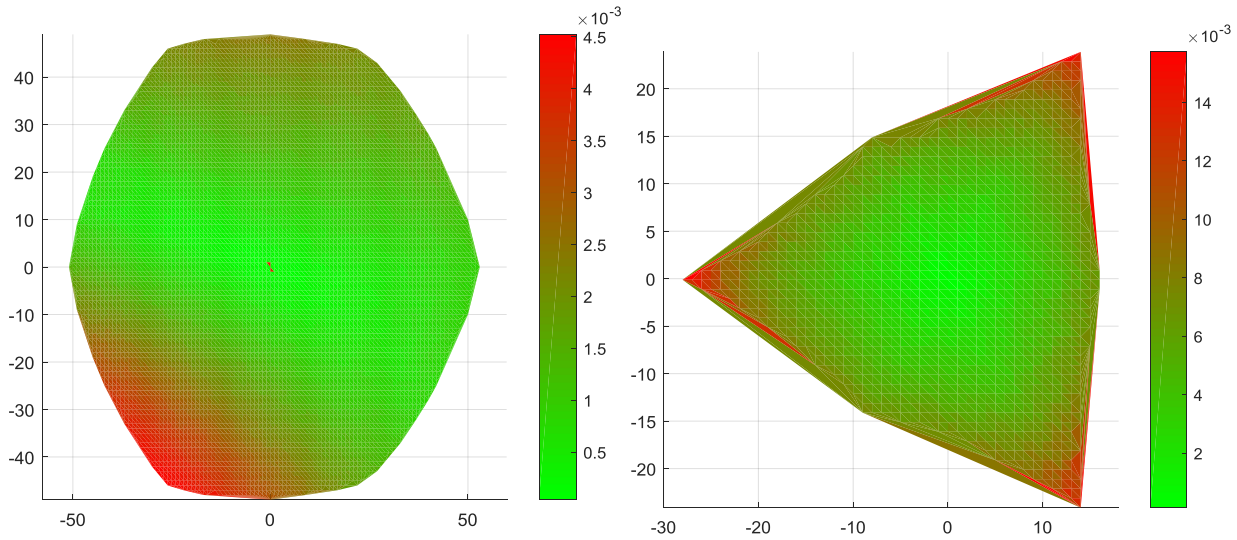

Figure 2 Error visualization for the general type (left) and rotary type (right) Stewart platforms

Conclusion of this paper is that these two types of parallel manipulators respond well to actuator errors. Actual position errors are expected to be always less than that of the actuators, very small in the middle, with the big errors only present near the edge of the workspace. The unexpected error zone on the general type is planned to be investigated with singularity analysis.

REFERENCES

[1] *Advanced Robotics and Mechanism Applications: Analysis and Synthesis of Parallel Robots for Medical Applications,* A.R.M.A. Research Laboratory, Columbia University, Department of Mechanical Engineering http://www.columbia.edu/cu/mece/arma/people/nabil_simaan/ms_research.shtml
[2] MICROMO: *Hexapod Surgery Assistant: Servo Motor Applications, Miniature Hexapods Used In Spinal Surgery*
[3] https://www.micromo.com/applications/medical-lab-automation-equipment/application-case-study-micro-precise-surgery-assistant
[4] D. Bodnár, S. Hajdu: *Kinematics and Workspace analysis of parallel manipulators, International Journal of Engineering and Management Sciences (IJEMS)* Vol. 3. (2018). No. 2 DOI: 10.21791/IJEMS.2018.2.1.
[5] *Symétrie Breva* http://www.symetrie.fr/en/products/positioning-hexapods/breva/
[6] *Mikrolar R3000 Rotopod*: http://mikrolar.com/r3000.html

TENSILE ANALYSIS OF 3D PRINTER FILAMENTS

HALÁPI Dávid, KOVÁCS Sándor Endre, PALOTÁS Árpád PhD, VARGA László PhD
Faculty of Materials Science and Engineering University of Miskolc
E-mail: halapidavid@hotmail.com

Keywords: PLA, 3D printing, mechanical properties, additive manufacturing, tensile tests.

3D printing technology is extremely widespread in the present days. There are numerous processes available for creating digital geometries via the „additive manufacturing" (AM) method, which is basically building the product from one or more materials.
Our investigatios were centered around the FDM (fused deposition modelling) 3D printing method, and the PLA (polylactic acid) which is used by this process. Our work was supported by the Philament Ltd. Miskolc company, 6 of their product were tested, each contained different kinds of strengthening additive material. The main goal of the investigations was to determine that how much each strengthening material actually contributes to the final strength properties.

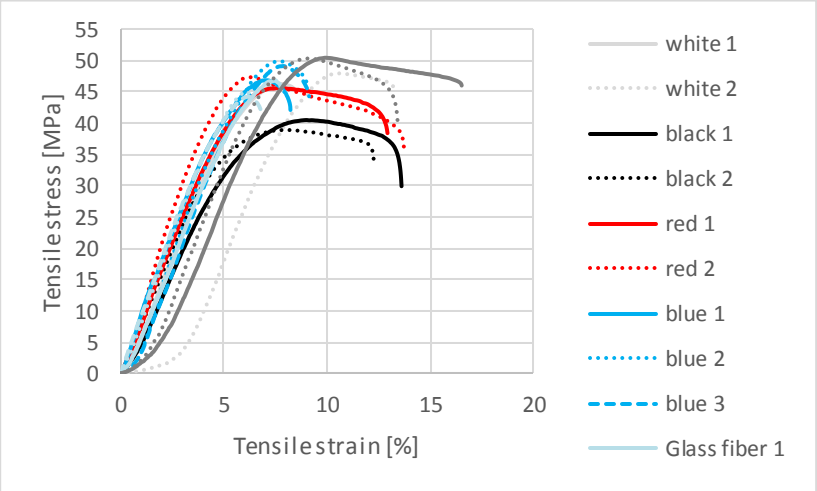

Figure 1 Tensile test: results of all filaments

We parted the examinations to two main groups. First, we tested the philaments strength properties, with an Instron 5566 type tensile tester. After processing and evaluating the data we earned from the tensile tests, we made SEM (scanning electron microscope) recordings for each fracture surface, which are showing perfectly the difference between the various materials.

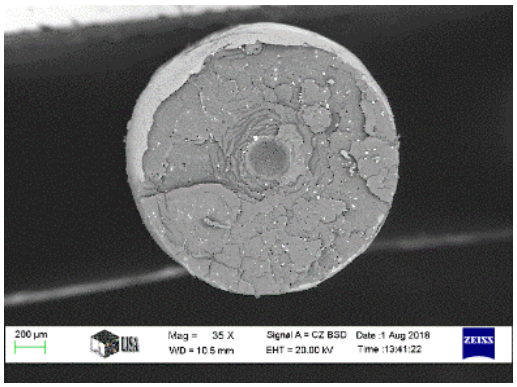

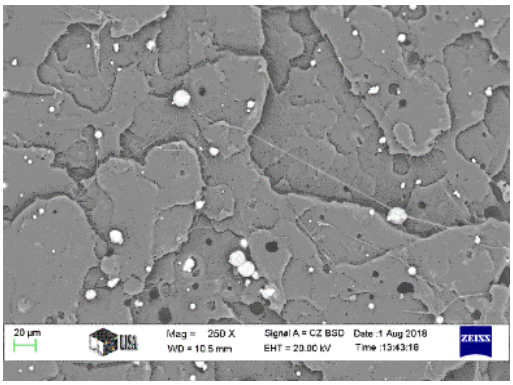

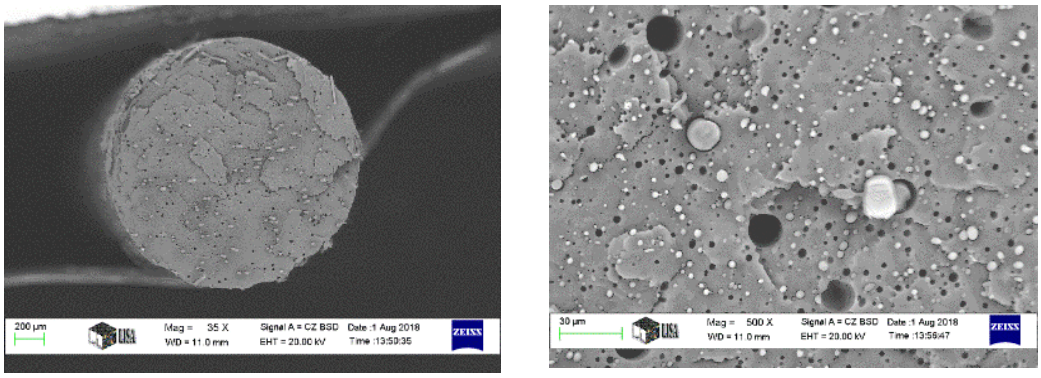

Figure 13 Cross section of the PLA+glass fiber filament by SEM nominal magnification 35×; 500×

Second, we printed tensile test specimens from each philaments, using the ISO 3167 1994 standard. The printing was executed via a Cetus3D type 3D printer, every printing settings were left on standard, with 100% fill rate. We tested each of them with the tensile tester mentioned above.
The measurements are showing that each additive materials have succesfully increased the strength properties of the printed test specimens. Furthermore, we want to perform additional measurements about how the fill rate, and the printing temperature influencing these examined properties of each tested specimens.

ACKNOWLEDGMENTS.
The authors express their sincere appreciation to Philament Ltd. (Miskolc), for the samples and Árpád Kovács for the SEM analysis.
"The described article/presentation/study was carried out as part of the EFOP-3.6.1-16-00011 "Younger and Renewing University – Innovative Knowledge City – institutional development of the University of Miskolc aiming at intelligent specialisation" project implemented in the framework of the Szechenyi 2020 program. The realization of this project is supported by the European Union, co-financed by the European Social Fund."

TRIBOLOGICAL BEHAVIOUR COMPARISON OF ABS POLYMER MANUFACTURED USING TURNING AND 3D PRINTING

[1,2]HANON Muammel M., [3]KOVÁCS Márk, [4]ZSIDAI László PhD
[1]*Institute for Mechanical Engineering Technology, Szent István University*
[2]*Baquba Technical Institute, Middle Technical University (MTU),*
E-mail: muammel_mmr_85@yahoo.com, Sharba.Muammel.M.Hanon@phd.uni-szie.hu
[3]*Faculty of Mechanical Engineering, Szent István University*
[4]*Institute for Mechanical Engineering Technology, Szent István University*

Keywords: Turning, 3D printing, friction, wear, ABS

In the present work, Tribological properties of Acrylonitrile Butadiene Styrene (ABS) polymer were examined experimentally and compared in two methods of manufacturing, (i) additive manufacturing (3D printing), and (ii) subtractive manufacturing (turning). FDM has been chosen as the 3D printer technique for this study. Some steps for developing the FDM 3D printer have been carried out seeking more accuracy and ease of use. This printer used to produce the 3D printed samples which are employed in the tribology measures, to determine the tribological properties of the 3D printed parts where there is a lack in the literature about it. Tribological measurements of the turned and 3D printed specimens have been achieved. Studying the difference between static and dynamic friction factors and the examination of wear values were included. A comparison of the tribological behavior of the turned and 3D printed ABS polymer has been investigated.

The printed test specimens were made by a 3D printer works according to the Fused Filament Fabrication (FFF), which is the most common technology in the 3D printing. The model of the used 3D printer is K8200 (Figure 1). The specimen model was designed using Solid Edge software.

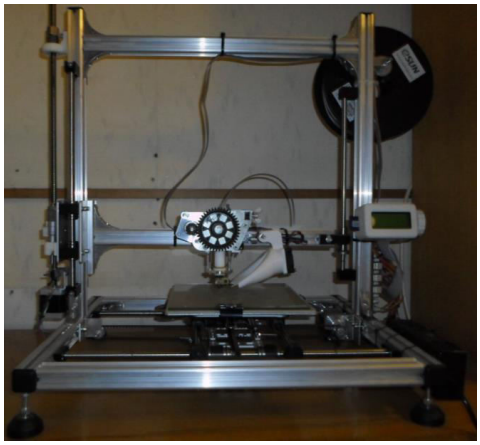

Figure 1 3D printer K8200

Figure 2 Turning and 3D printing test specimens

The ABS test specimens were prepared in the workshops of Szent István University using the industrial machining. Turning machine was used for the turned samples. The 3D printed test workpieces were made of ABS filament, its key features are presented in Table 1. The 7.5 mm diameter and 10 mm length specimens came out of the fundamental pieces. The work surface preheated approximately 60-70 °C for ABS Printing. It is treated for proper adhesion, due to ABS is more delicate for temperature fluctuations than some other polymers during printing. In case of insufficient cooling during printing, no optimum melting of the layers is reached, and brittle fracture of material takes place. Samples of the specimens that produced by turning and 3D printing of ABS polymer are shown in Figure 2.

Table 1 Main features of ABS filament

Print temperature	First layer temperature	Heated work surface	Available colours
220-260 °C	235 °C	Yes	Natural (White)

After printing the specimens, the measurements were performed at tribology test room in Szent István University under the laboratory conditions. The first step in the measurement process is to connect the measuring circuit, which consists of a computer, Spider 8 measuring converter, a tribotester and, an inverter. Before starting the measurement, a number of parameters must be defined which are given in Table 2.

Table 2 Tribology measurement parameters

Surface roughness of steel counterpart, [µm]	3.2
Test duration, t [s]	130
Load, F [N]	180
Alternating motion frequency, f [Hz]	10
Average speed, v [m/s]	0.05
Race length, [mm]	15
Relative humidity, Rh [%]	50

During the test, both static and dynamic friction factors were evaluated. The value of static friction factors is always higher than the relative dynamics. Wear rate measurements have been done for the ABS samples which are manufactured by turning, and 3D printing as well.
Figure 3 shows the maximum and most frequently used value of the dynamic friction coefficient. The blue column indicates the friction coefficient of the stabilized state, while the maximum friction value during the measurement period is indicated by the red supplementary column. The values shown here are from the average of multiple measurements. From the diagram, it is clear that the ABS-based specimens are in the same range of dynamic friction coefficient regardless of the machining method. But the turned ABS is a slightly higher in the mode value, which is almost negligible. In Figure 4, the average wear values of the individual specimens during the measurement were compared. It can be seen that the wear levels of the 3D printed ABS are somewhat lower than the turned ABS. This indicates that the features of the printed ABS got improved a bit regarding the tribological behaviour.

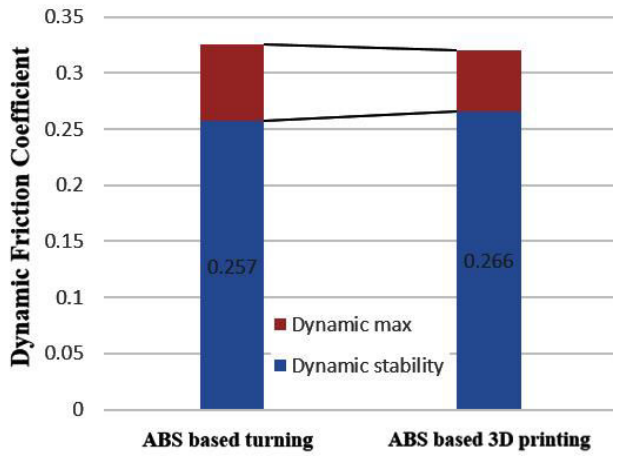

Figure 3 Measurement data of the dynamic friction coefficient

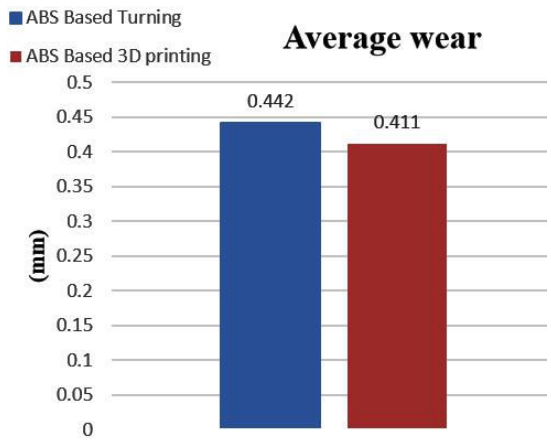

Figure 4 Average wear rate in the diagram

The alternating-motion system used during this research allows the measuring of the difference between static and dynamic friction factors and wear curves, so it is suitable for comparative tests of this type. The obtained tribological properties of the 3D printing and turning specimens of the same ABS material did not differ significantly, therefore, they could be considered as equivalent. Further research in this area would be worthwhile if it involves the other common commercial types of polymers like PLA with same and different colour materials.

ACKNOWLEDGMENT
This work was supported by the Stipendium Hungaricum Programme and by the Mechanical Engineering Doctoral School, Szent István University, Gödöllő, Hungary.

REDUCTION OF THE ENERGY DEMAND OF SOLVENT-GRADE BIOETHANOL PRODUCTION

HÉGELY László PhD, TÓBEL Kitti, DÉNES Ferenc PhD, LÁNG Péter DSc
Faculty of Mechanical Engineering, Budapest University of Technology and Economics
E-mail:hegely@mail.bme.hu, tobelkitti@gmail.com, lang@mail.bme.hu,denes@energia.bme.hu

Keywords: bioethanol, distillation, simulation, heat exchanger network, pinch method.

Bioethanol is a biofuel produced from the carbohydrate content of plants. First generation bioethanol is sugar- and starch-based and needs food plants as raw material, but second generation one is produced from lignocellulosic vegetable biomass (straw, waste wood). Although bioethanol is mostly known as a biofuel, it can be used as a solvent in the pharmaceutical and cosmetic industry. However, this application requires much higher purity, which means that the ethanol must be free from any organic pollutants. Beside ethanol and water, the beer contains several other organic pollutants, which are often neglected by other publications. Batista et al. [1] took into consideration further 16 organic components in the case of the distillation of fermented sugar cane beer. Bisgaard et al. [2] analysed the wheat straw beer composition from an existing plant producing solvent-grade bioethanol and found 13 significant trace compounds.
In the present work, the distillation separation technology of a less-studied, second generation solvent-grade bioethanol production process is investigated by computer simulation using the flowsheet simulator CHEMCAD. Our aim is to compare different heat integration (HI) possibilities for the reduction of external heating and cooling energy demand. The composition of the beer is the same as that of Bisgaard et al. [2], containing 3.49 wt% ethanol, 96.48% water and 0.03% organic pollutants: acetaldehyde, propanal, methanol, 1-butanal, ethyl acetate, 1-propanol, 2-butanol, trans-crotonaldehyde, 2-methyl-1-propanol, 1-butanol, 2-methyl-1-butanol, 3-methyl-1-butanol, benzaldehyde.
The bioethanol distillation plant consists of three distillation columns (*Fig. 1*). The first one is the Beer Stripper (1), which removes the majority of the beer's water content and the enzymes. It is operated in vacuum (0.242 bar), and has no condenser. Its distillate (D1) is then fed into the atmospheric Aldehyde Column (2). The distillate (D2) of the latter column contains practically the entire amount of acetaldehyde, propanal, and ethyl acetate. The bottom product (W2) is fed into the Rectification Column (3), which is operated at atmospheric or higher pressure. Its distillate (D3) is azeotropic alcohol vapour containing only water and very low amounts of methanol and 1-propanol as pollutants. Its dehydration is performed by adsorption by molecular sieve. The aqueous solution of organic polluting compounds (fusel oil) is withdrawn as side product (S3). The bottom product (W3) is pure water. Note that no HI is present in Bisgaard et al. [2].

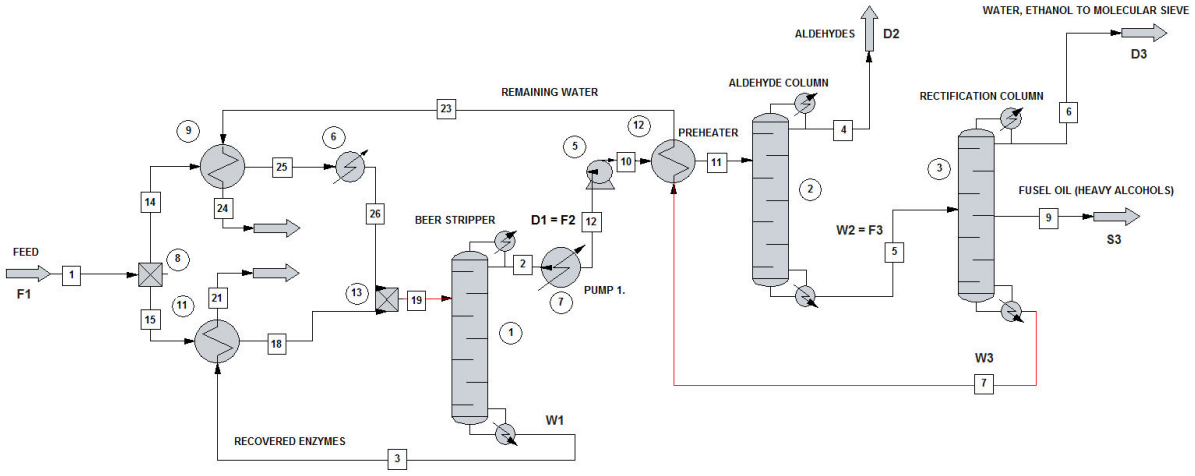

Figure 1 Model of the heat-integrated bioethanol distillation plant (CaseHI-A)

First, we performed the simulation of the process as described by Bisgaard et al. [2] (original case). The flow rate of the feed (of 20°C, F1) was 7585.9 kg/h. Specifications of the columns are given in *Table 1*. The top pressure of Column 1 was 2.929 bar. The feed of Column 2 (F2) was preheated to 85°C. S3 (16.04 kg/h) was taken from tray 25. The calculation results showed a good agreement with those of Bisgaard et al. [2]. The distillate of Column 3 (D3) contained 93.52 wt% ethanol. The reboiler of Column 1 requires more than the half of the total external heat input (*Table 2*), while the condensers of Columns 1 and 3 have high cooling duty. W1, W2, D2and S3 have to be cooled down to 30°C.

Table 1 Specifications of the columns for the original case.

	Column 1	Column 2	Column 3
Number of trays (excluding the reboiler)	18	30	40
Tray efficiency	0.5	0.8	0.55
Feed tray (counted from above)	1	6	30
Pressure drop, bar	0.05	0.1	0.1
Reflux ratio	0	12.5	12.3
Water content in bottom product, kg/h	6599.7	985.18	956.61

Table 2 External heating and cooling demands of the configurations being at different levels of heat integration

Case	**Heating demand [kW]**					**Cooling demand [kW]**							
	Feed preheating	Reboilers			**Total**	Condensers			Column products				**Total**
		QR1	QR2	QR3		QC1	QC2	QC3	B1	D2	S3	B3	
Original case	45.3	1140.0	43.6	960.4	**2189.3**	725.9	37.4	837.4	294.7	0.4	1.4	116.4	**2013.6**
Base case	45.3	1140.0	43.6	963.8	**2192.7**	725.9	37.4	879.9	294.7	0.4	1.1	81.2	**2020.6**
HI-A	35.1	774.6	43.6	963.7	**1817.0**	726.1	37.4	879.8	0.0	0.4	1.1	0.0	**1644.8**
HI-B	45.3	260.0	43.6	963.7	**1312.6**	726.1	37.4	0.0	294.7	0.4	1.1	81.2	**1140.9**
HI-C	0.0	0.0	43.7	963.6	**1007.3**	726.1	37.5	0.0	34.3	0.4	1.1	35.9	**835.3**
HI-C+VRC	0.0	0.0	43.7	145.2	**188.9**	39.4	37.5	0.0	34.3	0.4	1.1	81.2	**193.8**

The original case was modified by reducing the pressure of Column 3 to 1.024 bar and changing the location of withdrawal of S3 to tray 35 to increase the concentration of higher alcohols in the side stream. This increased the ethanol concentration of D3 to 94.34%, although the energy demand QR3 also increased slightly. This case served as basis for the various heat integration schemes: heat integration of the streams only (HI-A), that of Columns 1 and 3 (HI-B) and that of streams and columns (HI-C). The minimum ΔT was set as 10°C. Note that Column 2 is not included in HI schemes due to its low heat duties.

Four streams were considered for HI: F1 and F2 are cold streams C1 and C2 to be heated to 60.6 and 85°C, respectively, while W1 and W3 are hot streams H1 and H2 to be cooled to 30°C. For Case HI-A, by following the pinch method for heat exchanger network design, the minimum heating duty was found to be 35.1 kW and the whole system was above pinch temperature meaning that cooling was not necessary. C1 had to be divided (*Fig. 1*); 80.57% of it was coupled with H1, the rest with H2 previously coupled with C2. Heating energy demand was reduced by 17% compared to the base case, mainly because of the reduction of QR1 due to the preheating of F1.

In Case HI-B, the condenser of Column 3 was coupled with the reboiler of Column 1, drastically reducing its external heat demand. With this single coupling, the heating energy demand of the process was reduced by 40%.

Pinch analysis showed for Case HI-C that only the reboiler of Column 3 was above pinch point and thus needed external heating. The coupling from Case HI-B was also applied here, but preheating reduced QR1 and thus the remaining part of QC3 was used for the heating C1. At the same time, the couplings H1-C1, H2-C2 were applied. Compared to the base case, the heating energy demand was reduced by 54%.

Heating energy demand was reduced even further (91% of base case) by applying a heat pump. The top vapour of Column 1 was compressed to 2.50 bar to heat the reboiler of Column 3. The motor power required was 177 kW.

ACKNOWLEDGEMENTS. The described work was carried out as part of a project supported by the National Research, Development and Innovation Office – NKFIH, K120083.

REFERENCES

[1] F. R. M. Batista, L. A. Follegatti-Romero, L. C. B. A. Bessa, and A. J. A. Meirelles: *Computational simulation applied to the investigation of industrial plants for bioethanol distillation*, Comput. Chem. Eng., 46, 1-16. 2012.

[2] T. Bisgaard, M. Mauricio-Iglesias, J. K. Huusom, K. V. Gernaey, J. Dohrup, M. A. Petersen, and J. Abildskov: *Adding Value to Bioethanol through a Purification Process Revamp*, Ind. Eng. Chem. Res., 56, 5692-5704. 2017.

COMPARISON OF THE DIRECT SHEAR BOX TEST OF TWO AGRICULTURAL GRANULAR MATERIALS

HORVÁTH Dániel, POÓS Tibor PhD, TAMÁS Kornél PhD
Faculty of Mechanical Engineering, Budapest University of Technology and Economics
E-mail: horvath.daniel@mail.bme.hu, poos@mail.bme.hu, tamas.kornel@gt3.bme.hu

Keywords: direct shear box test, hulled millet, fodder corn, discrete element method.

In the soil mechanics studies, direct shear box tests are used to determine the macromechanical properties of different soil samples. The internal friction angle resulting from friction between the particles in an aggregate and e.g. the material's cohesion is created by its moisture content. In the spread of numerical models simulating the behavior of granular material sets, researchers began to apply a wide range of direct shear box devices using solids of larger size and irregular geometry (e.g. maize [1], rapeseed [2], crushed stone [3]) to determine the macromechanical properties with measurements and the micromechanical properties with simulation calibrations. In this research, the measurements of the direct shear box test of two grain cereal crops (one smaller and one larger size) were compared, taking into account their moisture content. As a result of the research, using the discrete element method [4], a proportional number was determined by the direct shear box's length in the shear direction proportional to which the largest size of the applied grains were, thus determining the minimum dimensions of the shear box applicable to the given materials. For the laboratory measurements a 60x60x30 mm direct shear box was used at the Department of Engineering Geology and Geotechnics at Budapest University of Technology and Economics which schematic design is shown in *Figure 1*.

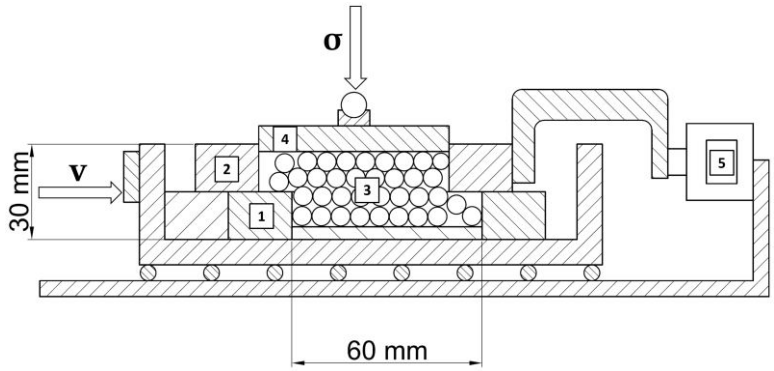

Figure 1 Schematic design of the direct shear box apparatus (1 - Lower shear box, 2 - Upper shear box, 3 - Granular material, 4 - Load plate, 5 - Load cell, σ – Normal stress, v - Shear velocity) [5]

The granular material was loaded into boxes 1 and 2 and then a σ normal stress was applied to the examined particle set from the top by means of a ball bearing. After that, box 1 was moved with a v = 0.02 mm/s velocity in the direction of shear. The shear force applied to the box 2 by the grain set was recorded by the load cell 5. Several normal stresses were used depending on the material and the evaluation to determine the failure envelope of an aggregate was carried out as described in standard MSZE CEN ISO / TS 17892-10 [6]. In this research the measurement results of two different materials were compared. One was the hulled millet which measurement results was presented in past research [7], and the other was the fodder corn. While the former has a spherical geometry with a typical median diameter of d = 1.8 mm, the latter has irregular geometry which can be described with three average dimensions, the length ($\bar{l} = 10.5$ mm), the width ($\bar{w} = 8.5$ mm) and the thickness ($\bar{t} = 5$ mm). The proportional number (ψ) was determined on the basis of the following equation:

$$\psi = \frac{H}{C}$$

Where H = 60 mm is the length of the shear box in the shear direction and C is the largest characteristic size of the particles, in the case of hulled millet $C = d = 1.8$ mm and for fodder corn $C = \bar{l} = 10.5$ mm.
Using the Yade [8] discrete element software, the model of direct shear box and materials were created which can be seen on the left side of *Figure 2*.

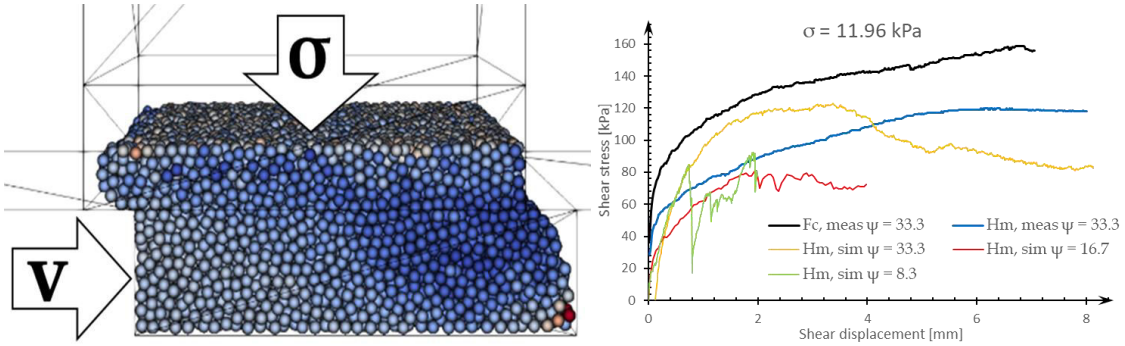

Figure 2 On the left the discrete element model (1:1) [5] and on the right the shear stress – shear displacement diagram for 23.6% moisture content on wet basis hulled millet (Hm) and for 27.1% moisture content fodder corn (Fc) (ψ - proportional number, meas - measured, sim - simulated)

Due to the nature of the task, because of the cohesion which was caused by the moisture content, a frictional-cohesional particle contact model (CohFrictMat [9]) was utilized to describe collisions and cohesive contacts between particles. After the validation of the discrete element model, in the case of hulled millet the size of the shear box was reduced, simulations were made and the proportional numbers were calculated. The resulted shear stresses - shear displacements were compared which can be seen on the right side of *Figure 2*. As a conclusion, it can be stated that changing the size of the shear box won't produce the same results as the 1:1 size. In further research the size of the particles should be changed and their material parameters should be recalibrated.

ACKNOWLEDGMENTS

This work was supported by Gedeon Richter's Talentum Foundation 19-21. Gyömrői street. 1103. Budapest. Hungary) and the Higher Education Excellence Program of the Ministry of Human Capacities in the frame of Water science & Disaster Prevention research area of Budapest University of Technology and Economics (BME FIKP-VÍZ). Special thanks to the Deparment of Engineering Geology and Geotechnics at BME for the support in the experiments.

REFERENCES

[1] C. J. Coetzee and D. N. J. Els: *Calibration of discrete element parameters and the modelling of silo discharge and bucket filling*, Comput. Electron. Agric., vol. 65, no. 2, pp. 198–212, Mar. 2009.

[2] K. Tamás, B. Földesi, J. P. Rádics, I. J. Jóri, L. Fenyvesi: *A Simulation Model for Determining the Mechanical Properties of Rapeseed using the Discrete Element Method*, Period. Polytech. Civ. Eng., vol. 59, no. 4, pp. 575–582, Oct. 2015.

[3] H. Huang, E. Tutumluer: *Discrete Element Modeling for fouled railroad ballast*, Constr. Build. Mater., vol. 25, no. 8, pp. 3306–3312, 2011.

[4] P. A. Cundall, O. D. L. Strack: *Discrete numerical model for granular assemblies*, Geotechnique, vol. 29, no. 1, pp. 47–65, Mar. 1979.

[5] D. Horváth: *Szemcsés anyaghalmaz műveleti paramétereinek modellezése diszkrételemes módszer alkalmazásával (Modeling of granular materials using discrete element method),* Master's thesis, Budapest University of Technology and Economics, Budapest, Hungary, 2018.

[6] *MSZ EN 12047:1998 standard: Solid fertilizers. Measurement of static angle of repose (ISO 8398:1989 modified)* 1998.

[7] T. Poós, D. Horváth, K. Tamás: *Modeling the movement of the granular material in a static equipment with discrete element method*, in Proceedings of the 5th International Scientific Conference on Advances in Mechanical Engineering (ISCAME 2017), Debrecen, Hungary, pp. 418–421. 2017.

[8] V. Šmilauer et al.: *Dem formulation. In Yade Documentation 2nd ed*., Yade Proj., p. 37, 2015.

[9] F. Bourrier, F. Kneib, B. Chareyre, T. Fourcaud: *Discrete modeling of granular soils reinforcement by plant roots,* Ecol. Eng., vol. 61, no. Part C, pp. 646–657, 2013.

DEPENDENCE OF MECHANICAL AND ELECTRICAL PROPERTIES OF SILVER NANOCUBES IMPREGNATED BACTERIAL CELLULOSE-SILK FIBROIN-POLYVINYL ALCOHOL FILMS ON LIGHT EXPOSURE

[1]HOSAKUN Worakan, [1]HOSAKUN Yanin PhD, [2]DUDIĆ Duško PhD, [2]DJOKOVIĆ Vladimir PhD, [1]CSÓKA Levente DSc
[1]Macromolecular Materials and Technology Research Group, University of Sopron
E-mail: worakan.hosakun@gmail.com, levente.csoka@skk.nyme.hu
[2]Vinča Institute of Nuclear Sciences, University of Belgrade

Keywords: bacterial cellulose, silver nanocubes, mechanical properties, electrical properties, flexible transparent film, light exposure

In recent years, the new transparent materials with good flexibility and high dimensional stability have been strong interest in development. A large number of materials are presently being investigated due to their possible application in flexible display technology [1,2]. Flexible and transparent substrate materials were fabricated by using bacterial cellulose (BC), silk fibroin protein (SF) and/or polyvinyl alcohol (PVA). The ten samples were prepared; BC-PVA, SF-PVA, pure PVA, BC-SF, and BC-SF-PVA films which obtained were further modified by impregnation with silver nanocubes (AgNC). Firstly, the field emission scanning electron microscope (FESEM) images were obtained as shown in Figure 1a and 1b. The surface structure of the BC-SF is characterized by a 3-D fibrous ultrafine network of well-arranged nanofibrils, stabilized by hydrogen bonds in PVA matrix. The isolated silver nanocubes with identical side lengths were presented. The influences of the silver nanocubes and white light illumination on the electric and viscoelastic properties of the films were investigated. Complex conductivity measurements showed that the films with PVA component are more sensitive to light exposure and there is an increase in conductance when the sample is illuminated. The films that contained silver nanocubes showed higher values of specific susceptance than their unmodified counterparts. DMA analyses revealed that the storage shear moduli of the films increase with addition of silver nanocubes. It was also found that the relaxation transition observed at elevated temperatures in the BC-SF-PVA-AgNC films is highly sensitive to the light exposure as shown in Figure 2a and 2b. Above the glass transition of PVA, both storage- and loss-shear moduli change dramatically if the sample is illuminated during the measurements with respect to the case when it was kept in the dark. Furthermore, differential scanning calorimetry (DSC), the thermogravimetric analysis (TGA) and derivative thermogravimetric (DTG) were observed for analyzing thermal properties. It was found that BC-SF-PVA-AgNC film has highly crosslink structure due to the absence of glass transition temperature. All samples have great thermal stability up to 265°C.

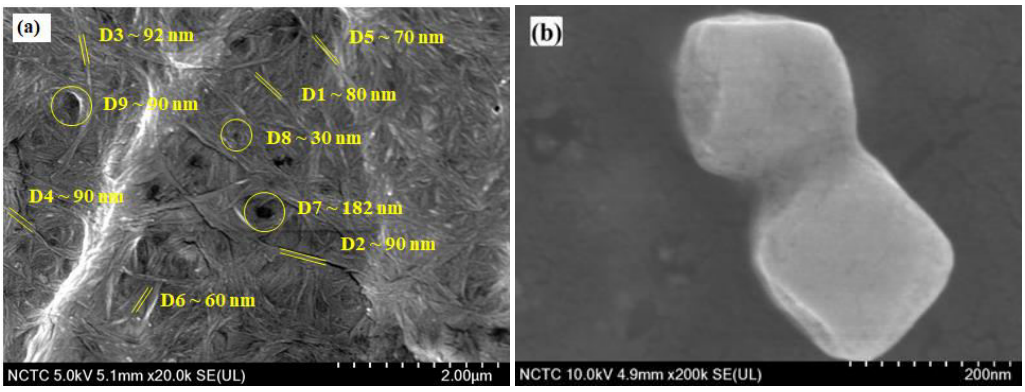

Figure 1 FE-SEM micrographs of a) BS-SF-PVA film, b) silver nanocubes.

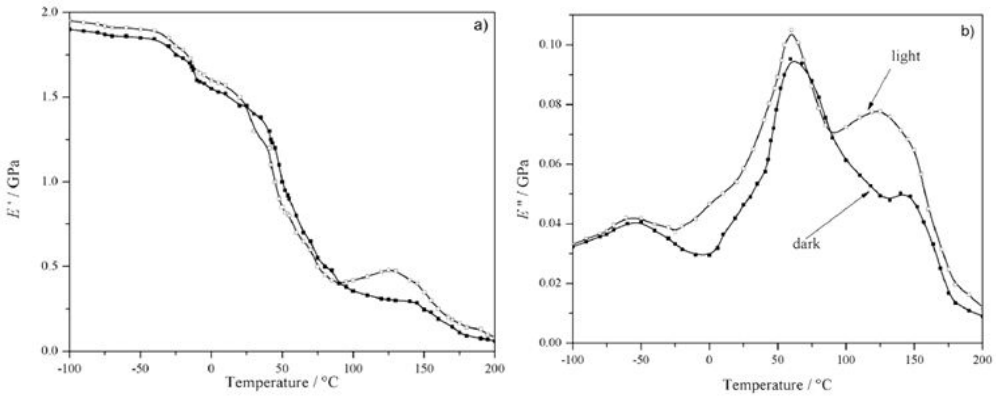

Figure 2 a) Storage and b) loss shear moduli of the BC-SF-PVA-AgNC (S7) film recorded in dark (full symbols) and under the white light illumination (open symbols). The frequency of the external force was 1 Hz.

Table 1 Realtive changes of specific conductance (ΔG) and susceptance (ΔB) of the films induced by illumination. Sample 7: BC-SF-PVA-AgNC, Sample 8: BC-SF, Sample 9: BC-SF-AgNC, Sample 10: BC-SF-PVA.

Frequency (kHz)	ΔG7	ΔB7	ΔG8	ΔB8	ΔG9	ΔB9	ΔG10	ΔB10
7	0.1	0.85	0.1	-0.3	1.5	1	1.1	2
22	0.02	1.04	-0.37	-0.32	0.96	0.78	2.1	1.7
70	0.25	1.3	-0.42	0.1	1	1.6	1.9	1.4
200	0.57	0.7	-0.15	0.25	1.1	1.1	1.8	1.2

ACKNOWLEDGMENTS

The authors would like to acknowledge the Human Resource Development Programme (HRDOP 3.6.1-16-2016-00018) "Improving the role of research + development + innovation in the higher education through institutional developments assisting intelligent specialization in Sopron and Szombathely" at University of West Hungary. This work was supported in part by the Ministry of Education, Science and Technological Development of the Republic of Serbia (Project Nos. 171029, 172056, and 45020).

REFERENCES

[1] J. Park, S. Heo, K. Park, M.H. Song, J.Y. Kim, G. Kyung, R.S. Ruoff, J.U. Park,F. Bien: *Research on flexible display at Ulsan national institute of science andtechnology,* Npj Flexible Electron 1 Article ID: 9. 2017.

[2] M. Aleksandrova*: Specifics and challenges to flexible organic light-emitting devices*,Ann. Mater. Sci. Eng. 4081697(8 pp). 2016.

BOUNDARY VALUE PROBLEM FOR A HEATED NANOFLUID FLOW IN THE PRESENCE OF MAGNETIC FIELD

HRICZÓ Krisztián PhD
Institute of Mathematics, University of Miskolc
E-mail: mathk@uni-miskolc.hu

Keywords: boundary layer flow, ferrofluid, magnetic field, similarity analysis.

The aim of this presentation is to introduce some new results on the magneto-thermomechanical interaction between heated viscous incompressible magnetic nanofluid and a cold wall in the presence of a spatially varying field.
Ferrofluids are an important smart material, synthesized by introducing ferromagnetic nanoparticles in a suitable non-magnetic carrier liquid. Scientists have been fascinated by the usage of magnetic fluids for many decades. We can observe a few applications in electrical instruments used commercially so like the hard disks, rotating X-ray tubes, shafts and rods etc. These liquids able to appear in sensors, densimeters, accelerometer or use as heat controlling agent in electric motors and hi-fi speaker, moreover in medical sciences alternating magnetic fluids can be applied to treat cancer and tumor [Zeeshan at al. (2016)].
Consider a two-dimensional steady flow of a viscous, electrically nonconducting and incompressible nanofluid, which involves ferromagnetic (e.g. magnetite) particles over a flat surface in the horizontal direction seen in Figure 1.

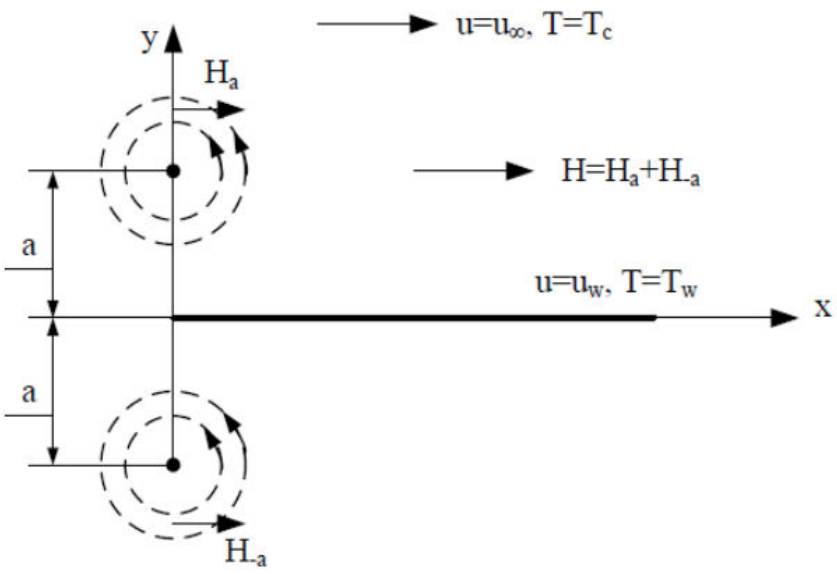

Figure 1 Parallel flow along a flat surface in magnetic field

The two magnetic dipoles are equidistant a from the leading edge. The filed is due to two-line currents perpendicular to and directed out of the flow plane.
The following four assumptions ensure the existence of our mathematical model [originat from Neuringer (1966)]:
(i) the applied field is of sufficient strength to saturate the ferrofluid everywhere inside the boundary layer,
(ii) within the temperature extremes experienced by the fluid, the variation of magnetization with temperature can be approximated by a linear equation of state, the dependence of M on the temperature T is described by $M = K(T_C - T)$, where K is the pyromagnetic coefficient and T_c denotes the Curie temperature as proposed in [Amirat and Hamdache (2012)].
(iii) the induced field resulting from the induced magnetization compared to the applied field is neglected; hence, the uncoupling of the ferrohydrodynamic equations from the electromagnetic equations and
(iv) in the temperature range to be considered, the thermal heat capacity c, the thermal conductivity k, and the coefficient of viscosity ν are independent of temperature.

The boundary layer equations for a two-dimensional and incompressible flow are based on expressing the conservation of mass, continuity, momentum and energy.
The governing equations are described as follows

$$\frac{\partial u}{\partial x}+\frac{\partial v}{\partial y}=0$$

$$u\frac{\partial u}{\partial x}+v\frac{\partial u}{\partial y}=-\frac{I_0\mu_0 k}{\pi\rho}(T_C-T)\frac{1}{x^2}+\nu\frac{\partial^2 u}{\partial y^2}$$

$$c\left[u\frac{\partial T}{\partial x}+v\frac{\partial T}{\partial y}\right]=k\frac{\partial^2 T}{\partial y^2}$$

where u and v are the parallel and normal velocity components to the plate, the x and y axes are taken parallel and perpendicular to the plate, respectively, ν is the kinematic viscosity and ρ denotes the density of the ambient fluid, which will be assumed constant. The system has the following boundary conditions at the surface (y = 0)

$$u(x,0)=0, v(x,0)=0, T(x,0)=T_w$$

with $T_w=T_C-Ax^{m+1}$ and

$$u(x,y)\to u_\infty, T(x,y)\to T_\infty$$

as y leaves the boundary layer $(y\to\infty)$ with $T_\infty=T_c$, and u_∞ is the exterior streaming speed which is assumed throughout the paper to be $u_\infty=\mathrm{U}_\infty \mathrm{x}^{\mathrm{m}}$ (U_∞ = const.). Parameter m is relating to the power law exponent. The values of parameter m are between -1 and 1, what refers to the temperature profile and exterior streaming speed.
One of the known ways to examine the solutions of the boundary value problem of the partial differential equations system, is the similarity analysis.
Similarity transformation is applied to convert the governing nonlinear boundary layer equations into coupled nonlinear ordinary differential equations. After than this system is solvable numerically for example using higher derivative method. The effects of governing parameters corresponding to various physical conditions are investigated. Numerical results are represented for the distributions of velocity and temperature, for the dimensionless wall skin friction and for heat transfer coefficients. Our results show excellent agreement with previous studies in special cases (depend on the values of parameters) and obtained a new solution in some other cases.

ACKNOWLEDGMENTS
Project no. 129257 has been implemented with the support provided from the National Research, Development and Innovation Fund of Hungary, financed under the *K_18* funding scheme.

THE INVESTIGATION OF THE PROPERTIES OF DIFFERENT FOUNDRY SANDS

HUDÁK Henrietta, VARGA László PhD
Faculty of Materials Science and Engineering, University of Miskolc
E-mail: ontheni@uni-miskolc.hu, laszlo.varga.mak@gmail.com, ontvlaci@uni-miskolc.hu

Keywords: foundry sand, quartz sand, specific surface, surface roughness.

The foundry moulds and sand cores are generally composed of 3 main components, which are: refractory, particulate material, which is always sand; binder, that holds together the sand particles, this can be organic or inorganic bonded; additive, which makes more preferential properties. Quartz sand is the most frequently applied type of foundry sands. Quartz sand is found in the nature in varying purity and is traded in varying quality for different industrial applications. The quality of castings produced depends largely upon the properties of the quartz sand utilized. A foundry mould must have the ability to withstand the high temperature of molten metal without damaging the contact surface between metal and sand. To ensure high quality castings the quartz sand must satisfy specifications such as permeability, grain fineness, moisture, bond strength and refractoriness. Smooth-surfaced and rounded sand are more suitable for binders because sand has small surface therethrough minimal binder consumption needed.

In this research we were used 4 different type of quartz sands and an artificial sand made of mullite crystals for our tests.

GBM 45 sand

SH 33 sand

H 33 sand

F35 sand

Kerabasic sand

Figure 1 Stereo microscopy image of foundry sands (N=10x and N=50x)

The comparative measurement of 5 different foundry sands were carried out.

Table 1 Measurement data of the investigated sands

	GBM 45	SH 33	H 33	F 35	Kerabasic
Average granularity (d_{50})	0,303 *mm*	0,333 *mm*	0,285 *mm*	0,226 *mm*	0,241 *mm*
AFS granularity number	61,7	51,9	60	81,6	73,3
Homogeneity degree	44 %	58 %	66 %	54 %	60 %
Angularity coefficient of sand	1,14	1,24	1,78	1,37	1,02
Specific surface (A_{BLAINE})	90 cm^2/g	110 cm^2/g	185 cm^2/g	195 cm^2/g	130 cm^2/g
Specific surface (A_{BET})	0,520 m^2/g	0,090 m^2/g	0,039 m^2/g	0,082 m^2/g	0,040 m^2/g

We compared two types of determination of the specific surface. Correlation between BET and the Blaine methods was not found to be excellent. The surface area of the sand as determined by BET method are presented in Table 1. In all cases the measured specific surface area by the BET method is higher than the one measured by Blaine. The difference between the surface areas measured by Blaine and BET could be attributed to the porosity and surface roughness of the particles. BET surface area is determined by the monolayer coverage of the exposed (pores and cracks included) surface of the particles by nitrogen molecules. If the particles are porous (including multi-particle agglomerates), or have a rough surface structure, the BET surface area will be greater than the Blaine surface area.

REFERENCES

[1] K. Löchte: *Working with the Cold Box Process in the Coremaking Department of a Foundry*. - Internet, 1998.
[2] V. Bechný: *Zukünftige Herausforderungen an Gießereisande*. - Giesserei-Rundschau, 2012 ¾. p.81-83. 2012.
[3] F. Iden, W. Tilch, H. J. Wojtas*: Die Haftungsmechanismen von Cold-Box-Bindemitteln auf der Formstoffoberfläche*. - Giesserei, 2011/5. p.24-36. 2011.
[4] F. Iden, U. Pohlmann, W. Tilch, H. J. Wojtas: *Strukturen von Cold-Box-Bindersystemen und die Möglichkeit ihrer Veränderung*. - Giesserei Rundschau, 2011 ½. p.3-8.
[5] http://giba.at/pdf/giba-de.pdf
[6] C. Ferraris, E. Garboczi: *Identifying improved standardized tests for measuring cement 2 particle size and surface area* - http://onlinepubs.trb.org/onlinepubs/nchrp/nchrp_rrd_382.pdf, 2012.

COMPARISON OF THE HYPERELASTIC MATERIAL MODELS IN THE FINITE ELEMENT INVESTIGATIONS OF RUBBER PARTS

HURI Dávid, MANKOVITS Tamás PhD
Department of Mechanical Engineering, University of Debrecen
E-mail: huri.david@eng.unideb.hu, tamas.mankovits@eng.unideb.hu
https://orcid.org/0000-0002-4782-1610

Keywords: finite element, Mooney-Rivlin material model, Yeoh material model, mesh design

In rubber product design finite element analysis is widely used. The investigated product is a rubber jounce which serves as a secondary spring in the air spring of the lorries. The operation circumstances need large deformations and under these conditions the rubber shows highly nonlinear material properties. In many cases the rubber product must fulfill customer needs. This predetermined special requirements led the study to geometry parameter based shape optimization. In this case the goal functions are usually complex functions evaluated using numerical models. The aim of this research is to elaborate a FEM model which is accurate and competitive for future shape optimization task. For this purpose the influence of the mesh locking problem and the choose of appropriate hyperelastic material model was investigated.
The exact mixture of the rubber material is unknown, therefore measurements on the base material are needed to determine the material constants used for finite element analysis. The main load of the rubber jounce is pressure so at least a simple compression test is required on a rubber specimen. Rubber behave as a nonlinear, elastic, isotropic and incompressible material, which can be described accurately with hyperelastic constitutive model. Within this several material models and material constants can be found. A successful finite element simulation of rubber parts hinges on the selection of an appropriate strain energy function and on the accurate determination of material constants. Because of material incompressibility, the strain energy function can be divided

$$W = W_D(\bar{I}_1, \bar{I}_2) + W_b(J)$$

where $W_b(J)$ denotes the volumetric terms of the strain energy function and J is for the Jacobian and $W_D(\bar{I}_1, \bar{I}_2)$is for the deviatoric terms of the strain energy function. The polynomial form of the strain energy potential is based on the first $\bar{I}_1$ and second $\bar{I}_2$ strain invariants of the right Cauchy-Green tensor

$$W = \sum_{i+j=1}^{N} c_{ij}(\bar{I}_1 - 3)^i(\bar{I}_2 - 3)^j + \sum_{k=1}^{N} \frac{1}{d_k}(J-1)^{2k}$$

where determination of c_{ij} and d_k material constants are required in material model. Mooney-Rivlin, Yeoh and Neo-Hookean material models are available within the polynomial form of the strain energy potential. The equation above with $N = 1$ substitution was applied because of the measured engineering stress-strain curve hasn't got inflection point.

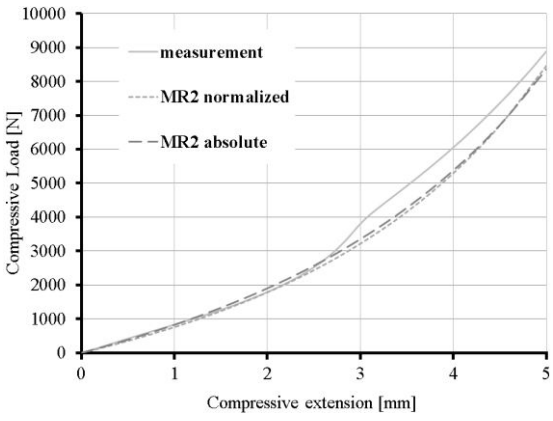

Figure 1 Finite element results using two-term Mooney-Rivlin material models

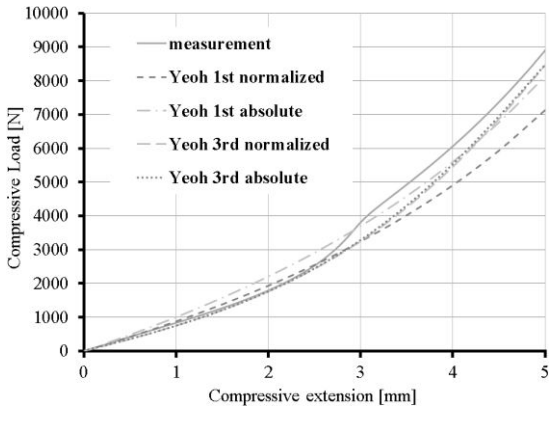

Figure 2 Finite element results using Yeoh material models

Curve fitting method was used for determining the material properties which are fitted to more hyperelastic material models. The determined models were used for the finite element analysis of the specimen and the exactness of parameters was compared with experimental data. First, the two term Mooney-Rivlin material model was analyzed and its results can be seen in *Figure 1*. The results show proper matching with the measured data until the middle of the whole deformation, then difference can be found but it can be accepted for rubber products. The cause of the difference was the friction which cannot be eliminated from the measurement process despite of lubrication, thereby an abnormal behavior can be seen in the middle range of the measured curves. This behavior cannot be modelled by finite element analysis, as the finite element model represented a frictionless boundary conditions.
Yeoh one- and three term material model was used for finite element analysis in *Figure 2*, and it was stated that we got more exact results in case of Yeoh material model if three term form is used. Sum of the squared differences (SSE) between each points of the run analysis results and the measured points was used to determine the material models goodness. Both models can be recommended for the future investigations of rubber jounce. However, considering the evaluated SSE error quantities, the three term Yeoh material model with the use of absolute error calculation for curve fitting process shows the best fit.

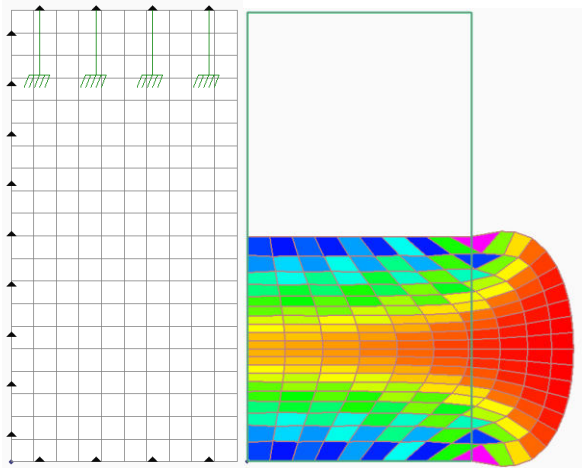

Figure 3 Deformation state of a rubber bumper with the use of quadrilateral elements for meshing

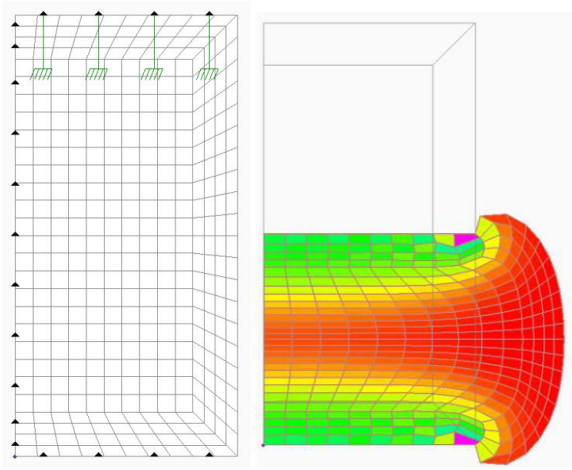

Figure 4 Deformation state of a rubber bumper with the use of quadrilateral elements and mesh design

Mesh locking problem of incompressible materials occured in case of large deformations. It can be analyzed with the investigation of the volume change of the element and with the sress distribution where local stress increasing can be seen in the locked elements. For large deformations higher order element need to be applied, therefore the finite element mesh was generated with the use of quadrilateral elements instead of the triangular elements. Despite of the higher order elements the mesh locking problem was still an existing problem. The *Figure 4* shows a solution for special meshing process due to this process the distortion of elements can be reduced compared with the *Figure 3*. It can be stated that with the use of mesh design the locking effect of quadrilateral elements can be reduced and as a result the deformation will be reasonable and there will be a reliable analysis running.

ACKNOWLEDGMENTS
The described work was carried out as part of a project supported by the EFOP-3.6.1-16-2016-00022 project. The project is cofinanced by the European Union and the European Social Fund. This research is partly supported by the ÚNKP-18-3 New National Excellence Program of the Ministry of Human Capacities.

NUMERICAL MODEL ANALYSIS OF NATURAL GAS COMBUSTION BURNERS

IBRAHEEM Amjd, SZODRAI Ferenc PhD
Faculty of Engineering, University of Debrecen
E-mail: amjdibraheem@gmail.com, szodrai@eng.unideb.hu

Keywords: combustion, boiler, burner, efficiency, CFD, Fluent

One of the most vital energy source and commonly used fuel for combustion process is natural gas. Which is considered now one of the main used fuel type in Europe. The ratios of the component in the natural gas can fluctuate, modeling the combustion process with different gas combinations and under various circumstances, can save us a lot of cost and time. Ansys Fluent 19.1 Academic version was used for the modelling, the mesh was built from 10^{-3} m large tetrahedrons, due to high velocity no inflation layer was applied. The energy equation and k-ε turbulence for the viscosity model was used, the air amount was calculated by dividing the oxygen amount consumed in the combustion process for 1 kg of fuel by the oxygen fraction of air, oxygen amount was defined from the chemical equations under stoichiometry, equivalence ratio $\Phi = 1$, and then the air–fuel ratio (AFR) [kg kg^{-1}] was calculated. The lower heating value was used to calculate the fuel mass flow (m_{fuel}) [kg s^{-1}] as the mass flow equals the power divided by the lower heating value, then and depending on the AFR the air mass (m_{air}) [kg s^{-1}] flow that was defined in equation 1.

$$AFR = m_{air} \cdot m_{fuel}^{-1}$$

In our case, the examined natural gas fuel contained methane as the main component besides carbon dioxide, nitrogen, ethane, propane, butane, and pentane. The detailed molar distribution can be seen in table 1.

Table 1 Used fuel composition

Carbon dioxide	Nitrogen	Methane	Ethane	Propane
1.1693 $_{mol}$%	0.9073 $_{mol}$%	94.3394 $_{mol}$%	2.7731 $_{mol}$%	0.8109 $_{mol}$%

The research started with a standard gas can combustor with a primary air inlet and fuel inlet and secondary air inlet as 75 $_{v}$% of air coming from the main inlet and 25 $_{v}$% from the secondary inlet:

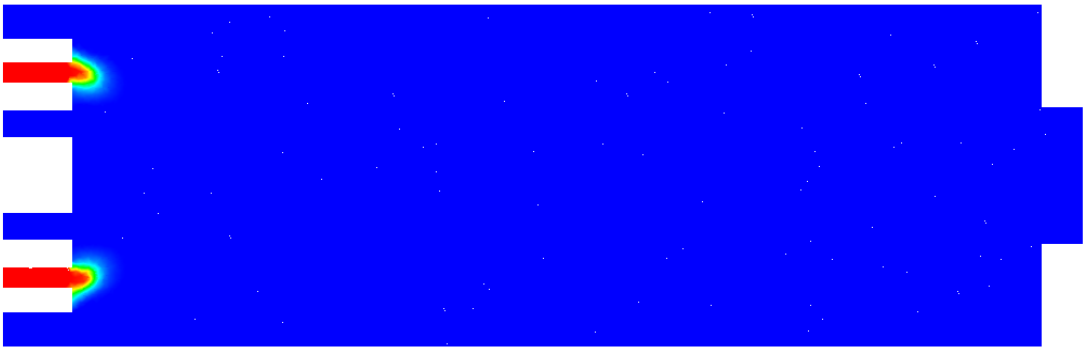

Figure 1 CH_4 volume fractions (colour code: red 100 $_{v}$%, blue 0 $_{v}$%)

From figure 2. it can be seen that the complete combustion happened, the CH_4 formation that was indicated with red color was consumed during the combustion. While it is observable in figure 2. that the fuel was converted into CO_2 during the process.

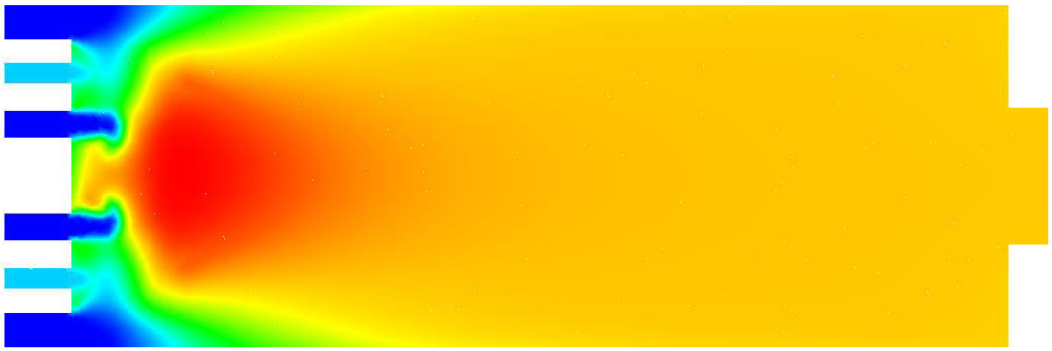

Figure 2 CO_2 volume fractions (colour code: red 11 $_v$%, blue 0 $_v$%)

For further calculation, the temperature distribution (figure 3.) can help us to optimize the boiler geometry and to make a more effective heat transfer surface.

Figure 3 Temperature distribution (colour code: red 2440 K, blue 388 K)

With the presented method, we were able to simulate a multi-species, complete combustion in ANSYS Fluent 19.1. Academic version. The simulation showed good convergence. Our further measurement goal to create a more precise geometry model of the AKH 7500M boiler. With measured gas composition and emissions, the emissions error can be calculated and by developing a finer model this error can be reduced. With good converging models it will be easier to design effective gas burners and with that, the CO_2 emissions can be reduced.

DETERMINATION OF DIFFERENT PARAMETERS OF HIGH STRENGTH STEEL CLINCH JOINTS BY FEA

JÓNÁS Szabolcs, TISZA Miklós DSc
Institute of Materials Science and Technology, University of Miskolc
E-mail: szabolcs.jonas@gmail.com, miklos.tisza@uni-miskolc.hu

Keywords: clinch joint, dual phase (DP) steels, mechanical joining, FEA

These joints are used mostly in automotive, computer and aircraft industries, but for instance according to the standards they are not allowed to be used in food industry. The clinch joints are quite new types of joints, the first patent was accepted in 1989. This type of joint can be done between 2-3 thin sheets. These joints can be comparable with spot welded joints. In the point of view of fatigue strength the clinched joints have longer life span. The static strength is usually lower that of the spot welded joints (~60 %). The cross section of a joint can be seen in *Figure 1*, which shows the main geometrical parameters of a joint (2 sheets were joined). The undercut size (C value) and the neck thickness (t_N value) are highly affecting the strength of the joints. In optimal case both of them are as high as it is possible. The material of the sheets can be ferrous or non-ferrous at the same time, so this joint can realize dissimilar joints without any added material (weld material or glue). The joint is made by metal plastic forming by a special tool. After creating the patent the increasing industrial needs of these types of joints led the researchers to analyse the joints much more deeply. Several studies have been carried out concerning the geometry optimization of the clinching tool to achieve better joints by different optimization methods. Other studies were carried out on the so-called hybrid joints. These joints have an adhesive layer between the sheets. These joints have higher strength but they need much more time because the drying of the adhesive layer is a time-consuming process. In this article different DP steels were analysed by FEA. The simulations were done in ANSYS Workbench 18.2. The goal is to determine their geometrical properties. After the simulation of the three different DP steels the results were analysed and compared to each other. As it can be seen in the *Figure* 2 the forming force is increasing to the effect of the increasing strength. The displacement is equal in each case. The difference between the DP 600 and the DP 1000 is around 10 kN in forming force. This observation is important because of the point of view of the clinching tool's load bearing capacity. Before testing, a fast prediction can save the tool save the tool against failure.

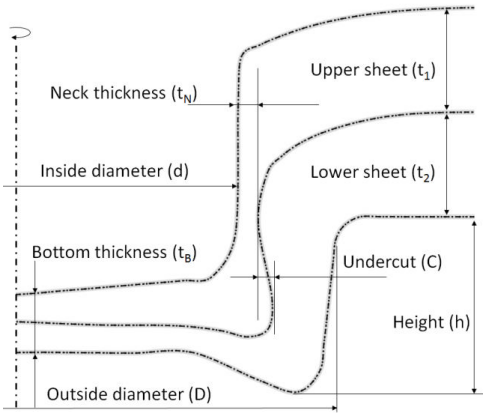

Figure 1 Cross section of a clinched joint and its main geometrical sizes

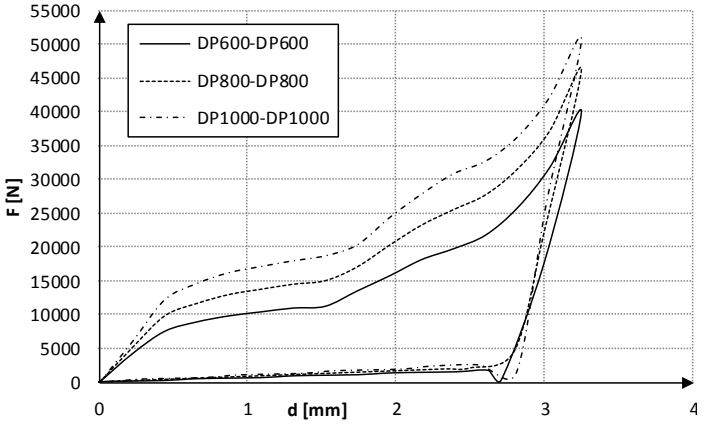

Figure 2 Comparison of the forming force-relative punching tool displacements in case of different steels

From the results the geometrical values were determined. The C value is decreasing with increasing the strength, the t_N is almost constant, due to the spring back effect; the t_B value is increasing with the strength and the height of the protrusion is decreasing. The *Figure* 3 shows the results in graphical way. The residual bottom thickness is highly dependent on the spring back effect. The spring back effect also has affected the undercut values. The neck thickness highly depends on the undercut values are important values for the joint strength prediction. basic equations take only the neck thickness into consideration. the neck thickness; which is almost constant, but the undercut size and angle of the undercut are also important parameters. The effect of shape locking is getting higher with the increasing undercut.

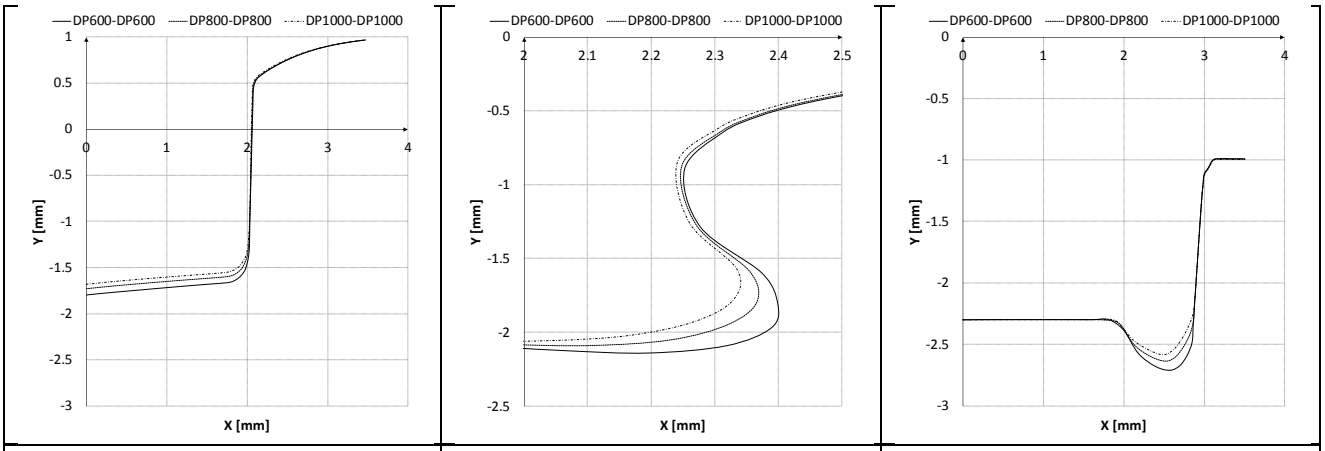

a) Spring back effect on punch side

b) Undercut (C) sizes

c) Height of the protrusion

Figure 3 Results of the simulations

From the results relationships can be derived (*Figure* 4). The C and t_B values according to the simulations are linear function of the R_m. The t_N is almost constant. The h value is a quadratic function of the ultimate strength. The R^2 values are close to 1, which means the regression function has a good fit to the results. The derived equations can be used to predict the geometrical values of other type of DP steels.

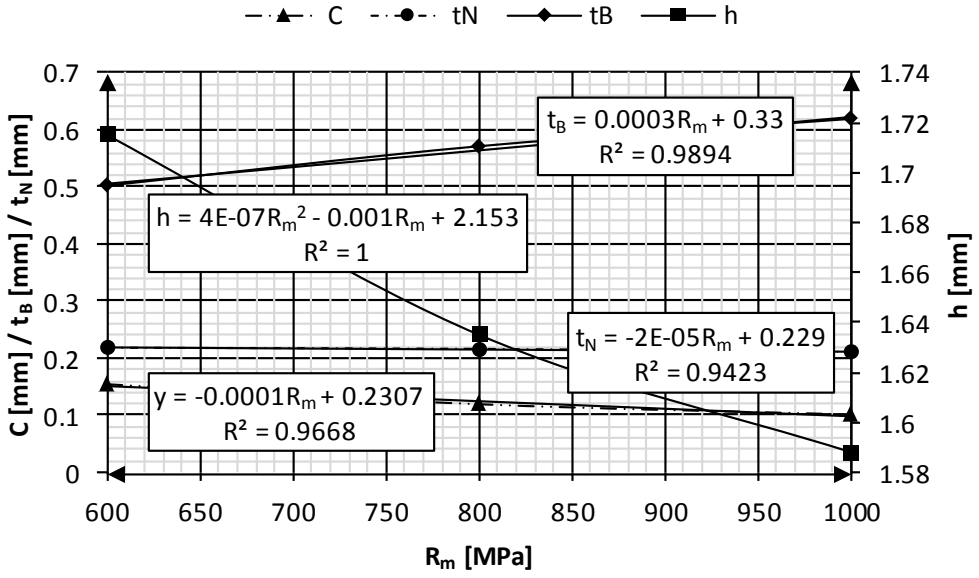

Figure 4 Relationship between the UTS and geometrical properties

CONCLUSIONS

Different strength DP steels were analysed by a 2D asymmetrical FEA model. From the results the geometrical properties of the clinched joints were determined. The article provides some equations to predict geometrical parameters of DP steels. From the predicted values with analytical formulas the strength of the joints can be predicted also. Further investigations are needed to apply the formulas to different types of steel or other types of materials. Tests are also needed to validate the results.

SURFACE ACTIVATION OF HIGH IMPACT POLYSTYRENE SUBSTRATE USING DYNAMIC ATMOSPHERIC PRESSURE PLASMA

JUHÁSZ Gergely, BERCZELI Miklós, WELTSCH Zoltán PhD
GAMF Faculty of Engineering and Computer Science, John Von Neumann University
E-mail: gregoryshepard.95@gmail.com

Keywords: Adhesive, Surface treatment, Surface tension, Wetting, Plasma

Over the last decade, the number of researches has increased in the field of bonding technologies. Researchers attempt to improve surface adhesion properties by surface treatments. Adhesive bonding is one of these bonding techniques, where it is important to see what surfaces will be bonded. One such surface property is wetting, which can be improved by several types of surface treatment. In recent years, atmospheric pressure plasmas have appeared, with which research is ongoing on surface treatments. In our research, we will deal with the effects of plasma surface treatment at atmospheric pressure and its measurement. In addition, we summarize the theoretical background of adhesion, surface tension and surface treatment with atmospheric pressure plasma. Our goal is to improve adhesion properties and thus the adhesion quality.
As material we used high impact polystyrene in a form of a sheet which thickness was 5 mm. The sheet table was cut to 25 mm wide and 55 mm long samples. The polymer sheet had a tear able film layer that protected the surface, so we did not need to clean the surface before the surface treatment. We used different parameters for the surface treatment. The parameters that we changed was the speed of the treatment and the distance between the substrate and the plasma jet. After the treatment we used static contact angle measurement. We used two liquid for the contact angle measurement which was distilled water and ethylene glycol. On the untreated samples we measured approximately 88° with water and approximately 63° with ethylene glycol as seen on Figure 1.

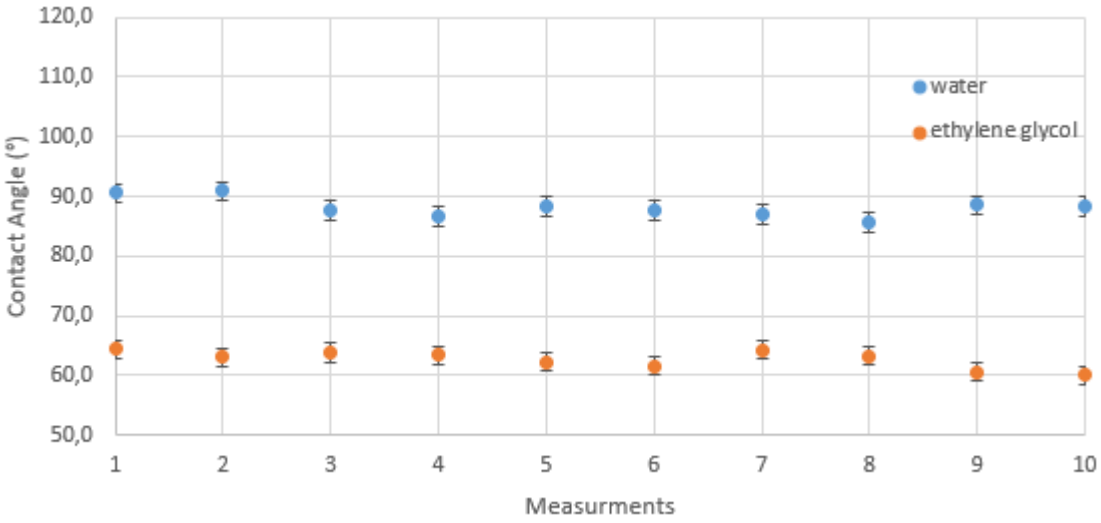

Figure 1 Contact angles on the untreated samples

After the surface treatment the contact angles decreased drastically as seen on Figure 2 and Figure 3.

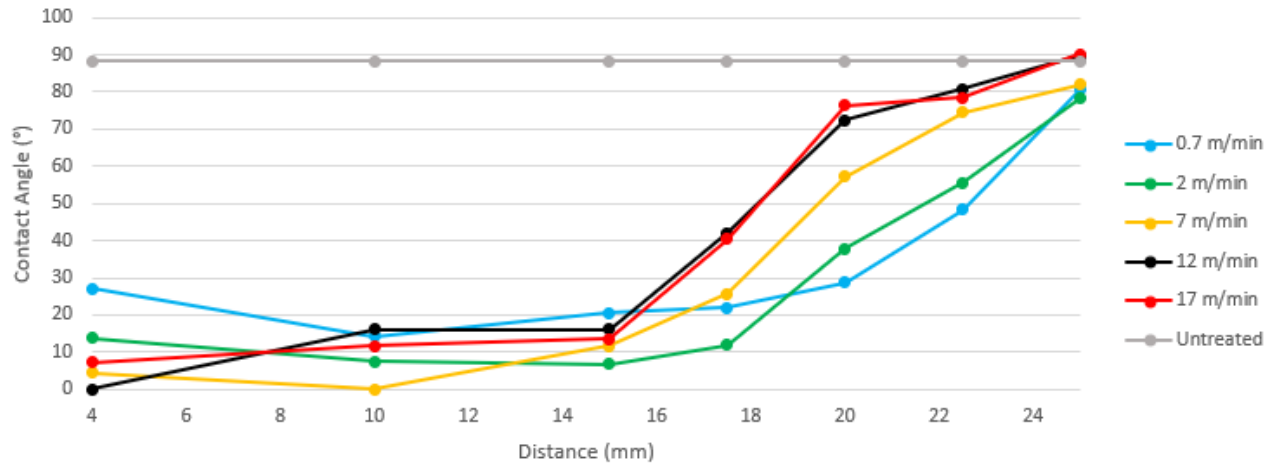

Figure 2 Measured contact angles of the treated samples with water

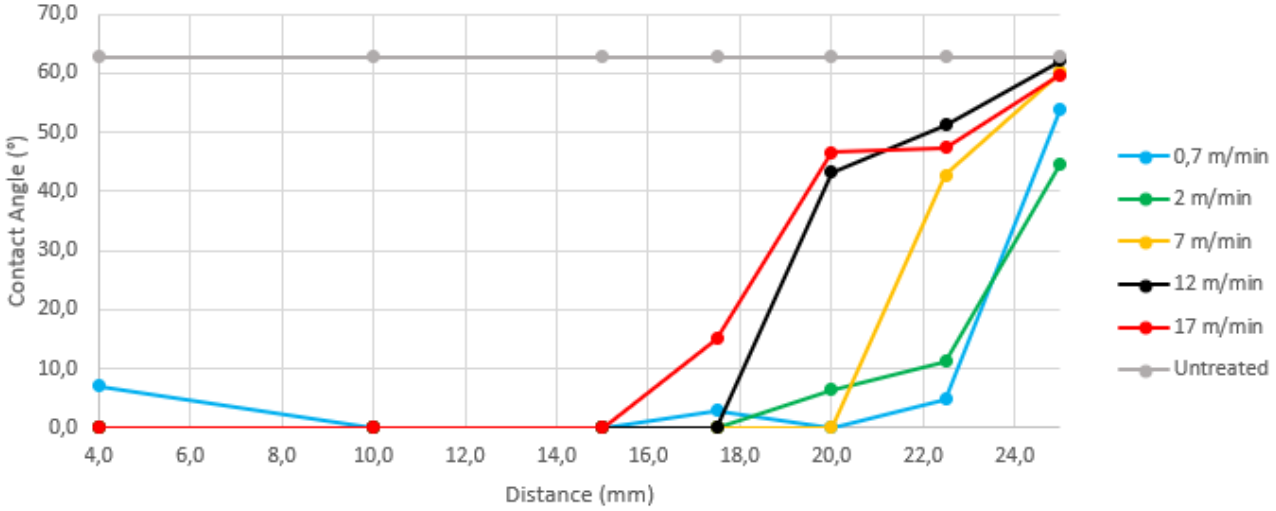

Figure 3 Measured contact angles of the treated samples with ethylene glycol

Based on these results the atmospheric pressure plasmas can improve the wetting of the solid substrate if we use the proper parameters and technique.

ACKNOWLEDGMENTS
This research was supported by EFOP-3.6.1-16-2016-00006 "The development and enhancement of the research potential at John von Neumann University" project. The Project is supported by the Hungarian Government and co-financed by the European Social Fund. Furthermore

KINEMATICS AND CONTROL OF A PLANAR CABLE ROBOT

KAPITÁNY Pálma, LÉNÁRT József
Robert Bosch Department of Mechatronics, University of Miskolc
E-mail:kapitanypalma@gmail.com, lenart.jozsef@uni-miskolc.hu

Keywords: inverted pendulum, LQR controlling, feedback

This paper deals with the kinematics of a planar cable robot [1], which is driven by four DC motors with gear. Cable robots are frequently used e.g., for the motion of cams in sport halls and stadiums and also in high storage logistical systems [2]. Main goal of this research work is to design and build a test bench with low budget, which can model the motion of real life cable robots.
The test bench of the cable robot is shown in Figure 1a. Four DC motors are mounted on the black corner plates of the rectangle frame structure, and a blue disk is hold and positioned by four tight cables connected to the axes of the motors M_1, M_2, M_3, M_4.

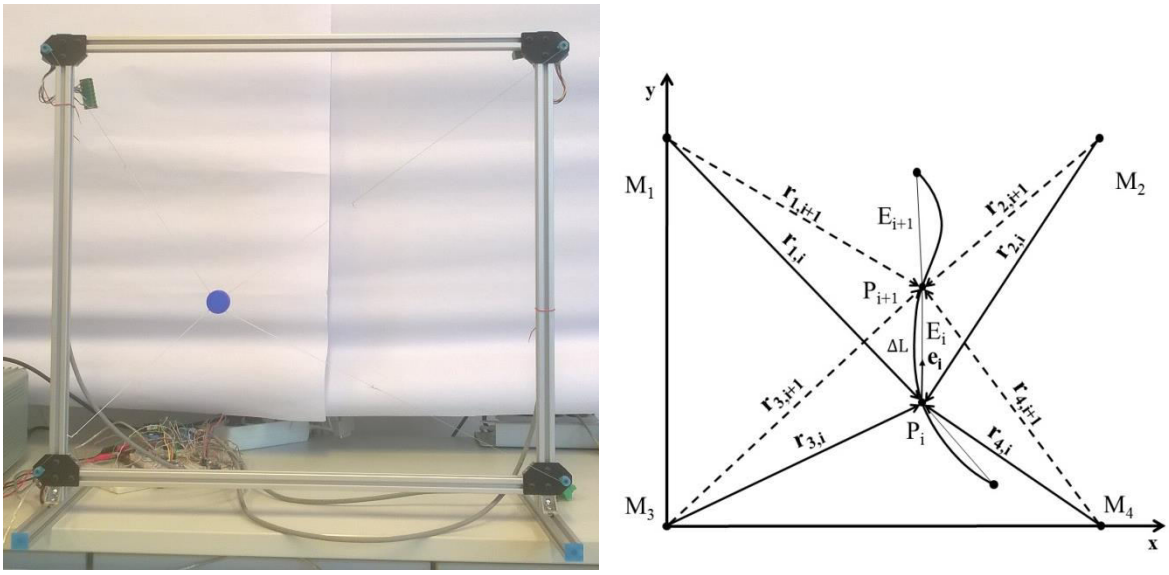

(a) (b)

Figure 1. a/ Structure of the cable robot, the end-effector is represented by a blue disk b/ Path of the end-effector

A curve path of the end-effector is approximated by polygon which is shown in Figure 1b. It is assumed that the velocity of the end-effector along a section of the polygon is constant, which is equal to the maximum of the cable velocity provided by the DC motor at nominal r.p.m. n_{max}. Velocities of the cables, i.e., the rotational velocity of the cable reel, can be determined by the use of notations shown in Figure 1b, where vectors are denoted by boldface letters. The i^{th} side of the polygon given as a vector

$$\Delta\mathbf{r}_{\mathbf{E,i}} = \Delta L\mathbf{e}_{\mathbf{i}}.$$

where $\mathbf{e}_{\mathbf{i}}$ is a unit vector.
The location vectors of the ends of the polygon sides denoted by $\mathbf{r}_{\mathbf{M,i+1}}, \mathbf{r}_{\mathbf{M,i}}$

$$\mathbf{r}_{\mathbf{M,i+1}} = \mathbf{r}_{\mathbf{M,i}} + \Delta L\mathbf{e}_{\mathbf{i}}, \qquad R_{M,i} = |\mathbf{r}_{\mathbf{M,i}}|, \qquad R_{M,i+1} = |\mathbf{r}_{\mathbf{M,i+1}}|,$$

where $R_{M,i}$ and $R_{M,i+1}$ are the lengths of the cables. The velocity vector of the end-effector is given as

$$\mathbf{v}_{\mathbf{E,i}} = \frac{\mathbf{r}_{\mathbf{M,i+1}} - \mathbf{r}_{\mathbf{M,i}}}{\Delta t} = \frac{\Delta L}{\Delta t}\boldsymbol{e}_i.$$

The absolute value of the velocity of the end-effector is calculated by the substitution of the nominal r.p.m. n_{max} of the DC motor, the reduction of gear ratio k and the diameter d of the cable reel

$$\left|\mathbf{v_{E,max}}\right| = v_{E,max} = \frac{\Delta L}{\Delta t} = \frac{n_{max}}{2\pi}\frac{60kd}{2} = \frac{60n_{max}\,kd}{4\pi}.$$

The velocity of the cable driven by motor M, i is calculated as

$$\left|\mathbf{v_{M,i}}\right| = v_{M,i} = \frac{R_{M,i+1} - R_{M,i}}{\Delta t}.$$

The DC motors are controlled by pulse width modulation (PWM), the controlling parameter of the motor M, i is

$$PWM_{M,i} = \begin{cases} 255\,\frac{v_{M,i}}{v_{E,max}}\ ; & if\ 255\,\frac{v_{M,i}}{v_{E,max}} \geq 45 \\ 45\ ; & if\ 255\,\frac{v_{M,i}}{v_{E,max}} < 45 \end{cases}.$$

It is noted that the motor starts to rotate at $PWM = 45$ and provides its maximum r.p.m. at $PWM = 255$.

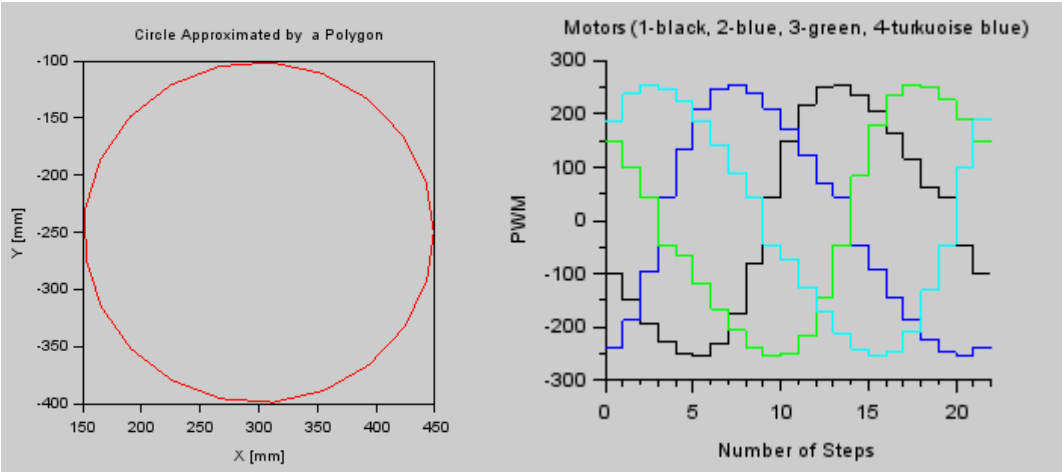

a/ b/

Figure 2 (a) Path of the end-effector, (b) Controlling parameters of the DC motors

In order to demonstrate the performance of the test bench, a circle path of the end-effector is prescribed, which is approximated by a polygon shown in Figure 2a. The computed controlling PWM parameters are displayed in Figure 2b. The lecture will also present an example for rectangle path of the end-effector.

ACKNOWLEDGMENTS

The described article/presentation was carried out as part of the EFOP-3.6.1-16-2016-00011 "Younger and Renewing University – Innovative Knowledge City – institutional development of the University of Miskolc aiming at intelligent specialisation" project implemented in the framework of the Szechenyi 2020 program. The realization of this project is supported by the European Union, co-financed by the European Social Fund.

REFERENCE

[1] X. J. Jin, I. K. Jun, A. Pott, S. Park,J. O. Park, S. Y. Ko: *Four-cable-driven parallel robot,* 13th International Conference on Control, Automation and Systems (ICCAS 2013), pp. 879-883, 2013.

[2] T. Bruckmann, W. Lalo, C. Sturm: *Application examples of wire robots*, In: Multibody System Dynamics, Robotics and Control / Workshop on Multibody System Dynamics, Robotics and Control ; Linz, 26.-27.09.2011 / Gattringer, Hubert; Gerstmayr, Johannes; (Hrsg.), S. 291 – 310, 2013.

THE EFFECT OF MMS LUBRICATION ON SURFACE ROUGHNESS DURING MACHINING

KÁRI-HORVÁTH Attila PhD, PATAKI Tamás PhD, SZAKÁL Zoltán PhD
Faculty of Mechanical Engineering, Szent István University
E-mail: kári-horváth.attila@gek.szie.hu, pataki.tamas@gek.szie.hu; szakál.zoltán@gek.szie.hu

Keywords: friction, machining, lubricant, cooling, surface roughness, MQL

I display this paper the chipping front metal of cutting allocated geometric, considering particular the friction. I catch the attention energy's balance sheet someday metal of cutting, open one new direction the manufacture technology. I display this new direction's metal of cutting condition. but built I delineate his paper final division this new policy searching programed, consumed trial instruments as well as the evaluation's mode.
The development of elements is not equal in the machine – cutting tool - cooling lubricant – workpiece systems, but one of the elements always enforces the development of the other system elements which result in the collective system development collectively. The goal of the present-work is to illustrate the uneconomic and environment pollution of lubrication technologies used until now. The development is imperative in this field. The minimal quantity lubricant (MQL) is one of the development trends (courses) immediate with which results can be got. Its further global advantage is the complete paradigm-shift in the mechanical engineering technology sometime in the future.
Complicated stress and deformation states are present in the cutting zone, Fig.1 shows this.

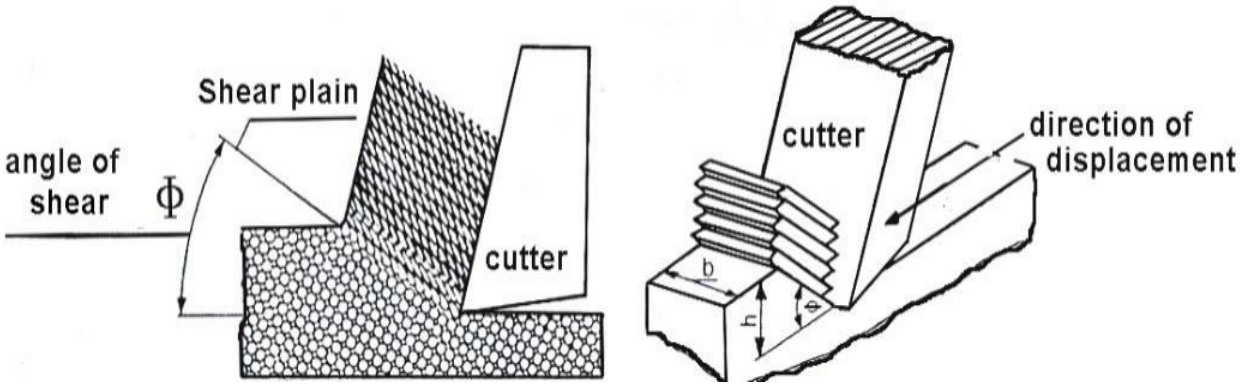

Figure 1 Process of cutting (the inside friction)

- As the cutter penetrates into the workpiece material it plastically deforms the material particles near the edge of the cutter. The particles slide on one another generally at one definite plane (shear plane) in the „h" thick layer. The chip-removal can be divided into three characteristic phases from a tribological point of view. These are:
- Internal friction arises in the material machined as a result of the sliding of particles on one another along the shear plane. The stress in the material layer near the edge of the cutter will be higher and higher, it reaches a critical level that the material can't resist and the material ruptures. That material rupture is called unconditional rupture, as it happens in every case independently from the cutting conditions. Two new surfaces are formed during material rupture: the chipped surface and the inner surface of the chip. The rupture can extend to the shear zone at certain conditions but only after the completion unconditional rupture. This is called conditional rupture.
- The removed particle (chip) slides mainly on the tool-face and a lesser amount on the tool-back from the deformation zone while friction resistance and wear are formed. This is called solid (external) friction.
- Fusions and solid material particles are also formed at the cutting edge of the tool, some part of which leaves between the tool-back and the fresh-machined surface, causing back-wear and surface damage.

I would like to present in the figure 2 the parameters, what we were changed during the whole machining process. We have three fundamental parameters, amount of the lubricant, the type of the liquid, and the technological parameters.

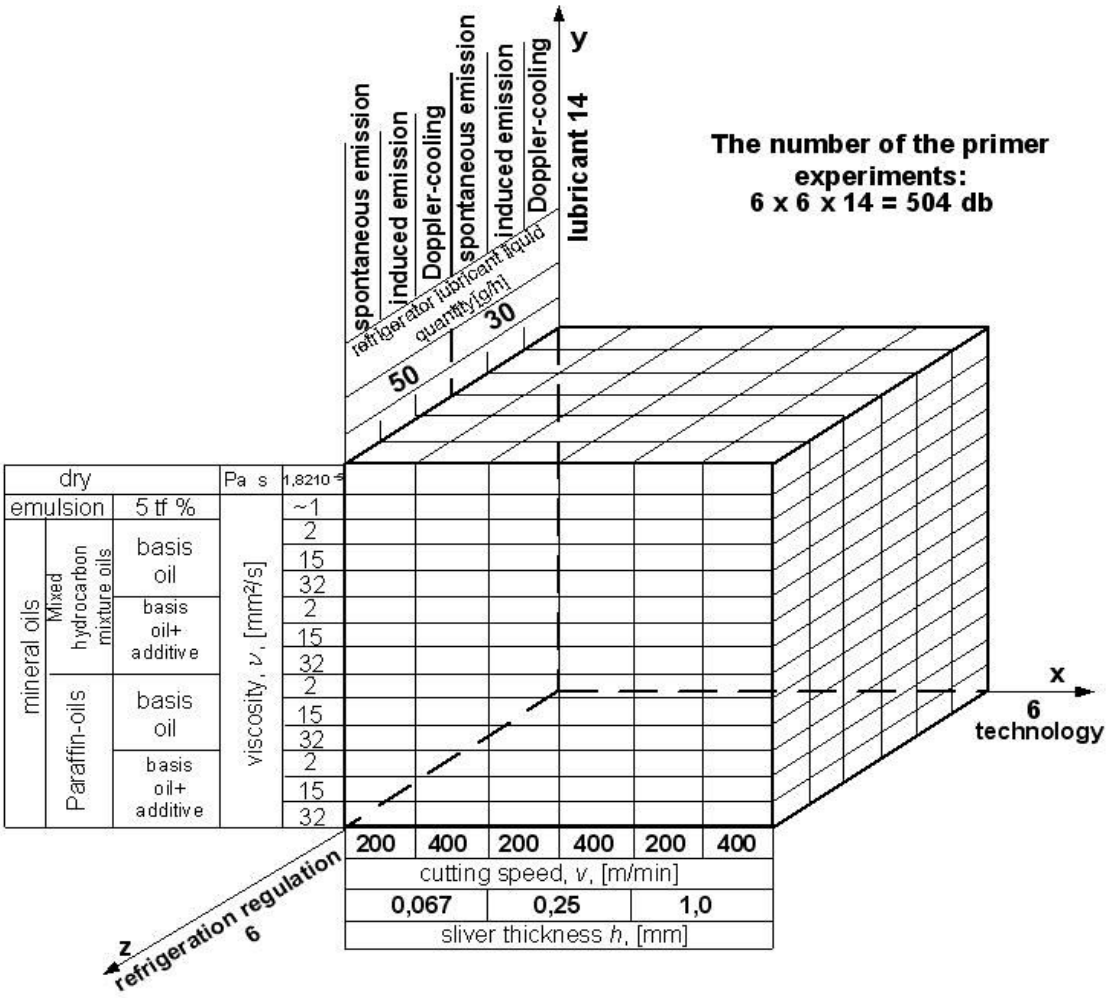

Figure 2 Experimental program

EVALUATION OF PVD COATINGS WEAR OF TOOLS FOR MECHANICAL JOINING

KAŠČÁK Ľuboš PhD, SPIŠÁK Emil CSc
Institute of Technological and Material Engineering, Technical University of Košice
E-mail: lubos.kascak@tuke.sk, emil.spisak@tuke.sk

Keywords: PVD coating, clinching, wear

Mechanical joining - clinching is one of the most widely used mechanical joining methods in sheet metal construction applications. Mechanical joining technologies, such as clinching, clinch-riveting and self-piercing riveting have been proved effective for joining lightweight materials with high strength. Lightweight constructions have gained considerable interest in recent years, because of their economic and environmental properties [1-3]. Various materials including galvanized steel sheets or non-ferrous sheets are joined by this method and thereby affecting the lifetime of the active parts of the clinching tool, the punch and the die. PVD coatings are used to decrease the wear of clinching tools (Figure 1).

Figure 1 Punch and die of clinching tool: a) ZrN coating, b) CrN coating and c) TiCN MP coating

Clinching process was studied by finite element method to evaluate the stress, strain and pressure levels in tools during the joint forming process (Figure 2). Simulation was carried out in 2D axisymmetric conditions due to rotational nature of tools.

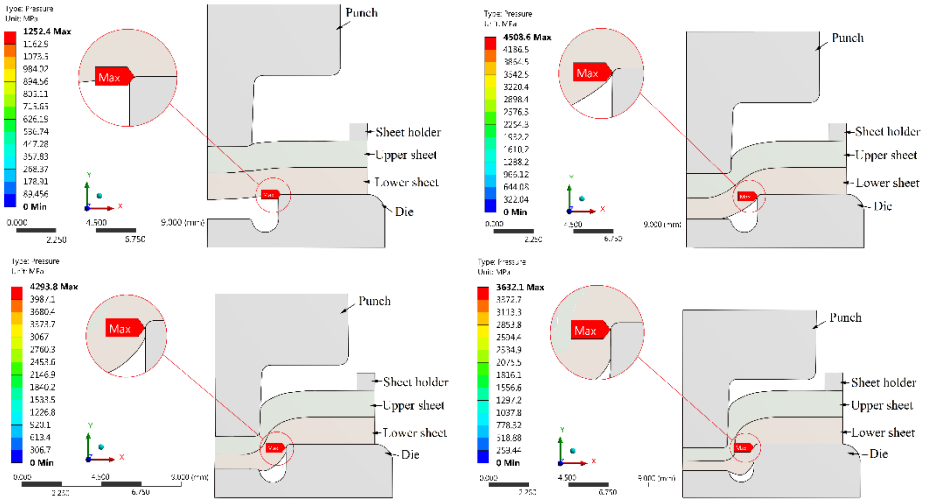

Figure 2 Clinching process: a) max. contact pressure during drawing, b) max. contact pressure during compression, c) max. contact pressure during interlocking, d) max. contact pressure during backward extrusion

FEM analysis localized the area on the shaped part of the die, in which high contact pressure values and a relatively intensive flow of the joined material occurred during the clinching process. According to the FEM analysis, surface wear can be expected on the shaped part of the die's surface.

Globulitic particles were detected on the surface of PVD coatings after deposition – Fig. 3. In these globulitic particles, zirconium in the ZrN coating, titanium in the TiCN MP coating and chromium in the CrN coating were detected by

qualitative EDX microanalysis. The presence of the globulitic formations, so-called macroparticles is directly related to the technology of cathodic arc sputtering. The number and the size of macroparticles is mainly affected by the deposition parameters used for the individual types of coatings, the appliance and the type of coated material. The macroparticles were metallic, formed at the end of the deposition process according to the type of PVD coating.

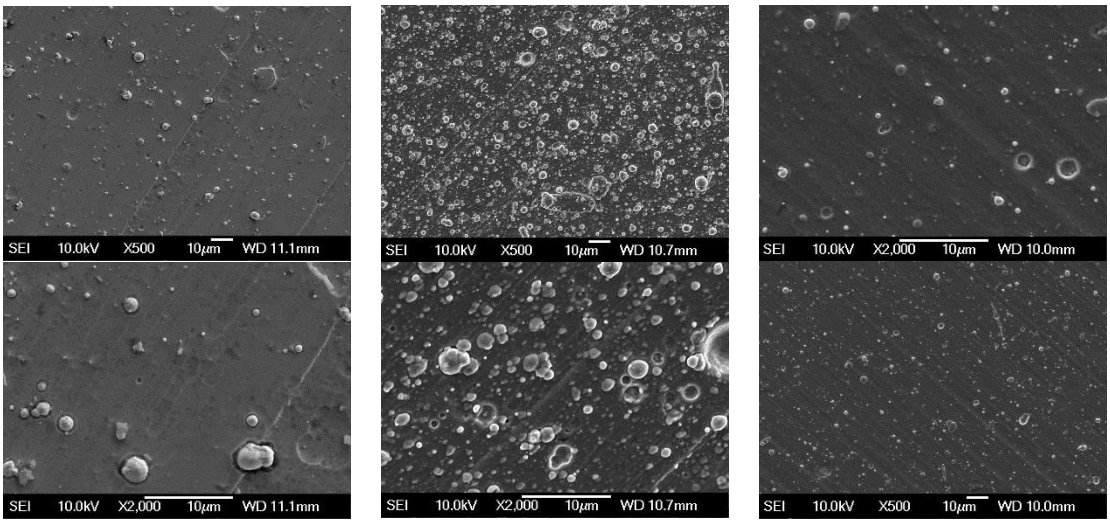

a) b) c)

Figure 3 Surfaces of: a) ZrN, b) TiCN MP and c) CrN coatings

The degradation process of the die of the clinching tool during the joining process is a superposition of multiple degradation mechanisms. A prediction of this mechanism is complicated, so utilization of the FEM analyses of the clinching process is needed.

FEM analysis identified the shaped part of the die and the segment of cylindrical surface of the die cavity as areas in which there is a high contact pressure and a relatively intensive flow of the clinched material during the joining process. After joining the observed steel sheets, zones with zinc galls were identified in the shaped part of the die and in the cylindrical surface of die cavity. The position of adhesive zinc galls on the shaped die surface followed the change of the location of maximum pressure during the clinching process, which moved towards the cylindrical surface of the die ϕ 5 mm. Out of the three types of PVD coating, the TiCN MP coating was intact on the entire surface of the die and the coatings ZrN and CrN were worn in the ROD area of the die. The wear resistance of PVD coatings mostly correlated with the indentation hardness values. The PVD coating TiCN MP had an indentation hardness value of 1.76 times higher than the values of ZrN coating and 1.89 times higher than the value of CrN coating.

ACKNOWLEDGMENTS

The described work was carried out as part of a project supported by the Slovak Research and Development Agency under project APVV-14-0834 "Increasing the quality of cut-outs and effectiveness of cutting electric sheets" and grant agency for the support of the project VEGA 1/0441/17 "Application of high-strength materials for exterior car body parts".

REFERENCES

[1] C. Chen, S. Zhao, M. Cui, X. Han, S. Fan, T. Ishida: *An experimental study on the compressing process for joining Al6061 sheets.* Thin. Wall. Struct., 108, 56–63. 2016.

[2] T. Jiang, Z. X. Liu, P. C. Wang: *Quality inspection of clinched joints of steel and aluminum*. Int. J. Adv. Manuf. Tech., 76, 1393–1402. 2015.

[3] Ľ. Kaščák, E. Spišák, Mucha, J. *Mechanical joining of various materials by clinching method.* Key. Eng. Mater., 662, 205–208. 2015.

VIRTUAL TESTING METHOD OF HUMAN KNEE PROSTHESIS

KHEIREDDINE Zehouhani, OLDAL István PhD
Faculty of Mechanical Engineering, Szent István University
E-mail: khaireddinezehouani093@gmail.com, oldal.istvan@gek.szie.hu

Keywords: *Biomechanics, Knee prosthesis, ADAMS program, knee*

Abstract: *In the human knee joint, a degenerative wear of the joint can be formed, the common treatment of this disease is the total knee prosthesis geometry replacement and prosthesis implanting, the aim of our research is the study of the human knee joint with applications in prosthesis, we will develop a method by creating a virtual knee prosthesis geometries, we will generate the geometries using the ADAMS program and examined on a special knee prosthesis qualification equipment.*

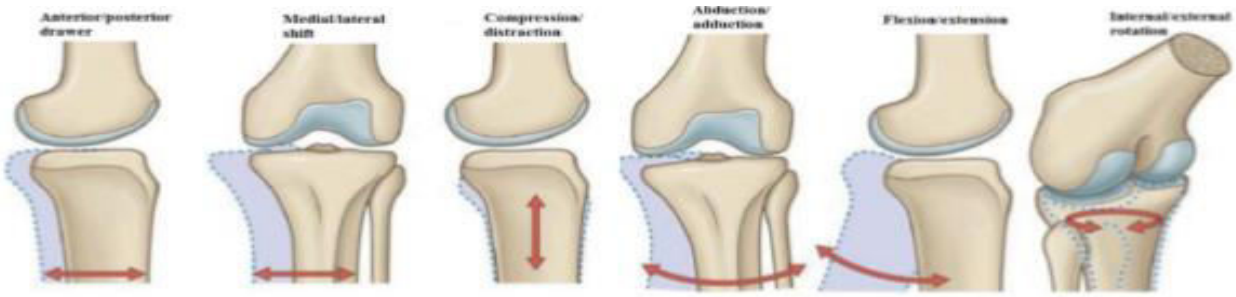

Figure1 knee joint motion in three dimensions, which is described using six independent variables (Standring,2008).

From these movements the most important is the tibia internal/external rotation values under the flexion/extension. If we want to create a good knee prosthesis is seeming obvious to copy an image of a healthy human knee joint geometry with a CT or MRI. However, this is not the good solution. Instead of the three main components: femur, tibia, meniscus the prosthesis consists of only two components (femur and tibia).

Kinematic analyses presented by different authors show large deviation (Figure 2). A mention must be made that several flexion-rotation functions of other authors in accordance with reality does not start from the origin. However, the starting point of the measured curves is transformed to the origin by most of the authors. Nevertheless, most of them do not indicate how this transformation is carried out. This problem will be further discussed in the article.

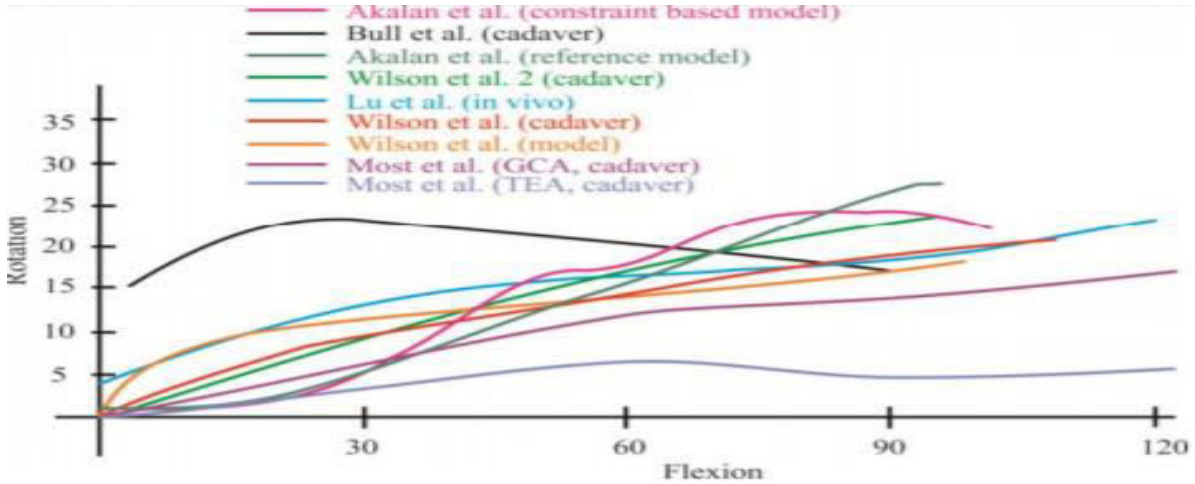

Figure 2 The results of different authors (Katona et al,2013)

The measurement performed on the experimental test machine shown in (figure 3), the flexion of the knee prosthesis components is performed by a stepper motor. The rotation-flexion values are recorded by two incremental rotary encoders with a resolution of 180°. Due to the high-stepping restore accuracy of the stepper motor, all measurement we will carried out in the same range flexion. Test machine is multifunctional, which is suitable for the determination of testing knee prostheses (Figure 3). and in case of different type of loads and it is also suitable for the knee kinematics and kinetics. The measurement performed on the experimental test machine shown in (figure 3), the flexion of the knee prosthesis components is performed by a stepper motor. The rotation-flexion values are recorded by two incremental rotary encoders with a resolution of 180°. Due to the high-stepping restore accuracy of the stepper motor, all measurement we will carried out in the same range flexion. Test machine is multifunctional, which is suitable for the determination of testing knee prostheses (Figure 3). and in case of different type of loads and it is also suitable for the knee kinematics and kinetics.

Figure 3 Knee prosthesis test machine.

REFERENCES

[1] Standring S. Gray's Anatomy. *The anatomical basis of clinical practice, New York: ChurchillLivingstone: Elsevier Press*, pp. 4300-4354. 2008.

[2] Katona G, M. Csizmadia B and Andrónyi K. *Determination of reference function to knee prosthesis rating. Biomechanica Hungarica,* 6 (1), pp. 293- 301. 2013.

FLEXIBILITY ANALYSIS OF INVENTORY COST MODEL WITH ERGONOMICS

KORKULU Sezen, BÓNA Krisztán PhD
Department of Material Handling and Logistics Systems, Budapest University of Technology and Economics
E-mail: sezen.korkulu@logisztika.bme.hu, krisztian.bona@logisztika.bme.hu

Keywords: Ergonomics, Inventory management, Endurance time, Rest allowance, Flexibility analysis.

The economic and environmental sustainability issues in inventory management have integrated by many researchers in the past decades. The ergonomics as a social aspect of sustainability had received a little attention by researchers. Therefore, the aim of the paper is analyzing the flexibility of developed inventory cost model with relaxation allowance and endurance time as a social aspect of sustainability. The effects of distance, unit weight of item and total number of items on relaxation allowance, the total cost of logistics operation and the EOQ model were investigated. As can be seen below, the analyzed mathematical model is a single operator-single material model which covered transportation of fixed amount of raw materials from storage plant to production plant by manual material handling with simple cart and picking, storing, pushing and pushing back with empty cart for manual handling of the products.

$$C(q) = \left(t_a \times q \times \left\lceil \frac{Q}{q} \right\rceil\right) \times \frac{c_h}{2} + \left[t_p(q) + t_s(q) + t_{push}(q) + t_{pushb} + \left(T_{R_{t_p}}(q) + T_{R_{t_s}}(q) + T_{R_{t_{pushb}}} + T_{R_{t_{push}}}(q)\right)\right] \times c_w \times \left\lceil \frac{Q}{q} \right\rceil$$

$$T_R(q) = 1800 \times \left(t \Big/ -1.5 + \frac{2.1}{fMVC} - \frac{0.6}{fMVC^2} + \frac{0.1}{fMVC^3} \right)^{1.4} \times (fMVC - 0.15)^{0.5}$$

The different parameter values applied for analysis such as total amount of handled items (Q) changes between 500 pcs to 2750 pcs, unit weight of item (w) changes between 0.1 kg to 1 kg, distance of movement by manual material handling for picking and storing motions (d1) changes between 2 m to 3 m and the distance between the storing equipment and the supermarket of the production line for pushing motion (d2) changes between 15 m to 20 m. As can be seen in Fig. 1 and Fig. 2, the results of the analysis indicated that the longer the distance of movement for all motions leads to decrease in savings of the model compared to EOQ model.

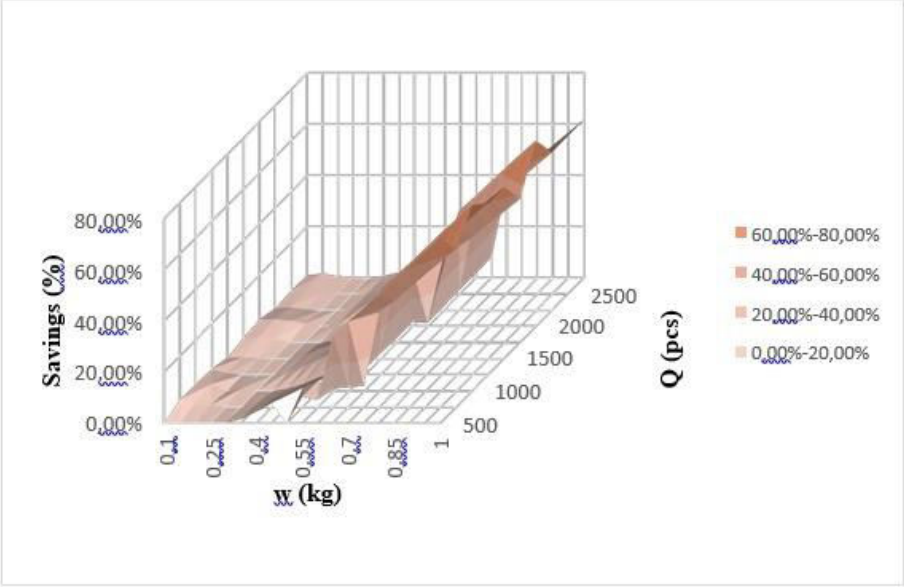

Figure 1 Savings of the model with d1=3 m and d2=20 m

The increase in unit weight of item is increase the savings obtained from application of our model and decrease the optimal lot-size. There was no specific change on savings or optimal lot-size as the total amount of handled item is increase.

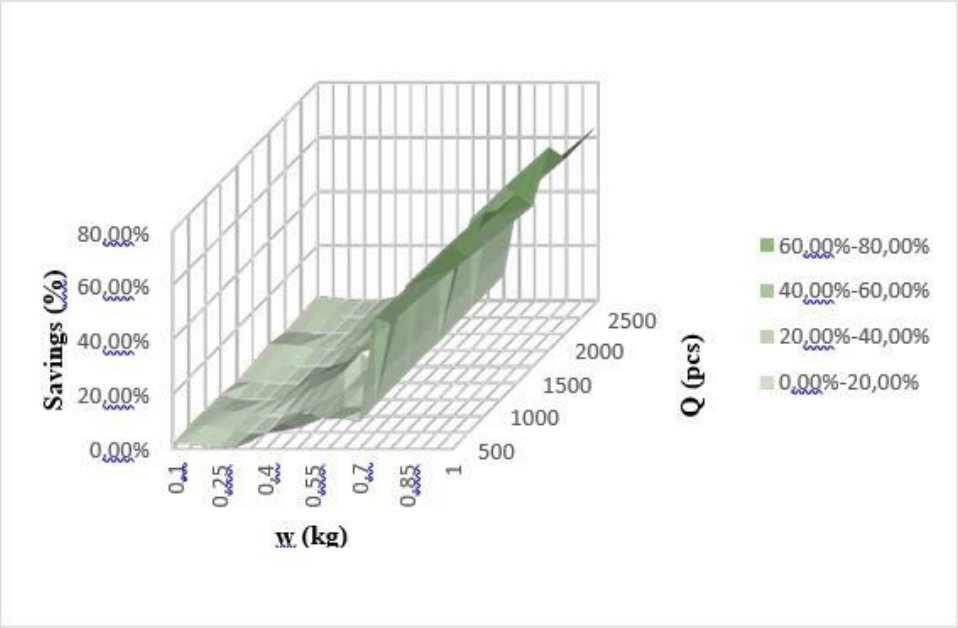

Figure 2 Savings of the model with d1=2 m and d2=15 m

The optimal lot-size for different unit weight of item and total amount of handled item were given in Fig. 3. The compared results indicated that an increase in d1 and d2 lead to an increase in optimal lot size and increase in total cost of the model.

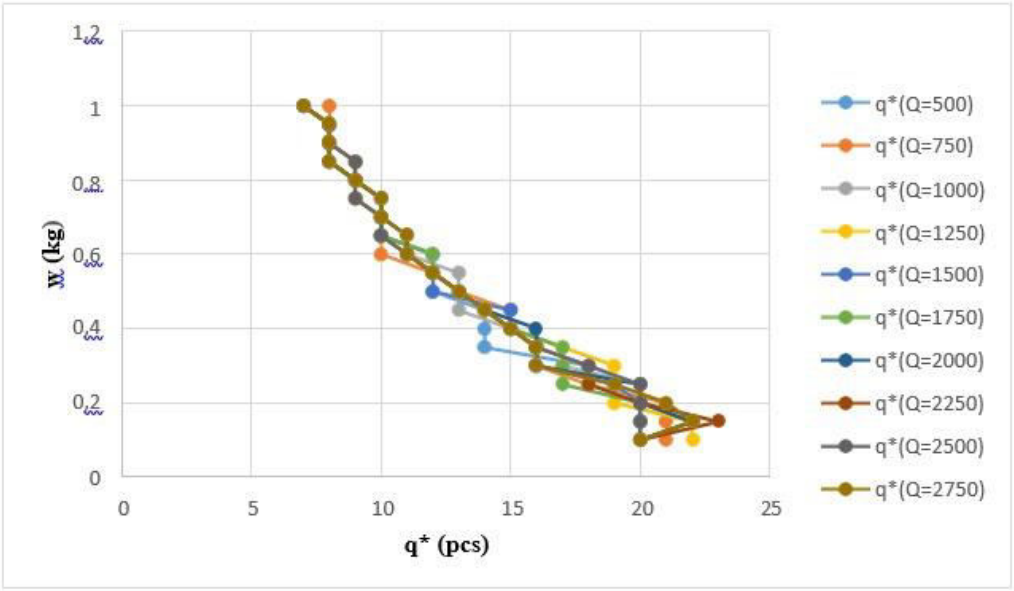

Figure 3 Optimal lot-size for different total amount of handled item and unit weight of item (d1=3 m and d2=20 m)

Consequently, the analysis has shown that a decrease in lot-size would be the better way to improve both ergonomic conditions and total cost of production in any different parameter values. Finally, the analysis of the inventory cost model with ergonomics was proved that this model is suitable for different industrial practices.

PRELIMINARY INVESTIGATION ON THE EFFECTIVENESS OF INDIRECT EXTERNAL CASTING CHILLS

KOVAČEVIĆ Lazar PhD, TEREK Pal PhD, MILETIĆ Aleksandar PhD, KUKURUZOVIĆ Dragan, ŠKORIĆ Branko PhD
Faculty of Technical Sciences, University of Novi Sad
E-mail: lazarkov@uns.ac.rs, palterek@uns.ac.rs, miletic@uns.ac.rs, kukuruzovic@uns.ac.rs, skoricb@uns.ac.rs

Keywords: feeding, risering, casting, casting simulation, steel.

One of the most common defects in steel castings is shrinkage porosity. This defect is a common cause for rejections and limits the use of steel castings in critical high-strength applications. In order to mitigate the occurrence of shrinkage porosity, foundries design feeders that compensate solidification contraction by providing liquid metal under pressure until the whole casting solidifies. In order for this system to work, the foundry engineers need to ensure that there is a directional solidification towards the feeder. The liquid metal connection between the feeder and solidification front needs to be continuous. However, in industrial castings that have complex geometries this task is very difficult to accomplish. One of few tools at engineer's disposal is the use of external chills [1]. By substituting the material of the small part of the mold, one can increase the cooling rate of adjacent casting sections. External chills can be direct or indirect [2]. The former type of chill is in direct contact with the melt, while the latter is separated from it by a small layer of sand. However, while direct chills are widely studied and their effectiveness is well understood, the indirect chills are less common and often are not even included in textbooks [1,2]. Although there is no published research with comprehensive studies regarding their performance, the widespread belief is that they are ineffective. The general conviction is that the sand layer that prevents their direct contact with the melt reduces heat transfer coefficient to the levels of regular sand molds. However, it is exactly that sand layer that mitigates a lot of problems regularly experienced with direct chills, figure 1. The goal of this research is to investigate the effectiveness of indirect chills in steel casting and provide possible guidance for their use.

Figure 1 Gas defects caused by improper use of direct chills in steel casting

The rules for determining feeding distance in steel castings are based on plate castings where an abundance of experimental data has been gathered. Therefore 400 x 140 x 25 mm plates made from Ck25 steel, were selected for this study. In order to determine effectiveness for different chilling arrangements, two sets of simulations were performed. For end chill simulations the plates are fed at the center by a single feeder that has diameter of 80 mm and height of 120 mm, figure 2. For drag chill simulations two feeders of the same size are positioned at the plate end points, figure 3. Simulations were performed in MAGMA^5 v5.3 software package by using internal database for material properties and boundary conditions. Niyama criterion was used as a common indicator for prediction of steel porosity [3].
The simulations have shown that for cases where the chills are used to increase length of the end zone, internal chills are indeed inadequate. Previous research has shown that in order to achieve ASTM level 1 of radiographic soundness in Ck25 steel grades, minimum simulated Niyama criterion values should not exceed 0.1 $(K\ s)^{0.5}mm^{-1}$ (cyan color in the images) [3]. This condition was fulfilled only when direct chills were employed, figure 2. For all sand gap sizes between the chill and the casting, it was found that indirect chills had no significant influence on predicted Niyama values. Opposite trend was observed when indirect chills were used between the feeders. Even when the gap between the chill and the casting was set to 10 mm, the use of indirect chills provided notable reduction in the predicted levels of porosity. For 2 mm gap size, indirect minimum Niyama criterion value was above 0.1, suggesting complete elimination of shrinkage porosity. When the gap was set to 5 mm, the minimum simulated Niyama values were approximately 0.07 that roughly correspond to ASTM RT shrinkage level 2, which is still a very good result.
Based on results of this study, indirect chills can be considered as ineffective when used as a tool to increase the length of the end zones. However, indirect chills were able to create end zone effect between two feeders. This increase in

lateral feeding distance offer significant possibilities to improve casting yield without being exposed to the risks that are present when using direct chills which are in immediate contact with the casting.

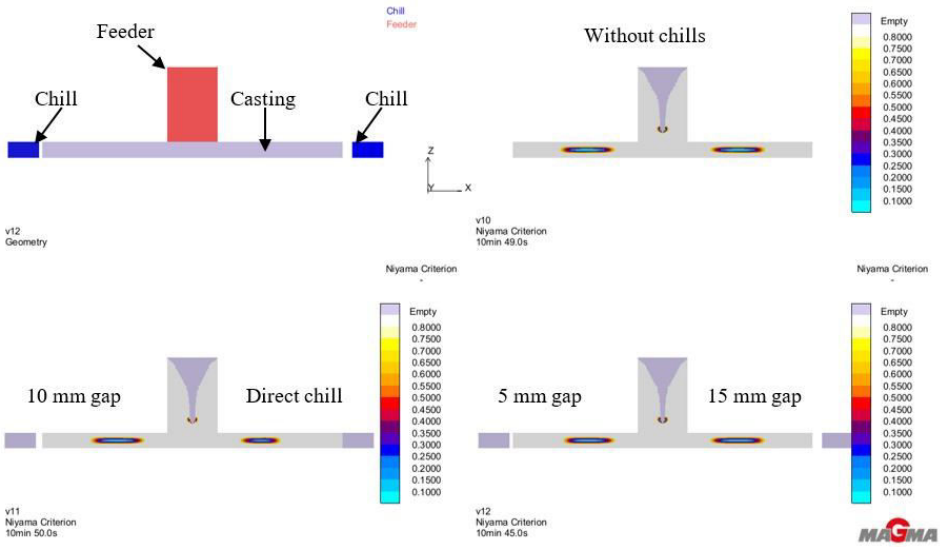

Figure 2 Simulated Niyama criterion values for end chills that increase end zone length

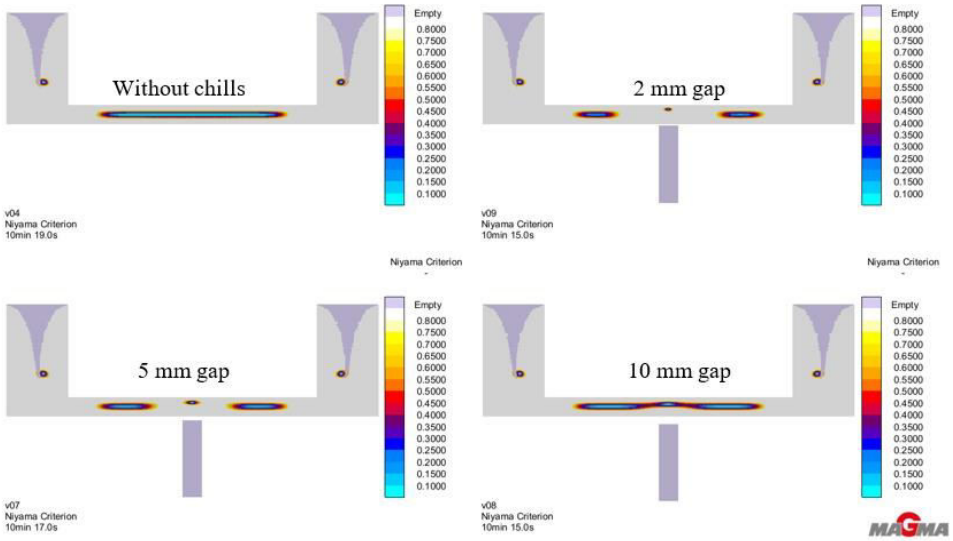

Figure 3 Simulated Niyama criterion values for drag chills that create end zone effect between two feeders

ACKNOWLEDGMENTS

This work was supported by the Ministry of Education, Science and Technological Development of the Republic of Serbia under grant No. III-45006. Authors would like to thank MAGMA Giessereitechnologie GmbH (Aachen, Germany) and their regional representative Exoterm-it d.o.o., (Kranj, Slovenia) for providing licenses for MAGMA[5] casting process simulation software

REFERENCES

[1] Peter Beeley: *Foundry technology*, Butterworth-Heinemann, 2001.
[2] P.L. Jain: *Principles of foundry technology*, Tata McGraw-Hill, 2009.
[3] K.D. Carlson, R.A. Hardin, S. Ou, C. Beckermann: *Development of new feeding-distance rules using casting simulation: Part I. Methodology*, Metall. Mater. Trans. B. 33 731–740. 2002.

PREPARATION OF Ni-COATED SiC CERAMIC POWDERS BY ELECTROLESS PLATING METHOD

KUMAR PAL Manoj, GERGELY Gréta PhD, GYÖKÉR Zoltán, HORVÁTH-KONCZ Dániel PhD, GÁCSI Zoltán DSc
Faculty of Materials Science and Engineering, Metal forming and Nanotechnology, University of Miskolc
E-mail: manojsantosh2002@gmail.com, femgreta@uni-miskolc.hu, femkhd@uni-miskolc.hu, zoltan.gacsi@uni-miskolc.hu

Keywords: SiC powder, surface coating, acidic pre-treatment, Ni layer, surface oxidation

ABSTRACT
In this study, the nickel formation on silicon carbide (SiC) ceramic powders was achieved through the electroless deposition method. Electroless nickel (EN) plating was used to coating of SiC particles, using two different pre-treatment methods (acidic pre-treatment, surface oxidation). The acidic pre-treatment is able to activate the surface of the particles hardly. A coherent oxide layer is developed on the surface of the substrate after the surface oxidation. This ensures the homogeneous nickel nuclei formation after using the electroless nickel plating. The surface morphology of the coated SiC particles showed a homogenous distribution of nanostructured nickel grains characterized by scanning electron microscopy. The nanostructures of the crystalline Ni coatings were observed to be attractive for achieving both good bonding and dense structure. The thin structure of Ni on the SiC surfaces was assessed as a beneficial reinforcement for possible metal matrix composite manufacturing.

INTRODUCTION
Due to its unique mechanical properties and chemical stability, SiC has been used to prepare composites to enhance composites mechanical properties and to fabricate resistance for high-temperature, high-frequency and high-emitting devices [1]. However, the devices produced with SiC particle-reinforced composites exhibit poor stability due to the agglomeration of ceramic particles and a poor interface bond between the matrix and reinforcement. Therefore, modifying the surface of ceramic particles is a significant way to enhance their dispersion and to provide them with new functions. Moreover, the modified reinforcing particles have been used for many important applications, especially in the production of anode materials, absorbing materials, alloy catalysts, composite materials and biomaterials [2]. The electroless nickel (EN) plating method is now widely used to modify the surface of various materials such as nonconductors, semiconductors and metals. The cost of the EN plating method is low, and the process yields a uniform coating over all surfaces of any profile of metallic or electrically non-conductive materials. This method has also attracted substantial interest in both micro and nano fabrications, in optics and in the decoration on carbon nanotubes, SiC and other kinds of powder, such as cenosphere particles [3]. Metal-coated ceramic powders refer to composite powders with a ceramic core and a metallic shell that can endow the ceramic powders with particular electrical, magnetic and chemical properties and can simultaneously improve the wetting properties between metal and ceramic materials. In this connection, EN plating has been recognized as one of the most effective techniques for preparing metal-coated ceramics powders [4].

EXPERIMENTAL (PRETREATMENT PROCESS OF THE SiC POWDERS)
SiCP with an average diameter of 2 μm was used in these experiments, which was purchased from Saint-Goba in silicon carbide Switzerland. The process of experiment contains stages: cleaning, pretreatment of SiCP and electroless nickel plating. Following process steps were carried out prior to deposition process:

1. Ultrasonic cleaning of the SiC particles with acetone (25ml) for 30 minutes at room temperature, (the purpose of cleaning is to move impurities on the surface of SiC_p).
2. Dry the SiC powder in the furnace at 105^0C for 20-30 minutes.
3. Use the sodium hypophosphite (1.5 g) and Lactic acid (1 ml) for the pretreatment of SiC_P.
4. Dry the SiC powder in the furnace at 85^0C for 20-35 minutes.
5. Then pre-treated SiC particles were EN plated by immersing them in to an acidic Ni bath, containing nickel sulphate ($NiSO_4 \cdot 7H_2O$) 28g/l, sodium hypophosphite ($NaH_2PO_2 \cdot H_2O$) 30g/l, sodium acetate hydrate ($CH_3COONa \cdot 3H_2O$) 35g/l, and lactic acid ($C_3H_6O_3$, 90%) 20ml/l.

Then, the pre-treated SiC particles were EN plated by immersing them in to an acidic Ni bath, containing nickel sulphate ($NiSO_4 \cdot 7H_2O$) 28g/l, sodium hypophosphite ($NaH_2PO_2 \cdot H_2O$) 30g/l, sodium acetate hydrate ($CH_3COONa \cdot 3H_2O$) 35g/l, and lactic acid ($C_3H_6O_3$, 90%) 20ml/l.

CONCLUSIONS

The electroless deposition on SiC surfaces with a grain size of 2µm was carried out using acidic pretreatment and oxidation process of nano-sized nickel coating. The coatings were created by changing process parameters, such as pretreatment concentrations and SiC powder concentrations into acidic Ni baths, to obtain optimum process parameters. The following conclusions can be drawn from the present study:

1. The Ni layer on the surface of SiC particles was deposited on the SiC particle surfaces through the acidic pretreatment and oxidation method with a relatively continuous and uniform structure.
2. The grain size of Ni on the surface of the SiC particles was between 150 and 300 nm, depending on the hypophosphate and the particle content in the acidic bath.
3. Increasing the amount of $NaH_2PO_2 \cdot H_2O$ resulted in the deposition of coarser Ni grains (a thicker coating layer) on the SiC surfaces, whereas increasing the particle content in the acidic bath produced finer grains (a thinner coating layer) on the SiC surfaces.

The present study shows that acidic electroless coating with specific experimental parameters will be useful in producing reinforced ceramic particles for possible composite applications.

ACKNOWLEDGMENTS

The described article was carried out as part of the GINOP-2.3.2-15-2016-00027 "Sustainable operation of the workshop of excellence for the research and development of crystalline and amorphous nanostructured materials" project implemented in the framework of the Szechenyi 2020 program. The realization of this project is supported by the European Union.

REFERENCES

[1] J. Pázmán, V. Mádai, J. Tóth, Z. Gácsi*: Powder Metallurgy Progress*, Vol.10 2010.
[2] M. Uysal, R. Karslio˘glu, A. Alp, H. Akbulut: *Applied Surface Science* 257 10601– 10606. 2011.
[3] Gui-Zhen Zou, Mao-Sheng Cao, Liang Zhang, Jin Gang Li, Hui Xu, Yu-Jin Chen: *Surface & Coatings Technology* 201 108–112. 2006.
[4] Guizhen Zou, Maosheng Cao, Haibo Lin, Haibo Jin, Yuqing Kang, Yujin Chen: *Powder Technology* 168 84–88. 2006.

DISPLACEMENT AND ROTATION. SIMILARITIES AND DIFFERENCES IN THE DISCRETE AND CONTINUOUS MECHANICAL MODELS

LÁMER Géza PhD
Faculty of Engineering, University of Debrecen
E-mail: glamer@eng.unideb.hu

Keywords: displacement, rotation, discrete model, continuous model.

To describe the mechanical behaviour of the deformable solid body, the theory of elasticity is used [8]. The kinematical variable in the theory of elasticity is the displacement field. In this theory the physical inhomogeneities, internal structure in the material cannot be taken into consideration. To generalizes theory of elasticity used the second kinematical variable, the rotation field (see [1-3]). A point can be shifted, but cannot be rotated. A rigid body with non-zero size can be rotated. On the contradictions in the theory of micropolar elasticity and their causes was discussed a few decades ago [5]. Kunin showed, the micropolar theories based on discrete systems [4]. Because of this the solid body with and without structure was analysed [6], as well as the construction of model of discrete and continuous system [7].
The purpose of the study is showing the difference between kinematical behaviour of the discrete and the continuous mechanical systems. So, the basic step is the motion of the Euclidean space.
The motion of the Euclidean space can be decomposed on displacement and rotation. The displacement as a map is commutative and does not have fix point, the rotation as a map is non-commutative and have a fix point. The two kind of motion of the Euclidean space based on two structure of the Euclidean space: The first one is the topological structure, that fix the order (successiveness) of the points of the space. The second one is the idea of distance. The motion is such a (topological) map, that the distance of any two points remains the same.
The bounded and closed domain of the Euclidean space is taken as a model of the rigid body.
The bounded and closed domain of the Euclidean space is also taken as a model of the deformable solid body. In the model one vector-value kinematical freedom, namely the displacement vector is used to order to every point of Euclidean space. The map – i.e. the displacement field – of the deformable solid body is continuous, but is not (necessarily) motion; the size and the shape of body can change.
The material has atomic-molecular structure. In compliance with it, the material can be comprehended as a discrete system. In this case the elements of the material, as an atom, molecule, grain, can be comprehended as either material point, or rigid body. In the first case the kinematical freedom is the displacement, in the latter case the displacement *and* the rotation.

rigid body displacement — rigid body rotation

Figure 1 Displacement and rotation of discrete system built by material points

In the study we analyse whether how the kinematical behaviour of the discrete and continuous system can be characterized by the displacement and the rotation. In the discrete system the two kind of motion are independent variables. In the same time, they characterize the movement in different way

locally homogeneous displacement = rigid body displacement — locally homogeneous rotation ≠ rigid body rotation

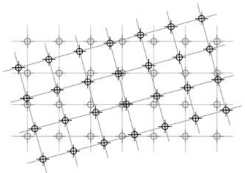

rigid body displacement of frame without locally homogeneous rotation ≠ rigid body rotation

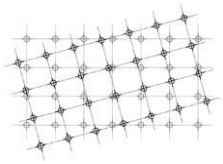

rigid body displacement of frame and locally homogeneous rotation = rigid body rotation

Figure 2 Displacement and rotation of discrete system built by rigid bodies

For instance, the homogenous local displacement "field" gives the global (rigid body) displacement, but the homogenous local rotational "field" does not give the global (rigid body) rotation. For the specification global (rigid body) rotation, the global rotation of grid of elements and the local rotation of element in accordance with the rotation of grid need at the same time. In the continuous system the two motion cannot interpret locally: a point cannot rotate; only rotation of a surrounding (neighbourhood) of any point or rotation of any direction can interpret.

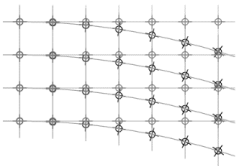

Independent displacement and rotation with parallel shift

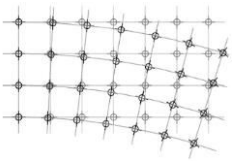

Independent displacement and rotation with bending of body

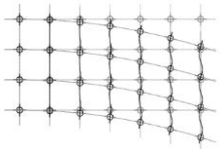

Bounded displacement and rotation with parallel shift

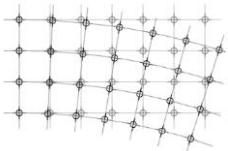

Bounded displacement and rotation with bending of body

Figure 3 The displacement and rotation cannot be independent in the continuous material

The kinematical characteristics of the continuous model, as displacement of a point, rotation of the surrounding of a point, and the rotation of direction are not independent quantities: the displacement (field) characterize the rotations unambiguously [8]. In accordance with this only displacement field can be interpreted in the deformable solid body as an independent kinematical variable.

REFERENCES

[1] Cosserat E. – Cosserat F.: *Théorie des Corps Déformables Hermann et Fils*, 1909. The Cornell University Library Digital Collections, Reprint 2017.
[2] Eringen A.C.*: Microcontinuum Field Theories.* Springer, New York, Berlin/Heidelberg, 1998.
[3] Kröner E. (ed.): *Mechanics of Generalized Continua. Proceedings of the IUTAM-Symposium on the Generalized Cosserat Continuum and the Continuum Theory of Dislocations with Applications*, Freudenstadt and Stuttgart (Germany) 1967. Springer-Verlag, Berlin - Heidelberg - New York, 1968.
[4] Kunin I.A.: *Elastic Media with Microstructure I.*, II. Springer-Verlag, Berlin - Heidelberg - New York, 2011-12, translated from Russian, 1975) 2011-12.
[5] Lámer G.: *Contradictions in the Theory of Micropolar Elasticity and Their Causes = Newsletter,* Techn. Univ. of Budapest, II (1), pp. 12-16 1984.
[6] Lámer G.: *Solid and Soft Body with and without Structure = In: Quasi-Static Deformations of Particular Materials. Proceedings of QuaDMP'03 Workshop*. 25-28 august 2003. Ed.: K. Bagi. P. Co. of BTU, Budapest, 2003. pp. 159-166. 2003.
[7] Lámer G.: *Continuous and Discrete Models in the Mechanics of Deformable Solid Bodies. Proceedings of the Annual Session of Scientific Papers.* Vol. XVII. (XXVII) "IMT Oradea" May 31. – June 1. pp. 125-130 2018.
[8] Lur'e, A.I.: *Theory of Elasticity. Springer*. Berlin - Heidelberg - New York, 2005.

APPLYING THE CAMBRIDGE ENGINEERING SELECTOR (CES) SOFTWARE DURING ALTERNATIVE MATERIALS SELECTION FOR AN IMPELLER OF A CAR AIR BLOWING ENGINE

LÁSZLÓ Noémi, MAROSNÉ BERKES Mária PhD
Institute of Materials Science and Technology, University of Miskolc
E-mail:metlnoe5@uni-miskolc.hu,maria.maros@uni-miskolc.hu

Keywords: materials selection, CES, impeller, automotive, industry

Materials selection is of great importance as the product made of them carries a load, conducts heat and electricity, is often exposed to wear and corrosive media and has a shape that should satisfy functional and / or aesthetic needs. This is only possible if there is a procedure that assists the rational choice of materials. Materials selection should be supported from the earliest stage of the engineering design. This is especially true for the automotive industry, where unique operational conditions of the components are complicated by manufacturability aspects. The Cambridge Engineering Selector (CES) [1] is a material and process selection software, based on Ashby's Material Choice Concept, providing a comprehensive information system for a wide range of materials and processes. CES EduPack software represents a powerful tool for searching information and browsing in the database. The software makes easy to understand the behaviour of each family of materials with visual tools, providing material property charts. The objective of the current paper is to introduce a case study on selection of alternative materials for the impeller of an air blowing engine. The component is currently made of 30% glass fiber reinforced polypropylene (PP GF30) by injection moulding, resulting inhomogeneity, large pores ($V > 2$ mm^3), as well as week collision lines (Figure 1). which may cause the component to break during operation.

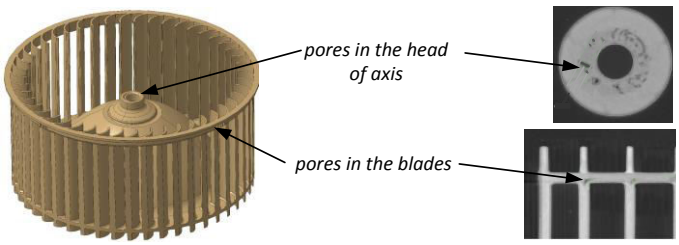

Figure 1 Material defects in the injection-moulded impeller

The case study reported in this paper has been investigated in the framework of an ongoing research programme aiming at improving the technological suitability of the base material of the impeller. Among the others, we wanted to reduce the number of material defects in the injection moulded product to improve the reproducibility of the manufacturing of the good quality products, to omit the final quality control or decrease its frequency, as well as to improve the reliability of the component during operation. The computer aided material selection according to the specified criteria given in Table.1. – with the aim of finding alternatives to the current wheel material – was performed using the CES software. We obtained 20 candidate materials satisfying the specified criteria (Table 1.). The candidates were ranked using statistical methods and material property charts (Figure 2.). Ranking was performed based on the following material properties: price, density, elastic modulus, fatigue strength, fracture toughness, maximum service temperature, mouldability, durability (against water, salt water, chemicals, grease), flammability and linear shrinkage. The summarized, i.e. final rank-place number was defined as the sum of the individual rank-places defined for candidate materials in case of each property. It is important to emphasize that during ranking the properties were taken with identical weight. From Table 1. it is seen that the currently used material has the rank-place number 16, but altogether 5 candidates of the possible 15 materials were qualified as suitable ones. The reason for this is that these candidates precede the current material just in terms of the summarized rank-place, but a detailed comparative analysis of the properties revealed that regarding the individual properties the candidates can be far behind the currently applied PPGF30 material. Some examples of this analysis are as follows: Epoxies would require costly technological modification of processing; The PF 40% glass fiber composite is the only cheaper alternative to the current material, which makes it desirable, however it possess extremely low fatigue strength, making it unsuitable for the given application. The PPA polymers containing 40, 45 and 51% glass fiber do not resist grease and oils, thus regardless of their otherwise good mechanical properties they should be excluded from the group of candidate materials. PCT with

40% GF is evaluated as suitable composite, though it has a higher price and density comparing to PP GF30, but it is better with respect to all mechanical features, has better mouldability and favourable self-extinguishing behaviour during combustion making it potentially a good alternative material. The liquid crystal polymer matrix composites, i.e. LCP-s with 40, 45 and 50% glass fiber have better mouldability (Figure 2.) and almost twice higher the fatigue strength compared to the current base material, therefore they are remarkably good alternatives. However, it should be noted that their density is 50 % higher, and their price is more than three times higher than those of the currently used material.

Table 1 The selection criterion system and results of the alternative materials selection with final rank-place numbers; (green: suitable materials, red: unsuitable materials)

Material selection criteria		Candidate materials obtained by materials selection using CES			
Criteria	**Limit or category**	**Unsuitable**	**Rank-place**	**Suitable**	**Rank-place**
Material	TP or TS polymer	DAP GF 50-70	20	LCP GF40	14
Max. service temperature	140 °C	Epoxy BC GF65	11	LCP GF45	10
Filler type and %	GF or MF; min 30%	Epoxy SMC GF60	2	LCP GF50	5
Price	Low	Epoxy SMC GF65	1	PCT GF40	12
Density	Low	LCP GF40+MF10	17	PF GF 30-60 HS	6
Young modulus	High	PF Novolac (GF+MF)40	21		
Fracture toughness	High	PEKK GF30	13	***PPGF30 current material***	***16***
Fatigue strengths	High	PEKK GF40	7		
Processing properties	Suitable for inj. moulding	PF GF40	4		
Durability (water)	Excellent	PPA (GF+MF)40	15		
Durability (salt water)	Excellent	PPA GF45	3		
Durability(chemicals)	Excellent	PPA (GF+MF) 51	8		
Durability(gear)	Excellent	PBT GF25	19		
Water absorption	Low	PBT GF30	18		
Linear mould shrinkage	Low	PBT CF30	9		
Flammability	Good				

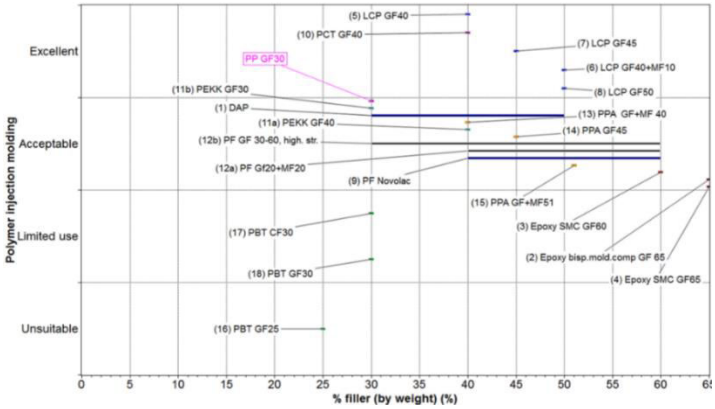

Figure 2 Influence of quantity of filler on the injection mouldability of the alternative materials of the impeller

At the current stage of research our findings in alternative material selection can be summarized as follows:

- Based on the summarized ranking-place of the candidate materials and analysing their technological and application properties, we cannot designate any alternative material that outperforms the currently applied one in all respect of the property requirements, including the price and density, as well.
- Since the basic objective is to improve the mouldability of the material, therefore in first approximation, improvement of this feature must be a decisive criterion for the selection of any alternatives.
- For more reliable ranking and selection of candidate materials a purposeful weighting of the different properties is indispensable, that requires defining and applying a weighting factor for each selection criteria.

This research was supported by the European Union and the Hungarian State, co-financed by the European Regional Development Fund in the framework of the GINOP-2.3.4-15-2016-00004 project, aimed to promote the cooperation between the higher education and the industry.

REFERENCES

[1] CES 2017 EduPack, Materials selection software, Granta Design, 2018.

EXPERIMENTAL STUDY REGARDING THE INFLUENCE OF COMPLIANT HINGES GEOMETRY IN MECHANICAL STRUCTURES

[1,2]LATEŞ Daniel PhD, [3]CĂŞVEAN Marius
[1] *"Petru Maior", University of Târgu Mureş*
[2] *iFOR Research and development center of IRUM, Târgu Mureş*
E-mail: lates.upm@gmail.com or daniel.lates@irum.ro
[3] *Accesa IT Systems, Cluj-Napoca, Cluj*
E-mail: marius.casvean@yahoo.com

Keywords: compliant mechanism, compliant joints, measurements, comparison, geometry.

Designing and developing any systems based on these type of mechanisms, which are compatible with precision movement, is a necessity in the micro-precision industry.
International papers on this subject are diverse, like Lin Cao presenting in his work a new optimization technology for designing compliant mechanisms that are effective in transferring movement, strength or energy, while they are strong enough to resist fatigue. The sustained philosophy here is that a compliant mechanism can benefit from the above mentioned properties if flexible hinges are located where they must be and also be dimensioned in a rational way.
In this work, a case study on a pentalater mechanism has been achieved, concerning hinges geometry of it. An attempt was made to design the hinges of the mechanism, having different geometry, on a pentalater structure. The mechanism that integrates these joints can be seen in Figure 1. This mechanism is made up of kinematic elements, compliant hinges, rigid structure and the end-effector of the mechanism. The motor element of this mechanism consists of two linear piezoelectric actuators which are positioned as shown below. The displacement of the actuators is done by means of a controller and an amplifier.

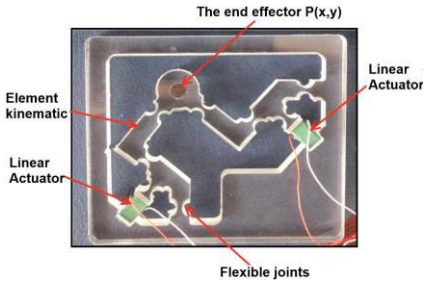

Figure 1 Pentalater mechanism

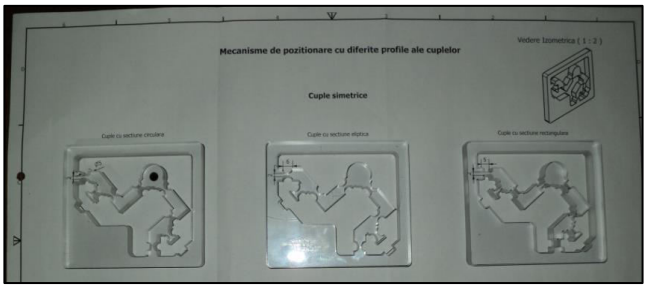

Figure 2 Sets of studied hinges

Each type of joint used has the same mechanism as shown in Figure 1. In this paper, each case will be taken for analysis and the results will be extracted, in terms of displacement of the moving parts, concluding which variant is more efficient from this point of view. In Figure 2 there are three sets of studied flexible joints. The precision of the movement and the maximum displacement that could be achieved, were followed.
The geometric characteristics of the three studied couplings are shown below. Figure 3a shows the design stage of the mechanism with circular profile hinges and its practical realization is presented in Figure 3b. The same description will be done for the other two types of mechanisms with different flexible joints geometry.


Figure 3a 3D model


Figure 3b Physically made model

The results are presented at the end of this paper. The experimental study was carried out at the Nyiregyhaza College at the Faculty of Engineering from Nyiregyhaza, Hungary, in 3D Measurements Laboratory. The measuring machine was an Axion brand and the software involved for this research was Aberlink 3D. Figure 4 shows the studied mechanisms and the clamping device. The mechanism's actuators are controlled by the Thorlabs amplifier controller, MDT693A model. The actuator displacement values are from 1 µm to 9 µm, the measurements being made in five steps. The measurement method was by touching several points of the end-effector.

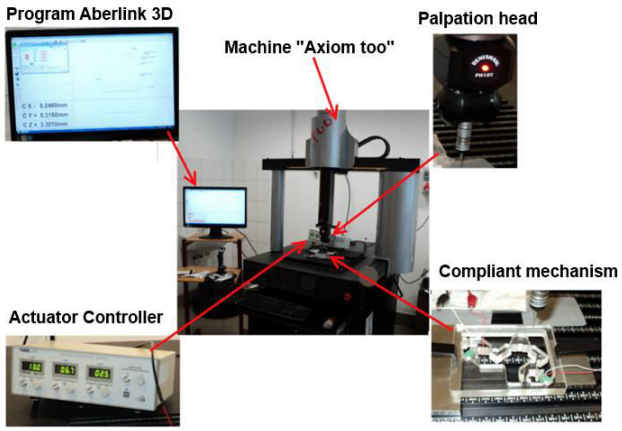

Figure 4 Experimental stand

Graphical data from the experimental case study are found in Figure 5a, for circular profile hinges, Figure 5b, for eliptical profile hinges and Figure 5c, for rectangular profile hinges.

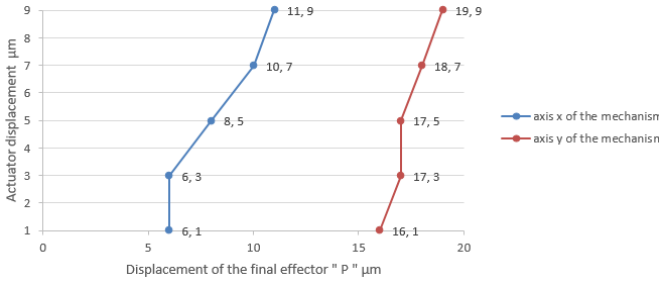

Figure 5a Circular joint profile

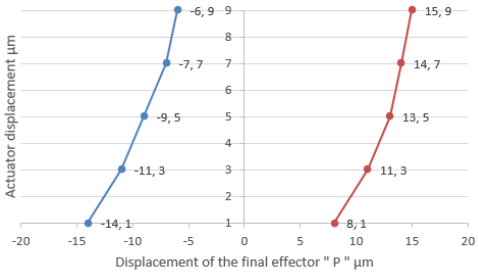

Figure 5b Elliptical joint profile

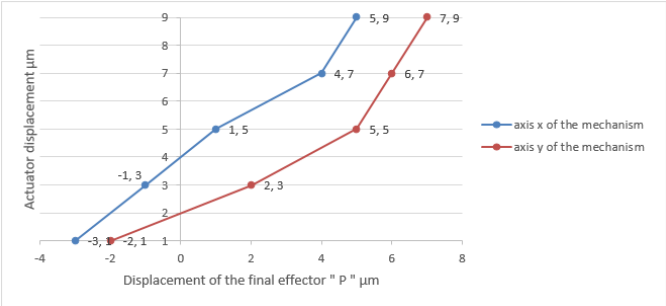

Figure 5c Rectangular joint profile

ACKNOWLEDGMENTS
We would like to express our gratitude to SC IRUM SA for the moral and financial support for the realization of this article. We also want to thank the organizers of the event for organizing such a scientific conference that helps us publish articles on engineering.

MODELLING THE THERMAL BEHAVIOR OF PERMANENT MAGNET SYNCHRONOUS MOTORS

LOTFI Abdelhakim, MARCSA Dániel PhD, HORVÁTH Zoltán PhD
Department of Mathematics, Széchenyi István University Of Applied Sciences
E-mail: lotfi@sze.hu, marcsa@maxwell.sze.hu, horvathz@sze.hu

Keywords: PM machine, electromagnetic losses, heat-transfer coefficient, equivalent thermal conductivity.

ABRIDGED VERSION OF THE PAPER

The main objective of our task is to develop a finite element model to analyse the thermal effects in electric machines during its various operating conditions. The application allows the predictions of simultaneous heat transfer in solid and fluid media with energy exchange between them and to determine the heat removal by natural convection from the machine surface. In electrical machines the permanent magnets and the insulation in the stator windings are sensitive to temperature variations, so a special attention must be paid to this part because the high temperature can affect the durability of the stator winding insulation and the efficiency of the permanent magnets. The prediction of the temperature distribution inside an electric motor is required at the machine design stage in order to control the temperature rise and to avoid overheating of the sensitive parts. The accuracy of the thermal model depends on the material properties and the knowledge of losses in electrical machine. In order to simplify the thermal model, the windings and the stator are treated as homogeneous medium with equivalent thermal parameters and the effective properties to characterize the thermal behaviour are calculated based on the volume-weighted average over all constituents. For heat transfer through the external surface of the machine, natural convection is considered. On the other hand the internal air gap is defined as solid and the effective conductivity to characterize the thermal behaviour of the air gap is calculated from empirical correlations. In the developed FEM model, total losses including winding loss and iron loss are simulated in Maxwell, ANSYS software and the estimated losses are then used as heat sources in the thermal model. This computation is made by coupling transient FEA thermal fields with the developed losses model.
The proposed thermal model is implemented using the open source Feel++ software. Two examples are presented to assess the accuracy of the developed coupled solvers and the numerical results are compared with the experimental ones, which are obtained from a prototype machine.
In section 2, the thermal field is described by the following equations:

$$(a.)\quad \rho c_p \frac{\partial T}{\partial t} + \nabla.(\lambda \nabla T) = Q, \qquad (b.)\quad -\vec{n}.(-\lambda \nabla T) = h(T_0 - T). \qquad (c.)\quad T(0) = T_0.$$

where λ is the thermal conductivity, T is the temperature and Q is the heat source.The heat equation (a) is solved in the whole domain including the air gap taking into account the boundary conditions (b) and initial condition (c).
In section 3, the method for computing the thermal parameters is developed. The machines parts are constituted of materials whose thermal conductivities are either isotropic or anisotropic. The stator is composed of layers of iron stacked in the axial direction and each lamination is insulated by a layer of varnish. Therefore in this work we use the whole model of equivalent stator to simplify the stator modelling. The calculation of equivalent thermal conductivity coefficient is approximated by the series and parallel models for two materials derived from equivalent thermal resistance network:

$$\text{Series:}\ \frac{1}{\lambda_{eq}} = \sum_{i=1}^{2} \frac{v_i}{\lambda_i} \qquad \text{Parallel:}\ \lambda_{eq} = \sum_{i=1}^{2} v_i \lambda_i$$

where $v_i, \lambda_i, i = 1,2$ are the volume fractions and conductivity of the constituent i.
The stator slot is occupied by the conductors and the insulation. To simplify the windings modelling, equivalent copper conductor and equivalent insulation are used with equivalent thermal parameters. In the developed FEM model, the windings and the stator are treated as homogeneous medium with equivalent thermal parameters and the effective properties to characterize the thermal behaviour are calculated based on the volume-weighted average over all constituents.
In 3D FEM, the air gap is defined as solid and the effective thermal conductivity is calculated by using the empirical relations. The heat generated by the electric motor is dissipated to the ambient air by a combination of conduction and natural convection. The heat transfer coefficient can be calculated using traditional empirical methods and it is

$$h_{na} = N_u \frac{\lambda_{air}}{D} \quad \text{and} \quad N_u = \begin{cases} 0.525(G_r P_r)^{0.25} & \text{(laminaer if } 10^4 < T < 10^9\text{)} \\ 0.129(G_r P_r)^{0.33} & \text{(turbulent if } 10^9 < T_a < 10^{12}\text{)} \end{cases}$$

where λ_{air} is the thermal conductivity of the air, N_u is Nusselt number, R_e is Reynolds number, P_r is Prandtl number, G_r is Grashof number and D is the outer diameter of the motor.

In section 4, we present the method of calculation for the electromagnetic losses in the PM motors. These losses are the source in thermal analysis. The mechanical losses are neglected during the thermal simulation. The main heat sources are the copper loss (Joule losses) of the stator windings and the iron losses, including eddy current loss and hysteresis loss of the stator, rotor and permanent magnet core. Electromagnetic computation is carried out with the aid of two 2D finite-element (FE) simulations on the cross-section of the PM motor *using* the Ansys Maxwell.

In section 5, two computations are presented to assess the accuracy of the developed coupled solvers. The transient 3D FE thermal were carried out using the open-source library Feel++ and applied to the BMW C1 11 kW and Toyota Prius 2004 electric motors. Figs. 1 and 2 show the temperature distribution of the motor at time t = 1600 s.

In this section we also present a comparison between the numerical results and the measured results taken from the prototype machine. Fig 3 shows comparison of the simulated and measured temperature variation obtained by a few thermocouples. Fig 3(a) shows the experimental value of Joule losses variation with time. The last section presents the conclusions of the research described in this work and *recommendations* for future *work*.

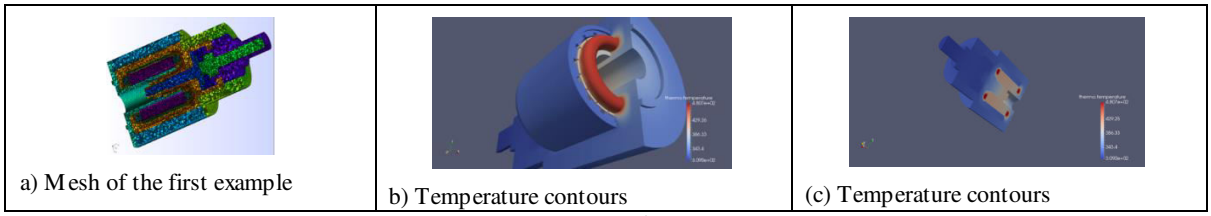

a) Mesh of the first example | b) Temperature contours | (c) Temperature contours

Figure 1

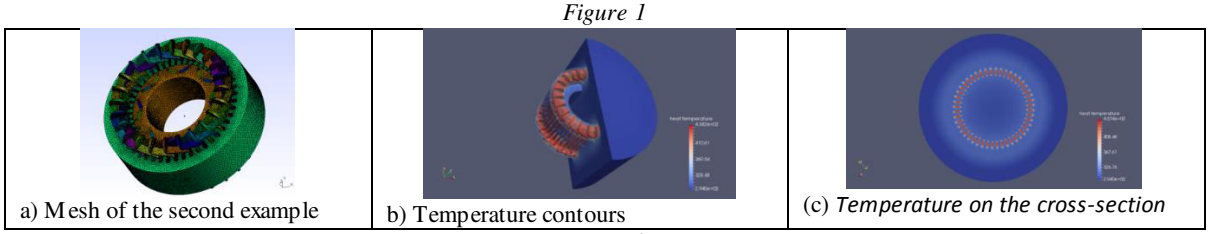

a) Mesh of the second example | b) Temperature contours | (c) *Temperature on the cross-section*

Figure 2

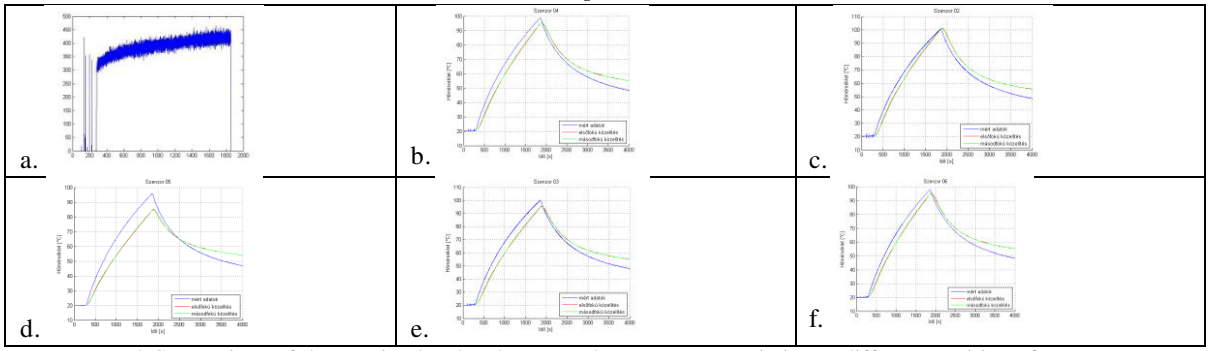

a. b. c. d. e. f.

Figure 3 Comparison of the FE simulated and measured temperature variation at different position of PM motor.

ACKNOWLEDGMENTS

This work was supported by the FIEK program (Center for cooperation between higher education and the industries at the Széchenyi István University, GINOP-2.3.4-15-2016-00003)

REFERENCES

[1] J. Gieras, R. Wang and M. Kamper:*Axial Flux Permanent Magnet Brushless Machines*, Springer 2008.

[2] P. H. Mellor, D. Roberts and D. R. Turner: *Lumped parameter thermal model for electrical machines of TEFC design* IEE Proceedings-B, 138 5, p. 205-218. 1991.

INCREASING THE LIFE OF MULCHING TOOLS

ĽUPTÁČIKOVÁ Veronika, HNILICA Richard PhD, ŤAVODOVÁ Miroslava PhD
Faculty of Environmental and Manufacturing Technology, Technical University in Zvolen
E-mail: luptacikovav@gmail.com, hnilica@is.tuzvo.sk, tavodova@is.tuzvo.sk

Keywords: mulchers, tool, wear.

Areas after mining or calamity are not amenable to immediate afforestation and require some adjustment. After removal of wood biomass, the rest of the residue is scattered throughout the area. To modify them, Several methods can be used to remove it. It is possible to remove the mining remnants (used for fuel or chips), put them in the waves (manually or mechanized), leave the surface to break apart, burn, crush and remove the surface. The optimal conditions for the planting environment and the subsequent adaptation process of the planting can be achieved by its mechanical, biological, chemical treatment. The basic prerequisite for a successful renewal of forests is their release from undesirable increases, in some cases from foams (trees) from mining waste. The area is also released when forest nurseries, seed plantations, etc. are established. The main purpose of the release of surfaces is to achieve the maximum throughput of the area for the machines to be moved. It is an important element in the technology of the production process. The basic mechanized treatment of the terrain and the preparation of the soil for the foundation and upbringing of the forest include cultivation of the environment, soil processing and incorporation of forest biomass into the soil, thus improving the soil. Adapters used to process stagnant forest biomass are unwanted shredders (mulchers). Their tools are in Figure 1.

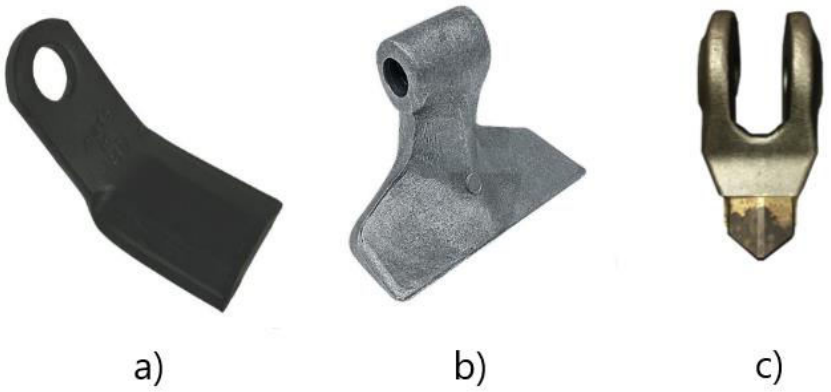

Figure 1 Mulching machine tools a) bolts, b) hammers, c) teeth

They wear during work. Wearing is a permanently undesirable change in the surface due to the interaction of functional surfaces or functional surface and wear medium. It appears to be removing or moving particles from the worn surface by mechanical effects, possibly accompanied by other influences (chemical, electrochemical, electrical).
A tool that does not have any editing can go into a state where it can no longer be used anymore. During the measurements, we created a 3D Scan of a new two-gear tool and a two-gear crusher tool that clearly shows the tool wear rate when folded from the rotor crusher. These scans were subsequently overlaid (Figure 2).

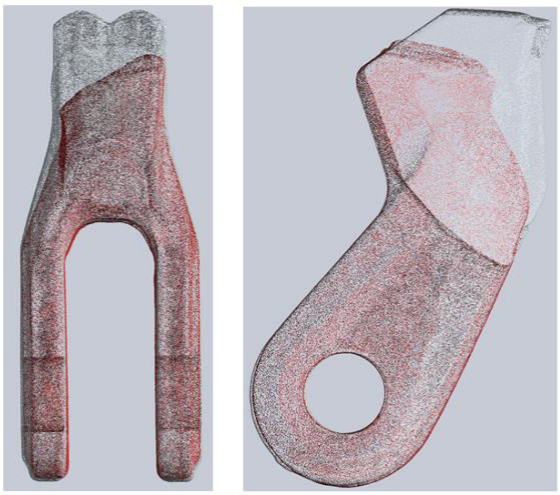

Figure 2 Loss of material displayed on the tool

An experiment was carried out in which 9 new teeth were placed on the rotor of the crusher and their wear patterns were observed (Figure 3).

Figure 3 Rotor of undesirable bumps

The tools were numbered from 1 to 9, with the tool on the left by the number 1, the tool moved one by the right to the number 2, etc. to the last position in the row of the rotor. With regular maintenance and inspection, it is not necessary to exchange all the tools at once, but only those that are so badly damaged that their working function is reduced to an unacceptable degree. Sometimes it happens that the tooth breaks on the tool and loses it. Such a tool is no longer usable. This is the case for the experiment 4 and 5 for the experiment. Next, we will try to continue using the tool, which we would like to achieve by applying the appropriate lifecycle methods. The article shows the progress of tool wear over time.

ACKNOWLEDGMENTS
The described work was carried out as part of a project APVV-16-0194, Research on the Impact of Innovation in Production Processes on the Life of Tools and Components of Forest Mechanisms.

COMPOSITION BASICS AND ANALYSIS OF VISUAL LANGUAGE OF THE PRODUCT

MARKOVA Kremena PhD
Technical University of Varna
E-mail: kremenacankova@abv.bg

Keywords: visual language, consumer's products, composition, informational expressiveness

The analysis of the visual language of the product demands deeper analysis of the user's profile and built behavioral patterns. There is an existing group of factors that have relatively constant nature - gender differentiation, age differentiation, belongingness to specific group – social status, place in hierarchy, race, religion, people with special needs, etc.
The analysis of the visual language of the product can be done by analyzing the basic arsenal of the composition - the means of composing form shaping:
Scale – It's related to the correct size of the products and their components, in other words – the properly designed dimensions provide operational and visual comfort. The elements that give the most accurate feature about the size of the entire product are called "scale indicators", such as spins, switches, handles, etc.
Proportions – Proportions are associated with organizing the form plastical and visual order of the whole and its parts. They are a selection of specific dimensional relationships that allow the whole to function as one system and ensures physical and visual balance. This balance allows the realization of the operating function of the product.
Contrast - A powerful mean of attracting the attention of the addressee. It can be related to the shape of the product - shaping patterns, number of elements, color, materials; may be semantic - to oppose the conceptual content of a physical model; to be bounded to past experience, atavism; to position a particular element in the whole or the whole itself in a specific way, etc.
Color – It's bounded to both formal characteristics and plasticity, as well as to contrast and its meaningful designation. It can be a mean of manipulating human emotions, for example, to provoke a desire for possession. The color can be related to certain fashion trends or combinations considered to be cultural evergreens. The perceptions of color depend on the features of visual perception and are a powerful factor in the formation of visual memory.
Plasticity. Plastic of the form - A basic tool of form shaping, linked to the proportions and scale, which determines not only the structural and formal characteristics of the products, but also the meaningful reading of the forms. It refers to both the structure, the construction of the shape and the nature of the surface, the coating or the characteristics of the materials used.
This tool often has the basic geometric patterns as the starting point, depending on the specifics of the visual perceptions and the simplicity and clarity of the model.
It should be noted here that the term " composing form shaping " in the papers is referred to the utilitary products, for the serial or mass production and not for works of art.
The analysis of the individual composite devices is demonstrated by Ingo Maurer's lighting fixtures, shown in Figures 1 and 2 as follows:

Figure 1 From left to right – „Oh Mei Ma Kabir" – 1997; „Jetzt 2" – 2015, an Axel Schmid's lighting fixture replica from 2009; „Lampampe" – 1980; „Luzy on the Wall" – 2018.

Figure 2 From left to right – „Dead Bulb Alive“ – 2000; „Holonzki“ – 2000; „Alizz T. Cooper“ – 2008; „Metall T. Cooper“ – 2009.

FORMABILITY INVESTIGATIONS OF ADVANCED HIGH STRENGTH STEELS

MEHDI Yassine, TISZA Miklós PhD
Institute of Materials Science and Technology, University of Miskolc
E-mail : om08@live.fr, tisza.miklos@uni-miskolc.hu

Keywords: Forming limit diagram, Sheet Metal Formability Testing System, Numerical Modelling, Materials Science

Car manufacturing has been significantly influenced by sheet metal forming developments, thus the requirements and developments in car manufacturing have decisive role in the development of sheet metal forming, too. The automotive industry is facing challenges of reducing body weight in consideration of environmental problems and higher collision safety. These requirements are being addressed by the application of various dual-phase steels, ultra and extra advanced high strength steels (UHSS, XAHSS). Forming Limit Diagrams (FLD) are the most appropriate tools to characterize the formability of sheet metals. Theoretical and experimental investigations of forming limit diagrams are in the forefront of todays' research activities. In this paper, an up-to-date research methodology elaborated and applied at the Department of Mechanical Technology at the University of Miskolc will be shown.

Sheet metal forming is one of the most important manufacturing processes. This is particularly valid for the automotive industry, where sheet metal forming has an even more important key position. The automotive industry is the leading sector in many countries and the main driving force behind the sheet metal forming developments as well.

As automakers are challenged to improve safety and fuel economy, they search for new materials to meet higher standards. Advanced high-strength steels (AHSS) help engineers meet requirements for safety, efficiency, lower emissions, manufacturability, durability, and quality at a low cost.

AHSS are a newer generation of steel grades that provide extremely high-strength and other advantageous properties, while maintaining the necessary formability required for manufacturing. They have been on the road for many years, but with additional research and development, automakers are using these newer grades in more applications

In general formability is the ability of sheet metal to undergo shape changes (plastic deformation) without failure by necking or tearing.

The most appropriate tool to characterize the formability of sheet metals is the Forming Limit Diagram (FLD).

Applying the Forming Limit Diagram, we can reliably estimate the forming behavior of metallic materials under various stress- and strain state as shown in Figure 1.

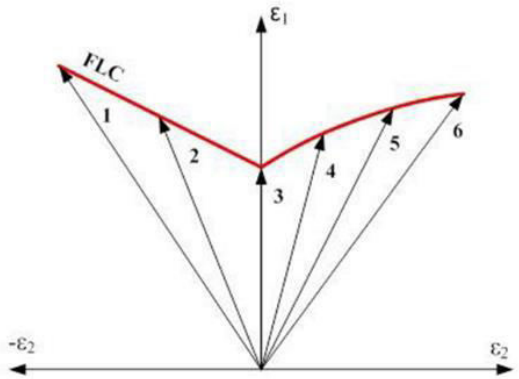

Figure 1 Forming Limit Diagram for various strain paths (1-pure shear, 2-uniaxial tension; 3-plain strain; 4, 5 6-different biaxial tension)

Forming limit diagrams (FLD's) offer a convenient and useful tool in sheet products manufacturing analysis. They show the critical combinations of major strain and minor strain in the sheet surface at the onset of necking failure. Formability in the context of multiple phase operations strongly depends of the deformation history and therefore demands an investigation of every particular case. This makes the experimental determination of FLD's unappreciative expensive and causes the necessity to develop an accurate and efficient theoretical method for formability prediction

In This article, we will introduce briefly the Advanced High Strength Steels (AHSS) and their broad range of properties as illustrated in the following diagram

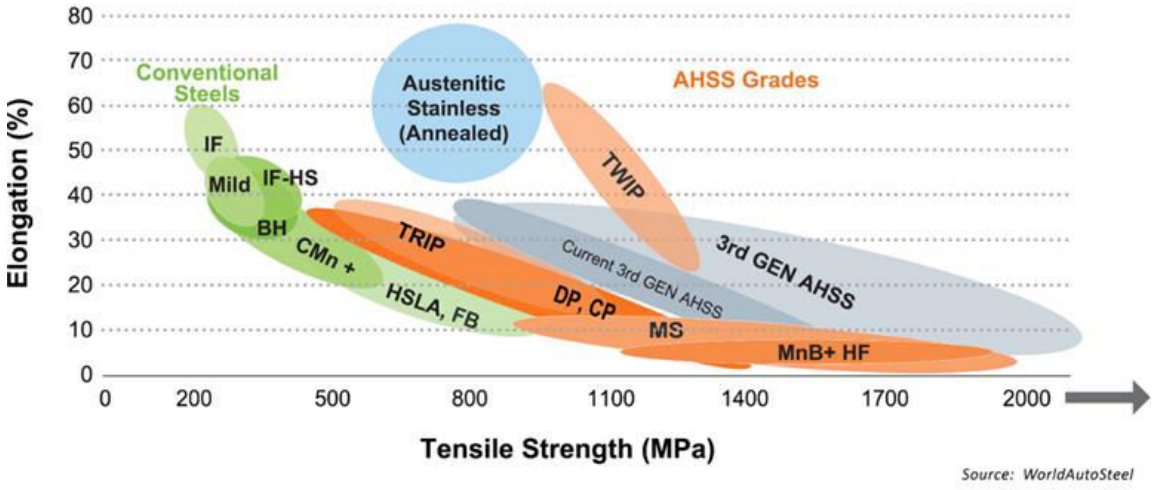

Figure 2 Steel Strength Ductility Diagram, illustrating the range of properties available from today's AHSS grades

Furthermore, a theoretical and practical demonstration regarding the generation of the forming limit diagram will be shown (Figure3)

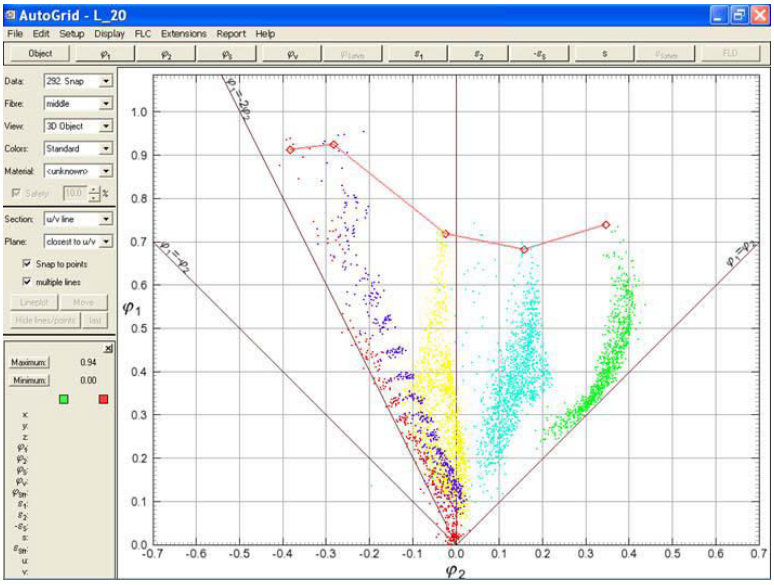

Figure 3 Graphical generation of FLC from the measured strains.

EXHAUST SYSTEM MUFFLER VOLUME OPTIMIZATION OF LIGHT COMMERCIAL VEHICLE USING TRANSFER MATRIX METHOD

[1]MOHAMAD Barhm, [1]KÁROLY Jálics PhD, [2]KERMANI Milad
[12]Faculty of Mechanical Engineering and Informatics, University of Miskolc-Hungary
E-mail: pywand@gmail.com, machijk@Uni-Miskolc.hu
[2]Faculty of Mechanical Engineering, University of Eastern Mediterranean-Cyprus
E-mail: mldkermani@gmail.com

Keywords: Muffler modelling; Audi A6; MATLAB Code; Transfer matrix method; Acoustic level control

Nowadays, the automotive industry is focused on weight and size reduction. Main advantae of this weight and size reduction are improving the fuel economy. The specific fuel consumption of a vehicle can be improved trough e.g. downsizing area of heat loss and weight reduction. Weight reduction can be done by replacing material or by changing the size (dimensions) of components. In the present work we have focused on Audi A6 muffler, troubleshooting and optimizing the muffler by changing pipe length of inlet and outlet, also by replacing the original mesh plate to porous pipe. Based on optimization, prototype has been built with the help of 3D design tool CATIA V5 and the calculations of transmission loss (TL) have been performed by MATLAB. Plane wave-based models such as the transfer matrix method (TMM) can offer fast initial prototype solutions for muffler designers. The principles of TMM for predicting the transmission loss of a muffler was used. Existing muffler has been analysed and then compared with vehicle level test observation data. Noise level have been optimized for new muffler design. Other literatures were played significant role for validate results.

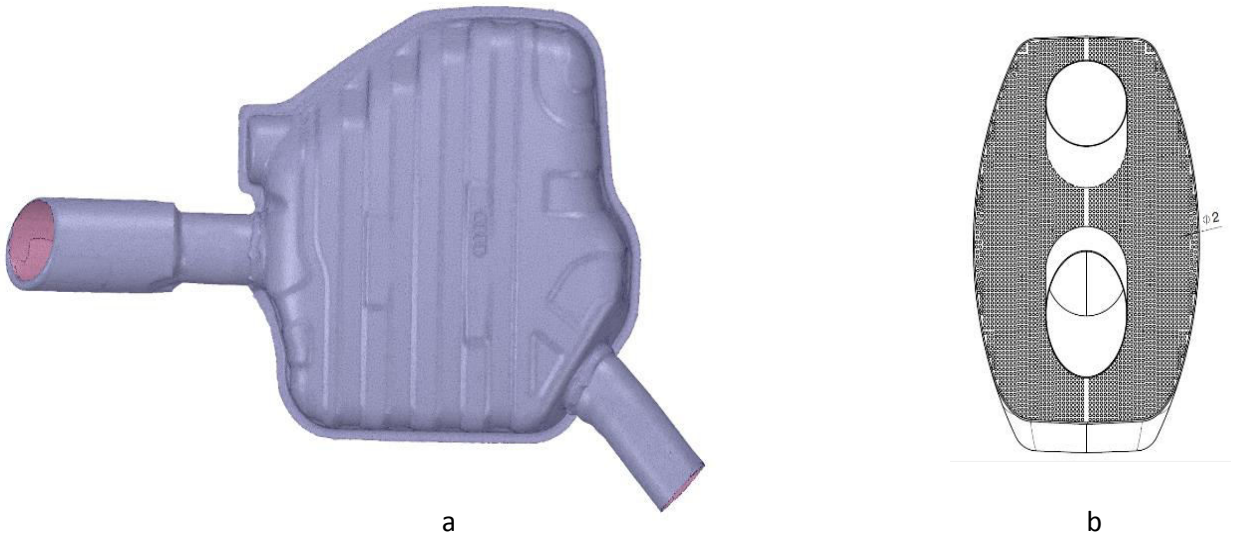

Figure 1 (a) Muffler geometry, *(b)* porous plate part inside the muffler

The noise reduction capability of a muffler can be defined as, insertion loss, or transmission loss. Noise reduction (R) related rather to rigid walls and not for mufflers. Insertion loss (IL) the reduction of noise level at a given location due to placement of a noise control device in the sound path between the sound source and that location. Transmission loss (TL) Measure of the airbone sound insulating properities, so IL and TL are used for mufflers. The transfer matrix method (TMM) uses the transfer matrix of a silencer element as a function of the element geometry, state variables of the medium, mean flow velocity, and properties of duct liners, if any. The results presented below correspond to the linear sound propagation of a plane wave in the presence of a superimposed flow. The basic formulation of the Transfer Matrix Method (TMM) has been summarized to predict the Transmission Loss of muffler elements. Neglecting the impacts of higher order modes is the cause of validation of the plane wave propagation.

Based on the geometry, the equation was applied utilizing the impedance analogy, the sound pressure P and volume velocity V at locations 1 (upstream end) and 2 (downstream end) in Figure 1 (x=0 and x=L, in order) can be stated by:

$$P_1 = AP_2 + BV_2 \qquad (1)$$
$$V_1 = CP_2 + DV_2 \qquad (2)$$

Where A, B, C, and D are usually called the four-pole constants. They are frequency- dependent complex values manifesting the acoustical characteristics of the tube. The equations (1) and (2) can be written in the way of matrix form as:

$$q_2 = T_1 q_2$$

Where $q_i = [P_i V_i]^T$ is a vector of thermally conductive state variables (i= 1, 2) and

$$T_1 = \begin{bmatrix} A & B \\ C & B \end{bmatrix}$$

Transmission loss can be written as:

$$TL = 10 Log_{10} \frac{W_i}{W_t}$$

Where W_i, W_t denote incident and transmitted sound power level of the acoustic wave present in the exhaust-duct system. Also, in the current analysis of an automotive muffler with porous plate inside, many useful results were obtained. The output from 3D analysis using Ansys-Fluent include acoustic level and 1D AVL-Boost calculation results includes transmission loss, see table 1.

Table 1 Data for the investigated muffler

Geometry		Numerical calculation	
Volume (v)	501480mm^3	TL of current muffler from TMM	55 dB
Inner diameter (D)	60mm	TL of modified muffler from TMM	65 dB
Outer diameter (d)	65mm	Frequency range (f)	0-2000 Hz
Porous diameter (D_p)	2mm	TL from 1D-Boost analysis	68 dB

This paper depict the modelling of mufflers using AVL _Boost software and discusses the ideas of the proper transformation of an Audi A6 muffler geometry to a linear acoustic calculation model as shown in figure 2.

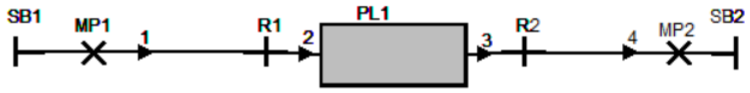

Figure 2 Muffler model using 1D -AVL Boost

A SLURRY-POT ABRASIVE WEAR TEST DEVICE FOR SEVERAL COMPOSITE MATERIALS

MUHANDES Hasan, KALÁCSKA Gábor DSc
Institute of Mechanical Engineering Technology, Szent István University
E-mail: hasanmuhandes@gmail.com, kalacska.gabor@gek.szie.hu

Keywords: slurry test – abrasive wear – composite materials.

To choose the proper material for agricultural machinery we tested several materials with abrasive cloth on the pin-on-plate test device. After having the pre-results, we launched more complex abrasive testing (slurry-pot) simulating more realistic mode with soils to investigate the abrasive wear mechanism and resistance of the selected up-to-date polymeric structural materials. For this, we developed a modified slurry-pot test machine that ensures the comparability of the materials over a wide range of conditions. Through this device, several parameters could be controlled like speed, the soil particle's hit angle on the tested surface.

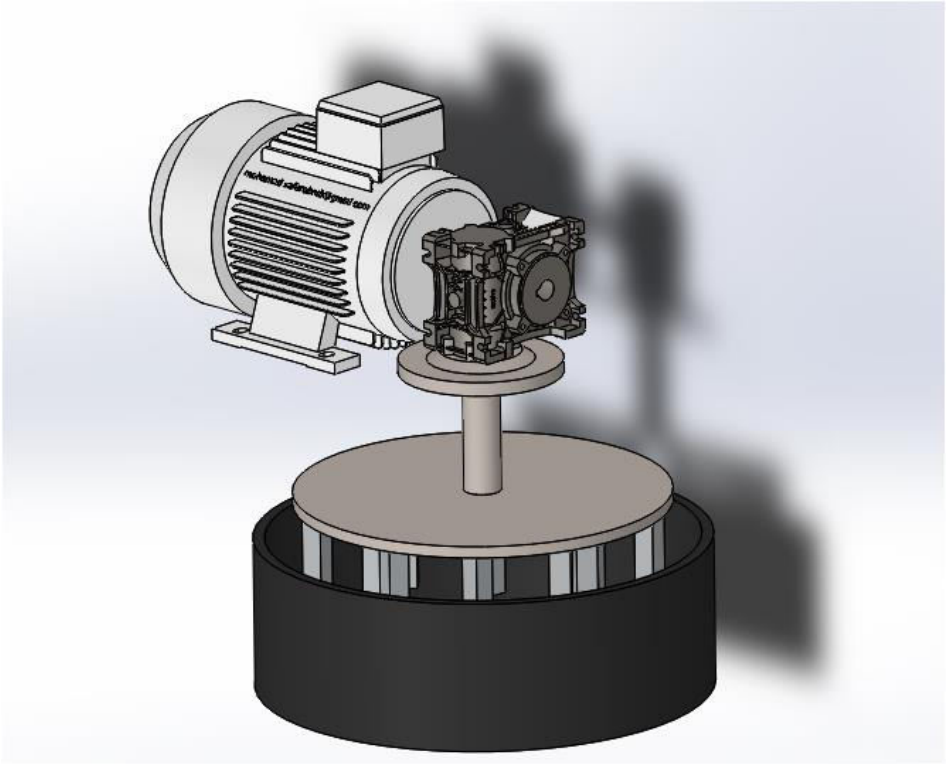

Figure 1 The slurry-pot abrasive wear test device

In our last research we tested several composite materials in the standard abrasive test, we wanted to check these materials in the real mode, in other words when these materials are in contact and friction with soils.
Three concepts were the main points for our design:
1- The size of the specimens.
2- The possibility to install and uninstall these parts every day since we want to take measurements every day.
3- Test the materials in the same conditions, which is an essential point.
To consider these three concepts, the first point in our design was that the sizes of the specimens and the size of the holders which will hold them. This size should be acceptable for testing in a laboratory device, the dimensions of the specimens were 120mm as length, 20 mm as width and 6 mm as thickness, so our starting position was the specimens' holder.
After deciding the size of the specimens, we wanted to test the materials with the same conditions. Having the same conditions every time is such hard or almost impossible thing, so the best choice is to test all materials at the same time, by that we will ensure the same conditions.

During the last research we had six composite materials and two speeds, and to test all the six materials with two speeds we have to use twelve holders.
As a linear motion, we are not able to have two speeds at the same time. So changing the design to a rotation motion was the solution for this case.
So we fixed these twelve holders on a disc with two positions by using two radiuses. An outer radius r_1 and an inner radius r_2.
The twelve holders were divided into six groups, one for each composite materials, each group has an outer and an inner holder, by that we can test and compare all materials with two speeds. The first speed is 1.456 $m.s^{-1}$, while the second one is 2.038 $m.s^{-1}$.
By immersion these twelve holders in a pot which contains the wear media this will ensure good contact and friction conditions between the composite materials and the wear media.
As a result of these step, we got this test device as shown in figure 1.
This device allows studying several factors:

- Study the effect of speed on wear rate.
- Study the effect of friction angle on wear rate.
- Study the effect of abrasive media on wear behaviour, since we can use several abrasive media.

DIFFERENCES IN THE BEHAVIOR OF NORMAL AND RACK RAILWAY VEHICLE'S BOGIE ON TRACK

NAGY Andor, LAKATOS István PhD
Széchenyi István University
E-mail:nagy.andor@sze.hu, lakatos@sze.hu

Keywords: rack railway, cogwheel railway, assimmetric rail bogie behavior, differences in axle box pressures

Usually, nowadays when I'm making a presentation, I start my speech with warning the audience, that they are supposed to forget mostly everything that they know about traditional railway systems. On the rack railway, we don't use the flanged rail wheel to transmit the force of traction or braking to the rail, but only keeping the vehicle on track. The traction and braking force is presented by a massive cogwheel per braked and/or traction and braking bogie, and some of the wheels are fixed on the axles, and some aren't. Just to mention, on rack railway there are (in historical order) Blenkinsop, Marsh, Fell, Riggenbach, Abt, Strub, Locher, Morgan, Lamella systems, and mixtures of the above. Basically, the difference lays in the cogwheel, and the rack connection. The Locher applies two cogwheels sideways of the rack (Pilatus Bahn), Abt uses two or more closely joint cogwheel, those teeth are shifted from each other (Harzbahn), Strub is a straight-faced cogwheel (Budapest, Strba .). All of them has its advantages, and disadvantages.

It can clearly be seen that all of the systems are limiting the movement of the axle, and indirectly the bogie and the vehicle on the track. Following the most recent derailments of Budapest Cogwheel Railway, I want to dig myself deeper to the almost forgotten science of the rack railways. The aim is to proof all aspects from vehicle side and track side, that may cause the vehicle to derail.

There are a very few regulations that are affecting the track layout of the rack railway, in Hungary:

a) There is no transition curve by the curves, there is the straight part of the track, then – boom – there is the curve. This limits the speed as well, as the side accelerations can be pretty big, and this single handedly can cause the train to derail. Due to the reduced speed of the operation the designers sacrificed the transition curve, not to mention its extremity to be designed, caused by the limited flexibility of the rack itself.
b) Superelevation is applied in all the curves, but extreme care must be taken, because we need to adjust the level of the rack as well, and its angle compared to the vertical perpendicular must be also carefully adjusted, in other case, the cogwheel will climb out of the rack. If the curve's outer rail is lower than the superelevated rack's outer edge, the wheel stops being as a support to the vehicle, and the rack will carry the weight, that supposed to be carried by the specific wheel.

The bogie itself is a complicated, and assimetric part. If we measure the pivot pressures on the wheels, we will find that the differences between the wheels, can be sometimes bigger than 5%! This is unacceptable by a traditional railroad vehicle, especially by high speed railways. (Over 120 km/h, 2% is acceptable) When we look at this bogie, it is far away from conventional. The center of gravity is on a parallel, but different vertical line than the center plate.

When tracing a normal bogie, we can experience the classic mechanical movement of a normal railroad bogie. Hypothetically, we assume that all the wheelsets are a part of a torsion system. But this is only true by the classic railroad bogie. Because of its mechanical design, not all of the axles can behave itself like a normal torsion system. The "clean" sinus movement of the axle center point cannot be realized. As one of the axles has bearing on both of its hub seats, one degree of freedom is taken away, so the figure above is modified by both of the traction bogie, and the brake bogie. This makes a huge difference in the behavior and the movement of this special bogie on the track.

As a conclusion, it can be stated, that by the traction axle, the angle speed of the two wheels, are not identical! So the wheels play only a support function on this specific axle, when it is not set to adhesive mode. The traction and braking forces are not attacking the rail via the wheel itself, as it happens by the classic rigid wheel joint.

Normally, if we talk about a stiff axle, with fixed wheels, the angular speed of the two wheels would be identical, so the wheel would normally not leave the rail. But here the angular speeds are different, and the axle gets elevated from the rail, as the cogwheel takes the weight what the specific wheel must carry, and as the centripetal force pushes it, the teeth slip out of the rack, and the bogie derails.

CONCLUSION

After numerous measurements on the track itself, and laser-modeling it, taking numerous video recordings, we can state that the rack railway traction bogie or brake bogie is significantly more sensitive to the track's super elevation, and the geometry of the rack between the two rails. The assimetric bogie weight distribution also helps to the bogie to turn around the center place, and this movement is also helped by the cogwheel. The measurement is currently in progress to determine the marginal force, and the minimum elevation of the curve's outer rail, for to avoid such derailments.

ACKNOWLEDGMENTS

The described work was carried out as part of NAGY Andor's Ph.D thesis work, supported by Budapest Transport Plc, Directorate of Railway Operations.

THE MEASUREMENT OF THE THREE COMPONENTS OF THE CUTTING FORCE DURING THE TURNING PROCESS

[1]NEMES Csaba, [2]LUBOMIR Javorek PhD, [1]BODZÁS Sándor PhD, [1]PÁLINKÁS Sándor PhD
[1]Faculty of Engineering, University of Debrecen
E-mail: csabanemes94@gmail.com, bodzassandor@eng.unideb.hu, palinkassandor@eng.unideb.hu
[2]Department of Manufacturing Technology and Quality Management, Technical University in Zvolen
E-mail: lubomir.javorek@tuzvo.sk

Keywords: cutting force, turning, machining, measurement, depth of cut.

We carried out the measurement of the three components of the cutting force as a function of the modification of the depth of cut during the longitudinal turning process. The results show that if we increase the depth of cut, all three components of the cutting force shows increasing tendency, regardless of how much the cutting speed and feed speed were performed during the measurements.

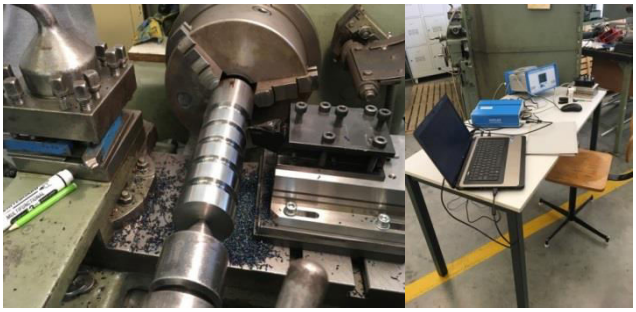

Figure 1 The lathe (E-400) and the instruments

We used the following measuring instruments:

- Kistler Type 9257B
- Kistler Data Acquisition System Type 5697A 22003583
- Kistler Multichannel Charge Amplifier Type 5070

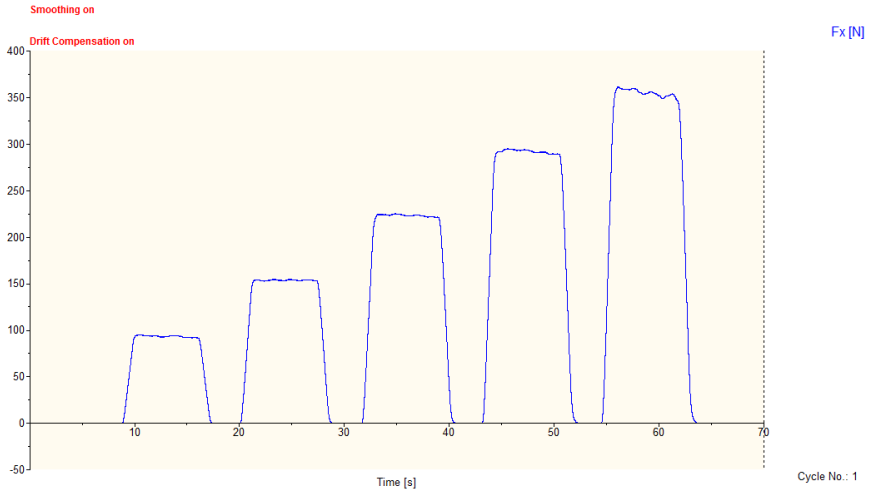

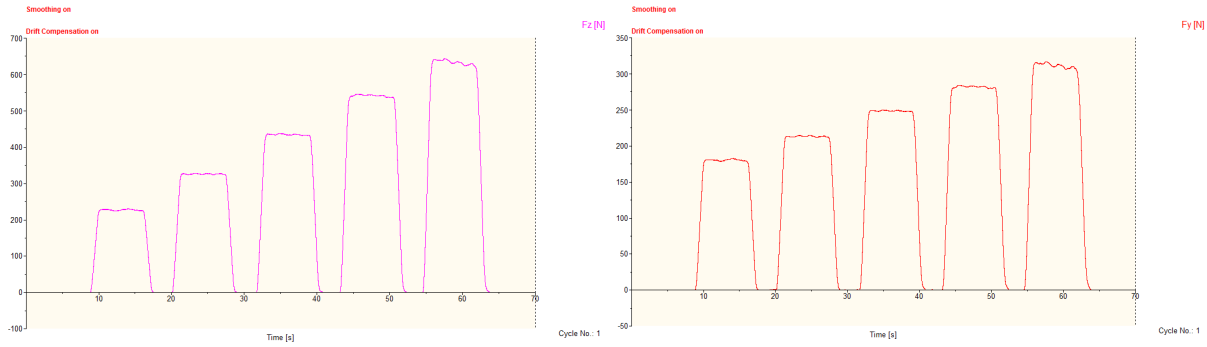

Figure 2 Measurement results

$$F_x = F_f = \textbf{feed force}$$
$$F_y = F_a = \textbf{passive force}$$
$$F_z = F_c = \textbf{main cutting force}$$

We made a total of six measurements. Comparison of measured and calculated results can be seen in the following diagrams:

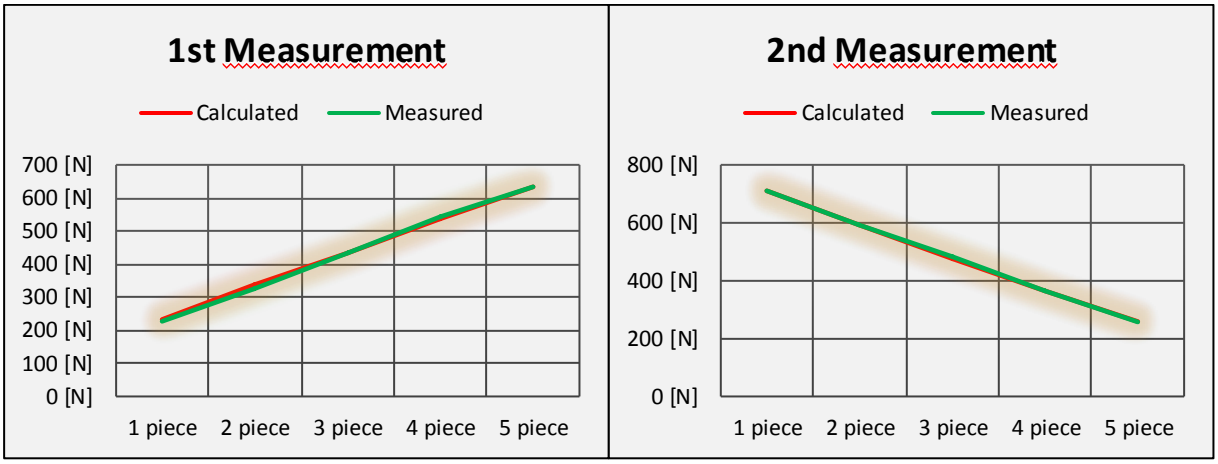

Figure 3 Comparison of measured and calculated results

The formula for calculating:

$$F_c = C_1 \cdot f^x \cdot e^y \cdot \sigma^n \cdot R^p \cdot \kappa^s \cdot {v_c}^b \cdot K_\gamma \cdot K_k \cdot K_h \cdot K_a \cdot K_\lambda$$

F_c: main cutting force
C_1: chipping factor
f: depth of cut
x: exponent of depth of cut
e: feed
y: exponent of feed
σ: tensile strength
n: exponent of tensile strength
R: corner radius
p: exponent of corner radius
κ: major tool cutting edge angle
s: exponent of major tool cutting edge angle
v_c: cutting speed
b: exponent of cutting speed
K_γ: tool rake dependent factor
K_k: tool wear dependent factor
K_h: tool cooling dependent factor
K_a: tool clearance dependent factor
K_λ: tool inclination angle dependent factor

ACKNOWLEDGMENTS
The project was implemented by the Ministry of Human Resources through the New National Excellence Program of the Higher Education Master's Degree Researcher's Scholarship. Project number: ÚNKP-18-2-I-DE-100.

REGENERATION OF A WASTE SOLVENT MIXTURE WITH TWO DIFFERENT BATCH COLUMNS

NÉMETH Bence, LÁNG Péter DSc, HÉGELY László PhD
Department of Building Services and Process Engineering, Budapest University of Technology and Economics
E-mail: lang@mail.bme.hu

Keywords: batch distillation, waste solvent regeneration, two column system.

INTRODUCTION

Distillation is considered to be the most widespread process for separating liquid mixtures, which is based upon the differences in volatilities of the components. Batch distillation is commonly used in the pharmaceutical and fine chemical industries for separating mixtures with varying composition and amount. In this work, an industrial waste solvent regeneration process is investigated by dynamic simulation. In the plant two columns of different size are used. The mixture contains in the order of increasing boiling point *A, B* and *C* components, from which *B* must be recovered in high purity. The quality criteria for the *B* product: (1) less than 0.05 vol% *A* and (2) less than 0.2 mass % *C*. The goal of our work is to maximize the B recovery by improving the current process. The model of the process is developed by using the ChemCAD professional flow-sheet simulator.

VAPOR-LIQUID EQUILIBRIUM OF THE MIXTURE

A and *C* forms a minimal boiling point heteroazeotrope (Hodgman, 1962) which boils at 38.8 °C and the azeotrope contains 99.6 mass % *A*. B forms tangent azeotropes both with *A* (Maczinski and Skrzecz, 1983) and *C* (Horsley, 1962) at high *B* content. This means that the separation is very difficult, when high B purity must be produced.
UNIQUAC thermodynamic model (which is frequently used for describing the vapor-liquid equilibria of non-ideal mixtures) was chosen for modelling the phase equilibrium conditions. We chose binary interaction parameters (BIP-s) from the literature or we generated where there was no available data. Those BIPs were selected which generated well-fitting equilibrium curves to the measured data. When we found better fitting BIPs than the ChemCAD default parameters, then those were swapped. Generated parameters were chosen for the *A-B* pair based on the measurements of Golubkov et al. (1979), for the *A-C* pair the ChemCAD default parameters were kept and for the *B-C* pair BIPs were taken from the literature (Brunjes and Bogart, 1943).
The composition of the mixture to be separated, can vary in wide ranges: 0.05-0.3 vol.% *A*, 60-80 vol.% *B* and 20-40 vol.% C. Calculations were performed with an average composition: 0.1 vol.% A, 69.9 vol.% B and 30 vol.% C.

PROCESS DESCRIPTION

The separation is performed in two batch columns with structured packings. The first column (Column 1) is a smaller one (providing ca. 3 theoretical plates (without the reboiler and total condenser)) and the second (Column 2) is a larger one (ca. 20 theoretical plates). In the present process the steps for the smaller column:

0. Heating up the column (not simulated)
1. Taking of 50 dm^3 fore-cut under finite reflux ratio (R≈5)
2. Taking of main cut until the *C* content in the accumulator reaches 2.5 vol.%

In Column 1 two batches are processed consecutively then the two main cuts are united and distilled again in Column 2 in the following steps:

0. Heating up the column (not simulated)
1. Taking of 100 dm^3 fore-cut under R≈8
2. Taking of main cut until the *C* content in the still reaches 9 vol.%

To reach higher B recovery, the stop criteria and the reflux ratios of these steps were optimized. We investigated two cases depending on the column, from which fore-cut is taken: only from Column 1 (Case 1) and only from Column 2 (Case 2).

PROCESS MODEL

We developed the ChemCAD model of the process (*Figure 1*). Unit 1 is the smaller and 6 is the larger column ("BATCH COLUMN"). Units 3, 4 and 8 are the distillate tanks (accumulators). Units 2, 5 and 7 are "SREF" units. SREF 2 and 7 create reference streams from the bottom of the smaller and larger columns, respectively. SREF 6 transfers the content of tank 3 after multiplying its amount by 2 to the larger column.

CALCULATION RESULTS

IN BOTH cases, we studied the effect of the stop criteria and reflux ratios in each steps on the *B* recovery and on the average specific product flow rate (SPF), which is the amount of *B* product divided by the total process time. Those parameters were chosen, which gave the highest *B* recovery and did not exceed any process limitations such as purity criteria or the minimal amount of liquid in the still of Column 2 (1 m^3) at the end of the process. The parameters chosen

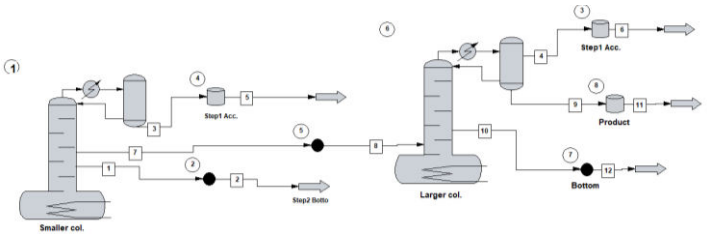

Figure 1 ChemCAD flowsheet of the process

are shown in *Table 1*, where Case0 is the present process, Main Cut 1 is the pot charge (after multiplying by two) for Column 2 and Main Cut 2 is the *B* product.

Table 1 Parameters for the present and new processes

	Fore cut 1	Main Cut 1	Fore cut 2	Main Cut 2	
Case0	<0.03 vol.% A in the still	>2.5 vol.% C in the accumulator	100 dm^3	>9 vol.% C in the still	Stop Criterion
	5	5	8	8	Reflux ratio
Case1	<0.02 vol.% A in the still	>2 vol.% C in the accumulator	-	>13 vol.% C in the still	Stop Criterion
	12	10	-	8	Reflux ratio
Case2	-	>1.7 vol.% C in the accumulator	<0.035 vol.% A in the still	>11 vol.% C in the still	Stop Criterion
	-	12	14	6	Reflux ratio

The summary of the most important results are presented in Table 2.

Table 2 Most important results for the present and new processes

	Case0	Case1	Case2
B recovery, %	68.86	82.21	67.49
SPF, kg/h	64.22	71.11	56.97
Capacity, t/week	~46	~40	~38

CONCLUSIONS

By both new operational policies the product quality criteria were reached, but Case2 proved to be worse than Case0 for both *B* recovery and SPF. In contrast, Case1 was much better than Case0 considering *B* recovery and SPF. However the weekly capacity of the process slightly decreased, but this might be improved by increasing the charge of the first column until a new process limitation is reached (e.g. reboiler volume of the larger column). The reason for being Case1 the best: the removal of *A* from *B* is easier when more *C* is present because *C* increases the relative volatility ($\alpha_{A,B}$). In Case2, in the charge of the larger column less *C* is present, but the *A/B* separation is more difficult.

ACKNOWLEDGEMENTS

This work was supported by the National Research, Development and Innovation Office – NKFIH, K-120083.

REFERENCES

[1] Brunjes A. S., Bogart M. J. P., Ind. Eng. Chem. 35, 255 (1943)
[2] Golubkov, Yu. V., Repneva, T. G., Skibarshina, V. T., Kotenkova, N. P.: Zh. Prikl. Khim. 52 (10), 2350 (1979)
[3] C. D. Hodgman (edit): CRC Handbook of Chemistry and Physics, 44th Edition. CRC Press, Cleveland, 1962.
[4] Lee H. Horsley, William S. Tamplin: Azeotropic Data-II. In Advances in Chemistry Series, No. 35. Washington, D.C., 1962.
[5] A. Maczinski, A. Skrzecz: Verified Vapor-liquid Equilibrium Data, Vol.7, Binary Two-liquids Systems of Water and Organic Componds, Warszawa, 1983.

DEVELOPMENT OF EFFICIENT DRIVE BASED ON SELF-HELP

NÉMETH Géza, PÉTER József PhD
Institute of Machine and Product Design, University of Miskolc
E-mail: machng@uni-miskolc.hu, machng@uni-miskolc.hu

Keywords: self-help, epicyclic traction drive, helical torsion spring.

There are a huge many principle of embodiment design, one of them is the principle of self-help [2]. When we develop a new machine element or a new machine structure so that the maximum stress occur only at the maximum load, we use the previously mentioned principle. Let us consider a pressure-cooker. The sealing force is increasing with the increment of the inner pressure. The experience is the same in case of the operation of mechanical seals. Of course, an initial sealing force should be applied to the seal at the beginning of operation, to assure the proper sealing also at shut down. The supplementary force is generated by the increasing pressure.
There are drives where the forces and torques acting to the elements can be proportional to the external load, almost automatically. In the case of a form closing drive, like a gear drive, the elements are unloaded when there is no external torque acting and the flank or root of teeth are loaded proportionally to the external torque. The friction drives are not so simple structures, considering this point of view. The geometry and the needs of manufacturing is less but not the proportional loading of the machine elements. Usually an extra machine element is required to assure the proper compressive force between the mating elements, or to assure the proportional compressive force, not to overload unnecessarily the elements.
The simplicity is also a useful principle. Try to integrate the function of the proportional compressive force and the power transmission element into a single machine element. There are some clutches, as the spring type clutch where the friction force is increasing proportionally with the increasing torque needs [2]. This principle is shown in Figure 1.

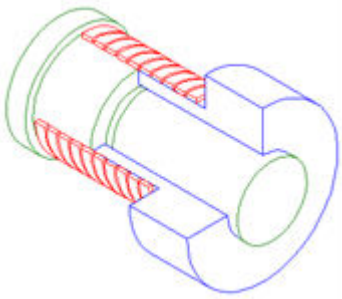

Figure 1 Spring type clutch [2]

The helical torsion spring that connects the input and output shafts works as a friction type free running clutch. It operates in unidirectional service, and the load of the connecting element (bending moment) is proportional to the external torque.
A similar structure is the helical spring bearing at Figure 2 that eliminates the unequal heat distribution and from that a special epicyclic traction drive can be originated.

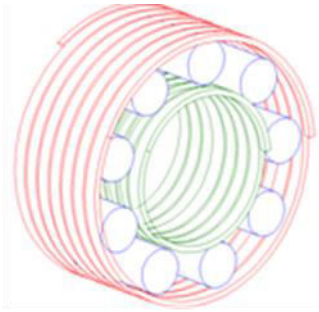

Figure 2 Helical spring bearing

The annular wheel or the sun wheel or both of them can be substituted by helical torsion spring. When the planetary wheels are installed to the planet carrier with radial space, the tightening (force applying) parts can be omitted. The helical spring has got a special load, due to the great number of contacts with the planet wheels, shown in Figure 3. The production technology of the spring can be manufacturing for the more accurate mechanical properties. Another advance of the manufacturing is the easy variability of the spring – e.g. for the proper initial tensioning the cross section at the free end, see Figure 4 the cross section can be increased. Hopefully the drive where the elastic element is stationary, can work in noiseless service and with low slippage. The main load of the strip (the helical spring) is bending, the load can be calculated analytically at any cross-section along the strip. Another advance of the manufactured spring is the merging of the functions, decreasing forward the number of elements.

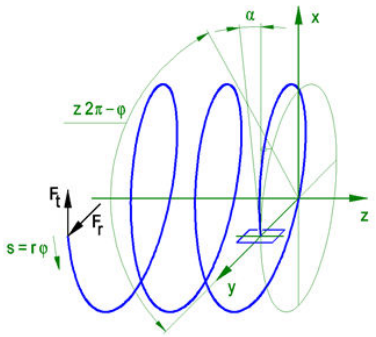

Figure 3 Modelling of the special helical torsion spring

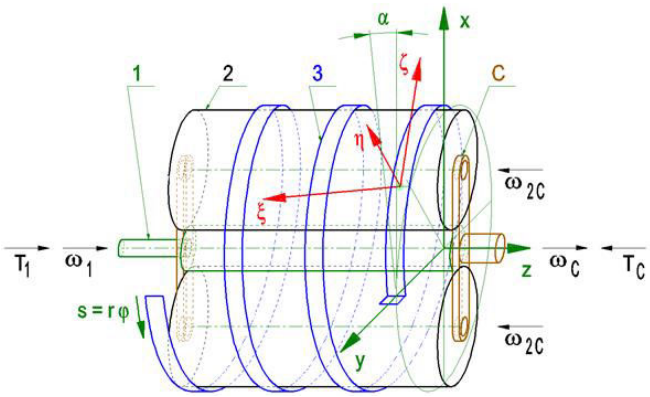

Figure 4 Modelling of the special epicyclic traction drive

The authors outlined a possible solution for this problem. The planet wheels are made of a series of deep groove ball bearings, the sun wheel is a simple circular rod, quenched and tempered and the spring has got also a high level hardness. The free radial displacement of the shaft of the planet wheels in the planet carrier is also essential. The greater the external torque acting the output element, C (planet carrier) the greater elastic deformation of the helical spring, 3 assure the greater contact force between the power transmitting elements due to the principle of self-help. The better efficiency and higher life rating are also the consequence of this principle.

ACKNOWLEDGMENTS

This work was supported by the European Union and the Hungarian State, cofinanced by the European Regional Development Fund in the framework of the GINOP-2.3.4-15-2016-00004 project, aimed to promote the cooperation between the higher education and the industry.

REFERENCES

[1] C. F. Wiebusch: *Dial Clutch of the Spring Type,* Bell System Technical Journal, Volume 18, Issue 4, October, p. 724–741. 1939.

[2] G. Pahl, W. Beitz: *Engineerin Design: A systematic Approach,* Springer-Verlag, London, p 257-267, 544p. 1996.

DEVELOPMENT OF A SMALL-SCALE PLASTIC RECYCLING TECHNOLOGY FOR 3D PRINTING

[1]OUSSAI Alaeddine, [1]BÁRTFAI Zoltán PhD, [1]KÁTAI László PhD, [2]SZALKAI István
[1]Faculty of Mechanical Engineering, Instutute of Mechanics and Machinery, Szent István University
[2]FKF Nonprofit ZRT
E-mail: alaoussai@gmail.com

Keywords: Recycling, plastic, polymeres, 3d printing, filaments

Abstract: *In our days, the fight against pollution has become a real challenge for the state. Recycling is one of the solutions that is adopted in several nations to reduce the rate of plastic discarded in nature. The amount of plastic waste has been increasing for decades contributing to the environmental pollution that is one of the most serious problem of the mankind. According to the statistics not only the household plastic waste, but the industry discharge is increasing because the utilization of plastic as a raw material is more and more extending. Plastic can be found in a lot of products,huge amount of bottles, plastic bags, computers, auto parts are sold every day. Although, plastic has become very useful in the everyday life, it is dangerous for the environment since most plastics are non-degradable in nature. The analysis and development of the manufacturing-, and utilization in 3D printing technology of the filament made of recycled plastic is an actual engineering problem. A successful research on this field can support the sensible, economic usage of the plastic waste , this is the main reason why I also would like to act on this field.*

In the case of waste plastics that are recyclable and reusable. The most widely used are polyethylene terephthalate (PET, used for synthetic fibers and water bottles), and second high-density polyethylene (HDPE, used for jugs, bottle caps, water pipes).

Figure 1 Worldwide PET bottle consumption and collection(PCI)

The current applications for using recycled plastics in fabrication and design are fairly limited, on a small scale, plastics (such as ABS, HDPE, or PET) are shredded and formed into pellets, and then either extruded into lament to be used in existing 3D printers, or injection molded into small parts and pieces of larger components. At a large scale, recycled HDPE is melted into sheets and either used directly as sheets in construction, or then heat formed from a sheet into components for construction. These methods of fabrication using recycled plastics are the norm because of their straightforward processes. Nevertheless, each method leaves some complexity to be desired.
In this paper we study the types of plastics and diagnose the pollution caused by the latter. This allowed us to design and size a recycling station of plastic into filaments for three-dimensional printers. This station which will contribute to the fight against pollution. The station consists of two machines for grinding of the plastic and the other for the

extrusion of the desired filaments. We were able to make a theoretical academic study on both machines and also we designed with SOLIDWORKS 2015. The theoretical study is spread of the mechanical calculations necessary to the design and validation of the structure using the tools. As the prospect of this project, we want to complete the achievement of this station while completing the crusher and extruder mechanically. Then switch to electric and electronic parts (introduction of engines, sensors and wiring...).
we show the environmental consequences of plastic solid waste are visible in the ever-increasing levels of global plastic pollution both on land and in the oceans. But although there are important economic and environmental incentives for plastics recycling, end-of-life treatment options for plastic solid waste are in practice quite limited.
Presorting of plastics before recycling is costly and time-intensive, recycling requires large amounts of energy and often leads to low-quality polymers, and current technologies cannot be applied to many polymeric materials.
Recent researches point the way toward chemical recycling methods with lower energy requirements, compatibilization of mixed plastic wastes to avoid the need for sorting and expanding recycling technologies to traditionally nonrecyclable polymers.
Mechanical recycling is the only widely adopted technology for large-scale treatment of plastic solid waste. In it the main steps are the removal of organic residue through washing, followed by shredding, melting, and remoulding of the polymer, which is often blended with virgin plastic of the same type to produce a material with suitable properties for manufacturing.

ACKNOWLEDGEMENT
The described work was carried out as part of a project supported by the National Research, Development and Innovation Office – NKFIH, K123456

REFERENCE
[1] M. C. Flores: *Plastic Materials and Environmental Externalities Plastic Materials and Environmental Externalities : Structural Causes and Corrective Policy Table of Contents Plastic Materials and Environmental Externalities Plastics Recycling* : Law and Economics. Lethbridge Undergraduate Research Journal, 3, 2–7. 2008.
[2] M. Grigore: *Methods of Recycling, Properties and Applications of Recycled Thermoplastic Polymers. Recycling*, 2(4), 24. https://doi.org/10.3390/recycling2040024, 2017.
[3] E. Hajekova, M. Bajus: *Recycling of low-density polyethylene and polypropylene via copyrolysis of polyalkene oil/waxes with naphtha: product distribution and coke formation*. J Anal Appl Pyrolysis;74:270e81, 2005.
[4] MA Huneault, H. Li: *Comparison of sorbitol and glycerol as plasticizers for thermoplastic starch in TPS/PLA blends.* J Appl Polym Sci; 119:2439e48, 2011.
[5] JCR*: Plastics recycling. Final Assessment Report,* St. Catherine's College JCR, University of Oxford, UK. Available at: http://hadriel.caths.cam.ac.uk/jcr/html/ 2006.
[6] A. Oussai: *Bartfai Z. study design and sizing of a plastic recycling station into filaments 3d printer*,Szent Istvan Egyetem 2017.
[7] H. Kang, J. M. Schoenung: *Electronic waste recycling: a review of U.S.infrastructure and technology options.* Resources, Conservation and Recycling 45 (4), 368–400. 2005
[8] Mercosur. *Mercosure technical regulation of packages of food grade post-consumer recycled poly(ethylene terephthalate) (PET) (food grade PCR-PET) intended to come into contact with foodstuffs*. Mercosur/GMC/Resolution Nr 30/07; 2007
[9] Minnesota *Office of Environmental Assistance (MOEA)*, Recycling used electronics report on Minnesota's demonstration project, July, 2001
[10] M. Vaezi, S. Yang: *2 - Freeform fabrication of nanobiomaterials using 3D printing Rapid Prototyping of Biomaterials,* pp. 16-74. 2014.

APPLICATION OF COLD AND HOT METAL POWDER SPRAYING

[1]PÁLINKÁS Sándor PhD, [2]FAZEKAS Lajos PhD, [3]GINDERT–KELE Ágnes PhD, [4]MOLNÁR András
[1,2,3]Faculty of Engineering, Department of Mechanical Engineering, University of Debrecen
E-mail: palinkassandor@eng.unideb.hu, fazekas@eng.unideb.hu, battane@eng.unideb.hu
[4]Faculty of Mechanical Engineering and Informatics, Department of Mechanical Technology, University of Miskolc
E-mail: a.molnar2007@gmail.com

Keywords: wear, abrasive wear, agricultural equipments, tillage tools

Flame spraying belongs to the group of thermal spraying methods and constitutes a well-established technique of surface engineering. Its advantages include ease of application and low cost compared with other spraying processes. With relatively low thermal input, its "cold" variant can be performed, which involves preheating the substrate up to about 100 ºC and deposition of coating, whereas the temperature of the system does not exceed 250 ºC. In spite of the relatively mild conditions, good bonding between the substrate materials and a wide range of alloys can be achieved, especially if intermediate bonding layers are applied. Cold flame spraying of coatings may be the final step in the production technology or may constitute itself a surface restoration technology. Applications include corrosion protection, repair of worn shafts in sliding bearing areas, etc. In agricultural engineering the technology is also used for shaft renewing typically operating in hostile environment and the replace with new parts means extra costs.
Thermal spraying is already used in industry to protect mechanical parts against wear and corrosion, but results are not always satisfactory due to porosity, microstructures and mainly bond strength. The thermal spraying underwent on spectacular development in the past decades and the development goes on nowadays, too. The method is also used at such advanced technical application as renewing, repairing parts of jet propelled power plant. The cold flame spraying is a wide – spread method renewing shafts worn in normal work renewing sliding bearing surfaces, or other sliding surfaces well identifiable (Figure 1). The main advantage of the technology is it can be also used in case of alloyed shafts as avoiding heat effect higher than 200-300 ^{0}C the get hardening, the texture change can be avoided. The size-decrease or breaking as well as the surface quality of parts exposed to significant wear and load can be improved by building up a new surface by using the traditional surface-layer welding and the different metal powder spray fusing technologies (Figure 2). By this, the construction of machine elements can be simplified and it is significant from economical point of view as well as it is not necessary to replace the whole workpiece. A lower specific flame intensity is used during the surface-layer welding; the seams are not deep but they are wide instead. A significant wear of machines used in the different fields of agriculture can be experienced. As a significant part of people living in Hungary deals with agriculture, it is very important to know how to ensure the cost-efficiency and the efficient agriculture. During the recent period of our research work, made experimentally hot metal powder spray fusing of cultivator tines in order to investigate their durability.

Figure 1 Rotor repair with cold spray process

Figure 2 Renovation of the mold in the glass industry

The use of complete workpieces for soil preparation: The experimental workpieces were given to János Illyés agricultural entrepreneur in Hajdúszovát who mounted them on the combinator and performed the soil-preparation of a land of 200 hectare. The mass of tines was measured both before using them and after the soil-preparation of the land of

200 hectare. The obtained results are demonstrated in Table 1. It can be stated that Sample No. 5 (indicated by bold letters in the Table) and Sample No. 7 (indicated by bold letters in the Table) wore in the less extent of the samples treated by hot metal powder spraying. Such a result could be anticipated at these samples as this powder had got the highest hardness (60 HRC).

Table 1 The mass of cultivator tines before and after use

No of sample	Performed procedures: Spray welding by using	Mass of workpiece [g]		
		Before use	After use	Difference
1.	10009 Borro Tec powder	246,89	199,1	46,98
2.	10009 Borro Tec powder	245,82	187,33	58,49
3.	10009 Borro Tec powder	251,57	198,41	53,16
4.	N 60 Mogul powder	248,54	197,34	51,2
5.	**N 60 Mogul powder**	**258,01**	**227,24**	**30,77**
6.	N 60 Mogul powder	248,66	193,21	55,45
7.	**Deloro 60 powder**	**253,49**	**220,09**	**33,4**
8.	Deloro 60 powder	249,83	191,27	58,56
9.	N 40 Mogul powder	265,92	159,05	106,87
10.	N 40 Mogul powder	256,94	184,68	72,26

In case of the samples No. 9 and 10, a powder-type with a hardness of 40 HRC was applied – a significant material loss was experienced at these samples – so we are not going to deal with this type of powder during our further experiments. A scattering can be observed as far as the material-loss of samples treated by the powders of identical types is concerned. It can be explained by the fact that the load of cultivator tines mounted on the agricultural machine was not equal; the tines overlap each other and the tines working in the tractor wheel track were exposed to a higher abrasive power owing to the compression of soil.

The pre-experiments of long-term research work performed at the Department of Mechanical Engineering of Technical Faculty of University of Debrecen are described in our present paper. In the course of our earlier research work, cultivator tines were made by means of free-forming forging for experimental purposes. The cultivator tines were a wear-proof layer was developed of tines by means of the hot metal powder spray fusing. In order to investigate the durability of these tines, they were given to an agricultural entrepreneur who used them for soil-preparation in real circumstances. By utilizing the results obtained during our present experiments, our research work will be going on in the future as well. The workpieces produced such a way will be used in agricultural circumstances as well in addition the metallographic investigations of these workpieces will also be performed. The research work aiming at the increase of agricultural productivity is of an extraordinary significance as the topsoil is of an excellent quality in Hungary and the agriculture plays a determining role in the economic life of our country.

ACKNOWLEDGEMENTS

The publication is supported by the EFOP-3.6.1-16-2016-00022 project. The project is co-financed by the European Union and the European Social Fund.

INVESTIGATING DIFFERENCES BETWEEN THE WORKLOAD FACTORS OF EXECUTIVE AND PLANNING AIR TRAFFIC CONTROLLERS

PESTI Dorottya Luca, SZÁMEL Bence Domonkos, SZABÓ Géza PhD
Budapest University of Technology and Economics
E-mail: pesti.dorottya@mail.bme.hu, szamel.bence@mail.bme.hu, szabo.geza@mail.bme.hu

Keywords: aviation, air traffic control, workload, complexity

The safety of air traffic is mainly ensured by the air traffic control service, where human controllers are responsible for maintaining the separation between the aircraft. The air traffic control (ATC) is divided into three main parts at the controller level:
ACC – Area Control Center – They are responsible for managing traffic in the upper airspace and for keeping the separation minima between the aircraft;
APP – Approach – They are responsible for managing traffic in the Terminal Movement Area (TMA) which is within 100 km of the airport. They supervise approaching and departing aircraft keeping the separation minima between them;
TWR – Tower – They are responsible for all the movements on the ground level of the airport and for ordering the approaching and departing aircraft.
In the ACC air traffic controllers are working in so-called sectors. The main purpose of the sectorization is to keep the controllers' workload in the optimum interval which means ca. 75-80%.
The focus of our article is the ACC area where two controllers (EC/Executive Controller and PC/Planning Controller) operate in one sector. The current ATC researches provide methods and procedures for predicting or calculating the actual workload of the controllers and for determining the sector-configuration to be used, but these methods and procedures do not take the two controllers into account, and use only 'a controller' in general. Our aim is to validate if the single controller approach in a two controller configuration is applicable (e.g. because the workload of the two controllers is the same or nearly the same; or because the workload of one of them is significantly higher in every work situation). Besides this, the purpose of our article is to investigate the factors which influence the workload of the EC and PC and what differences can be identified.
There are several methods to measure the workload of the air traffic controllers. Some of them focus on the complexity of the traffic, but there are other approaches as well which use only a few number of factors; and the simplest method only takes the number of the aircraft in the sector into account. Now we emphasize two methods which are complexity-related, because our research is based on complexity-based approaches.
Eurocontrol has created a complexity-related measurement which consists of three parts:

- ATC-procedures related complexity
- Traffic characteristics based complexity
- External complexity

These three parts above give the dimensions of the complexity and the interactions are the base of this measurement. Interaction means two aircraft in one cell simultaneously from the perspective of both aircraft. The fourth dimension is the time one aircraft spends in the cell. Based on this model the complexity is the multiplication of the density and the structural index which we get from the three parts mentioned above. (Eurocontrol, 2016; Delehaye, 2000)
Another Eurocontrol method is a task-based measurement. They defined so-called macro tasks which are the tasks related to aircraft entrying the sector, the perception of descending/climbing aircraft and conflicting aircraft and the solution of these conflicts.
They assign a time value to each macro tasks and these factors give the workload of the controller. We show this formula in (1)

$$WL = t_{AC} * O_{AC} + t_{Cnf} * O_{Cnf} + t_{CID} * O_{CID} \qquad (1)$$

Our purpose is to research the ACC controllers' workload based on complexity measurements. Thus first we have to explore the factors which are complexity elements and influence the workload of the EC/PC. As a first step we created a survey to get information about the subjective judgment of the workload from the ACC controllers at Hungarocontrol, the Air Navigation Service Provider in Hungary.
The survey consists of three parts: general, complexity factors and questions about the change of sector configuration. The general questions refer to personal data like age, sex, professional experience, etc. (this information will be used for evaluating dependencies). The third part of the survey contains questions about the time controllers spend on sector

configuration change. The point is the complexity factors part. We identified 16 complexity factors (based on previous studies e.g. Számel and Szabó, 2016) which we wanted to get information about. These factors are the followings:

- Number of climbing aircraft
- Number of descending aircraft
- Relative directions of aircraft (convergence / divergence of traffic)
- Coordination between the sectors
- Diversity of aircraft velocities
- Number of arriving, departing and en-route aircraft relative to each other
- Number of aircraft pairs on converging route
- Spatial distribution of the traffic
- Number of pilot requests (altitude, heading)
- Number of available flight levels
- Quality of verbal communication
- Number of active special use airspaces (e.g. military) (inside the sector or in the adjacent sectors)
- Weather conditions
- Geographic extent of the sector
- Load of the radio frequency
- Condition of the technical equipment

The controllers had to check for each factor a value in a 1-5 scale which means the degree of influence of these complexity factors on the controller's workload.
The paper presents the primary results of the survey and the main evaluation sentences. Table. 1 shows the general information about data.

Table 1 Some statistical features of the answers given to the questions in the complexity factors part

	EC	*PC*
Expected value	3,6094	3,599
Deviation	0,43	0,55
Relative deviation	11,95%	15,35%

During the evaluation we have determined some statistical features in general and furthermore we have investigated the relations between the age of the controllers and the complexity factors. According to this testing there are some factors which are worthy of dealing with because there are differences between the EC's and PC's results in relation to the relation between their ages and the affected complexity factors. Later we would like to work on a decision support tool which would be able to help controllers reduce their workload in certain work situations.

ACKNOWLEDGMENTS
The described work was carried out as part of a research supported by Hungarocontrol Zrt.

REFERENCES

[1] Complexity Metrics for ANSP Benchmarking Analysis. ACE Working Group on Complexity, Eurocontrol, Brussels, Belgium 2016.
[2] Delahaye D., S. Puechmorel: *Air Traffic Complexity: Towards Intrinsic Metrics. 3rd USA/Europe Air Traffic Management R&D Seminar*, Napoli 2000.
[3] Számel B., G. Szabó: *Analyzing the Relationship of Simplicity and Accuracy in ATC Workload Estimation Methods.* In: Rolandas Makaras, Robertas Keršys, Rasa Džiaugienė (szerk.): Proceedings of 20th International Scientific Conference Transport Means 2016. 789-793. 2016.

CALCULATION METHOD OF EVAPORATION AT HEATED WATER

POÓS Tibor PhD, VARJU Evelin, BATÓ Mihály András
Faculty of Mechanical Engineer, Budapest University of Technology and Economics
E-mail: poos@mail.bme.hu, varjuevelin@mail.bme.hu, batomisi@gmail.com

Keywords: Evaporation, heat- and mass transfer, calculation method, heating performance.

Evaporation plays an important role in the field of physiological, meteorological and technological applications. During our research the evaporation of water was investigated, because it is one of the most essential liquids related to life and technology. It is important to know the evaporation processes during operation of the pumped hydro energy storage systems if the upper reservoir is an open design, because in case of a large uncovered water surface, evaporation loss can be significant. We also need to consider heat loss by evaporation. A considerable part of heat flow loss from outdoor pools and wellness facilities is used up for evaporation. There are different equations to determine the evaporation loss of water, and these equations differ in precision depending on the circumstances. There is no such general equation in the literature, which can provide the evaporation rate, independently of the type of liquid, in a wide range of temperature.

Literature of evaporation can be found mainly amongst the past hundred year's publications, although the first equation of the evaporation rate was made by Dalton in 1802. In our work the typically laboratory measurements of evaporation with forced flow were reviewed, where the evaporating liquid was heated. The investigation of Himus and Hinchley [1], Rowher [2], Leven [3] and Pauken [4] were presented and the results of Raimundo et al.'s research [5] were also dealt with in this work.
Basically five cases are distinguished during evaporation of liquids depending on the direction of heat- and mass flow:

1. The air temperature is higher than the temperature of the liquid surface, the air transmits heat to the liquid and the diffusion flux points from liquid to air.
2. The temperature of air is lower than the temperature of the liquid surface, the liquid transmits heat to the air and the diffusion flux points from liquid to air.
3. The temperatures of air and liquid are the same, but partial pressure of the vapour in the air is lower than the saturated vapour pressure on the surface, so the diffusion flux points from liquid to air.
4. The temperature of air is higher than the temperature of the liquid surface, but it is lower than the dew point temperature, so the diffusion flux points from air to liquid and the vapour is condensed.
5. The temperatures of air and liquid are the same, and there is no difference in partial pressure between air and surface of liquid, so there is neither heat- nor mass transfer.

During our research a calculation method was elaborated, which is applicable to the first three cases. The heat balance of the system can be written as:

$$Q_{evap} = Q_{cond} + Q_{conv} + Q_{loss},$$

where Q_{evap} [W] is the heat of evaporation, Q_{cond} [W] is the heat transferred to the liquid on conductive way, Q_{conv} [W] is the heat transmitted from air to liquid on convective way, Q_{loss} [W] is the heat loss. The parts can be written separately:

$$Q_{evap} = NrA,$$

where N [kg/(m^{2}s)] is the evaporation rate, r [J/kg] is the latent heat of evaporation, A [m^2] is the evaporation surface.

$$Q_{conv} = \alpha(T_G - T_f)A,$$

where α [W/(m^{2}K)] the heat transfer coefficient, T_G [°C] is the temperature of the airflow, T_f [°C] is the heat of the liquid surface. The liquid tank applied during our research is well insulated, so we were able to dispense with the heat loss. The conductive heat of heating of the liquid is a measured value.
The calculation algorithm was tested by using the data of Raimundo et al. [5]. During their measurements they evaporated water form a heated tank that was located in a wind tunnel. The temperatures of liquid surface and air were recorded, the velocity and the relative humidity of the air were measured, and the quantity of evaporated liquid was monitored by an electronic scale. To specify the heating power in our case, according to the equations above, the

knowledge of the heat transfer coefficient is required. For this purpose, the heat transfer coefficient was calculated in two ways, on one hand by the Chilton-Colburn analogy, on the other hand by the Nusselt equation which can be written with dimensionless numbers. In Figure 1/a can be observed the difference between the heat transfer coefficients as a function of air velocity on the parameter of temperature difference between air and liquid. It can be seen that the higher the velocity or the temperature difference is, the greater the difference gets between the else ways calculated values. So, measurement of conductive heat, namely the heating power is recommended to accurate determination of the heat transfer coefficient.

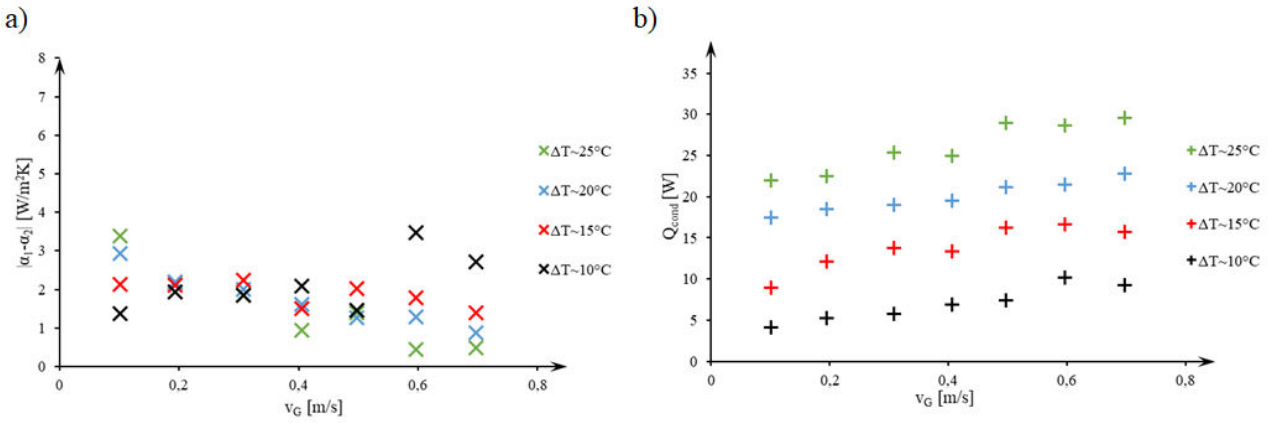

Figure 1 a) Difference between the heat transfer coefficients as a function of air velocity, b) Conductive heat as a function of air velocity

The conductive heat was specified by the heat transfer coefficient that was calculated from the Nusselt equation. The calculated conductive heat can be seen in Figure 1/b as a function of air velocity at different temperature gaps. It can be observed that the conductive heat increases when air velocity or temperature difference is increased.
Although the value of the heat transfer coefficient with the heat- and mass transfer analogies can be specified, for the sake of a simplified calculation method and the knowledge of a more precise value, measurement of the heating power is required.

ACKNOWLEDGMENTS
This work was supported by Gedeon Richter's Talentum Foundation (19-21, Gyömrői street, 1103, Budapest, Hungary). The research reported in this paper was supported by the Higher Education Excellence Program of the Ministry of Human Capacities in the frame of Water science & Disaster Prevention research area of Budapest University of Technology and Economics (BME FIKP-VÍZ).

REFERENCES
[1] G. W. Himus és J. W. Hinchley: „*The effect of a current of air on the rate of evaporation of water below the boiling point", J. Soc. Chem. Ind.,* köt. 43, sz. 34, o. 840–845, 1924.
[2] C. Rohwer: *Evaporation from free water surfaces*. Washington: U.S. Dept. of Agriculture, 1931.
[3] K. Leven: „*Beitrag zur Frage der wasserverdunstung", Warme Kaltetechnik*, köt. 44, sz. 11, o. 161–67., 1942.
[4] M. T. Pauken: „An experimental investigation of combined turbulent free and forced evaporation", *Exp. Therm. Fluid Sci.*, köt. 18, sz. 4, o. 334–340, 1998.
[5] A. M. Raimundo, A. R. Gaspar, A. V. M. Oliveira, és D. A. Quintela: „*Wind tunnel measurements and numerical simulations of water evaporation in forced convection airflow", Int. J. Therm. Sci.,* köt. 86, sz. Supplement C, o. 28–40, 2014.

DESIGN AND IMPLEMENTATION OF LABORATORY ABSORPTION/ADSORPTION TEST FACILITY

POÓS Tibor PhD, HORVÁTH Máté, VARJU Evelin
Faculty of Mechanical Engineer, Budapest University of Technology and Economics
E-mail:poos@mail.bme.hu, mate.horvath94@gmail.com, varjuevelin@mail.bme.hu

Keywords: absorption, adsorption, design.

The processes of absorption and adsorption are widely used, and applied in various industrial technologies mostly in different gas and liquid cleaning processes. Both have an important role in chemical-, pharmaceutical and environmental protection industries. The two processes are used for separating agents. The essence of the adsorption process is, that a selected component from gas, vapour or liquid is bonded, by physical or chemical forces, on the surface of the adsorbent, which is a solid material. However absorption is similar but in this case the absorbent is not a solid material, but a liquid, mostly water and is used only for gases and vapours.
In the laboratory „Stokes" of the Department, an absorber measuring station was already available but certain parts of which had to be upgraded. The department also had an adsorber for the same reason, there was in an urgent need for its modernization and restoration. Due to the fact that the two devices needed the same engineering and instrumentation, we designed and built them into one frame structure, led by space and cost-saving motivations. The mechanical designing was followed by the implementation, during which development possibilities were taken into account.
Several operating states have become possible with the new equipment, such as the independent operation of the adsorption and the absorption as well as the combination of the two processes. This has led to a lot of new possibilities by for researching measurements, for instance an air flow mixed with ammonium can be cleaned in the absorption column and then in the adsorption column the smell components can be cleaned on an activated carbon bed, or the humidity level can be reduced on a silica gel bed. Furthermore with the installation of an air-heating coil the temperature of the flowing gas can be raised so evaporating examinations can be made and the temperature dependence of the effectiveness of adsorption can be examined too.

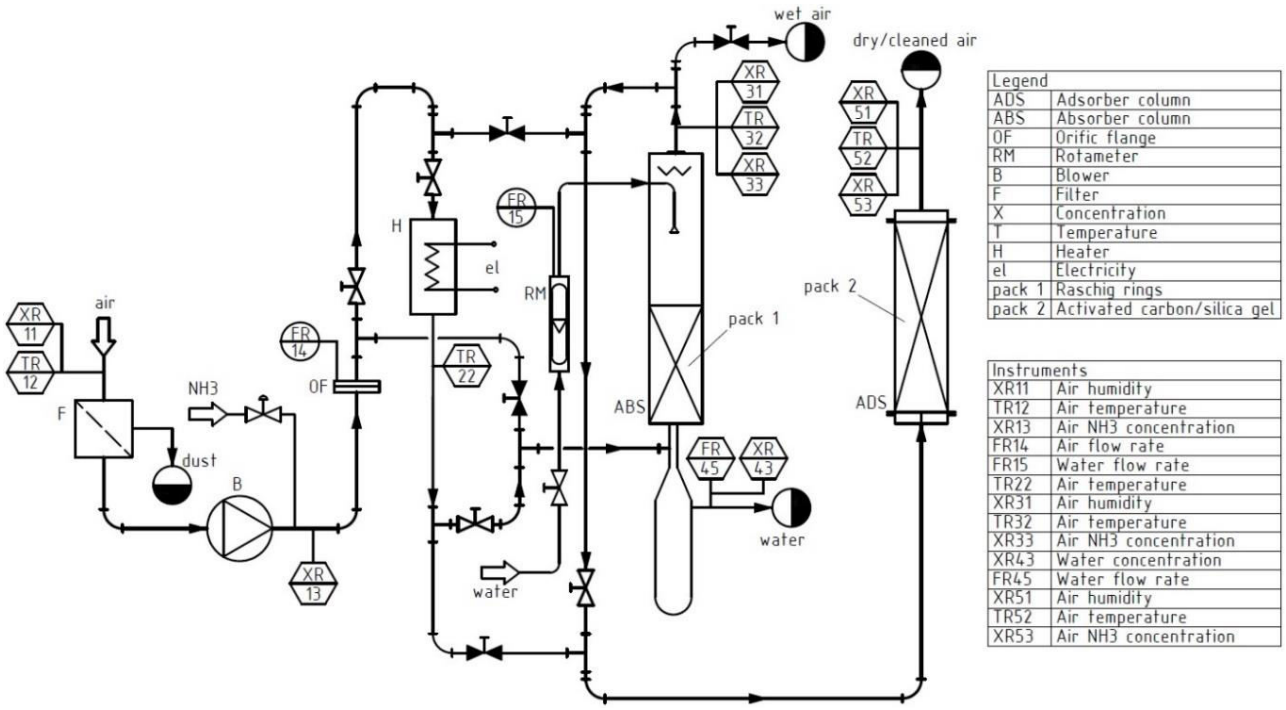

Figure 1 Piping and instrumentation diagram of the test facility

The flow rate of air is controlled between 0÷200 m^3/h by changing the speed of the Effepizeta SCL V5 blower which is installed on the equipment. The efficiency of the adsorption depends on the temperature of the gas, which can be raised to a maximum value of 45°C through a VENTS NK 100-1,6-1 type heater via 1600W which is regulated by a Jumo 8662-61-72 controller. This way the effect of the temperature of the air can be examined in the case of the adsorption

and the absorption. Another advantage of the equipment is, that with simple modifications the absorbent losses forced by evaporation can be determined. The pipeline is made of DN63 PVC pipes, the inner diameter of the absorber is 120mm and the adsorber is 100mm. In case the blower or other essential parts of the equipment require repairing, before and after these parts detachable joints have been fitted into the pipe system. The P&I diagram of the equipment is shown in Figure. 1.

Abs. column inner diameter	120 *mm*
Ads. column inner diameter	100 *mm*
Silica gel bed height	500 *mm*
Rasching ring pack height	750 *mm*
Blower flow rate	0÷200 m^3/h
Air temperature province	15÷50 *°C*

Figure 2 The 3D model and setup intervall of the test facility

Also we have created the parametric 3D model of the equipment with the Autodesk Inventor Software's Frame Generator module, which served as a basis for the implementation. With the help of the new equipment our students are able to familiarize themselves with two significant processes widely applied in various industrial environments.

ACKNOWLEDGMENTS
The research reported in this paper was supported by the Higher Education Excellence Program of the Ministry of Human Capacities in the frame of Water science & Disaster Prevention research area of Budapest University of Technology and Economics (BME FIKP-VÍZ). This work was supported by Gedeon Richter's Talentum Foundation (19-21, Gyömrői street, 1103, Budapest, Hungary).

PHYSICAL INTERNET – A NOVEL APPLICATION AREA FOR INDUSTRY 4.0

PUSKÁS Eszter, BOHÁCS Gábor PhD
Faculty of Transportation Engineering and Vehicle Engineering, Budapest University of Technology and Economics
E-mail: eszter.puskas@logisztika.bme.hu, gabor.bohacs@logisztika.bme.hu

Keywords: Physical Internet, Logistics, Industry 4.0, Simulation

INTRODUCTION

The Physical Internet (PI or π) is one of the most decisive ideas for future logistics systems. The idea behind it is to implement logistic systems which apply the principles of Internet information flow. Simultaneously technological innovations of Industry 4.0 have also appeared. Our current research deals with the applicability of the tools of Industry 4.0 technology in the PI system. Following the literature review we analyse the individual technological tools that could improve the functioning of PI components. Subsequently we will detail the usability of a specific Industry 4.0 tool and finally determine the future research steps.

BASICS OF THE PHYSICAL INTERNET AND THE INDUSTRY 4.0

As a result of globalization and individualization of the world, pressure on the performance of logistics systems is increasing. This global market change has a major impact on the functioning of systems, which will make the current operating conditions unsustainable. This problem must be addressed in social, economic and environmental terms. The Physical Internet concept provides a solution to address problems and create a sustainable network.

As a solution for delivering products efficiently the researchers are investigating the design of the standard container called π-container. The essence of this box is that each product uses the best possible volume utilization to fit a modular container and represents the goals of the Physical Internet, which is recyclable, environmentally friendly, intelligent and compatible with each other. The π -hub and π -transit centres are very important in the future logistics network. The biggest change is that they are open to everyone. These centres would use renewable energy sources to protect the environment and autonomous operation of the system would help increase effectiveness. The π-sorters are important parts of the transfer points that provide the containers with the right truck in the correct sequence and time. The system of open centres is closely linked to examining the sharing of vehicles to improve utilization and efficiency. Furthermore, in order to increase flexibility, the shipment within the logistics network would follow the hub and spoke transport strategy.

Industry 4.0 is a new paradigm that is characterized by its intensive use of both the old-established and new information and communications technology innovations. It is based not on the equipment and systems, but rather on an approach to how people and machines could create a common system. The presence of Industry 4.0 integration can be determined by deciding whether a function is Industry 4.0 compatible or not. First of all, it was concluded that there is no unambiguous classification of technologies for the inclusion into Industry 4.0. In the past, several researchers reviewed the Industry 4.0 technologies. In our article we overview three of these researches. The classification created by the different principles are shown in Figure 1. There are similarities between the groupings listed items (for example cloud or CPS), but they also have some different thought such as system integration or 3D printing.

Technological Pillars of Industry 4.0		
Cyber Physical Systems	Cybersecurity	Big Data & Analytics
The Cloud	The Cloud	Autonomous Robots
Virtualization	Mobile technologies	Simulation
Real-time capability	Machine to Machine	System Integration: Horizontal and Vertical
Modularity	3D Printing	Internet of Things
Decentralization	Advanced Robotics	Cyber security & Cyber Physical Systems
	Big Data & Analytics	The Cloud
	Internet of Things	Additive Manufacturing
	RFID technologies	Augmented Reality
	Cognitive Computing	

Figure 1 Main pillars of Industry 4.0

APPLICABILITY OF INDUSTRY 4.0 TECHNOLOGIES FOR THE IMPROVEMENT OF THE PI COMPONENTS

Table 1 shows which Industry 4.0 technology device can be used for components appearing in the Physical Internet system. It can be noted that the technical elements and components defined by the two trends have many common intersections, but there are also some technological tools that are not relevant to PI, such as 3D printing. The density of "X" shows which Industry 4.0 devices are of the outstanding importance for the Physical Internet.

Table 1 Industry 4.0 devices that affect PI components

INDUSTRY 4.0 / PHYSICAL INTERNET	π - container	π - hub	Track & Trace solution	Smart objects	π - sorter	Hub-and-spoke transport	Unified framework	Open Global Logistics Web	Open monitoring system	Webbed reliability
Cyber Physical Systems		X						X		
Cyber securty										X
The Cloud		X	X	X			X	X	X	
Mobile technologies	X		X	X				X	X	
Machine to Machine		X	X			X		X		
3D Printing										
Advanced Robotics		X			X					
Autonomous Robots		X			X					
Big Data & Analytics		X	X		X		X	X		
Internet of Things	X			X	X					
RFID technologies	X	X		X	X					
Cognitive Computing			X		X					
Virtualization		X			X				X	
Real-time capability		X	X						X	
Modularity	X			X	X			X		
Decentralization		X	X	X	X			X		
Simulation		X	X		X	X		X		
System Integration (Horizontal and Vertical)		X	X			X		X		
Additive Manufacturing	X									
Augmented Reality		X								

The π-container and smart objects components would operate with intelligent tools in the future logistics system. Creating this is supported by a number of Industry 4.0 technology tools, such as IoT or RFID technology. The π-hubs are the core of the open logistics network, which form the basis of the system as fixed and accessible points. Because of the complexity of its task, most technological innovations can be integrated into the hub system, in particular the existence of the CPS system and the use of simulation for optimization.

The logistics network constructed by the Physical Internet principles is based on the hub and spoke transport strategy to make the system more flexible. The operation of this kind of system is improved by the development of horizontal and vertical integration and the simulation defined as Industry 4.0 tool for the appropriate use of resources and optimization of operation. In addition to its delivery and storage functionality, the entire Physical Internet system has been defined in an open, global logistics network. This approach as a PI component is supported by Industry 4.0 system technologies such as CPS, cloud, M2M, Big Data & analytics, modularity, decentralization, simulation and integration.

Among many technological tools, we consider that simulation is one of the most important tools that will surely help in the future logistics system. Using the tools of Industry 4.0 in the PI system, the objects will be interconnected and intelligent in order to create an efficient and sustainable network. The simulation tool is suitable for the design of ever-growing complex systems, highlighting special events by trying different cases.

CONCLUSION AND FUTURE WORK

Several researchers concur that the current logistics networks can be defined as complex systems. The future Physical Internet system will also have to face this complexity. The behaviour of a compound system cannot be predicted solely by examining the behaviour of individual components. Thus, we need a model of the entire system. As simulation used extensively by Industry 4.0, we suggest this has to be the first approach to improve the components of Physical Internet. The next step in future research is to find a theoretical model that can be used for the Physical Internet based logistics network. When constructing the model, it is necessary to examine how each π-hub fits into the hub and spoke transport structure, meaning how the transport, storage and movement between and within the centres will be realized. After developing the theoretical model, it is required to optimize each module of PI. It is important to use the simulation to validate the model of the complex system, then we can analyse the modifications due to different impacts.

PVC/LDPE BLENDS: RELATIONSHIP BETWEEN THERMAL/MECHANICAL PROPERTIES, STRUCTURE AND BLEND BEHAVIOUR

ROMÁN Krisztina, ZSOLDOS Gabriella PhD
Institute of Ceramics and Polymer Engineering
E-mail:krisztinaroman@gmail.com, hugezs@coloplast.com

Keywords: blends, foam, SEM, DSC analysis, mechanical properties

In this paper the structural changes of low-density polyethylene (LDPE) and polyvinyl chloride (PVC) foam and the effects of LDPE content are investigates. Polyvinyl chloride (PVC) is widely used in the construction and consumer products industries. Nowadays, the use of polymer blends has become increasingly important in the development of advanced engineering materials. Through the combination of polymers, new and improved properties such as impact strength, chemical and heat resistance have been achieved. We examine the effects of addition of low-density polyethylene (LDPE), in an attempt to understand how LDPE can have an effect on the structural changes of PVC in the blends and changes in glass-transition (Tg). These parameters often provide important information related to the overall macromolecular structure of the polymer. The thermal analysis techniques such as differential scanning calorimetry (DSC) often require substantial sample modification. The effect of the miscibility and composition of the PVC/LDPE foam blends on the thermal stability were investigated. Signs of thermodynamic incompatibility of PVC and LDPE polymers were observed during the SEM analysis *(Figure 1)*.

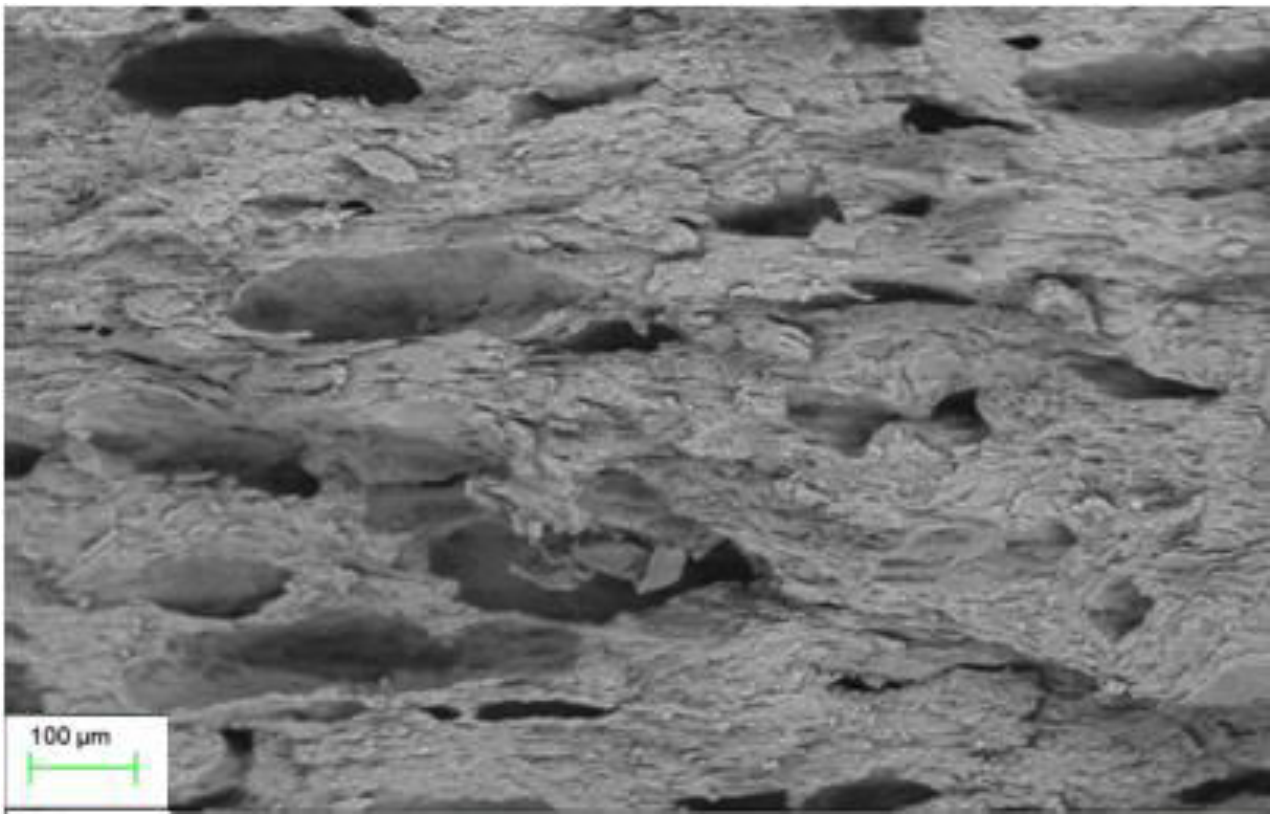

Figure 1 Scanning Electron Microscope fractured structure of PVC/LDPE foam

Various mechanical tests were performed, such as hardness-, tensile- and impact test. From the mechanical tests we can examine the foam properties compared to an origin PVC (sample without LDPE). We can be determine the differences of the properties and the modifier effects of the LDPE. The result shows that, the LPDE has an ineffective additive into the PVC, the properties of the composite was deteriorated. As a result, we have experienced the formation of different phases. To solve the inhomogeneous needed to use interface agent to increase the compatibility between the two materials. It is necessary to use a coupling agent or another way to produce the specimens, which gives stable structure

of the PVC/LDPE composite foams. From the results of the DSC analysis structural changes of composites were observed. DSC curves of the blends show shift of the PVC glass transition temperature which means that these blends are not heterogeneous.

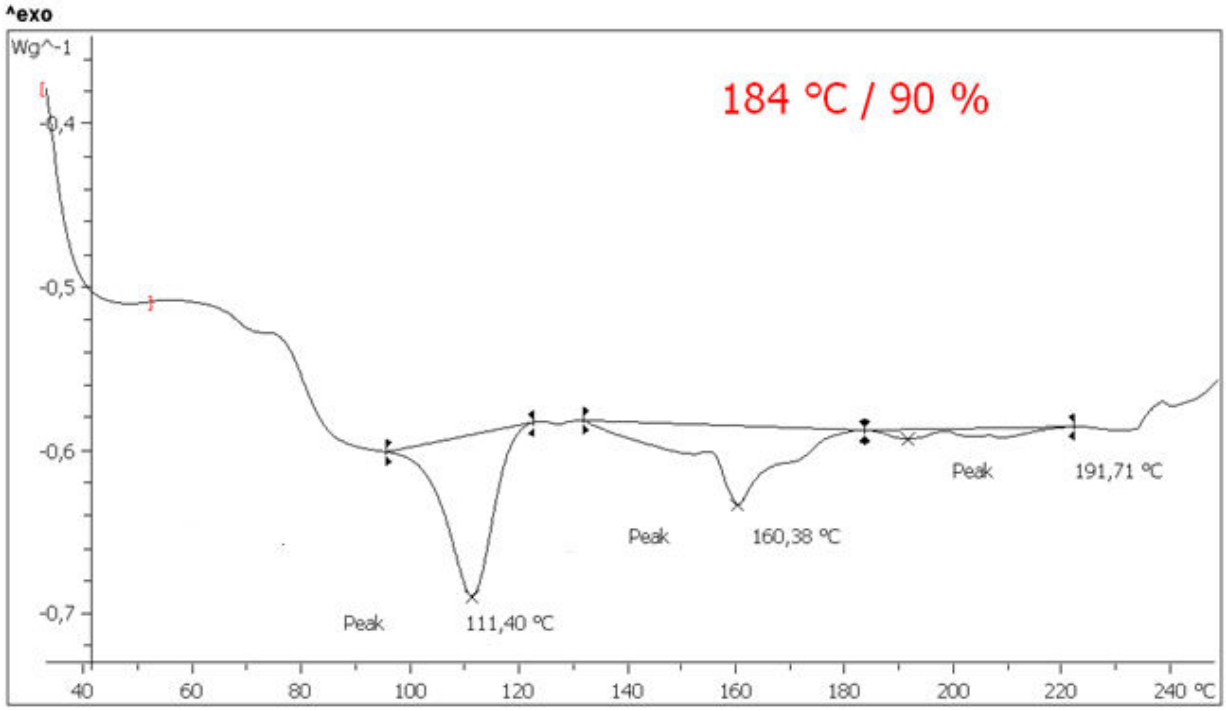

Figure 2 DSC curve of PVC/LDPE foam blend

ACKNOWLEDGMENTS

"The described study was carried out as part of the EFOP-3.6.1-16-2016-00011 "Younger and Renewing University – Innovative Knowledge City – institutional development of the University of Miskolc aiming at intelligent specialisation" project implemented in the framework of the Szechenyi 2020 program. The realization of this project is supported by the European Union, co-financed by the European Social Fund."

NUMERICAL MODEL ANALYSIS OF MYRING-SAVONIUS WIND TURBINES

SALEH Mahmoud, SZODRAI Ferenc PhD
Faculty of Engineering, University of Debrecen
E-mail: mhmodsalh84@gmail.com, szodrai@eng.unideb.hu

Keywords: wind turbine, Myring, Savonius, Ansys, CFX

Nowadays the importance of renewable energy is growing and the utilization of the wind energy potential is crucial. Turbines with low tip speed ratio such as the Savonius wind turbines can generate an adequate amount of torque at low wind velocities. The geometry of the blade has a strong connection to the efficiency of the device. The primary objective of this paper was to decrease the force acting on the convex surface of the blade by modelling the effect of wind on it. For the sake of simplicity, a 2D cross-sectional area was investigated in the simulation with Ansys CFX 19.1. Academic version. In our paper the blade geometry was based on so-called Myring equation. The formula of the Myring equation is:

$$Y = b\left[1 - \left(\frac{x}{a}\right)^2\right]^{\frac{1}{n}}$$

In this study we focus on one of the effect that has impact on the turbine performance. In equation 1. the b=0.25 m and n=2 used as a constant, while the factor a varied from 0.375 m to 0.450 m. For every blade geometry, the inlet velocity was set to the following values 1 m s^{-1}, 1.5 m s^{-1} and 2 m s^{-1}. A steady flow simulation was carried out. To allow for the full development of the upstream flow, an 8 m long 2 m wide computational domain was created, that can be seen in figure 1.

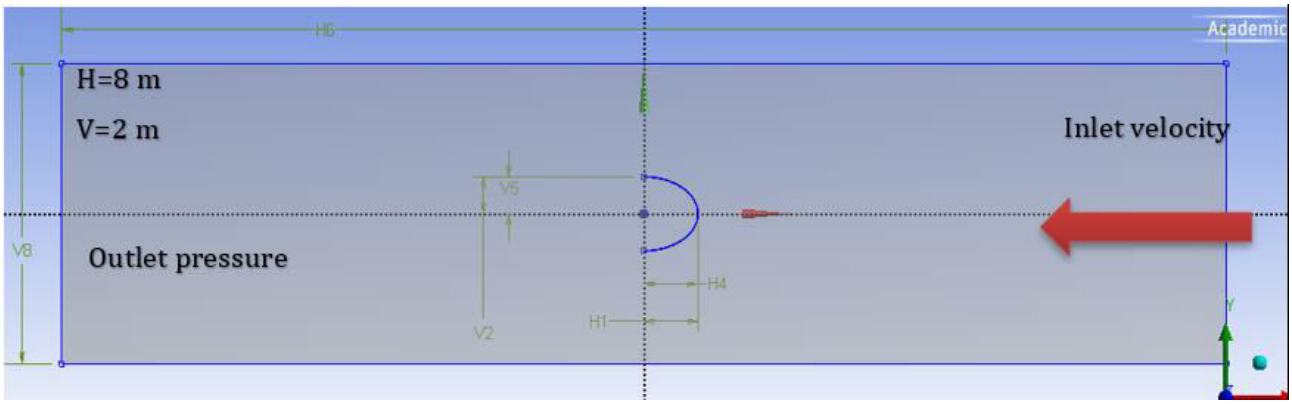

Figure 1 The computational domain

The blade was placed midway between the top and bottom boundaries, at the distance of 4 m from the inlet. To avoid the near-wall effect, a symmetry boundary was applied at the both sides of the domain. The mesh generated from 0.02 m large tetrahedrons and the inflation was applied around the blade surfaces to increase the calculation accuracy on that blade surface area. According to the figure 2. in every case the highest-pressure values were appeared on the peak of the surface. Table 1. shows the magnitude of the force acting on the convex surface of the blade with respect to the factor (a) when the inlet velocity was 1 m s^{-1}, 1.5 m s^{-1} and 2 m s^{-1}. It can be seen that the magnitude of the force increases with the increase in factor (a). At 1.5 m s^{-1} inlet velocity we can notice that when the factor a varies from 0.375 m to 0.400 m, the force roughly remains the same. The force reaches the highest magnitude when a=0.425 m and when a=0.450 m the force drops significantly to 80.40 10^{-4} N. It can be noticed from the 2 m s^{-1} column that the force increases with increase in the factor a when this factor was between 0.375 m and 0.425 m, but it decreases when a=0.450 m.

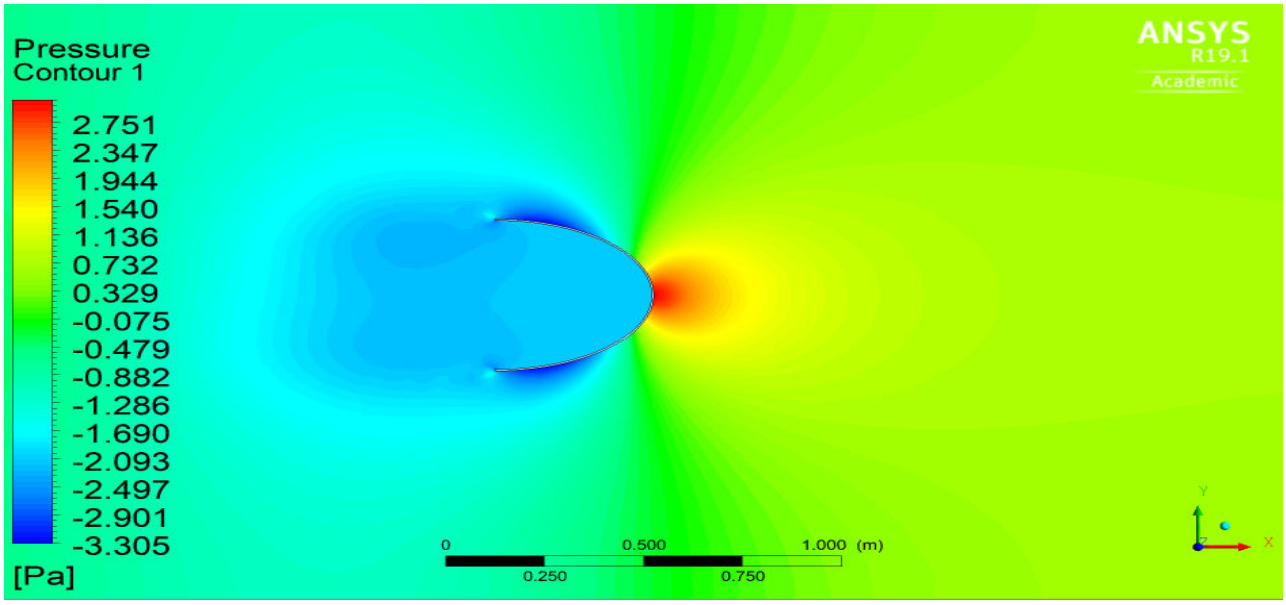

Figure 2 pressure distribution around the surface of the blade

Table 1 The force acting on the convex surface of the blade

Case	Inlet velocity		
	1 m s^{-1}	1.5 m s^{-1}	2 m s^{-1}
(a) a=0.375 m	32.67 10^{-4} N	83.27 10^{-4} N	133.92 10^{-4} N
(b) a=0.400 m	34.54 10^{-4} N	83.12 10^{-4} N	140.79 10^{-4} N
(c) a=0.425 m	39.30 10^{-4} N	86.15 10^{-4} N	148.96 10^{-4} N
(d) a=0.450 m	36.08 10^{-4} N	80.40 10^{-4} N	150.93 10^{-4} N

A STUDY OF PRESSURE – SINKAGE RELATIONSHIP USED IN TYRE- TERRAIN INTERACTION

[1,2]SALMAN NIHAL Dawood.,[1]KISS Péter PhD
[1]Institute of Process Engineering, Faculty of Mechanical Engineering, Szent István University.
[2]Middle Technical University (MTU), Baquba Technical Institute, Baghdad, Iraq.
E-mail: nihald2005@yahoo.com

Keywords: Terra-mechanics, Pressure-sinkage relationship, Bevameter technique, Soil properties.

Modeling the interaction of a vehicle with the terrain is the key part of the vehicle performance evaluation. Tyre/terrain interaction is a very complex research topic in Terra-mechanics, transportation and pavement engineering. It generally covers issues on terrain compaction, tire traction, dynamic terrain response, mobility and rolling resistance. The study of tyre/terrain interaction has been qualitatively understood that ground response is directly related to the tire structure, inflation pressure, soil properties, tyre/ terrain interface properties, and vehicle load.
The mechanical properties of terrains are usually divided into bearing (which is characterized by pressure–sinkage relationship equations) in the normal direction and shearing in the tangential direction. The pressure-sinkage models play an essential role in terra-mechanics. The performance metrics such as thrust, and drawbar pull can be obtained from the pressure-sinkage models. Throughout the years, a wide variety of models have been developed for formulating the pressure sinkage model. The degree of complexity for these models is based on the application and accuracy. Generally, these models can be categorized into empirical models and semi-empirical models.
This study reviewed the conventional models with a brief description of the proposed method and limitations. In addition, the modified models based on the conventional models were discussed.
Regarding the empirical model, Bekker M.G. developed the Bevameter technique (Figure 1) is one of the techniques for measuring the terrain response to the applied loading, it consists of two separate tests, a plate penetration test and a shear test. The normal pressure-sinkage relationship is measured from the penetration test, with two sizes of plates (radii b1< b2), that are forced into the soil.

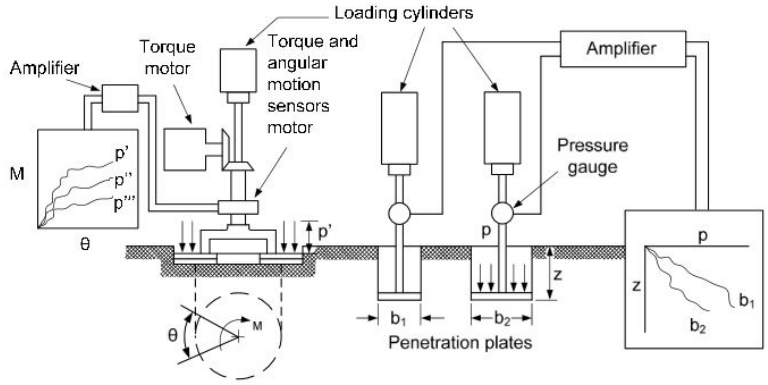

Figure 1 Schematic diagram of a Bevameter

Table 1 illustrates the most classical semi-empirical models of pressure-sinkage and its limitation.

Table 1 Conventional pressure sinkage models

The model finder	The equation	Features	Limitation
Bernstein	$p \cong kz^{0.5}$	-	-
Goriatchkin	$p = kz^n$	Fundamental pressure/sinkage relation.	k and n are constants for a given soil and plate size.
Bekker	$p = \left(\frac{k_c}{b} + k_\phi\right) z^n$	Reduce some of the uncertainties and variations found with the usage of the Bernstein Goriatchkin equation	Parameters k_c and k_ϕ depending on the value of the exponent n.

Reece	$p = \left(c\grave{k}_c + \gamma b\grave{k}_\emptyset\right)\left(\frac{z}{b}\right)^n$	The using of empirical parameters $k`_c$, $k`_\varphi$ and n resolve the problem of not being able to predict soil parameters.	The new values still 'non-invariant' and had a dependency on plate dimensions.
Saakyan	$p = k\left(\frac{z}{D}\right)^n$	Replaced the flat plate pressure sinkage with circular disk	D is the diameter of a flat circular disk, not wheel diameter.
Kacigin and Guskov	$z = \frac{B_i}{k_z}\, arctanh\left(\frac{p}{B_i}\right)$	K_z and B_i parameters are independent of the plate shape and dimensions and depend only on soil type and moisture content.	There are no connections of k_z and B_i parameters with real invariant soil parameters used in classical soil mechanics.

Table 2 reveals the modifications that carried out based on the conventional pressure-sinkage models.

Table 2 Modification on classical pressure-sinkage models

Author (The model)	Features	Basic of the model	Exponent (n)
Lyasko M. (LSA model)	1- $p = \frac{1}{\frac{D_1}{B_i}+\frac{D_2}{Ez}w\beta\xi}$ 2- Helps users to evaluate load–sinkage curves of rigid plates of different shape and dimensions 3- Uses invariant soil parameters which do not depend on plate shape, size or plate–soil boundary conditions.	The LSA model based on a test observed relationship of stress distribution in the soil under a plate contact area.	-
Meirion G. G and Spenko M,	1- $p = \hat{k}z^{\hat{n}}D^{\hat{m}}$, $p = \hat{k}r^{\hat{n}}(\cos\theta - \cos\theta_s)^{\hat{n}}(bl)^{\hat{m}}$ 2- This models comprehensive pressure-sinkage for small diameter wheels on compactive soils. 3- Considering the effect of the diameter and width of the small wheel on the pressure sinkage.	Modified bekker and reece model	Const.
Ding L. et. Al., (New perspective and related equations on characterizing pressure sinkage relationship)	1- $p = k_s z\lambda_N$ 2- The model with two meaningful parameters can fit the results of Bekker's model with three parameters and high goodness of fit 3- The model applied to small rigid wheels that move on deformable terrain. 4- It can be applied to estimating the pressure–sinkage relationship during wheel-terrain interaction with dynamic sinkage.	Based on Bekker model	variable
R.A. Irani et. al., (Model to capture and predict the dynamic oscillations)	1- $p = \left(c\grave{k}_c + \gamma b\grave{k}_\emptyset\right)\left(\frac{z}{b}\right)^n + \left(k\grave{_g}\ \bar{\sigma}_p + k\grave{_a} l_c d_\gamma\right)\sin\left(\frac{\omega_w}{n_g}t + \Phi\right)$ 2- The new relationship can capture the dynamic oscillations observed for a wheel with grousers. 3- the numerical simulations were carried out in the MATLAB/Simulink environment	Modified Reece model	Const.

The conventional pressure-sinkage relationships whether empirical or semi-empirical are poor in adaptability and extrapolation ability. The modified models showed high fidelity results with keeping the computational effort and number of model variables low.

ACKNOWLEDGMENT
This work was supported by the Stipendium Hungaricum Programme and by the Mechanical Engineering Doctoral School, Szent István University, Gödöllő, Hungary.

ANALYSIS OF VIBRATION DURING TURNING PROCESS OF DIFFERENT MATERIALS

SARANKÓ Ádám, KALÁCSKA Gábor DSc, KERESZTES Róbert PhD
Institute for Mechanical Engineering Technologies, Faculty of Mechanical Engineering, Szent István University
E-mail: saranko.adam@gmail.com, kalacska.gabor@gek.szie.hu, keresztes.robert@gek.szie.hu

Keywords: vibration, turning, polymers, Polyamide 6

In this article we would like to introduce the problems caused by vibrations in case of polymer turning processes. The finished surface roughness is highly depending on the vibrations between the workpiece and the machining tool. In practice the operators should chose the machining parameter well, to achieve the desired surface roughness. Nowadays there are a lot of research in this topic, to avoid the unnecessary phenomena of vibrations. The two most common method are the Spindle Speed Variation (SSV), and the Vibration Assisted Machining (VAM). In case of SSV the CNC machine can increase and decrease the speed of spindle continously during turning which can significantly reduce the effects of chatter. This method is very useful for longer workpieces when there is no any support except the chuck. Vibration assisted machining can be used to minimize the problems caused by vibrations. VAM combines precision machining with small-amplitude tool vibration to improve the fabrication process. It has been applied to a number of processes ranging from turning, drilling to grinding. Except these methods, regarding to the machining processes, vibration is always a disadvantageous factor. With these measurements we wanted to get some datas about the vibration during turning, what we can use in our future work.
Based on the enumerated above we made some trial measurements about the basic vibrations of the shank of the turning tool. The tests were done on a NCT EUROturn-12B CNC machine which can be found in the workshop of our institute. The tested material was cast polyamide 6, because this is the most commonly used basic polymer in the industry. The equipments were served by a specialist from SPM Budapest Kft. The first figure shows the used equipments.

Figure 1 The measuring equipments (from left: Leonova Diamond – DIA 300 processing unit, SLD-144S vibration measuring unit, TRA73 shock pulse meter and TTP10 laser tacho/temperature meter)

For safety reasons we saw the workpiece across to the middle in axial direction making the flowing chips break at each rotation. We also used this method in our previous cutting force measuring tests.

At first we measured the vibrations (acceleration, speed, and amplitude) in axial direction and the shock pulse in tangential direction. After that we changed the devices. As we expected, the second method proved to be a more conveninent solution. The second figure shows this setup. We held the measuring devices in our hands for take the picture about the setup.

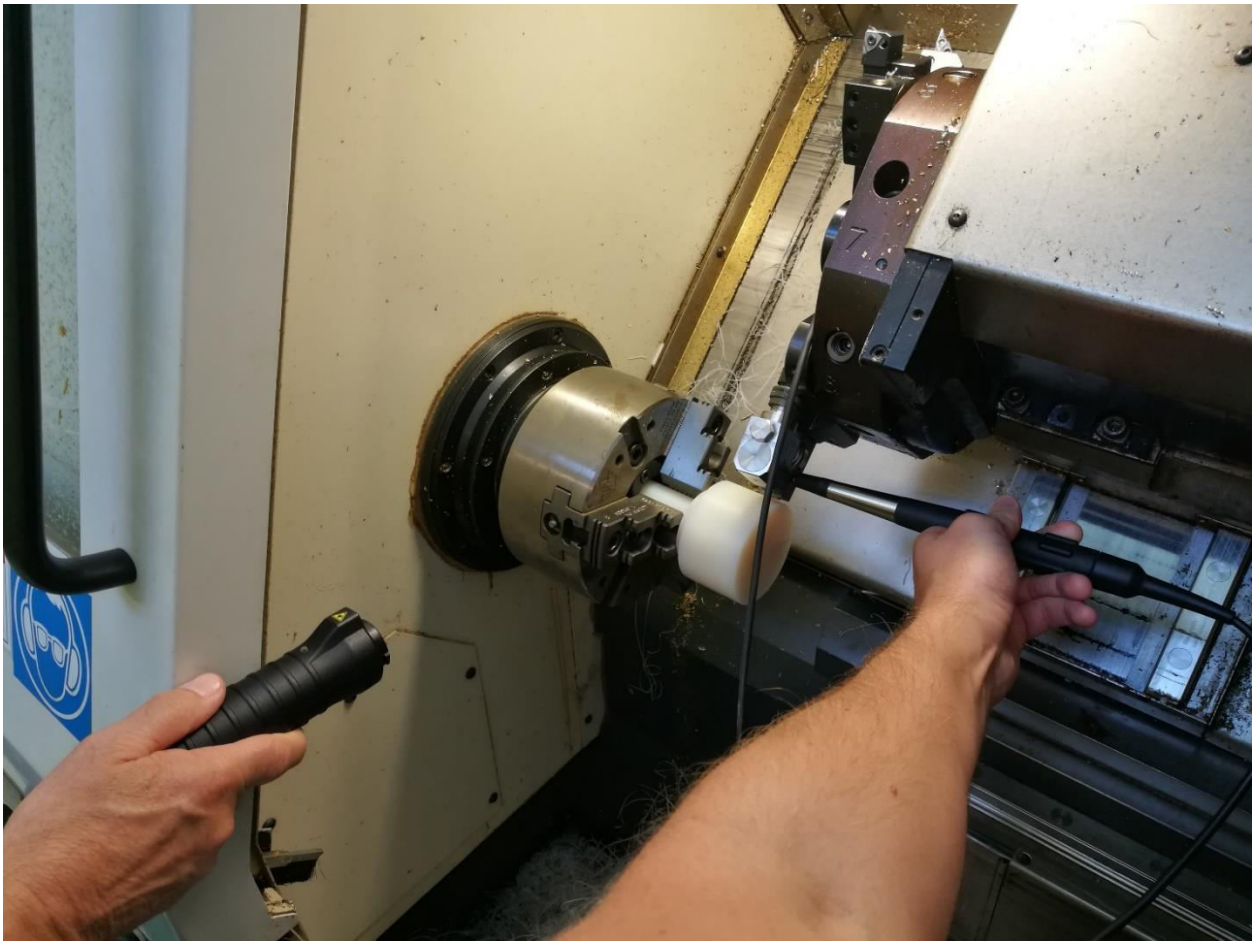

Figure 2 The setup for measuring the spindle speed, the vibration in tangential direction, and the shock pulse in axial direction

After some tests, we found that the shock pulse is too low, so later we measured only the vibration in tangential direction while the spindle speed was also measured continously. We got result by using the processing unit and a special SPM software called Condmaster Ruby. With these tests, our goal was to make sure that the equipments, and the measuring setup are suitable for our future research. Diagrams of the vibration speed were made by a computer connecting to the processing unit.

After processing the datas, we found that the vibrations are very low, because of the polymer workpiece and the parameters (cutting speed: 150 m/s, depth of cut: 1 mm, feed: 0,1 mm/rev.) we used in these tests. When higher cutting speeds or higher depths of cut were applied, the influence of the sawing was too significant. The structure of a modern CNC machine is also an influencing factor. The measuring method and setup were suitable for measuring the tangential vibrations of the tool shank. However we have to use workpieces without sawing, because this fact had a strong influence for the tests.

In the future we would like to test some other basic and composite polymer materials too. We will avoid the sawing to get the best results.

POSITION CONTROL OF PNEUMATIC DRIVES

SÁRKÖZI Eszter, FÖLDI László PhD
Institute for Mechanical Engineering Technology, Szent István University
E-mail: sarkozi.eszter@gek.szie.hu, foldi.laszlo@gek.szie.hu

Keywords: Servopneumatic drive, Position control, Optimization criteria, Air consumption, Energy saving

ABSTRACT
Despite pneumatic drives are widely used in industrial automation their application in position controlled solutions still faces challenges. One of these challenges is the high energy consumption of this systems. In this paper an optimizing method is presented and evaluated, which can be used as an energy saving solution without constuctional changes.

INTRODUCTION
In industrial circumstances in order to achieve linear motion, pneumatic, electromagnetic and hydraulic actuators are typically used. The pneumatic actuators have several advantages: they are fast, cheap, have an outstanding power-to-weight ratio. Beyond these there are challenges as due to the piston friction and the characteristics of compressed gas flow the behaviour of the system is non-linear. In the last decade with the use of high speed controllers servopneumatic systems are also capable for positioning purposes. Evaluating the positioning result control quality indicators are mainly used, but also the air consumption is an important consideration. Reducing the air consumption during the positioning has great importance, as the pressured air is one of the most expensive energy form used in the industry.

OBJECTIVES
In this article our main objective was to examine the potential of energy saving by a new optimization criteria of the tuning method of control algorithm. Null hypothesis was that if the air consumption is taken into consideration as a part of the optimization criteria, then the air consumption will decrease during positioning, but other control parameters will deteriorate.

EXPERIMENTAL APPARATUS
As an actuator a double acting rodless pneumatic cylinder was applied. An analogue displacement encoder with 0,01 mm travel resolution was attached to the cylinder. The applied encoder is a potentiometer which provides a voltage signal in proportion to the displacement. The used way-valve was a 5/3 proportional valve.

CONTROL ALGORITHM AND TUNING METHOD
The applied control algorithm was the status controller, which is based on the classic proportion controller with the addition that it takes into account the first and second derivative of the feedback signal. The controlled variable was the position, the first derivative is the velocity and the second derivative is the acceleration. The velocity and the acceleration have negative impact, so they are a dampings proportionally to the velocity and the acceleration.
The selected tuning method is optimizing the control parameters by genetic algorithm combined with a gradient fminsearch method. Both algorithms perform large number of settings, so the optimization was implemented on an identificated system model.The solvers needed a criterion for the optimization. The first used one is the Integral of Time multiply by Absolute Error (ITAE) criterion

$$\mathrm{ITAE} = \int_0^\infty t|e(t)|dt$$

These ITAE criterion takes into consideration the control error (e) - which is the difference between the set point (in case of positioning this is the target position) and the present value (the present position)- and the elapsed time (t).
In this paper we have examined the effect of an expanded ITEA criterion, that contained an additional part, which was proportional to the air consumption, as the nominal air consumption (Vn) is weighted by an air consumption coefficient (AC), so the new optimization criterion is:

$$\mathrm{Cr_{AC}} = \mathrm{AC} * V_n + \int_0^\infty t|e(t)|dt$$

RESULTS

Based on the results it can be declared that the null hypothesis was right, as increasing of air consumption coefficient value causes decreasing of nominal air consumption and increasing steady-state error and settling time during the positioning. The decreasing of air consumption has limitation, because the movement during the positioning needs compressed air.

INNOVATIVE RESIDUAL STRESS AND ANISOTROPY INVESTIGATION BY ROBOT ARM BASED X-RAY DIFFRACTOMETER

SEPSI Máté, MERTINGER Valéria PhD, BENKE Márton PhD
Institute of Physical Metallurgy, Metalforming and Nanotechnology, University of Miskolc
E-mail:femsepsi@uni-miskolc.hu, femvali@uni-miskolc.hu, fembenke@uni-miskolc.hu

Keywords: non-destructive test, XRD, residual stress, texture

Centreless X-ray diffractometers are developed for the sample-cutting free determination of residual stresses (Fig.1.). The residual stresses strongly affect the lifetime of any object and is in a strong correlation with the production method and use of crystalline matters. The non-destructive feature makes it possible to apply them in such cases when sample cutting of the component is not allowed due to the unique character or value feature of the objects. Our purpose is to introduce a newly developed technique with which information can be obtained about the anisotropy of crystalline materials using centreless X-ray diffractometers besides their stress measuring method. Centreless diffractometers have never been used to describe anisotropy previously. The innovation and usability of the method stands in that it can be applied directly on the objects without the need of specimen cutting. The technique has literally no size limitations and it does no harm to the examined objects. Measurement and calculation methods for non-destructive texture tests were developed to determine the identical crystalline plane series distribution in centreless and in the conventional diffractometers.

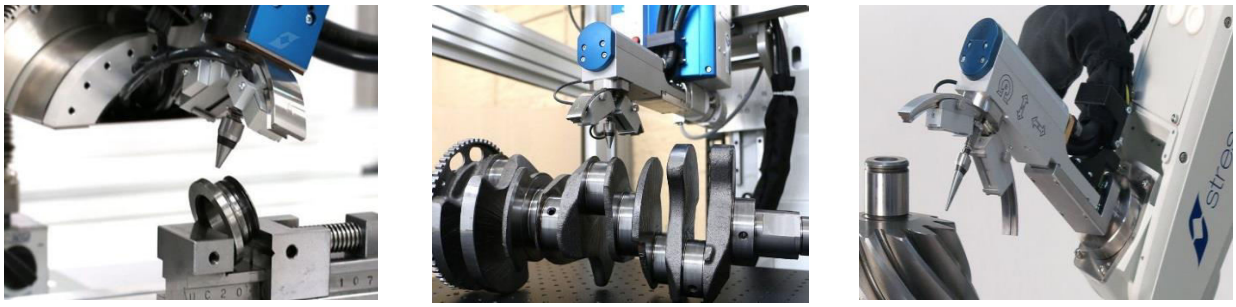

Figure 1 Technical solution for centerless Xray diffractometers

Residual stress in engineering practice appears to be a serious problem in many cases [1]. The stress generated during operation or further machining always superimposes to the residual stress. If the magnitude and direction of the residual stress is unknown due to improper design, the process may often cause distortion or failure. Therefore, controlling the residual stress is essential. Typically, it is problematic during forging or cutting [2], thus, in the case of sheet or strip products, the stress relieving heat treatment is unavoidable before cutting, which increases the cost of the final product. Otherwise, the misplacement of the sheet during cutting may cause the breakdown of the cutting device due to the release of residual stresses. A typical example for this situation is laser cutting, where the laser head is dangerously close to the surface of the sheet having residual stress.
Further processing of the sheet and strip products often involves deep drawing. In this case, the texture of the base material is also a key issue for the development of earing (Fig.2) [3,4,5]. For certain aluminium alloys, the evolution of texture during thermomechanical treatments can be very sensitive to the degree of rolling even along the width of the rolled strip [6,7,8,9,10]. In this case, the possibility of a rapid texture test method can greatly assist the prediction of earing.
The most common method for determining texture is X-ray diffraction, which can be realized with conventional diffractometers equipped with Eulerian cradles. For such equipment, samples must be cut with the size of a few 100 mm2. Although X-ray diffraction itself is a non-destructive method, the need for sample cutting makes it a destructive technique at the end. Centreless diffractometers do not require sample cutting and virtually have no sample size limits. Such diffractometers are designed to determine residual stress in a non-destructive manner of machine parts, even under industrial conditions. Those devices have never been used to determine texture. In this paper, new texture measurements method will be introduced and presented on a rolled aluminium alloy plate that could not be subjected to sampling. The new texture test method was validated with a conventional diffractometer. The new method was applied on a Stresstech G3R type centreless X-ray diffractometer while Bruker D8 Advance equipped with Eulerian cradle was used for validation.

Figure 2 The earing represented after deep drawing

ACKNOWLEDGMENTS
The described work was carried out as part of a project supported by the National Research, Development and Innovation Office – NKFIH, K123456. and also supported through the New National Excellence Program of the Ministry of Human Capacities.

REFERENCES
[1] Totten G, Howes M, Inoue T: *Handbook of Residual Stress and Deformation of Steel* (Materials Park: ASM International) 2008.
[2] Navas V, Gonzalo O, Bengoetxea I: "*Effect of Cutting Parameters in the Surface Residual Stresses Generated by Turning in AISI 4340 Steel," International Journal of Machine Tools & Manufacture,* pp. 48-57, 2012.
[3] Engler O, Randle V: *Introduction to texture analysis* (CRC Press) 2010.
[4] Kocks F, Tomé C and Wenk H: *Texture and Anisotropy- Preferred Orientations in Polycrystals and their Effect on Materials Properties* (Cambridge: Cambridge University) 1998.
[5] Suwas S and Ray K R: *Crystallographic Texture of Materials* (London: Springer-Verlag) 2014.
[6] Rollet A, Humphreys F, Hatherly M: *Recrystallization and Related Annealing Phenomena* (Oxford:Elsevier) pp 256-274, 2012.
[7] Vatne H, Engler O and Nes E: *Materials Science and Technology* 13 pp 93-102, 1997.
[8] Engler O: *Materials Science and Engineering A* 538 pp 69-80, 2012.
[9] Rodrigo P, Zschommler H: *Dierk R: Particle Stimulated Nucleation in Coarse-Grained Ferritic. Metallurgical and materials transactions A*, 469-478. (Vol. 44A, January 2013).
[10] Kashihara K, Inagaki H.: *Effect of Precipitation on Development of Recrystallization. Materials Transactions*, 528-536. 2009.

THE IMPACT OF ELECTRIC VEHICLES ON SUSTAINABILITY: JORDAN AS A CASE STUDY

SHATNAWI Malak
Bánki Donát Faculty of Mechanical and Safety Engineering, Óbuda University
E-mail:malak.shatnawi@phd.uni-obuda.hu

Keywords: Electric Vehicles, Sustainability, Energy Consumption, Environment.

The Global concern nowadays is moving toward making a revolution in favor of exploitation of renewable energy in order to limits emissions and waste within the planet, minimizes consumption of non-renewable resources and minimizes production of noise and all other kinds of pollutions as well as to achieve sustainable systems aimed at preserve planet's natural resources and to ensure progress and prosperity for any society. In this context, it is necessary to focus on the transport sector as it contributes at least 30% of the total primary energy consumption. Therefore, a set of rules and laws must be developed to address the problem so as not to Increase their severity and lead to economic, environmental and social disasters and these cannot be done unless there are joint measures from governments, companies, manufacturers and users.

Unfortunately, the Jordanian transport system depends on the individual transport which supported by passenger cars and different types and forms of taxis, and that because of the weak role played by the public transport sector, especially in the capital, Amman.

The sudden unexpected increases in population caused by several waves of internal and external immigrations from the neighbouring countries goes together with a high growth in the number of vehicles which created a pressure on the country infrastructure and seriously has its effect on sustainability dimensins.

The study aims to assess the impact of adoption of electric cars on sustainability, based on the global trend to replace Internal Combustion Engine vehicles (ICE) powered by fossil fuels by Electrical Vehicles (EV). To anticipate these effects on sustainability elements in terms of economic, social and environmental dimensions, the analysis will study first the number of passenger cars for a period of time and the expected annual increase, determine historically used fuel quantities and their financial cost and vice versa, also predicting the impact on sustainability of the annual growth rate in the number of EV.

Statistics show that the trend to buy hybrid cars (internal combustion engine + electric motor) and Electrical Vehicles (EV), in the past few years in Jordan is increasing, so it is necessary to start theoretical assumptions through studing different scenarios to carry out forecasting of replacement the current vehicles (passenger cars) by electric vehicles in order to predict the future fuel cosumption and emissions to compare them with the base situation.

To forecast the future, it is well known that in the field of transportation, data analysis is probably the most important and widely used research tool for analysis.

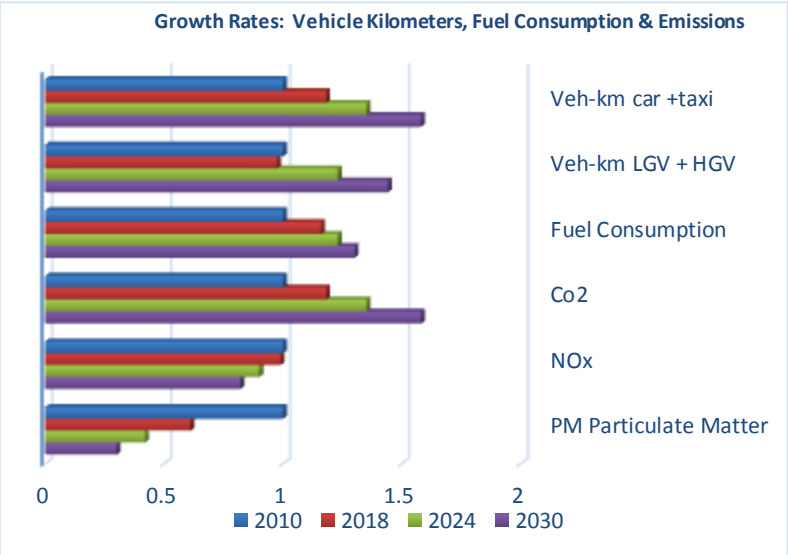

Figure 1 Growth Rate: Vehicle kilometers, Fuel Consumption and Emissions

Gasoline consumption shows the historical and the future prediction best fit achieved by linear regression relationship with $R^2 = 97\%$.
forecasting models were made related to gasoline and electricity consumption to study the growth rate and the positive and negative impact of replacement ICE by EV.
There is no doubt that there will be an impact on the present infrastructure since the current filling stations of gasoline and diesel will be affected and replaced gradually by electric charging points in the stations, in the parking areas and houses, also there are serious limitations regarding the EVs battery capacity, the driving range and charging time which will cause changes in the style of fuel refilling (refuelling) /electric charging, to be compatible with the period that required for refuelling / charging and the frequently number of visits, not to mention the concern of indirect and direct environmental effects in the manufacturing ,operating and recycling of electric motor batteries through the life cycle of the cradle to the grave.
This issue will have a direct impact on gas station that will affect the revenue of such companies, also it will have a direct impact on labour since electric charging station is not a labour intensive in addition to the adverse impacts on the current car industry because EV manufacturing is not a labor intensive industry.

BALL-ON-DISC WEAR TEST OF DUPLEX (PN+PVD) LAYERS PRODUCED ON X42Cr13 STEEL

SIDDIQUI Shiraz Ahmed, MAROSNÉ BERKES Mária PhD, SZILÁGYINÉ BÍRÓ Andrea PhD
Institute of Materials Science and Technology, University of Miskolc
E-mail: ahmedshiraz432@gmail.com, maria.maros@uni-miskolc.hu, biro.andrea@uni-miskolc.hu

Keywords: *Plasma nitriding, PVD coating, Duplex treatment, Ball-on-disk test, wear*

INTRODUCTION

The wide range of techniques and recently developed methods in the field of surface engineering and coating technology have brought immense changes in the properties and behaviour of materials. These techniques are used to protect the manufactured components from thermal or corrosive degradation, impart wear resistance and hardness to the surface while retaining the toughness and ductility of the bulk component and enhances the aesthetic appearance [1]. Duplex heat treatment is one of the innovative technologies which is a combination of two or more different surface technological processes which builds a two or multi-layer composite structure surface on the substrate material with the objective to improve the wear resistance, frictional behaviour and improves the loadability, durability of the components [2].

The presented research deals with the investigation of the tribological performance of the surface layer produced by duplex heat treatment, namely combination of plasma nitriding at two different nitriding temperatures (520 °C and 550 °C) and PVD coating. The material of investigation is X42Cr13 plastic mould tool steel which has a wide range of industrial applications. Nitriding is a thermochemical heat-treating process of diffusing nascent nitrogen onto the surface of steels and cast iron. The plasma nitriding is a method of surface hardening using the principle of glow discharge phenomenon, widely used to increase the surface hardness, fatigue strength and wear and corrosion resistance [3] [4].

The current research aims at investigating the effect of the duplex treatment applied onto the given tool steel and most importantly to compare the effect of the different nitriding treatments on the friction behaviour of specimens having glass bead blasted (GBB) or polished (P) substrate surface below the PVD produced DLC coatings.

EXPERIMENTAL PROCEDURE

Material and bulk heat treatment

The investigated samples were steel discs having diameter of 50 mm, height of 10 mm and grinded surface quality before the bulk heat treatment of the substrate. The applied bulk heat treatment, i.e. precipitation hardening is commonly used for these type of tool steels. This treatment was followed by nitriding with the combination of the following technological parameters: temperature 520 °C and 550 °C, holding time: 8 hours, pressure: 2 mbar, voltage: 600 V, source of nitrogen: decomposed ammonia.

Surface preparation and coating

Before producing the superhard DLC coating by PVD process, the surface of the substrate material has been prepared in two different ways: polishing (P) and glass bead blasting (GBB).

Ball-on-disc test

Ball-on-disc test using the UNMT-1 tester at the Institute of Materials Science and Technology laboratory at the UM was carried out to examine the wear and friction behaviour of sample. The parameters of test were as follows: normal force: F=90 N; total sliding distance: L=180 m; nominal diameter of the wear track: d=6 mm. The test machine records the friction coefficient which forms the basis of the evaluation of the wear resistance.

RESULTS AND DISCUSSION

The Table 1. shows the optical microscopic images of the wear track for each sample that was investigated. Each sample had different nitriding treatment followed by different surface preparation i.e. glass bead blasting and polishing as indicated also in Table 1. The images show that samples which are duplex treated i.e. nitriding followed by PVD coating gives better wear resistance and good adhesion properties. In case of polishing the sample, which was nitrided at lower temperature indicates less debris and finer microscopic image of the wear track than the sample which was nitrided at higher nitriding temperature. Whereas, in case of GBB the sample which was nitrided at higher temperature gives lower value of μ_{ss} (steady state friction coefficient) indicating less distortion to the coating and better adhesion properties as compared to sample which were treated at lower temperature and untreated specimen (GBB+PVD).

Table 1 Steady state friction coefficient and the corresponding images of the wear track of differently treated samples having polished (P) glass bead blasted (GBB) surface below the PVD produced DLC layer

Nomination	Nitriding	PVD	Surface preparation before PVD	Steady state friction coefficient (μss)	Images of the wear track
P+PVD	-	Yes	Polished	0.32	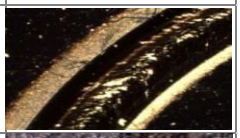
GBB+PVD	-	Yes	Grinded	0.28	
N(520° C)+GBB+PVD	520°C, 8h	Yes	Grinded	0.18	
N(520° C)+P+PVD	520°C, 8h	Yes	Polished	0.16	
N(550° C)+P+PVD	550°C, 8h	Yes	Polished	0.14	
N(550° C)+GBB+PVD	550°C, 8h	Yes	Grinded	0.15	

The important establishment is that the applied duplex treatments resulted in unambiguously better wear performance, comparing to the reference samples that have an identical DLC coating produced by PVD process on the un-nitrided substrate steel material.

ACKNOWLEDGMENTS

This research was supported by the European Union and the Hungarian State, co-financed by the European Regional Development Fund in the framework of the GINOP-2.3.4-15-2016-00004 project, aimed to promote the cooperation between the higher education and the industry.

REFERENCES

[1] Mittemeijer, E. J., Somers, M. A. J.: *Thermochemical Surface Engineering of Steels. Woodhead Publishing*. ISBN: 978085709592, 2014, Chapter 1, pp. 23-25.
[2] C.K. Jones, S.W. Martin: *Nitriding, sintering and brazing in glow discharge.* Feb 1964, Chapter 4. pp. 94-98.
[3] Xu, D. Z., Xiong F. F.: *Plasma Surface Metallurgy, Springer Nature*, 2017. pp. 12-18., DOI 10.1007/978-981-10-5724-3_2
[4] Bell, T., Bardet, W. P.: *Surface Engineering*, ASM Int. Handbook, Vol. 5, 1994. pp. 1800-1810.

TESTING OF MICRO SWITCHES FOR GARDEN TOOLS

SIPKÁS Vivien, VADÁSZNÉ BOGNÁR Gabriella DSc
Institute of Machine and Product Design, University of Miskolc
E-mail: machsv@uni-miskolc.hu, v.bognar.gabriella@uni-miskolc.hu

Keywords: micro switch, failures, Weibull- distribution, lifetime

The estimation of product reliability has attracted wordwile attention during the past decades. The estimation produce usually begins with parameter estimation based on test date. The aim of this paper is to introduce the Accelerated Life Testing (ALT) method for the testing of micro switches. The analysis aims to take many effecting factors into account, to provide statistical assurance of the reliability and to give statistically reliable lifetime data in brief time. The shape of the characteristic cure representing the frequency of the failure as a time parameter called 'bathtube' characteristic curve. This curve shape contains many information.

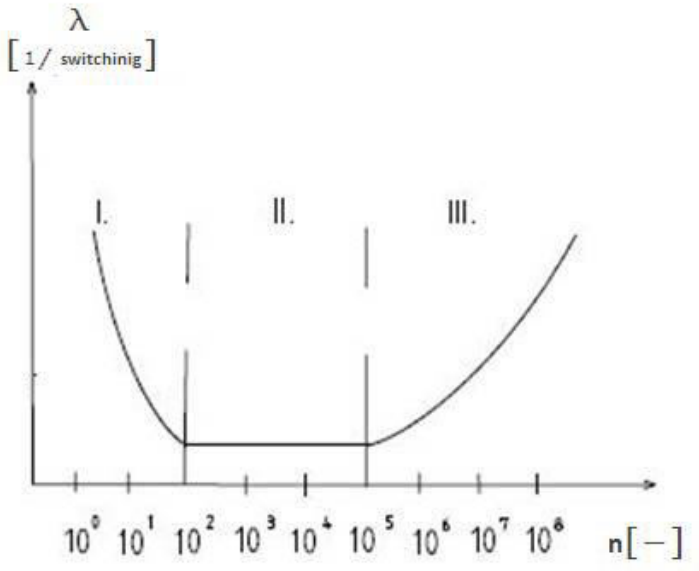

Figure 1 The 'bathtube' curve

The Weibull distribution is applied for the investigation of the failure rate in the product's 'bathtube' lifetime curve. Weibull distribution capable of modelling bathtub shaped hazard rate function is defined. The importance of this distribution lies in its ability to model monotone as well as non-monotone failure rates, which are quite common in lifetime problems and reliability

In recent years new classes of distributions were proposed based on modifications of the Weibull distribution to cope with bathtube –shaped failure rate. Among these, the exponentiated Weibull distribution introduced by Mudholkar et al. (1995, 1996) the additive Weibull distribution (Xie and Lai, 1995), the extended Weibull distribution presented by Xie et al. (2002), the modified Weibull distribution proposed by Lai et al. (2003) [10].Our aim is to analyze the Weibull distribution density function, failure rate function and time-diagram of the load to determine the failure rate of the micro switches in garden tools.

Reliability means that a product maintains its initial quality and performance at certain period of time, cycle, distance etc under given condition without failure. This conditions include both enviromental condition and operating condition. Environmental condition means a common natural ambience such as humidity, vibration, temperature and working condition means an artificial enviroment such as voltage, current load, place for installment, and hours of use, which occurs during the life of the product,

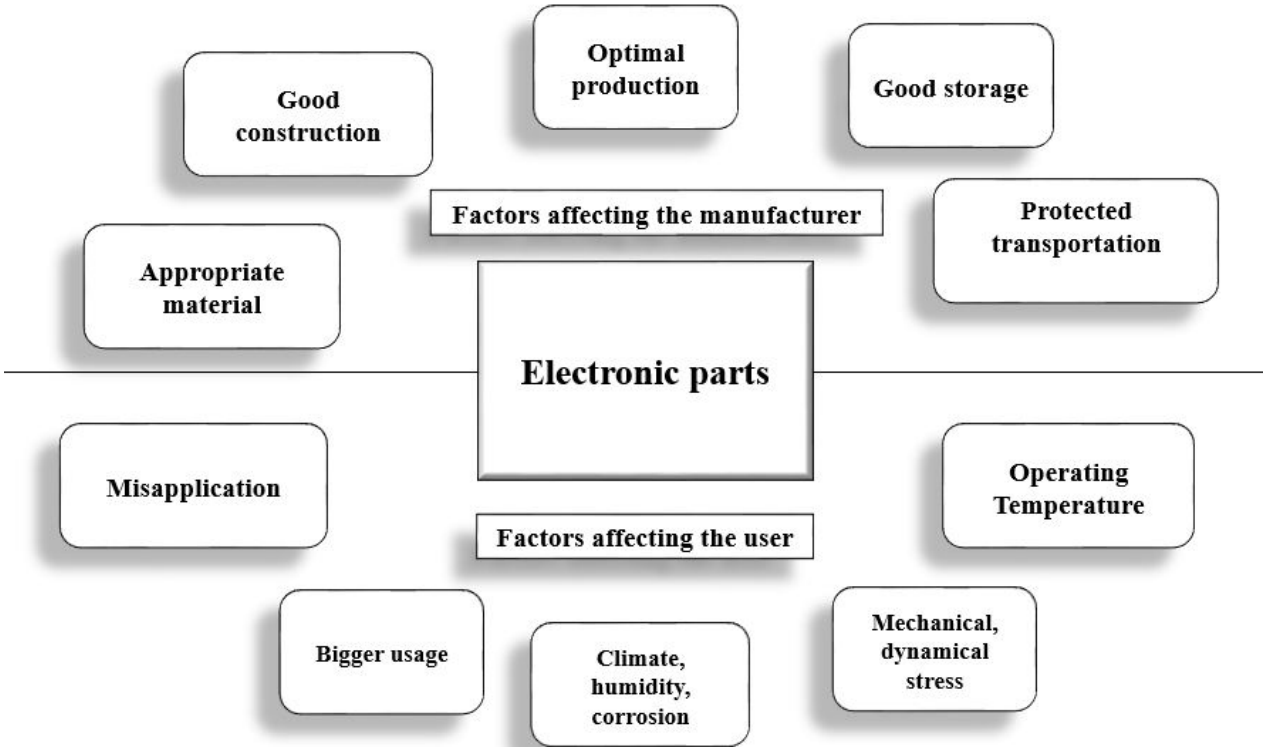

Figure 2 Some example factors affecting the manufacturer and user

This article prepares the planning and design of a test equipment and the literature research of mathematical methods. Furthermore the most common failures of the micro switches have been collected, which are essential for testing and understanding the design of test equipment. It is necessary to learn more about the probability and frequency of these failures.

ACKNOWLEDGMENTS

„ SUPPORTED BY THE ÚNKP-18-3-I-ME/19.NEW NATIONAL EXCELLENCE PROGRAM OF THE MINISTRY OF HUMAN CAPACITIES

HAZ CHARACTERIZATION OF AUTOMOTIVE DP STEELS BY PHYSICAL SIMULATION

[1]SISODIA Raghawendra, [1]GÁSPÁR Marcell PhD, [2]GUELLOUH Noureddine
[1]Institute of Materials Science & Technology, Faculty of Mechanical Engineering & Informatics, University of Miskolc
E-mail: metraghu@uni-miskolc.hu, gasparm@uni-miskolc.hu
[2]Institute of Energy and Chemical Machinery, University of Miskolc
E-mail: noureddine.guellouh94@gmail.com

Keywords: Dual phase steels (DP), Gleeble simulation, Heat-affected zone (HAZ), Rykalin 2D model

The development of high strength weldable steels has diversified the field of application, range of design alternatives subjected to more severe operation conditions than previous time. High strength steels promise higher strength, ductility, good formability as well as weldability. DP steel contains islands of martensite with ferrite matrix and this soft ferrite matrix has significant effect in providing DP steels excellent ductility. The lower strength ferrite surrounds the island of martensite which gives high work hardening rate. This hardening rate and excellent ductility together give DP steel higher ultimate tensile strength because of these features it found intensive application in the field of vehicles industry. The paper focuses on HAZ hardening and softening analysis of different grades of dual phase (DP) steels for automotive application. HAZ softening is the key issue in the DP steels that weakens the joints and affect the mechanical properties. The hardening of HAZ leads to the higher risk of crack susceptibility in DP steels.
A Gleeble 3500 thermomechanical simulator was used to simulate the welding thermal cycles of all the sub zones of the heat-affected zone for MIG welding of DP steel. In order to simulate the sub-zones of the heat-affected zone, samples were heated to different peak temperatures (650 °C, 775 °C, 950 °C and 1350 °C), two cooling time ($t_{8.5/5}$ = 5 sec and 30 sec) and Rykalin 2D model were selected. The hardness and microstructure of the specimens were then tested and analysed using Vicker's hardness test and optical microscope respectively.
The material investigated was a commercial uncoated cold-rolled DP 600, DP 800 & DP1000 steel supplied by Swedish Steel (SSAB) with a thickness of 1 mm and the steel sheet were cut in the rolling direction. The full chemical composition determined by optical emission spectroscopy (OES) and the mechanical properties of this steel are shown in Table 1 and Table 2 respectively.

Table 1 Chemical composition of the investigated base materials in mass percent

Steel	C	Si	Mn	P	S	Cr	Ni	Mo	V	Ti	Cu	Al	Nb	B	N	CEV
DP600	0.088	0.19	0.84	0.012	0.002	0.03	0.03	0.00	0.01	0.00	0.01	0.039	0.016	0.0001	0.003	0.24
DP800	0.136	0.20	1.55	0.013	0.003	0.03	0.04	0.00	0.01	0.00	0.01	0.046	0.016	0.0003	0.003	0.41
DP1000	0.132	0.19	1.50	0.010	0.003	0.03	0.03	0.00	0.01	0.00	0.01	0.041	0.014	0.0002	0.004	0.39

Table 2 Mechanical properties of the investigated base materials

Steel	$R_{p0.2}$, *MPa*	R_m, *MPa*	A_8, %
DP600	405	650	21.0
DP800	585	871	15.5
DP1000	821	1074	9.5

The programmed HAZ thermal cycles for the two technological variants 5 s and 30 s are shown in Figure 1(a) & (b).

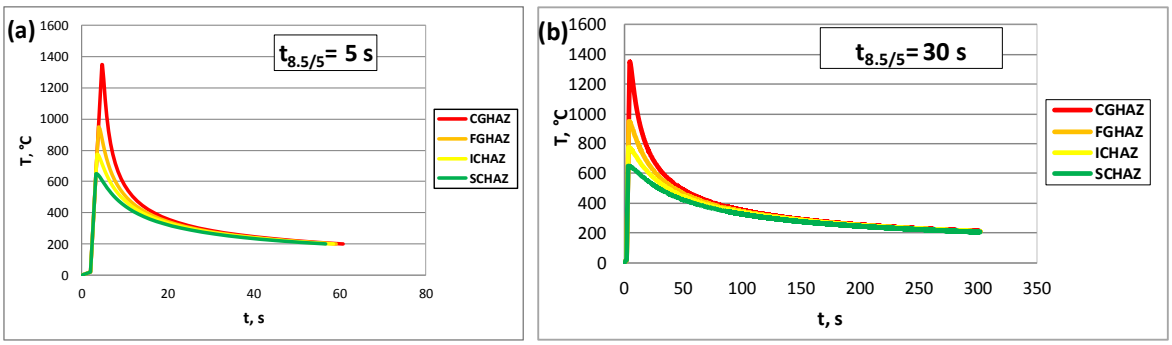

Figure 1 Thermal cycles (a) $t_{8.5/5}$ = 5 s and (b) $t_{8.5/5}$ = 30 s

The average hardness values for simulated HAZ of DP600, DP800 & DP1000 in the function of the distance from the fusion line are presented in Figure 2(a) and (b). The average hardness values of the base material of DP steels used in this work were measured by using HV10 hardness test are 207, 270 and 329 for DP600, DP800 and DP1000 respectively.
The results show that the simulated HAZ is wider in case of long cooling time compared to short cooling time. The following graphs represent the hardness structure profiles of the simulated HAZ for all types of dual phase steels used (DP600, DP800 & DP1000), where we can see how the hardness changes in the function of the distance from fusion line (y) (or welding centreline). Evaluation was performed according to the EN ISO 15614-1 standard which permits HV_{max} = 450 HV10 for non-heat treated welded joints (including HAZ) of high-strength steels belonging to the group 3^b of CR ISO 15608, and HV_{max}= 380 HV10 for the groups (1^a, 2) of CR ISO 15608 also. DP steels are not included EN ISO 15608.

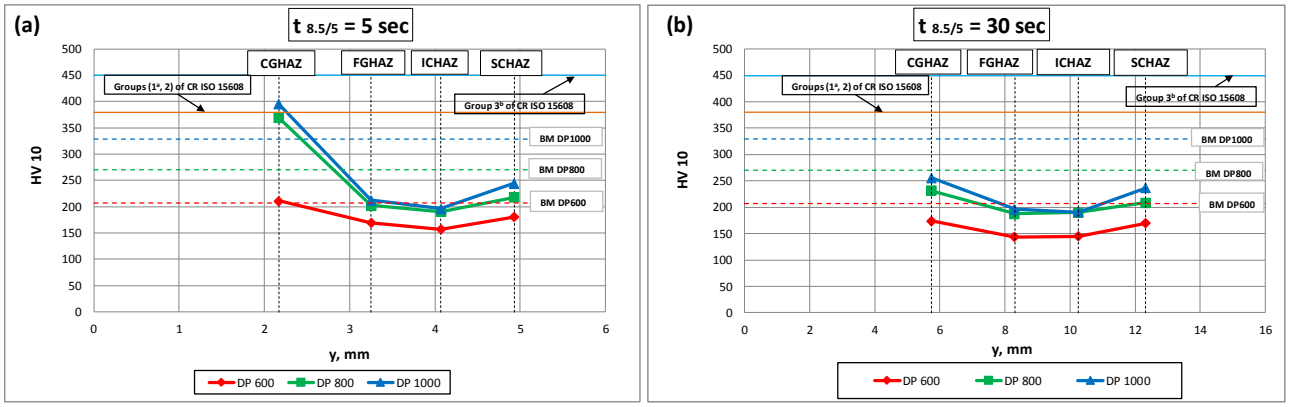

Figure 2 Hardness of simulated HAZ (a) $t_{8.5/5}$ = 5 s and (b) $t_{8.5/5}$ = 30 s

It can be seen that the results obtained from the HAZ hardness examinations did not exceed the permitted maximum hardness value for group 3^b of CR ISO 15608 (450 HV10), but the hardness values in CGHAZ of DP1000 with short cooling time slightly exceeded the permitted value of HV_{max} for groups (1^a, 2) (380 HV10). Also, we can see that, when T_{max} is 1350 ºC and $t_{8.5/5}$= 5 sec, the HAZ average hardness of simulated DP600 is slightly higher than base metal, which has an average hardness of 211 HV and ranges from 200 HV to 219 HV. The HAZ average hardness of DP800 is significantly higher than base metal, which has an average hardness of 369 HV and ranges from 363HV to 374 HV. For DP1000, hardness is higher than the base metal also exceeded the permitted value of HV_{max} for groups (1^a, 2) (380 HV10). For T_{max} =950 ºC and $t_{8.5/5}$= 5 sec, the HAZ average hardness of simulated DP600 is lower than base metal, which has an average hardness of 170 HV and ranges from 163 HV to 177 HV. The HAZ average hardness of DP800 is much lower than base metal, which has an average hardness of 203 HV and ranges from 197 HV to 213 HV and for DP1000, hardness is 213 HV which is much lower than the base metal, ranges from 204 HV to 224 HV. Similarly, For T_{max} =775 ºC & T_{max} =650 ºC and $t_{8.5/5}$= 5 sec, the average hardness of simulated HAZ is significantly much lower than base metal. Therefore, softening of DP600, DP800 and DP1000 steels occurs when T_{max} =950 ºC, 775 ºC & 650 ºC for shorter cooling time i.e $t_{8.5/5}$= 5 sec but the softening is higher in intercritical HAZ compared to other sub-regions for all the types of DP steel with short cooling time ($t_{8.5/5}$ = 5 sec). However, the hardening zone in the CGHAZ occurs when T_{max} is 1350 ºC for DP600, DP800 & DP1000 steels but it is more prominent in DP800 as compared to others two steel grade.
For longer cooling time ($t_{8.5/5}$= 30 sec), we observed that softening occurs in all grade of investigated DP steels to sub-regions CGHAZ, FGHAZ, ICHAZ and SCHAZ but in general the fine grained HAZ and the intercritical HAZ were the sub-regions where we recorded the highest decrease in hardness for all DP steels. So, we can say that softening occurs almost in all sub-zones with all DP steel grades as the cooling time increases.

ACKNOWLEDGEMENT
The research work presented in this paper based on the results achieved within the TÁMOP-4.2.1. B-10/2/KONV-2010-0001 and TÁMOP-4.2.2/A-11/1-KONV-2012-0029 projects in the framework of the New Hungarian Development Plan. The realization of this project is supported by the European Union, and co-financed by the European Social Fund.

PERFORMANCE OF DUPLEX, NANOCOMPOSITE AND NANOLAYERED THIN FILMS

ŠKORIĆ Branko PhD, KOVAČEVIĆ Lazar PhD, TEREK Pal PhD, MILETIĆ Aleksandar PhD, KUKURUZOVIĆ Dragan
Center for Surface Engineering and Nanotechnology, University of Novi Sad
E-mail: skoricb@uns.ac.rs

Keywords: thin film, duplex, nanocomposite, nanolayer

Thin ceramic coatings have been widely used for protecting the surfaces of various manufacturing tools and mechanical components. Different physical vapor deposition techniques are used for their preparation. A typical duplex process involves plasma nitriding and the coating treatment of materials. In the paper are presented characteristics of hard coatings deposited by PVD (physical vapor deposition) and IBAD (ion beam assisted deposition). The synthesis of the TiN film by IBAD has been performed by irradiation of Ar ions. The evolution of the microstructure from porous and columnar grains to dense packed grains is accompanied by changes in mechanical and physical properties. In industrial physical vapor deposition systems substrates move in a planetary-like manner to ensure uniform coating deposition on all surfaces. In this study, influence of the type of substrate rotation on phase composition, crystal orientation, microstructure and surface morphology of nanolayered TiAlN/TiSiN coatings was investigated. The mechanical properties on coated samples were characterized using a Nanohardness Tester (NHT) developed by CSM Instruments. Nanoindentation testing was carried out with applied loads in the range of 10 to 20 mN. A Berkovich diamond indenter was used for all the measurements. The data was processed using proprietary software to produce load–displacement curves and the mechanical properties were calculated using the Oliver and Pharr method.
Scratch adhesion testing was performed using commercially available equipment (REVETEST CSEM). Acoustic Emission (AE) is an important tool for the detection and characterization of failures in the framework of non-destructive testing. The analyzed AE signal was obtained by a scratching test designed for adherence evaluation. Detection of elastic waves generated as a result of the formation and propagation of micro cracks.
X-ray diffraction studies were undertaken in an attempt to determine the phases present, and perhaps an estimate of grain size from line broadening. The determination of phases was realized by X-ray diffraction using PHILIPS APD 1700 X-ray diffractometer. The X-ray sources were from CuK_{α} with wavelength of 15.443 nm (40 kV, 40 mA) at speed 0.9°/min. The surface roughness was measured using stylus type (Talysurf Taylor Hobson) instruments. The most popular experimental XRD approach to the evaluation of residual stresses in polycrystalline materials is the $\sin^2\Psi$ method. The method requires a Θ-2Θ scan for every Ψ angle around the selected diffraction peak and, in order to emphasize the peak shifts. Scanning electron microscopy, transmission electron microscopy, atomic force microscopy, X-ray photoelectron spectroscopy and nanoindentation technique were applied for coating characterization.
AE permits an earlier detection, because the shear stress is a maximum at certain depth beneath the surface, where a subsurface crack starts. Critical loads are presents inTable 1.

Table 1 Critical load for different type of coating.

	pn/TiN(IBAD)	pn/TiN(PVD)
Lc1	-	23
Lc2	100	54
Lc3	138	108

The critical load Lc1 corresponds to the load inducing the first crack on the coating. No cracks were observed on sample 1.The critical load Lc2 corresponds to the load inducing the partial delamination of the coating. The critical load Lc3 corresponds to the load inducing the full delamination of the coating. AE permits an earlier detection, because the shear stress is a maximum at certain depth beneath the surface, where a subsurface crack starts (PVD), figure 1.

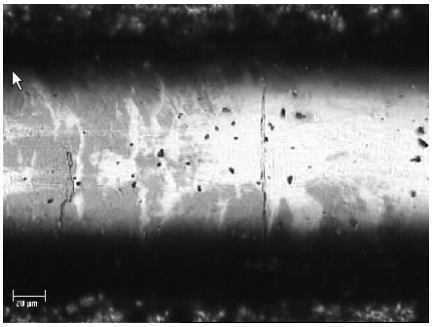

Figure 1 Partial delamination of coating

It was found that the plasma-nitriding process enhanced the coating to substrates adhesion. In some places of hard coatings cohesive failure of the coating and the delamination of the coating was observed (Fig. 2).

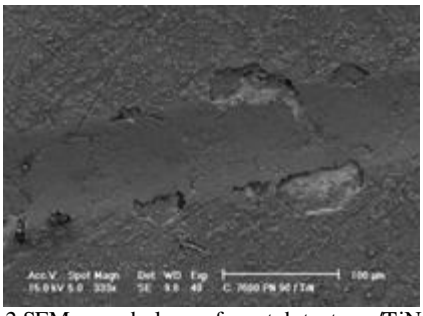

Figure 2 SEM morphology of scratch test: pn/TiN(PVD).

It was found that the type of rotation greatly influences both crystal orientation and microstructure. Coating prepared with single rotation was of columnar and porous microstructure with crystallites oriented in (111) and (200) directions. Conversely, there were no signs of columnar growth for coatings prepared with double and triple rotations which were of compact and dense microstructure with crystallites oriented in (200) direction. As a result, coatings prepared with higher number of rotations were smoother and of considerably higher hardness.

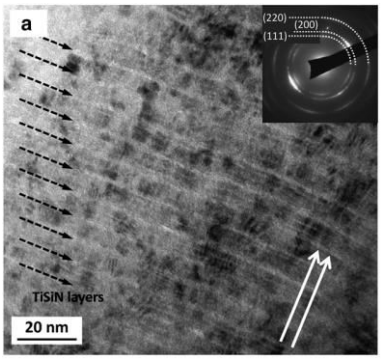

Figure. 3 TEM micrographs of TiAlSiN coating (image with the electron diffraction pattern)

ACKNOWLEDGMENTS
The authors would like to thank to The Provincial Secretariat for Higher Education and Scientific Research of Vojvodina, which supported this work by grant.

REFERENCES

[1] J.C.A. Batista, C. Godoy, A. Matthews, A. Leyland: *Developments Towards Producing Well Adherent Duplex PAPVD Coatings*, Surface Engineering, 2003.
[2] B. Škorić, R. Schrittwieser, A. Cavaleiro: *Nano metrology in biomedical engineering*, ETIKUM 2014, 2015.

FREQUENCY DOMAIN ANALYSIS OF TRACTOR TIRE ENVELOPING PROPERTIES

STOJIĆ Boris PhD
Faculty of technical sciences, University of Novi Sad
E-mail: bstojic@uns.ac.rs

Keywords: agricultural tractors, mechanical vibrations, agricultural tires, uneven ground

Main source of vibration excitation for off-road vehicles are ground profile undulations. Most unprepared terrains are characterized by wavelength of unevenness that is of the order of magnitude of the contact length between tire and ground, so that, due to its shape and elasticity, tire actually behaves as geometric low-pass filter transforming real road profile geometry into effective vehicle vibration excitation as shown in Figure 1.

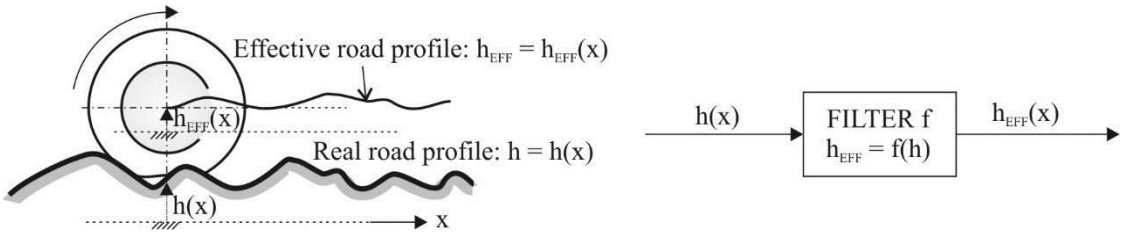

Figure 1 Tire as geometric low-pass filter for road undulations

Since this effective profile represents real vehicle excitation, it is of interest to study this filtering behavior in more depth. In this work, investigation of this kind of tire response has been studied for agricultural tractor tire rolling quasistatically over singular obstacle of rectangular cross section. In sense of geometrical filtering, the process can be considered as rectangular pulse excitation passing through low-pass filter. Experiment principle and general shape of response curves obtained are shown in Figure 2.

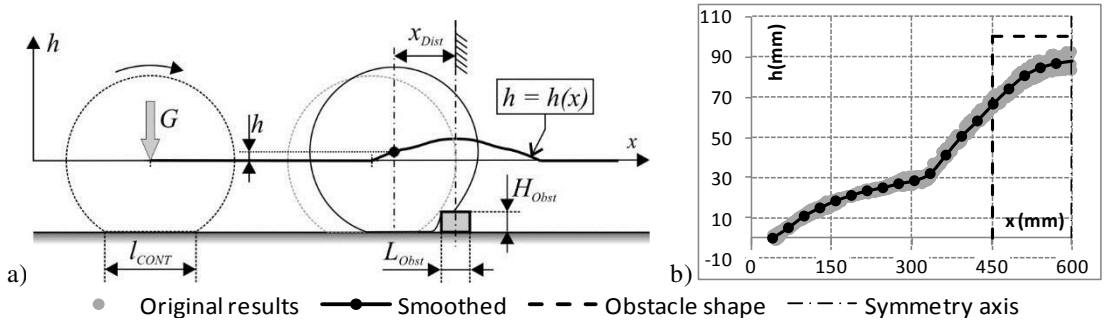

Figure 2 a) Example of the tire enveloping curve for the singular ground obstacle of rectangular cross section: h - effective road profile height, x - longitudinal wheel travel, $h=h(x)$ - enveloping curve, G - vertical force exerted at the wheel, l_{CONT} - tire contact length on the level ground, x_{Dist} - wheel position with respect to the obstacle, L_{Obst}, H_{Obst} - obstacle dimensions; b) Graphical representations of typical test results (only first half of input and output curve shown, i.e. up to the vertical axis of symmetry)

Based on results obtained in spatial domain, frequency analysis of both excitation and response curves has been carried out so as to obtain frequency response function of the filter in terms of its magnitude, by dividing spectra obtained. Since magnitude spectrum of rectangular pulse contains equidistant zeros, whose distance is proportional to pulse duration (i.e. to the length of the obstacle), obstacles of different lengths are used. In order to assess linearity of tire as system in the context observed, excitation magnitudes i.e. obstacle height values were also varied. Dimensions of all obstacles used in experiments are shown in the Table 1.

Table 1 Dimensions of rectangular obstacles used in investigation

Obstacle no.	1	2	3	4	5	6	7
Length L_{Obst} [mm]	100	200	300	100	200	300	200
Height H_{Obst} [mm]	50	50	50	100	100	100	150

In some cases, intensive dissipation of measurement results was observed, sometimes not only in term of noise in data but also in shape of the curves obtained as shown in the Figure 3(a). This phenomenon can be caused by uneven distribution of tire radial stiffness. In order to avoid problems connected with transformation to frequency domain of such set of experimental data, results obtained by using validated tire model with radial and inter-radial springs are used instead because of their repeatability and unambiguousity. Schematic view of the model and comparison between model prediction and experimental results for one set of data are shown in Figure 3 (b) and (c) respectively.

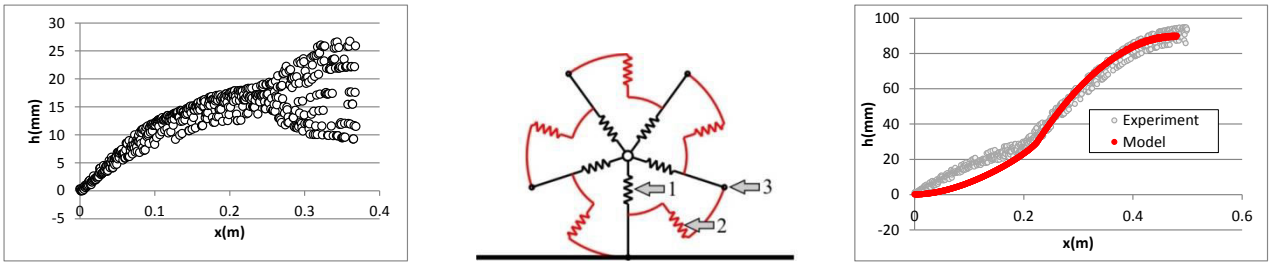

a) b) c)

Figure 3 a) Unambiguous results of the response curve obtained experimentally; b) Schematic view of tire model with radial and inter-radial springs used to simulate tire behavior; c) Comparison between model prediction and experimental results

Excitation spectrum obtained by using FFT algorithm was compared to analytical expression for single rectangular pulse in order to check whether adequate data sampling frequency was chosen. Since, by the nature of considered process, response is obtained by passing input signal through low-pass filter, this sampling frequency was also appropriate for output data. Magnitude spectra of excitation and response are shown in the Figure 4, a) and b) respectively. These curves were obtained for all 7 instances of experimental conditions according to Table 1.

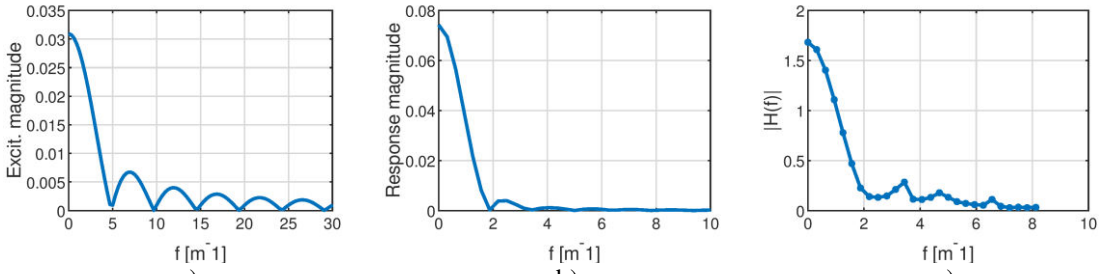

a) b) c)

Figure 4 a) Magnitude of the input spectrum; b) Magnitude of the output spectrum; c) Averaged frequency response function magnitude

For all experimental data sets, frequency response function magnitude curves were obtained dividing input by output spectra. As final result, these curves were averaged to give approximate frequency response magnitude of the low-pass filter. It can be seen that filter cut-off spatial frequency lies very low, somewhere between 2 and 6 m^{-1}. Unevenness that can be observed in the curve shape could be consequence of numerical process of dividing small numbers since it is apparent that output spectrum magnitudes are all very low above ~2÷3 m^{-1}. Conclusion can be drawn that it is necessary to carry out more in-depth experimental study, obtaining more experimental data sets with broader range of parameter values, as well as to improve accuracy and precision of numerical data. That way it would be possible to determine some appropriate empirical mathematical function for frequency response. Moreover, this would enable final check if the properties of the tire as dynamic system at all permit to define this quantity in proper manner, regarding above all system linearity.

NEURAL NETWORK BASED ENVELOPING MODEL OF AGRICULTURAL TIRE

STOJIĆ Boris PhD
Faculty of technical sciences, University of Novi Sad
E-mail: bstojic@uns.ac.rs

Keywords: agricultural tractors, mechanical vibrations, agricultural tires, uneven ground

The vibration properties of agricultural tractor tires significantly influence its response in terms of the exposure of the human operator to mechanical vibrations, which is still one of the key problems in the design and exploitation of tractors. The need to solve this problem plays a significant role in the process of developing and optimizing the tractor's design parameters. The behavior of the tire in this sense is significantly influenced by the mechanism of geometric filtering of the short-wavelength unevenness of the unprepared ground mostly encountered by tractor during in-field operations. Herein, this aspect of tire behavior was studied by using singular road obstacle of rectangular shape as described in the Figure 1. Experiments were carried out with tire rolling quasistatically in order to eliminate all other kinds of influences and to isolate geometric filtering from other mechanisms manifested by the tire.

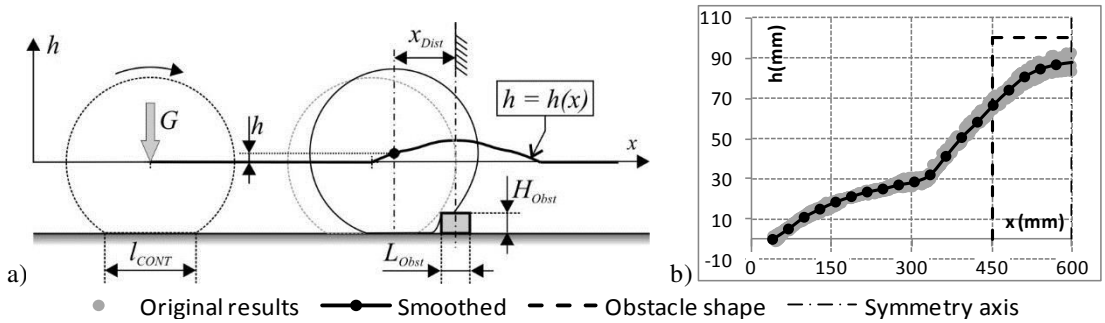

Figure 1 a) Example of the tire enveloping curve for the singular ground obstacle of rectangular cross section: h - effective road profile height, x - longitudinal wheel travel, $h=h(x)$ - enveloping curve, G - vertical force exerted at the wheel, l_{CONT} - tire contact length on the level ground, x_{Dist} - wheel position with respect to the obstacle, L_{Obst}, H_{Obst} - obstacle dimensions; b) Graphical representations of typical test results (only first half of input and output curve shown, i.e. up to the vertical axis of symmetry)

When developing tire model able to take ground profile filtering mechanism into account, one can distinguish between physical and empirical approach. First one, taking into account tire structure and nature, is more flexible and comprehensive, but on the account of complexity and slow execution. Empirical approach, on the other hand, does not have advantages of analytical methods, but can be far more computationally efficient which makes it especially appropriate for usage in vehicle dynamics simulations. Topic of this paper is development of an empirical model of tractor tire enveloping behavior based on the artificial neural network, by which the contact of the tire with a surface with pronounced short-wavelength undulations is taken into account. Concept of model principle and application is illustrated in the Figure 2.

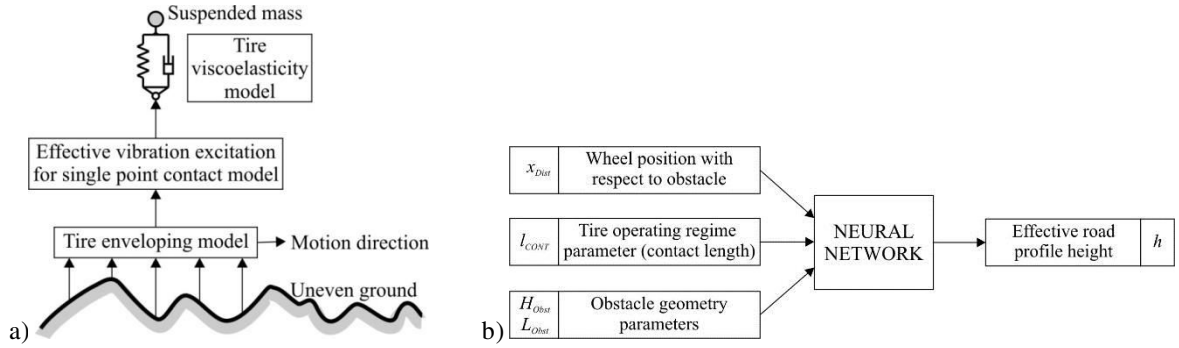

Figure 2 a) Schematic view of separation of the tire model into parts responsible for road profile filtering and for tire viscoelasticity; b) Structure of NN based empirical model of tire enveloping behavior for rectangular shaped obstacle

Tire enveloping model is integral part of overall tire model, consisting of this part itself and the part that describes response of the viscoelastic structure of the tire. The first one generates effective vibration excitation for the second one, which then describes tire dynamics, giving at the same time feed-back information to the enveloping model. The main purpose of this feed-back signal is to define input data for enveloping model in view of tire operating regime through some appropriate parameter, which may be e.g. ground force, or its equivalents such as radial deformation or contact length.

Characteristics of neural network adopted as optimal model structure were as following: type of network - feed-forward, back propagation; number of input neurons - 4 (wheel position, tire contact length, obstacle height, obstacle length); number of hidden layers - 1; number of neurons in hidden layer - 8; number of output neurons - 1 (effective road profile height); connectivity - forward directed, full connectivity of adjacent layers; training algorithm - Standard Backpropagation algorithm; activation function - Logistic function, $\Phi(x) = 1/(1+e-x)$. Figure 3 One example of model prediction of effective road profile, compared to experiment result, is shown in the Figure 3.

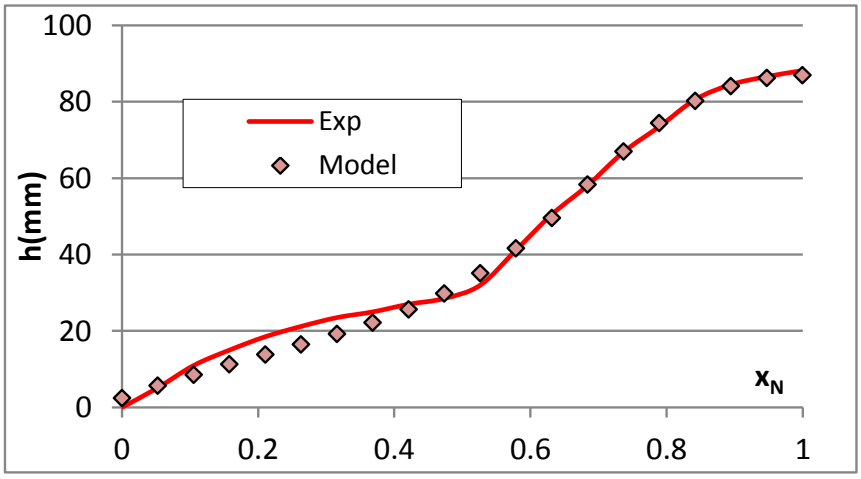

Figure 3 Example of model prediction of effective road profile, compared to experiment result

Neural network based model is characterized by high computational speed, whereby it fulfils this important requirement for use in vehicle dynamics simulations. Other main requirements in this view, accuracy and generalization ability are fulfilled in satisfactory level but through future work it should be checked out whether these can be further improved. As main characteristics of the model, the following can be named:

- Versatility, i.e. modelling approach can be used for other kind of tires as well, since experimental investigations shown that tractor tires behave similarly to other tires in view of enveloping behavior;
- Simplicity and few significant input quantities, contributing to high computational speed;
- Satisfactory accuracy and generalization ability;
- Model parameterization is carried out automatically, parameters (synaptic coefficients values) are hidden from user so there is no need for explicit parameterization procedure which makes model use more simple;
- Developing effort is high since there are no unambiguous criteria for optimal choice of neural network topology, training data set etc. so a lot of work has to be carried out based on the method of trial and error;
- Intensive experimental work on the collecting and processing empirical data for neural network training is necessary;
- Lack of flexibility regarding tire design changes, since no connection exists between physical properties of the tire and model parameters.

POSSIBILITY OF IMPROVING THE GEOMETRICAL ACCURACY OF CIRCULAR HOLES PRODUCTION USING WIRE EDM TECHNOLOGY

STRAKA Ľuboslav PhD, DITTRICH Gabriel
Technical University of Kosice
E-mail: luboslav.straka@tuke, gabriel.dittrich@tuke.sk

Keywords: geometrical accuracy, quality, wire electrode, progressive technology.

Electro-erosive machining technology is one of the finite technologies with a high quality machined surface. Therefore, even a very small variation of geometric accuracy can have a negative impact on the final quality of the machined surface. The aim of the paper is to describe the possibilities of improving the geometrical accuracy of EDM with a thin wire electrode. At the same time, it contributes to an existing database of knowledge that defines the influence of selected aspects on the geometrical accuracy of the machined area in the production of circular openings. Electro-erosive machining technology is characterized by the high quality of the machined surface. Therefore, even small geometric deviation from the desired shape, position, orientation or runout can have a significant impact on the functionality of the finished component. Its range is largely influenced by the accuracy of the applied electroerosion device, the precision of the workpiece and tool setting, the machining method, but also the combination of each other and the adjustment of all process parameters. In the end, they result in the resulting quality of the machined surface not only in terms of roughness parameters, but also in terms of geometric precision of the machined surface.

GEOMETRICAL ACCURACY OF MACHINED SURFACE AFTER WEDM

The geometrical accuracy of the machined surface after WEDM is largely influenced by the precision and reliability of the CNC electro-erosion machine and by the combination of process parameters (1). These input factors are the creators of the resulting quality level of the machined surface. On the geometric precision machined surface also it affects, e.g. oscillating the wire tool electrode. The oscillation of the tool electrode during wire electrical discharge machining is formed as a result of the inappropriate combination of electrode material and workpiece (2), but also setting the technological parameters. This unwanted effect during eletro-erosive machining (3) can be partially eliminated, e.g. by correctly choosing the combination of electrode material and workpiece material, but also by reducing the speed of wire electrode rewinding, by constantly stretching it to the desired size, decreasing the rinsing pressure, and the like.
With respect to all these aspects, the geometric deviation of the precision of the machined surface at WEDM is approximately ±4 μm to ±500 μm. The following table 1 presents a basic overview of the achieved quality of the machined surface at wire electrical discharge machined in terms of dimension deviation

Table 1 The size of the geometric deviations of the area after WEDM

Size of geometric deviation	Type of operation
±100 to ±500 μm	*High performance operations*
±50 to ±100 μm	*Standard operations*
±10 to ±50 μm	*Fine operations*
±4 to ±10 μm	*Precise finishing operations*

MATERIAL AND METHODS OF WORK

In the experiments, the FANUC ALFA C600iA electro-erosion machine was used to make the samples (Fig. 1). It is a three-dimensional vertical CNC electro-erosion device that is used in practice to cut materials. Its application is mainly in the production of complicated shear tools from hard-to-machinable materials.

Basic device parameters	Maximum range
max. Axis Travel X/Y/Z	600×400×310 mm
max. Work Table Size	1050×820×310 mm
max. Workpiece Weight	1000 kg
Speed rewinding wire	0-15 m.min^{-1}
Diameters of the wire electrode	0.10-0.30 mm
Wire tension	250-2500 g
Total machine weight	3050 kg
Dielectric fluid	950 l

Figure 1 FANUC ALFA C600iA electro-erosion machine

Thome Rapid CNC 3D measuring devices (Fig. 2) were used to measure circularity deviations on experimental samples.

Basic device parameters	Maximum range
Axis Travel X/Y/Z	600×500×400 mm
Resolution	0,0001 mm
Fast feed	250/430 mm.min^{-1}
Max. workpiece weight	450kg
Air consumption	25 l.min^{-1}

Figure 2 3D Thome Rapid CNC measuring devices

RESULTS OF EXPERIMENTAL MEASUREMENTS

The following graph in Fig. 3 shows the magnitude of the maximum geometric deviations of the circularity of the machined surface with diameters in the range ϕ_w = 10.0 – 80.0 mm after WEDM with wire electrode ϕ_e = 0.25mm.

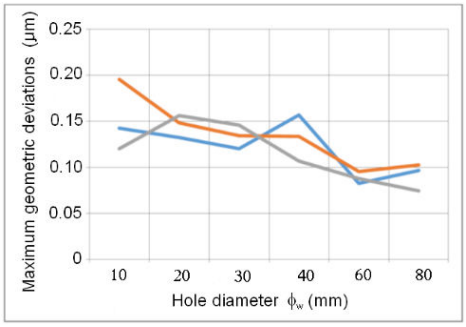

Figure 3 Size of the maximum geometric deviations of circularity of the machined surface with diameters in the range ϕ_w = 100 - 80.0 mm after WEDM with wire electrode ϕ_e = 0.25mm.

Based on the results of experimental measurements of circularity deviations that describe graphical dependencies on Fig. 3, the trend of increasing circularity deviations with decreasing hole diameter has been shown. The reason for the increasing deviation of circularity with decreasing diameter is probably the interpolation error with which the electro-erosion device is operating. These interpolation errors are most visible at small diameters. Two solutions have been proposed to eliminate these deviations. The first solution is suitable for relatively small diameters up to ϕ200 mm. The design consists of a housing, bearings, a worm wheel that is powered by a servo motor. A work table that is attached to a worm gear has conventional "T" grooves to hold the jig, the vice or the clamp such as CNC milling machines. The hole in the table has a diameter of 250 mm and the table size is 500×500 mm. The total assembly, outside the table diagonal, has a maximum width of 650 mm and the height from the base to the edge of the table is 127 mm. The second solution is suitable for making holes with a diameter of over 50 mm. It consists of a servo motor and a work table. The diameter of the rotary table is ϕ45 mm and height 10 mm. This table has a built-in electromagnet, since implementation of another clamping method would be complicated.

CONCLUSION

Designed solutions for the production of holes are applicable to most of the currently used electro-erosion devices. This solution will allow you to eliminate the main drawback of the inaccuracy of interpolation. When connected to the machine control system, it will form one compact unit.

REFERENCES

[1] S. Hašová, Ľ. Straka: *Design and verification of software for simulation of selected quality indicators of machined surface after WEDM. In: Academic Journal of Manufacturing Engineering,* vol. 14, no. 2, p. 13-2, ISSN 1583-7904. 2016.

[2] Ľ. Straka: *Analysis of Wire-Cut Electrical Discharge Machined Surface*. LAP Lambert Academic Publishing, Germany, 98 p., ISBN 978-3-659-64435-1. 2014.

[3] Ľ. Straka, S. Hašová: *Assessing the influence of technological parameters on the surface quality of steel MS1 after WEDM*. In: MM Science Journal, vol. 2016, no. 11, p. 1194-1200, ISSN 1803-1269. 2016.

THE INFLUENCE OF CHEMICAL COMPOSITION OF THE WORKPIECE MATERIAL ON MATERIAL REMOVAL RATE AT EDM

STRAKA Ľuboslav PhD, DITTRICH Gabriel
Technical University of Kosice
E-mail: luboslav.straka@tuke, gabriel.dittrich@tuke.sk

Keywords: Material Removal Rate (MRR), machining, tool steel, electrode

The paper describes the results of experimental research aimed at identifying the extent of influence of chemical composition of material on the intensity of workpiece material removal at EDM. The experiments were carried out using an Aggregron Hyperspark 3 electro-erosion machine on selected tool steels. As a tool electrode material, EX-60 graphite was chosen for experimental purposes because of its practical advantages. For electrical discharge machining the hardness of the workpiece material is not a decisive criterion (1). However, an important parameter is its electrical and thermal conductivity. These properties of the workpiece material primarily specify its chemical composition. From it to some extent depends not only the resulting quality of the machined surface (2), but also the intensity of the workpiece material removal. In the case of very low workpiece material removal there is a substantial loss of productivity in the electro-erosion process (3). This consequently makes this machining process less economical.

MATERIAL AND METHODS OF WORK

In the experiments, Agietron Hyperspark 3 electro-erosive equipment (Fig. 1) from the Swiss company GF Agie Charmille was used to make the samples. It is a three-dimensional vertical CNC electro-erosion device which is used in practice for digging. Its application is mainly in the production of complex molds for casting metals under pressure and complex instruments for the forming of difficult to machine materials.

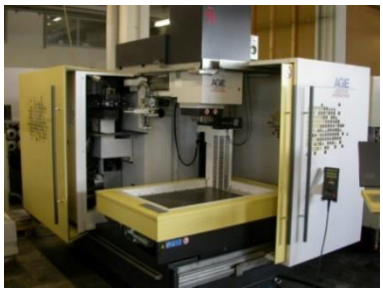

Figure 1 Agietron Hyperspark 3 electro-erosion machine used for the production of experimental samples

The SPEKTRO TEST CCD spectrometer was used to determine the exact chemical composition of the experimental samples. It is a device that is used in practice to verify or identify a material based on a chemical composition analysis. Using the device was made a detailed spectral analysis of samples of materials used. The analysis was carried out in a protective atmosphere of argon. In the production of samples, graphite with the designation EX-60 was used as tool electrode material. This type of material has been chosen because it has many advantages over Cu tool electrodes. This is in particular the higher productivity of the electroerosion process and thus the favorable economic efficiency in machining with this progressive technology. In the experiments, the tool-shaped electrodes of circular cross-section with a diameter ϕ5mm and a length of 100mm were used. It is a material that has a versatile application in electro-erosive machining. It can be used for both roughing and precision finishing operations. Experimental samples (Fig. 2) were made of tool steels. From each group of tool steels, i.e., unalloyed, alloyed and high-speed steels, one material was chosen. It was specifically the tool carbon steel EN C45W, tool alloy steel EN X36 rMoV5 and tool high speed steel EN HS6-5-2.

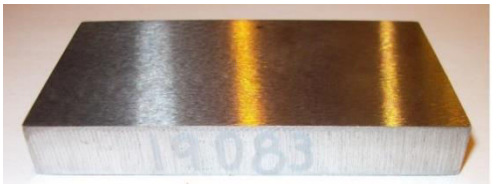

Figure 2 Experimental sample of carbon tool steel EN C45W (W. No. 1.1730) used in the experiment

Based on experimental measurements using Spectrometer SPEKTRO TEST CCD, the chemical composition of the tool steels was found. The identified percentages of their chemical elements are shown in the following Tab. 1.

Table 1 Measured values of percentages of chemical elements of steels EN C45W, EN X36CrMoV5 and EN HS6-5-2

Chemical composition of steel									
Steel marking	Percentage of elements (%)								
	C	Si	Mn	Cr	Mo	V	W	P	S
EN C45W	0.40	0.35	0.78					max. 0.030	max. 0.030
EN X36CrMoV5	0.41	0.26	0.49	4.28	1.28	0.37		max. 0.035	max. 0.035
EN HS6-5-2	0.82	0.27	0.38	4.50	4.83	2.02	6.24	max. 0.030	max. 0.030

Table 2 Selected physical properties of tool steels used in the experiment.

Steel marking	Electrical conductivity [S.m.mm^{-2}]	Electric resistivity [Ω.mm^2.m^{-1}]	Thermal Conductivity [W.m^{-1}.K^{-1}]	Melting point [°C]	Density (kg.dm^{-3})
EN C45W	8.33	0.12	50	1450	7.85
EN X36CrMoV5	7.25	0.35	45	1500	7.8
EN HS6-5-2	6.54	0.54	42	1600	8.14

RESULTS OF EXPERIMENTAL MEASUREMENTS

Based on the results of the experimental measurements, the graphical dependencies were subsequently constructed, describing the impact of these parameters on the MRR. The graphs in Fig. 3 detail the dependence of MRR on the electrical and thermal conductivity of machined material for EDM of tool steels EN C45W, EN X36CrMoV5 and EN HS6-5-2 with graphite tool electrode EX-60.

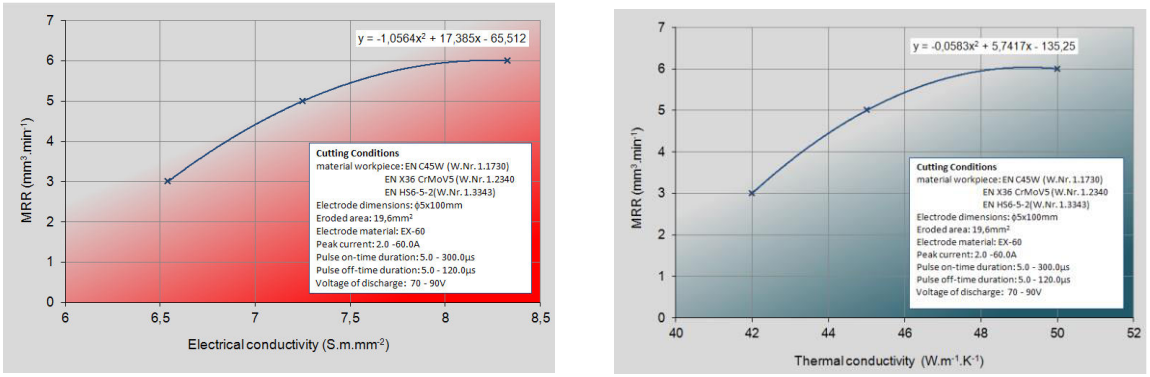

Figure 3 Dependence of MRR on electrical and thermal conductivity of machined material for EDM of tool steels with graphite electrode EX-60

CONCLUSION

The aim of the paper was to identify, on the basis of the preliminary analysis and subsequent experimental measurements, the influence of the electrical and thermal conductivity of the workpiece material on the EDM of tool steels EN C45W, EN X36CrMoV5 and EN HS6-5-2 with graphite tool electrode EX-60. On the basis of the measurement results, it was found that increasing the value of the electrical and thermal conductivity increases the value of the MRR parameter.

REFERENCES

[1] Marafona, J., Wykes, C., (2000), *A new method of optimizing material removal rate using EDM with copper–tungsten electrodes*. Int. J. Mach. Tools Manuf., 40, 153–164.

[2] Singh, S., Maheshwari, S., Pandey, P.C., (2004), *Some investigations into the electric discharge machining of hardened tool steel using different electrode materials*, J. Mater. Process. Technol., vol. 149, p. 272–277.

[3] Straka, Ľ., (2014), *Analysis of Wire-Cut Electrical Discharge Machined Surface*. LAP Lambert Academic Publishing, Germany, 98 p., ISBN 978-3-659-64435-1.

CHARACTERIZATION OF UNIT CELL MODELS WITH THE USAGE OF FINITE ELEMENT ANALYSIS

SZABÓ Dániel, MANKOVITS Tamás PhD
Department of Mechanical Engineering, University of Debrecen
E-mail: szabo.daniel995@gmail.com, tamas.mankovits@eng.unideb.hu

Keywords: biomechanics, additive manufacturing, unit cell, finite element analysis, elastic deformation

In the field of biomedical implant application there is a great need for materials which are biocompatible and mimic to the mechanical properties of human tissues, e.g. bone tissue in the field of orthopaedics. Human orthopaedic implants manufactured from solid materials (e.g. titanium and its alloys) are available in the market, but experience revealed issues regarding their long time performance. The solid type biocompatible implant structures are way stronger than the surrounding bone tissue they're implanted to, and with time a process called stress shielding occurs. Stress shielding means that the implant, which is stronger, bears most of the occurring loads, and with time the surrounding human tissue weakens. This can lead to the loosening of the implant, bone breaking, etc, of which neither scenario is good. These issues usually lead to surgery and a new implantation. Surgery always come with a risk, especially for the elderly, therefore the aim of our research is to find a way to mimic the mechanical properties of human bone tissue with biocompatible materials to increase the success rate of implantations and their expectable lifetime.
With the help of micro Additive Manufacturing, we have the possibility to design and create trabecular scaffolds made up from unit cells with controlled porosity, therefore by weakening the structure, we can manipulate the mechanical properties of the biocompatible structures. With this method, the use of finite element analyses and the verifying tests, we can create biomedical implants which have very similar properties to the replaced and surrounding tissues, therefore supposedly have a much higher success rate and lifetime.
The unit cells these scaffolds are built up from can be described by type, size, pore size, volume ratio and pore ratio. In this experiment we have used cubic type unit cells with an edge length of 0,5 mm, with varying pore sizes.

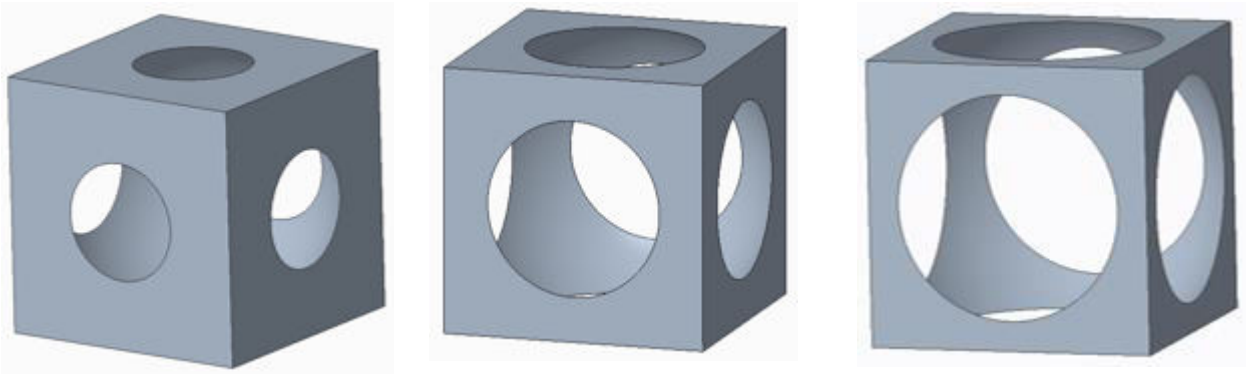

Figure 1 CAD models of the different unit cell models

To be able to design and create such trabecular scaffolds, first we need to calculate how different unit cell types react to different loads. For this purpose, finite element analysis was used. With FEA we can predict the behavior of the investigated structures, and can possibly come to a conclusion of which types can we use in different situations, according to the demands.
First of all we used FEA to investigate the behavior of each unit cell in the elastic region. In result of this investigation we got their force-displacement curves as a function of varying pore ratio.
In this study we used Ti6Al4V material with an elastic modulus (Young's modulus) of 114 500 MPa and with a Poisson's ratio 0.34, and the average element size of 0.034 mm. The study consisted of a compression test, therefore the top and bottom surface have been constrained, and on the top surface prescribed displacement was applied. The compression force was recalculated from the allowable maximum stress level according to Von Mises equation. For the analyses the quarter model of the unit cell was investigated and the symmetric properties were taken into account as constraints.

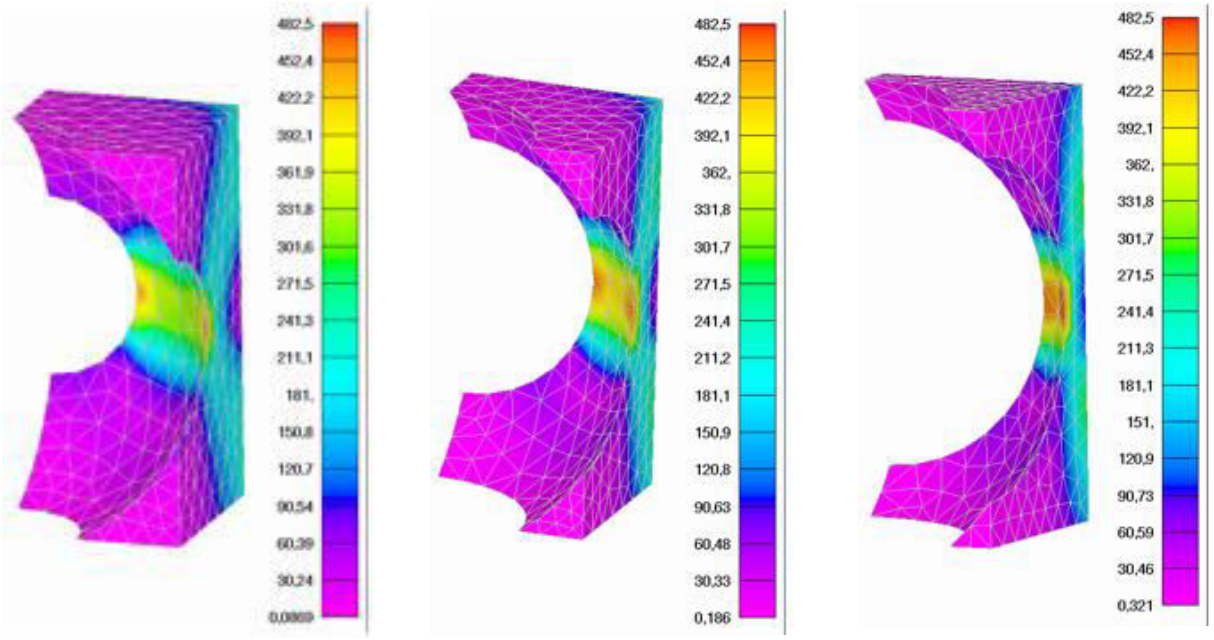

Figure 2 FEA results of the unit cell models

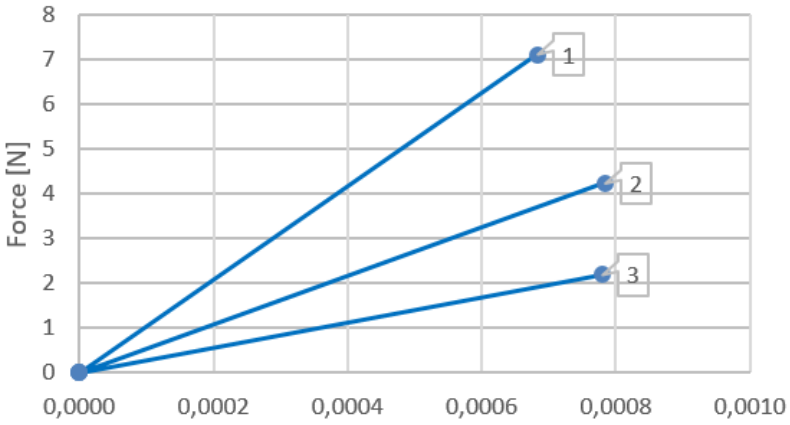

Figure 3 Force-displacement curves of different unit cell models

ACKNOWLEDGMENTS
This research is partly supported by the GINOP-2.2.1-15-2017-0005 project.
This research is partly supported by the EFOP-3.6.1-16-2016-00022 project.
The project is co-financed by the European Union and the European Social Fund.

INSTRUMENTAL MEASUREMENT AND EXAMINATION WITH LIFE SUBJETCS OF THE THERMAL ENVIRONMENT

SZABÓ János PhD, KAJTÁR László PhD
Faculty of Mechanical Engineering, Budapest University of Technology and Economics
E-mail: szaboj@epget.bme.hu, kajtar@epget.bme.hu

Keywords: PMV, AMV, thermal comfort, desired thermal sensation

Thermal comfort sensation can be predicted in the most exact way based on Fanger's PMV model. This evaluation method takes all the six influencing factors into consideration: air temperature and humidity, air velocity, mean radiant temperature of surrounding surfaces, clothing insulation and occupants' activities. Fanger's PMV method was developed for temperate climate and European people, with the participation of university students as subjects. Many researchers had investigated its validity in different geographic locations (i.e. climatic conditions, people) and under non-laboratory circumstances. The other group of researchers analysed the thermal environment in which subjects at different geographic locations sense thermal neutrality. These studies were made mainly in torrid climate zone of Asia. In their research they analysed, which thermal environmental condition was judged neutral by occupants in real buildings. J. van Hoof summarized the results of ten surveys in the topic of neutral and desired temperatures. Other researchers were also investigated the evaluation of the subjective and objective thermal comfort: D.W. Yoon et. al., V.M.D. Araújó and E.H.S. Araújó, E. Mayer, de Paula Xavier, A.A. and Roberto, L.
PMV ("Predicted Mean Vote") is an index that expresses the quality of the thermal environment as a mean value of the votes of a large group of persons on the ANSI (American National Standards Institute) ASHRAE (American Society of Heating, Refrigerating and Air-Conditioning Engineers) seven-point thermal sensation scale. PPD ("Predicted Percentage Dissatisfied") is an index expressing the thermal comfort level as a percentage of thermally dissatisfied people, and is directly determined from PMV.

Table 1 Seven-point thermal sensation scale according to ANSI/ASHRAE Standard 55-2010

Value	Thermal sensation
–3	Cold
–2	Cool
–1	Slightly cool
0	Neutral
+1	Slightly warm
+2	Warm
+3	Hot

During the last decades thermal comfort was evaluated by our research team using subjective scientific questionnaires and applying the objective Fanger's model in several office buildings in Hungary. The relation between the PMV and AMV („Actual Mean Vote") values were analysed based on these results. Investigations were carried out under steady-state conditions in winter time. We performed objective thermal comfort evaluations based on instrumental measurements using the PMV theory. Parallel to this we assessed the subjective thermal sensation using scientific questionnaires. The mathematical relationship between AMV and PMV was defined according to the evaluated thermal environment.
Based on the PMV model many thermal comfort assessments were conducted in office buildings by our research team. Thermal comfort measurements were completed with the use of the thermal comfort scale. The relation between the values of PMV and AMV was determined. In Hungary only a few similar research has been carried out. The results relate to Hungarian office buildings and office job.

The researchers determined the PMV – PPD function in the course of the validity analysis of the model. According to the researchers the primary reasons for the difference between the Fanger equation and their own result were the following:

- the measurements were field studies,
- there was natural ventilation in the rooms,
- the environmental parameters differed from the European weather conditions.

In a given comfort space the thermal sensation number quantified by comfort questionnaires was named AMV. The researchers determined the relation between PMV – AMV with the help of living subjects, considering the climatic conditions, clothing habits and working culture in their own country. The thermal comfort was analysed with measuring instrument and it was evaluated on the thermal comfort scale using comfort questionnaires as well.
In office buildings the thermal comfort and indoor air quality determine the comfort sensation and influence productivity of occupants. To be efficient at work, one needs to be provided with comfortable environment regarding thermal sensation and indoor air quality. International literature proves that the geographical location and its climate also influences the PMV model. We processed the results of our thermal comfort field studies conducted in office buildings in winter time. We carried out comfort analysis in summer time as well. In this case further effects are added to the dissatisfaction with thermal comfort. To avoid the draught effect of cooled fresh supply air, it is necessary to design, construct and operate in a professional way. However, the increased personal draught sensitivity cannot be eliminated totally.
In the office building two kinds of thermal comfort analysis were conducted. On one hand, PMV was determined by measurement, on the other hand subjects judged thermal sensation using a seven-stage thermal comfort scale. The results were treated and evaluated applying the scientific research methods.

By PMV theory analysis two parallel thermal comfort evaluations were made in the office building:

- measuring PMV values and air-condition parameters,
- thermal comfort analysis using scientific questionnaires, which can be expressed in average actual mean vote (AMV).

Evaluating the thermal comfort, the following activity and clothing were taken into account (considering the characteristics of the local enclosures):

- activity level: M/ADu = 1 met (quiet sitting)
  M/ADu = 1.2 met (office work, using computer)
- clothing: Icl = 1.0 clo (suit, typical businessman clothing)
  Icl = 0.8 clo (suit without a coat)

Evaluation of the questionnaire survey was carried out with the help of the seven-stage thermal comfort scale (cool, slightly cool, neutral, slightly warm and warm) which is also applied in international studies.
It is not that straightforward when discrete and continuous probability variables are compared. In this case, the distribution cannot be the same. However, the comparison is valid, as both variables measure the same physical characteristic, only on a different scale. The problem can be analysed for connected variables with a regression method. There are limited mathematical tools when the samples are independent, as in this case. The thermal comfort data can be collected by seven-point scale questionnaire (AMV) and measurement (PMV). The AMV data was seven value discreet variable while the PMV was a continuous variable on range. Therefore the momentum of the variables can be compared.
The next step was to determine how the two variables can be transformed to each other, so to express X (AMV) as a function of Y (PMV) or vice versa. Continuous probability value is more difficult to fit with a discreet probability variable. However, if there are sufficient data points for X, then the average follows normal distribution based on the central limit theorem. The results of the thermal comfort questionnaires approach with high accuracy the results of PMV measurements considering clothing insulation and the activity level that represents the office work. Under Hungarian circumstances based on measurement results of conditioned office studies it can be ascertained, that the Fanger's PMV – PPD method for thermal sensation evaluation is applicable adequately. The difference between PMV and AMV values is minimal. In Hungary such a complex thermal sensation research and field study had not been conducted before. The presented results clearly certified the applicability of the PMV model.

ACKNOWLEDGMENTS
The research reported in this paper was supported by the Higher Education Excellence Program of the Ministry of Human Capacities in the frame of Artificial Intelligence research area of Budapest University of Technology and Economics (BME FIKP-MI/SC).

COMPARISON OF CRITICAL SPEED VALUES OBTAINED BY CALCULATION AND MEASUREMENT

[1]SZABÓ József Zoltán PhD, [2]DÖMÖTÖR Ferenc PhD
[1]Donát Bánki Faculty of Mechanical and Safety Engineering, Óbuda University
E-mail: szabo.jozsef@bgk.uni-obuda.hu
[2]Faculty of Transport Engineering and Vehicle Engineering, Budapest University of Technology and Economics
E-mail: ferenc.domotor@gjt.bme.hu

Keywords: Critical speed, natural frequencies, vibration measurement

The main cause of vibration in rotating machinery is the unbalance of the rotor. This is especially dangerous, if the rotational speed is near to the critical speed. This is the reason why the accurate calculation of the critical speed has a special importance. However, as this type of calculation is a common and frequent task in engineering, so consequently there is simply no time to use always a complicated software. Sometimes, simple methods have to be used. On the other hand, the accuracy of simple methods must be checked and always kept under control. In this paper the results of calculation by using two different models and measurement data of tests carried out on the "Laval shaft" module of „VIBROTESTER" test rig shall be presented. The test rig itself was developed at the Óbuda University Bánki Donát Faculty of Mechanical and Safety Engineering for demonstration purposes.

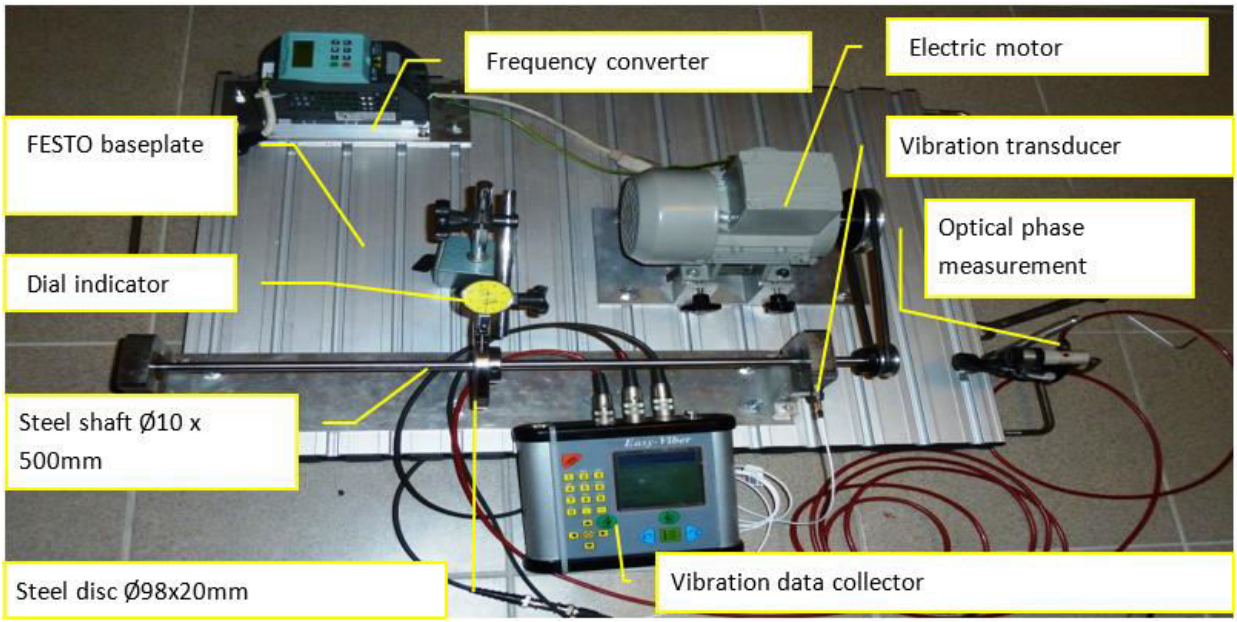

Figure 1 Test rig developed at the Óbuda University

The authors have used two types of beam models for the calculation. One of them is the beam with a concentrated mass. The other one is the continuous mass distribution method of the Bernoulli beam. The calculated results were compared on one hand to each other and on the other hand to the measured values. For the measurements an Easy Viber 64 type of vibration data collector was used.
The results of the comparison provide an evidence, that in simple case there is an acceptable difference between the results obtained by using different models. However, one of the numerous problems is, that several types of forces and torques act on the rotor, influencing the mechanical vibrations. These can be taken into consideration or neglected, depending on the requirements.

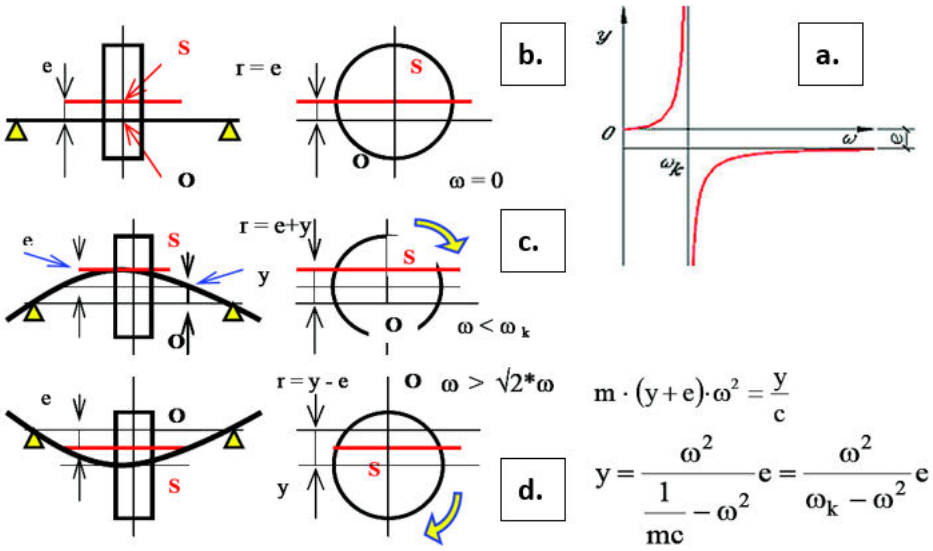

Figure 2 The critical speed of the rotor

The authors checked the critical speed in two different cases (rigid and elastic foundation). Also the so called ODS (Operation Deflection Shape) method was used to demonstrate the effect of the foundation. Results obtained during the tests and calculation can be successfully used both in the industry and the education.

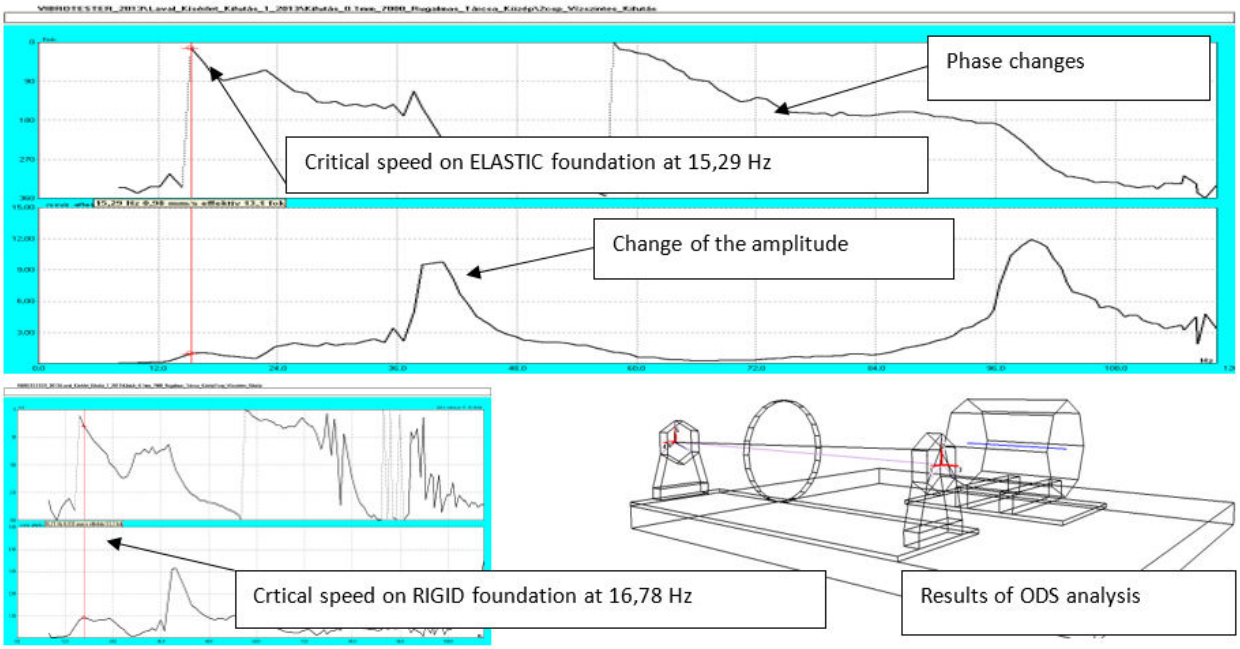

Figure 3 Results of the measurements

DETERMINATION OF DRYING PROPERTIES OF GRANULES IN FLUIDIZED BED DRYER

SZABÓ Viktor, POÓS Tibor PhD
Faculty of Mechanical Engineering, Budapest University of Technology and Economics
E-mail:szabo.viktor@mail.bme.hu, poos@mail.bme.hu

Keywords: fluidized bed drying, falling drying rate period, moisture ratio, volumetric heat transfer coefficient

A drying study is proposed which may be used to describe the drying characteristics of granules during fluidized bed drying. The main objective of drying is to reduce the moisture content of the material. Modelling the drying properties of agricultural granular products is a complex problem involving simultaneous heat and mass transfer between material and gas. Convective heat transfer coefficients between the two phases are one of the most critical parameters required for the simulation of the drying process. According to our previous work [1] the application of a volumetric heat transfer coefficient and modified dimensionless numbers for mathematical modelling the fluidized bed provides favourable opportunities to describe the drying process. The drying process can be characterised by the drying curves with generally two regions: the constant and falling drying rate periods. The constant drying rate period is characterised by an almost free water evaporation from the surface of the particles. The falling drying rate period is a complex phenomenon, where the mass transfer generally takes place inside the particles. Solution of the partial differential equations that represents the heat and mass transfer during the full drying period demands important calculations, particularly the dependence of properties with moisture content of the particles taken into account [2]. There are several papers on the literature on heat transfer during the falling drying rate period for various materials. The general equation for the heat transfer coefficient between gas and the surface of the material as a function of current water content during the falling drying rate period [3]:

$$\frac{\alpha - \alpha^*}{\alpha_{const} - \alpha^*} = \left(\frac{X - X_{eq}}{X_{crit} - X_{eq}}\right)^n,$$

where α is the actual heat transfer coefficient, α^* is the heat transfer coefficient uncomplicated by mass transfer, α_{const} is the heat transfer coefficient for the constant drying rate period. X is the actual moisture content of material dry basis, X_e is the equilibrium moisture content, X_{crit} is the critical moisture content and n is a constant for a given material. Assuming a linear variation with the free water content in the falling drying rate period, the heat transfer coefficient can be described [4]:

$$\alpha = \alpha_{const}\left(m + (1-m)\frac{X - X_{eq}}{X_{crit} - X_{eq}}\right),$$

where m is also a constant for the given material determined by experiments. Determination of the volumetric heat transfer coefficient for fluidized bed dryers on the falling drying rate period is less elaborated in the literature. Based on the literature the volumetric heat transfer coefficient for fluidized bed drying on the falling drying rate period:

$$\frac{\alpha a - \alpha a^*}{\alpha a_{const} - \alpha a^*} = \left(\frac{X - X_{eq}}{X_{crit} - X_{eq}}\right)^n.$$

The volumetric heat transfer coefficient for the constant drying rate period (αa_{const}), and the uncomplicated by mass transfer (αa^*) can be determined from dimensionless $Nu'=f(Re)$ equations based on experiments. The material properties, in this case the critical and equilibrium moisture content can be determined from the sorption isotherms of the material.

The aim of our work is to study the variation of the volumetric heat transfer coefficient on the falling drying rate period based on experiments. During the evaluation of the experiments, the variation of the volumetric heat transfer coefficient as a function of moisture content of the material, and the dimensionless moisture ratio as a function of drying time are examined. The experiments were performed using a pilot plant fluidized bed dryer equipment in the laboratory of the Department. Figure 1 presents a photo of the test facility. An experimental result is illustrated in Figure 2. The temperature of drying gas was 61 °C and the velocity of gas was 4,2 m/s and the dried material was hulled millet during this measurement. The volumetric heat transfer coefficient decreases with decreasing moisture content.

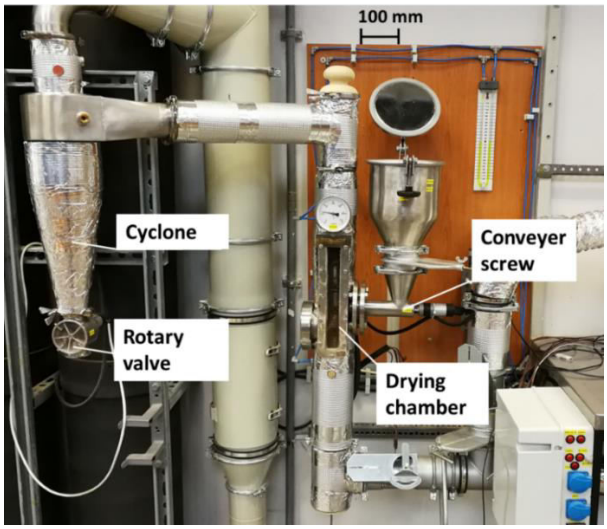

Figure 1 Photo of the fluidized bed dryer

The relationship between the volumetric heat transfer coefficient and the moisture content of the material ensures a more accurate description of fluidized bed drying. The purpose of our work is to use the experimental results to create a mathematical model for the description of fluidized bed drying on the falling drying rate period.

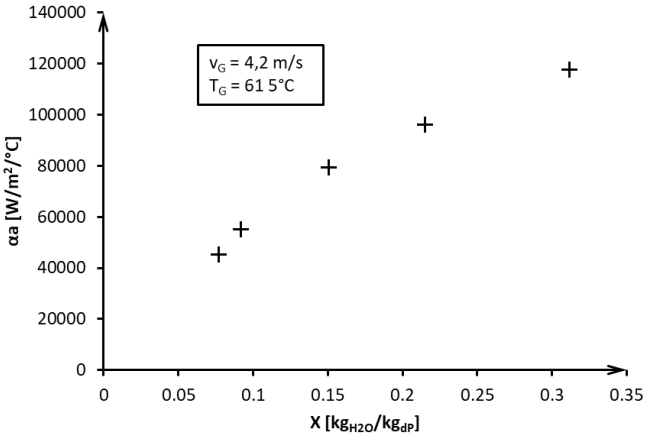

Figure 2 Volumetric heat transfer coefficient versus moisture content dry basis

ACKNOWLEDGMENTS

The research reported in this paper was supported by the Higher Education Excellence Program of the Ministry of Human Capacities in the frame of Water science & Disaster Prevention research area of Budapest University of Technology and Economics (BME FIKP-VÍZ).

REFERENCES

[1] T. Poós, V. Szabó: *Volumetric Heat Transfer Coefficient in Fluidized-Bed Dryers*. Chemical Engineering & Technology, 41 (3), 628–636., 2018.

[2] C. Ratti, G. H. Crapiste: *Determination of heat transfer coefficients during drying of foodstuffs*. Journal of Food Process Engineering, 18 (1), 41–53., 1995.

[3] V. A. Knysh: *Heat transfer in the period of falling drying rate for plywood*. Journal of engineering physics, 19 (4), 1261–1263., 1970.

[4] C. Peishi, D. C. T. Pei: *A mathematical model of drying processes*. International Journal of Heat and Mass Transfer, 32 (2), 297–310., 1989.

THE MECHANICAL PROPERTIES OF 3D PRINTED CuZn28 BRASS SPECIMENS WITH DIFFERENT ORIENTATIONS

SZAKÁL Zoltán PhD, KÁRI-HORVÁTH Attila PhD, PATAKI Tamás PhD, ODROBINA Miklós
Institute for Mechanical Engineering Technology, Szent István University
E-mail: szakal.zoltan@gek.szie.hu, kari-horvath.attila@gek.szie.hu, pataki.tamas@gek.szie.hu, odmiklos@gmail.com

Keywords: 3D printing, metal powder, mechanical properties, orientation.

3D printing is widely used in industry. We can produce not only metal models but also metal parts. Three-dimensional object can be manufactured using laser melting from metal powders. With 3D metal printing technology, external and internal free surfaces or so-called “impossible design" shapes can be created but they cannot be produced using traditional manufacturing technologies. The new 3D metal printing technology is better than the traditional 3D printing, as the parts, which are manufactured by this technology, are not only models, but also ready for use. Three-dimensional objects are produced by new technology that can be directly incorporated into machines after machining.
According to the technical literature, the mechanical properties of 3D printed part vary in different orientation, so, the cause of anisotropy can be attributed to the solidification process. The difference depends on the direction of the particle growth. The particles typically start to grow from the colder side to the warmer side. During laser sintering, the colder side is the bottom of the melt, the material there is already melted and solidified. The heat conduction of cooled solid material is much higher than the heat conduction of powder. The top of the melt pool is heated by the laser beam, and the gas atmosphere adjacent to the surface has a much weaker heat transfer ability than a solid metal. Material represents orthotropic behaviour due to the different temperature zones in the build area. The mechanical properties of 3D printed metal materials depend on the building direction, they are not identical within the printed solid.
This study focuses mainly on the change of mechanical properties of the copper alloy powder (CuZn20) due to the modifications in manufacturing parameters. The machine settings have been varied to achieve the highest strength. It was a question of whether the manufacturer's strength values could be produced with the best technological parameters.

Factors influencing the strength of the finished product:

- The moisture content of the raw material.
- Lighting and sintering strategy.
- Laser energy.
- Backfill.
- Printing orientation.

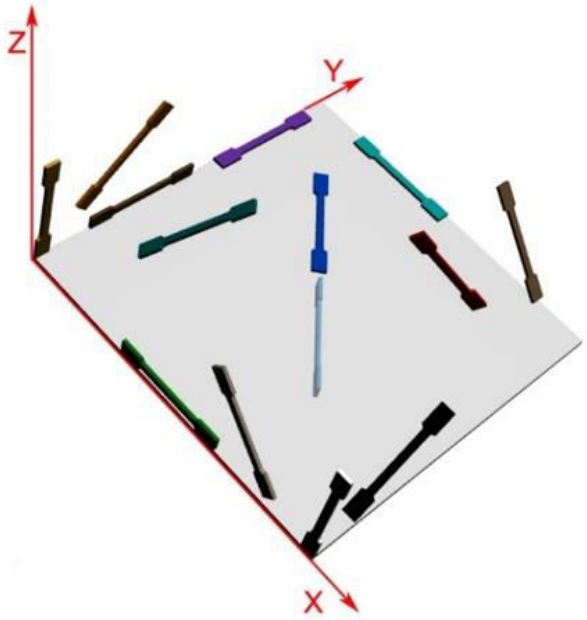

Figure 1 Samples in the build area of 3D printer

The building directions affect not only the print time, but also the mechanical properties of the workpiece as well as the amount of support material and the surface quality of the workpiece. In this study, the notable 3D printing directions of the machine are investigated. Various parameters were measured by tensile testing machine according to MSZ EN 6892-1:2012 standard. Measurements were repeated five times each time. For the measurements, a Zwick Roel Z100 universal tensile test machine was used. The specimens were produced by Thinkspace CL/CTS2 Pro 3D printer. The different print arrangements can be seen in Figure 1.
The samples are labelled as follows: the first two characters represent the plane of the print and the third character indicates the building direction (e.g. xy_x).
The results of the measured strength parameters are shown in Table 1. The yield strength (Rp0,2), the ultimate tensile strength (Rm) and the modulus of elasticity (E) have been determined.

Table 1 Results

	Direction	**$R_{p0,2}$ [Mpa]**	**R_m [Mpa]**	**E [GPa]**
1	**xy_x**	433	577	12,3
2	**xy_y**	423	573	11,9
3	**xy_45**	408	498	25,5
4	**xz_x**	412	502	12,6
5	**xz_z**	431	505	12,8
6	**xz_45**	423	474	28,9
7	**yz_y**	411	524	12,2
8	**yz_z**	403	567	12,5
9	**yz_45**	414	516	26,7
10	**xyz_45**	421	553	45,1

It was found that the values of the strength parameters do not depend on the direction of printing. The average yield strength is $R_{p0.2}$ 417 MPa. The average tensile strength is R_m 529 MPa. On the contrary, the modulus of elasticity is largely dependent on the orientation of the printing in this case. The modulus of elasticity can be up to 3.5 times the same strength parameter, but the highest value is only 45 GPa. On this basis, it is considered that the highest modulus of elasticity is half of the material produced by traditional technology.

VEHICLE MODELLING AND SIMULATION IN SIMULINK

SZÁNTÓ András, HAJDU Sándor PhD
Faculty of Engineering, University of Debrecen
E-mail: andras.szanto.0503@gmail.com, hajdusandor@eng.unideb.hu

Keywords: Simulink, vehicle model, Pacejka, downforce, ABS control

In this paper a vehicle dynamics model is presented, which is an example that contains all the necessary aspects of making a decent vehicle model. Several examples show the use of such a model: basic vehicle dynamics phenomena can be recognized with the simulation of a detailed vehicle model. We are dealing with the connection between downforce and under/oversteering in this paper. In addition, the use of numerical simulations in the field of control systems is pointed out by an example of simulating an ABS control for the vehicle.
The build of a vehicle model can be separated into at least 3 sections. First is the modelling of the rigid body system that can represent the vehicle with all its mechanisms and suspensions. In this example, a car with MacPherson suspension is modelled. Several environments can be used for rigid body dynamics modelling. In this paper MATLAB/Simulink is used because it has a library called Simscape providing convenient resources for multibody dynamics.
The other 2 sections are the modelling of the contacts and the wheels. Of course, these are the extensions of the rigid body model, in fact, the equations of motion are manipulated by adding the contact and wheel forces to the rigid body model. The reason for mentioning these parts of the model separately is that several wheel and contact models can be realized and the quality of these models has a huge effect on the vehicle model with respect to accuracy and the capabilities of the model. For example, a tyre model dealing with all 6 forces and torques is more suitable for approximating the behaviour of real tyres. The elastic behaviour of the tyre results in an increase in the DOF of the tyre: these behaviours also can be simplified and modelled in the rigid body model [3].
The presented vehicle model uses the semi-empirical Pacejka tyre model [1] with all equations and constants. The contact is modelled with a simple sphere-plane contact. A method is shown with which a surface can be visually designed by 3D softwares to add a friction scale to the road the vehicle moves on. Random effects taking place on the surface can be simulated this way which may be necessary for the development of vehicle control systems. Another random effect connected to the surface could be the fact that real surfaces are not planes but uneven surfaces. This effect is not covered by this paper and the contact is simulated as simple as a sphere-plane contact.
The concept and experience of modelling a complex system with several hundred constants and variables - like this vehicle - can be used for a wide variety of other kinds of models too. However, there could be other demands connected to vehicle models - for example real time simulation - that is not covered in this paper. For real time, Simulink solvers may not be adequate in the case of complicated stiff equations mainly caused by the wheel and tyre models in a vehicle simulation [2]. But for general simulation purposes, an environment where the tools and resources of applied mechanics are collected at hand, can be extremely useful.
Lastly, I would like to summarise the vehicle model by presenting the build-up of the MATLAB struct that contains all parameters and constants of the model. The main concept is that the Simulink model has all parameters defined outside Simulink in a MATLAB script. The reason for this is that the model can be more transparent and modifying these parameters is easier, even an automated simulation management can be used.
The Simscape field includes 17 parameters and 4 structs. The parameters are mass properties and initial conditions of the body, and a file path which contains the file that describes the friction properties of the surface (this can be interpreted as a lookup table). The other 4 structs describe the suspension geometry properties of the 4 wheels and it also include the characteristics of the +2 DOF (per wheel) with respect to tyre elasticity. Summing up the Simscape field we find 137 parameters in it.
The next field is the suspension, there are 4 of these too. The stiffness characteristics can be defined in a lookup table, the other characteristics are simplified as linear models. To model the different damping activities with respect to velocity direction, and to model the rubber bumpers we need 9 constants.
The wheel model contains 145 parameters derived from the Pacejka tyre model. Apart from this, we need brake properties and some thresholds for simulation purposes for the tyre and braking, so 149 parameters are included in the wheel struct for each wheel.
The model contains 768 parameters and 5 lookup tables all together. This is just a pure vehicle dynamics model without any driveline models, and several other effects are not included either like air resistance. It was not the aim of this paper to model every effect, our purpose was to model the basics of a vehicle which are the suspensions, wheels and tyres.

There are 12 base inputs for the model. 4 driving torques and 4 brake normal forces (resulted in 4 brake torques) effect between the wheels and the body, so these are internal torques. Besides, 2 steering angles can be defined for the front wheels.

Of course, these inputs can be resulted by other models and algorithms. For example, a theoretical ABS model – that is presented in this paper - produces the normal force inputs for the brakes by a brake force model. This brake force model is controlled by standard inputs of an ABS algorithm: a brake force increase, decrease or stay-the-same request can take place by the ABS algorithm.

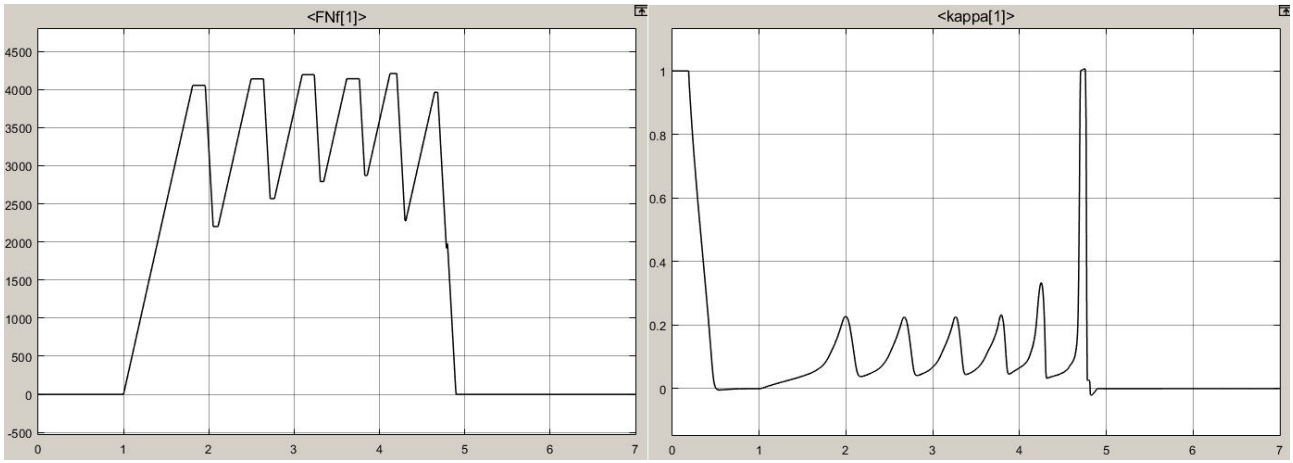

Figure 1 Brake force resulted by an ABS controller and the corresponding slip

REFERENCES

[1] H. Pacejka: *Tire and Vehicle Dynamics* (ISBN: 9780080970172)

[2] M. Carpinelli, M. Gubitosa, D. Mundo, et al.: *Multibody Syst Dyn* 36: 67. https://doi.org/10.1007/s11044-015-9455-x, 2016.

[3] Georg Rill, T. Measy -- : *A Handling Tire Model based on a three-dimensional slip approach*. 2013.

HEAT TRANSFER IN REINFORCED FOAMS

SZEPESI Gábor PhD, SIMÉNFALVI Zoltán PhD
Institute of Energy Engineering and Chemical Machinery, University of Miskolc
E-mail: szepesi@uni-miskolc.hu, simenfalvi@uni-miskolc.hu

Keywords: CFD, heat transfer, reinforced foams, composites

This paper shows a mathematical and a numerical model for the calculation of a 2D heat conduction in anisotropic composites. The main goal to investigate the effect of the biomass as a reinforcement element to the heat fluxes in insulation foam materials. The general equation for the 2D heat transfer equation is:

$$\rho c_p \frac{\partial T}{\partial t} = \frac{\partial}{\partial x}\left(k_x \frac{\partial T}{\partial x}\right) + \frac{\partial}{\partial z}\left(k_z \frac{\partial T}{\partial z}\right) + Q_{source}$$

The 2d heat conduction can be solve numerically with finite element (FEM), finite volume (FVM) or finite different method (FDM) several methods exist in the relevant literature. The easiest way is the FDM with explicit formula, but this method can be instable if the CFL is lower than 0.25.

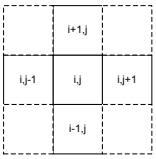

Figure 1 The nodes for numerical scheme.

The FDM explicit formula can be write with the following equation:

$$\frac{T_{i,j}^{n+1} - T_{i,j}^{n}}{\Delta t} = k\left(\frac{T_{i,j+1}^{n} - 2T_{i,j}^{n} + T_{i,j-1}^{n}}{(\Delta x)^2} + \frac{T_{i+1,j}^{n} - 2T_{i,j}^{n} + T_{i-1,j}^{n}}{(\Delta z)^2}\right) + \frac{Q_{i,j}^{n}}{\rho c}$$

The main problem for this formula that the investigated material is not isotropic and the solution need another approach. Let us the following figure where the heat fluxes can be seen which has an effect of the i,j cell:

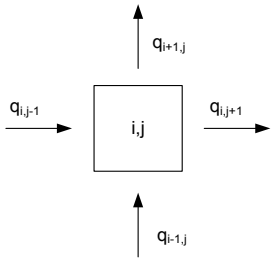

Figure 2 Heat fluxes for cell i,j

The heat fluxes can be calculated with the following formulas, if only heat conduction taken into account:

$$q_{i,j-1} = \frac{k_{i,j-1}}{\Delta j}\left(T_{i,j-1} - T_{i,j}\right), q_{i,j+1} = \frac{k_{i,j+1}}{\Delta j}\left(T_{i,j} - T_{i,j+1}\right), q_{i-1,j} = \frac{k_{i-1,j}}{\Delta i}\left(T_{i-1,j} - T_{i,j}\right), q_{i+1,j} = \frac{k_{i+1,j}}{\Delta i}\left(T_{i,j} - T_{i+1,j}\right)$$

These fluxes causes the enthalpy change in the cell i,j:

$$\rho_{i,j} c_{i,j} \Delta i \Delta j \frac{\partial T}{\partial \tau} = q_{i,j-1} + q_{i,j+1} + q_{i-1,j} + q_{i+1,j}$$

The solution of the above equation provides the time dependent temperature field.

In case of 2D solution, a matrix can help to determine the correct material properties. This research project would like to point out that case when the organic material (wood, or other waste) can distribute randomly at the volume. For a simple example the following distribution was used:

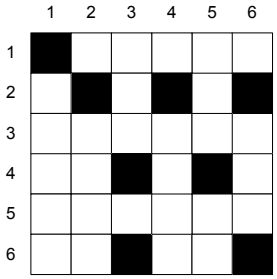

Figure 3 Distribution of the organic material at the volume

where the black cells shows an organic material and the white cells belongs to foam material.
A commercial CFD code (SC/Tetra) was used for the calculation of the heat fluxes. Two different biomass distribution was investigated. At first case the volume ratio of the biomass and the foam was 2% (biomass volume was 900 mm^3, and the foam volume was 49100mm^3). The calculated heat flux without the biomass was 7.34 W/m^2. According to the CFD result the given heat flux is 7.53 W/m^2, which is 2% higher than the original. At second case the amount of the biomass was two times higher than the first case. It means the volume ratio was 4%. The given heat flux for the composite was 7.61 W/m^2, which is 1.038 times greater. The result shows that the amount of the biomass effect is non-linear for the heat flux changes.

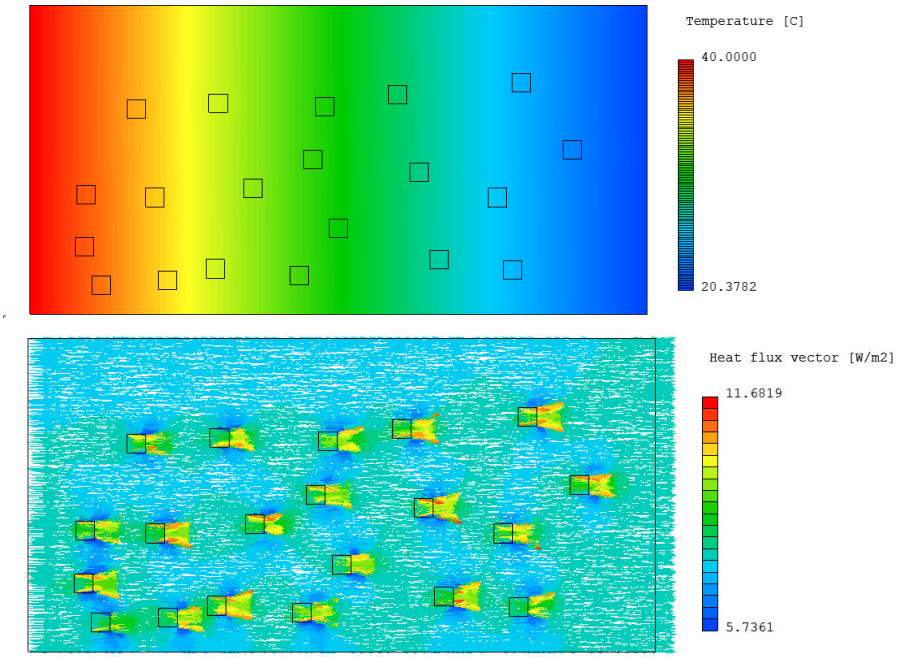

Figure 4 Temperature distribution and heat flux vectors.
(Cedar wood used as biomass and Polystyrene used as base material)

CONCLUSION

According to the results the biomass reinforced elements has an effect of the heat fluxes, it means the composite material heat conduction is higher than the base material, but the function of the biomass volume and the heat conductivity is not linear. Further investigation needed to determine the optimal reinforce element quantity which increases the strength of the composite, but the heat conductivity coefficient is still acceptable.

DETERMINATION OF THE DYNAMIC PARAMETERS OF ELECTRIC MOTORS

SZIKI Gusztáv Áron PhD, SZÁNTÓ Attila, SARVAJCZ Kornél
Faculty of Engineering, University of Debrecen
E-mail: szikig@eng.unideb.hu, szanto.attila93@gmail.com, sarvajcz@eng.unideb.hu

Keywords: series wound DC motor, dynamic parameters, simulation, test measurements.

In a previous publication [Szíki, G., et al. Measurement 109, 111-118., 2017.] a detailed study about the measurement process and the results of the electromagnetic and some of the dynamic characteristics of a series wound DC motor were presented. Moreover, a locked rotor test was performed on the motor and experimentally obtained current- and torque-time functions were compared with simulated ones. The simulation was performed by our own simulation program that had been developed in Matlab- Simulink previously.

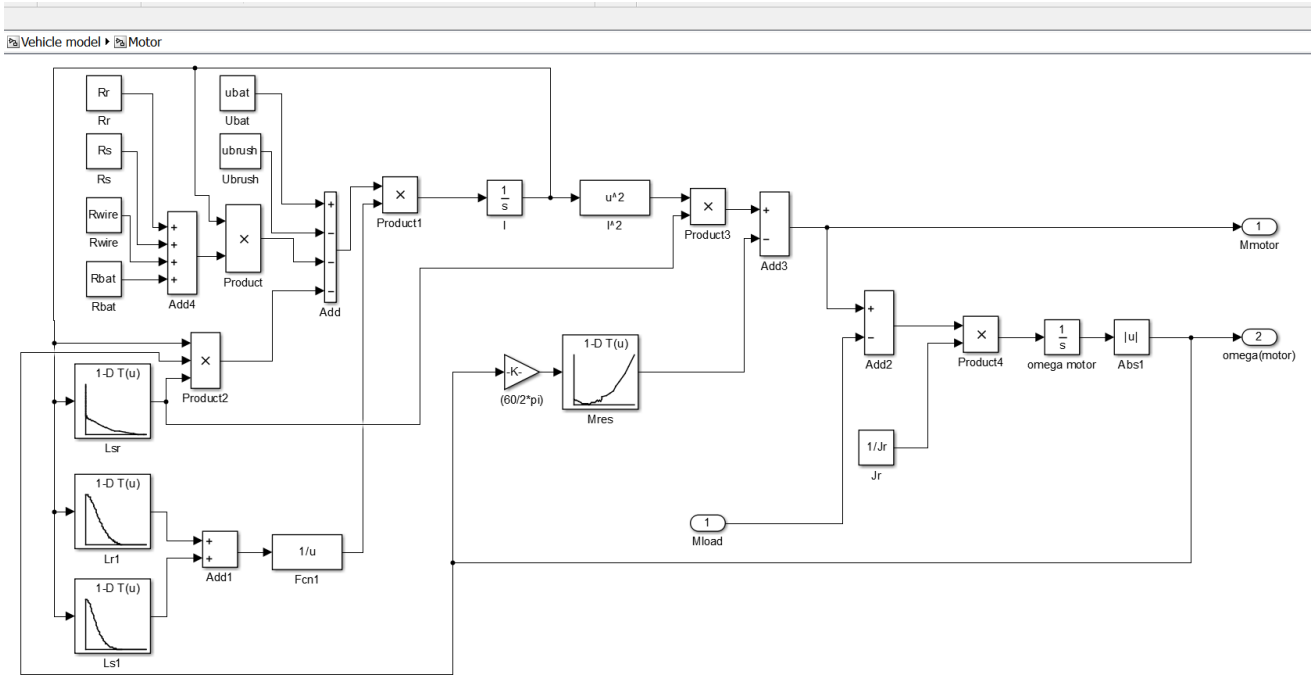

Figure 1 The simulation program in Matlab-Simulink

The measured and simulated results were in a good agreement. At that time the moment of inertia of the rotor was unknown and the experimental setup was not suitable for performing dynamic test measurements. By that time, we had solved most of the critical problems, but an accurate moment of inertia and also bearing and brush friction resistance torque values are still missing.
The recent publication is a detailed discussion about the different measurement procedures of the moment of inertia and bearing and brush friction resistance torques of an electric motor, together with their drawbacks and benefits. A short discussion about the advised experimental setup for dynamic test measurement is also presented here. The figure below represents the setup mentioned above.

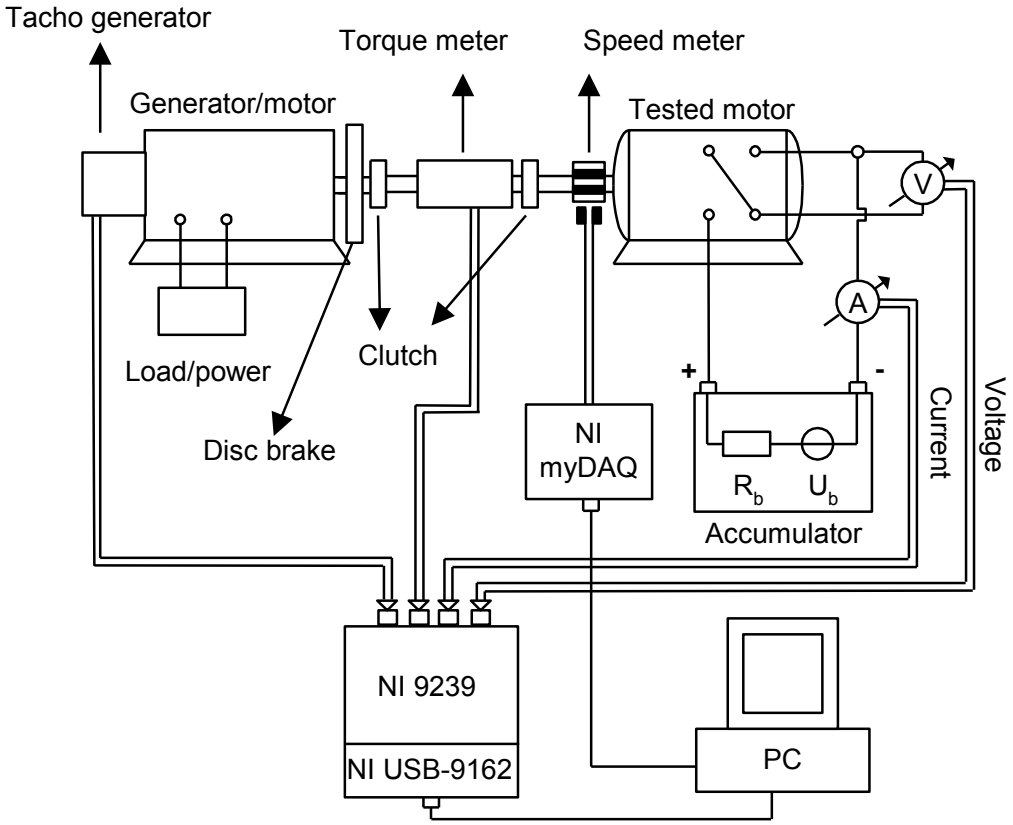

Figure 2 The measurement layout

ACKNOWLEDGMENTS

„ SUPPORTED BY THE ÚNKP-18-2 NEW NATIONAL EXCELLENCE PROGRAM OF THE MINISTRY OF HUMAN CAPACITIES"

IMPROVEMENT OF HIGH STRENGTH AUTOMOTIVE STEELS WETTABILITY PROPERTIES USING CO2 LASER SURFACE TREATMENT

TAJTI Ferenc PhD, BERCZELI Miklós, WELTSCH Zoltán PhD
GAMF Faculty of Engineering and Computer Science, John Von Neumann University
E-mail: cbfferi@gmail.com

Keywords: High strength steel, Laser, Surface treatment, Wettability, Surface tension

As a result of stricter environmental and safety standards, vehicle manufacturers have to reduce the weight of the vehicles, because 10% weight loss cause 8-10% reduction of fuel consumption. To reduce car's weight and increase safety, vehicle manufacturers use high-strength steels. Further weight reduction can be achieved by using corresponding bonding technology (soldering, sticking) and optimizing these technologies can increase the strength of the joints. According to literature research, the improvement of interface properties has a large effect on bonding technologies. In order to improve interface properties, we can use multiple surface treatments. In our research we investigate the effects of CO_2 laser surface treatment on high strength steels, because CO_2 lasers are often used in the vehicle industry. In order to detect the effect of surface treatment, we investigate the wettability of the treated and untreated steels. In our research we measure the surface tension of treated and untreated steels. Our main goal is to improve wettability properties thus the bonding technology.
In our research we used DP 600 high strength steel sheet with the thickness of 1 mm. We cut the steel sheet to 25mm wide and 55mm long workpieces. Before the surface treatment, the workpieces had to be cleaned and degreased using methanol. We searched for parameters that do not cause any visible changes on the surfaces. Among the parameters of the treatment we were able to change the output power of the laser. We used contact angle measurement to examine the wettability. We used distilled water and ethylene glycol to the contact angle measurement. On the untreated workpiece we measured 89°contact angle on distilled water and 68°contact angle on ethylene glycol and we found that the contact angles decreased with the increase in laser output power as seen on Figure 1.

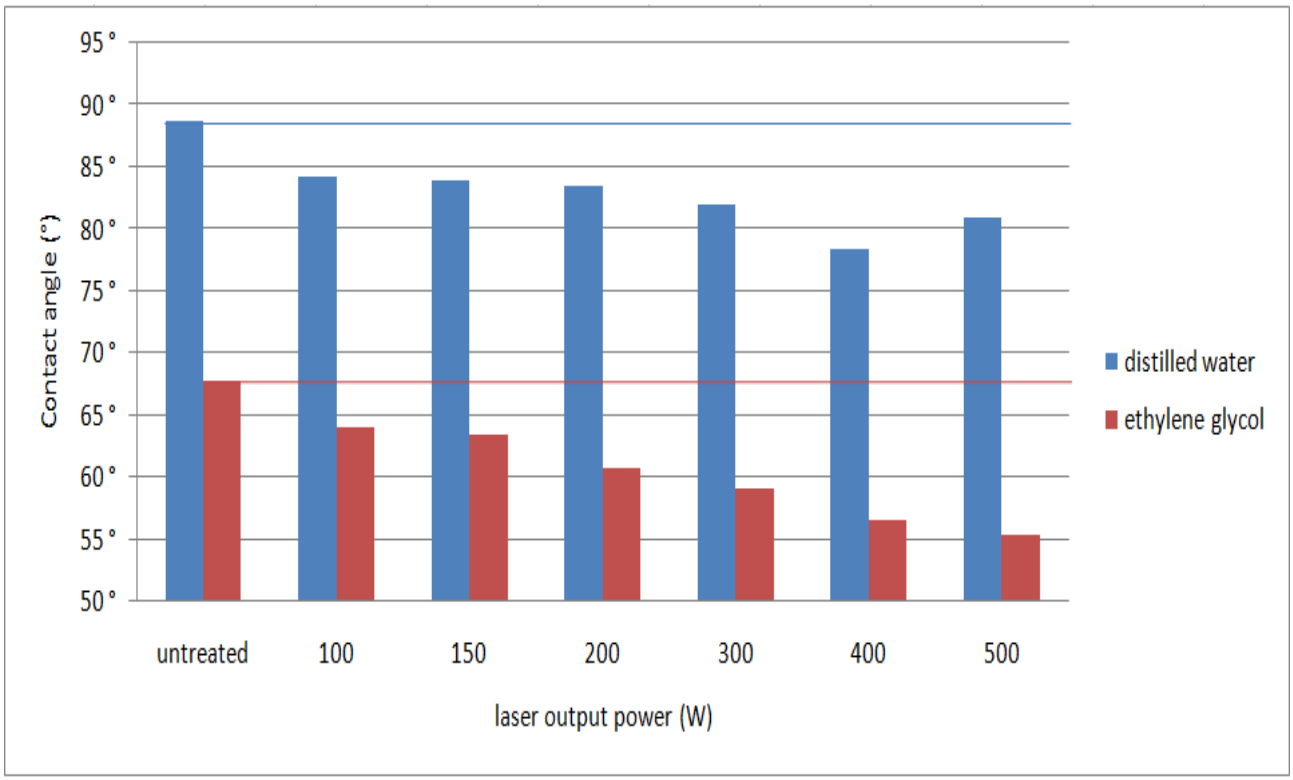

Figure 1 Distilled water and ethylene glycol contact angles on laser treated surface

We also investigated the spread of methanol drops on treated workpieces which shows changes in wetting properties as seen on Figure 2.

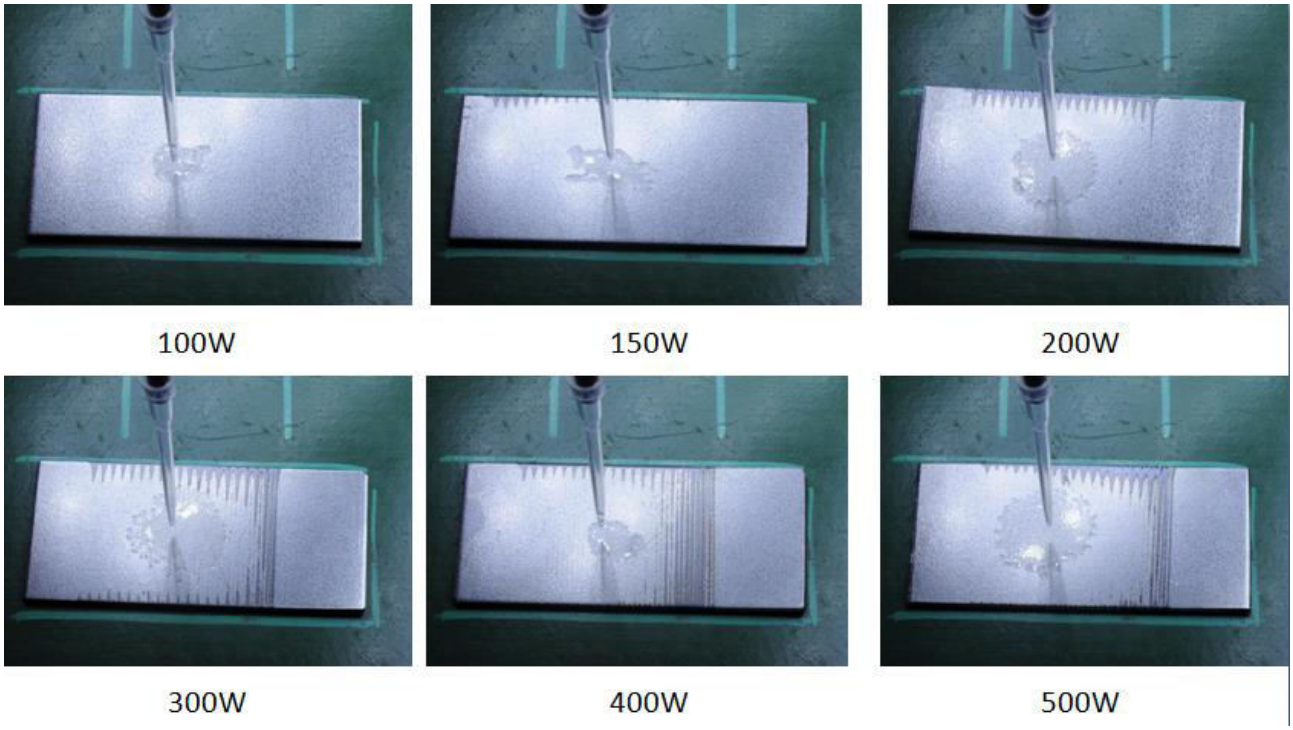

Figure 2 Methanol spread on treated workpieces

We found that laser surface treatment can improve the wettability of high strength steels thus joints strength should improve.

ACKNOWLEDGMENTS
This research was supported by EFOP-3.6.1-16-2016-00006 "The development and enhancement of the research potential at John von Neumann University" project. The Project is supported by the Hungarian Government and co-financed by the European Social Fund.

BIOBASED PLASTICIZERS FROM THE KITCHEN

TAMÁSI Kinga, MAROSSY Kálmán PhD
Institute of Ceramic and Polymer Engineering, University of Miskolc
E-mail: k.tamasi@accell-group.com, k.marossy@gmail.com

Keywords: biopolymer, natural rubber, plasticizers, vegetable oils

Plasticizers used in the Plastic Industries are often based on esters of polycarboxylic acids with linear or branched aliphatic alcohols of moderate chain length. These compounds are selected on the basis of many critieria including low toxicity, compatibility with the host material, nonvolatility, and expense. Phthalate esters of straight-chain and branched-chain alkyl alcohols meet these specifications and are common plasticizers. Ortho-phthalate esters have traditionally been the most dominant plasticizers, but regulatory concerns have led to the move away from classified substances to non-classified which includes high molecular weight ortho-phthalates and other plasticisers, especially in Europe.
In our study, we investigated 5 different natural based plasticizers in natural rubber mixtures: olive oil, plam oil, rapeseed oil, coconout oil and sunflower oil. The aim was to change the hazardous substances of plasticizers to the healthier compounds.

Figure 1 The applied oils "from the Kitchen": olive, palm, rapeseed, coconut and sunflower oils

This study aims to mechanically characterize through compression resistance and shore hardness tests, the mixture of hevea brasiliensis natural rubber with different vegetable oil-based plasticizers. For each of the studied mixtures increased by 10% the content of oils in the mixtures; each test consisted of carrying out five tests of compression resistance and five tests of Shore A hardness and aging-processes (t=30, 60 and 90 min.). The specimens were vulcanized on a temperature of 145°C, during an approximate time of 10 minutes, and the equipment used in the performance of the mechanical tests were an INSTRON and the thermomechanical tests were by DMTA universal machine. The Shore A Hardness results show the difference between the samples:

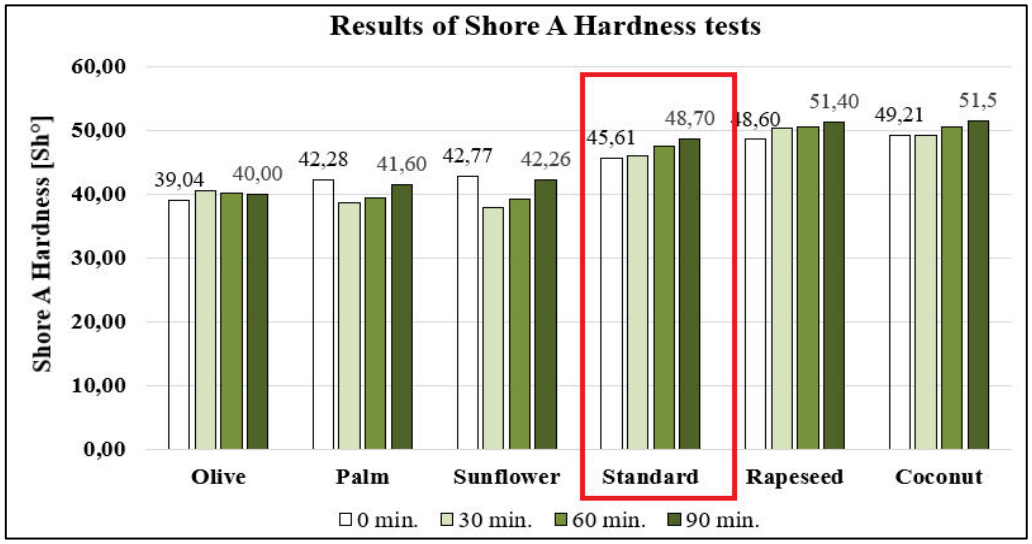

Figure 2 The results of Shore A Hardness tests

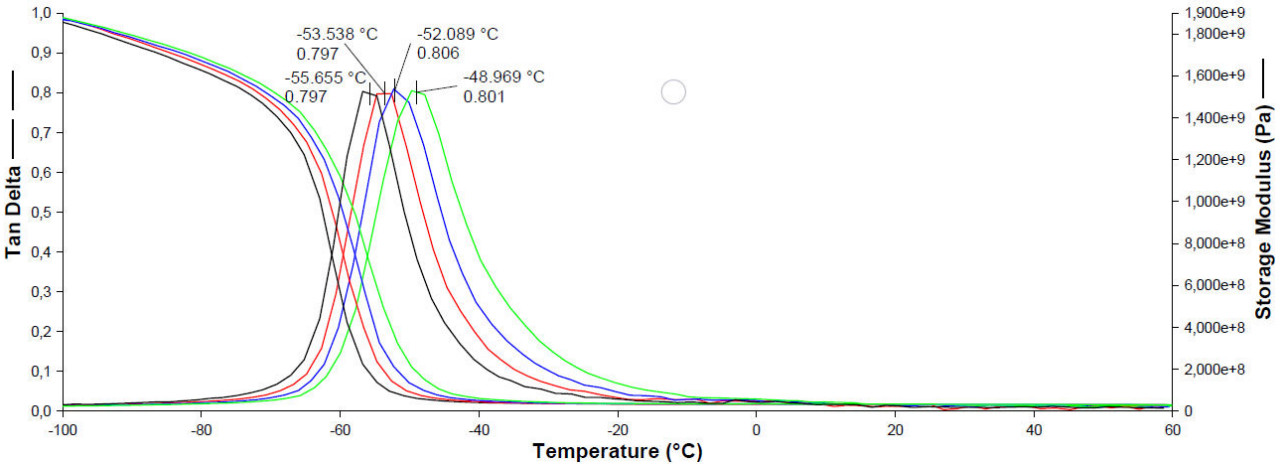

Figure 3 DMTA curves of Coconut oil mixed sample on different frequencies: **0,3**; **1,0**; **3,0** and **10,0** Hz

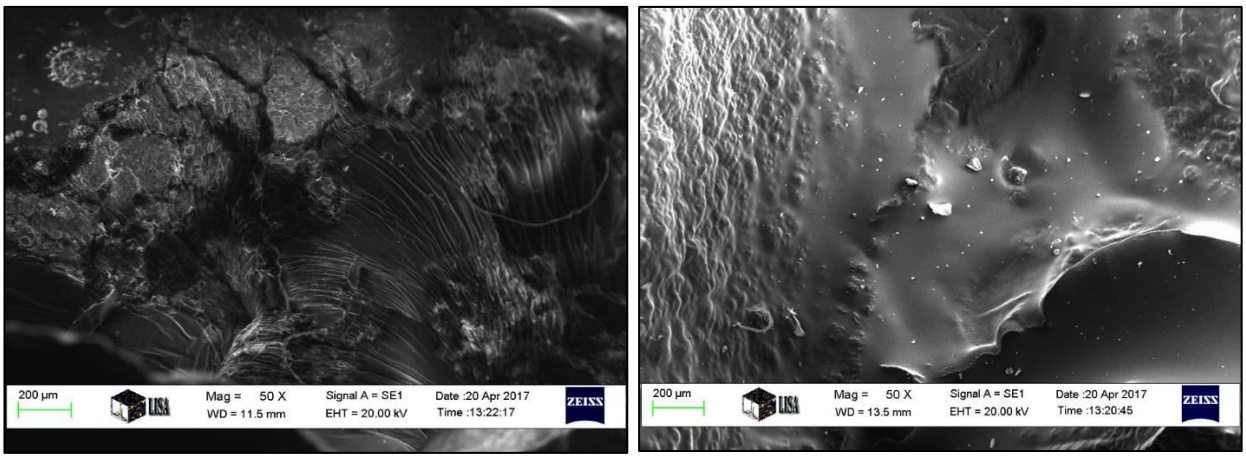

Figure 4 SEM microscopy results of Coconut oil mixed sample on 50x magnification

ACKNOWLEDGMENTS

"The described article/presentation/study was carried out as part of the EFOP-3.6.1-16-00011 "Younger and Renewing University – Innovative Knowledge City – institutional development of the University of Miskolc aiming at intelligent specialisation" project implemented in the framework of the Szechenyi 2020 program. The realization of this project is supported by the European Union, co-financed by the European Social Fund."

DESIGNING ASPECTS AND CLASSIFICATION OF BEARING INDUSTRY BOX HANDLING APPARATUS

[1]TIBA Zsolt PhD, [2]FEKETE-SZŰCS Dániel
[1]*Department of Mechanical Engineering, University of Debrecen*
E-mail: tiba@eng.unideb.hu
[2]*AFT Soft Ltd*
E-mail: fszdani@unideb.hu

Keywords: Handling manipulator, guide of axes, rigidity of frame

It has been an accepted tendency in the industrial practice since the last third of the 20th Century to decrease the living labour demand of the manufacturing processes. One of the main tools of it is the automation of production. In the design, the construction and the programming of the developed automata, the results of electronics, informatics and mechatronics can be used. All of the scientific fields mentioned above undergo intensive development. By the application of the results achieved in the design of the applications, the monotonous, dangerous and tiresome work not requiring expertise can be assigned to machines. In the longer run, the application of the automata is beneficial also in financial aspect, since the costs of living labour are continuously growing, while that of the mechatronic and technological devices show a rather decreasing tendency. Reliability is also an important aspect. It is well known for everyone that a well-designed and programmed automatic device performs its task without mistakes. If there is any objection or breakdown, on the basis of the currently valid safety technology rules, the machine stops, does not trigger any damage and after its repair, work can be continued.
During the manufacture of roller bearings, one of the important processes is the production of roller elements. Its first technological step is the automatic preparation and the washing of the raw roller manufactured from the wire billet by cold extrusion afterwards, the rollers are subject to heat treatment, grinding and sometimes super finishing. The roller press is integrated with the washer and its operation is fully automated. The produced billet arrives to the collection place on a conveyor belt and it gets into a box. The full boxes are put onto a trolley, see Fig. 1 and they are carried close to the machines and devices performing the further technological processes.

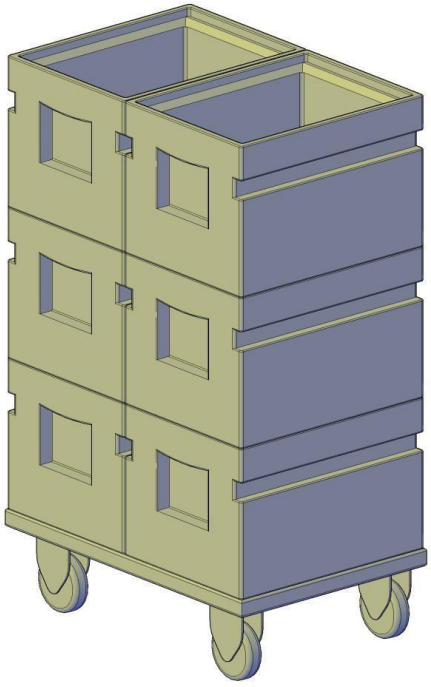

Figure 1 Trolley loaded with boxes

The filling of the boxes is automatic and the trolleys are organised into sets of wagons pulled by industrial forklift trucks. The removal of the empty boxes from the trolleys and the replacement of the full boxes onto the trolley have

been performed by the manual work of skilled workers. The aim of the development detailed herein is the automation of the loading and the filling of the boxes and the decrease of the need for living labour. This paper describes one of the main subsystems of the manipulator constructed during the development, the axis system of the unit moving the boxes. The other important element of the development, i.e. the design of the mechanism for the filling of the box is not part of this thesis. This thesis focuses on the machine design formation of the device and the electronic modules and the programming are not subject to this thesis either.
During the design and development, the aim is the creation of a fully automatic, fault tolerant, long life and low energy consuming automaton which makes possible the release of two unskilled people.
The side and bottom view of the implemented apparatus may be seen in Fig. 2. and Fig. 3.

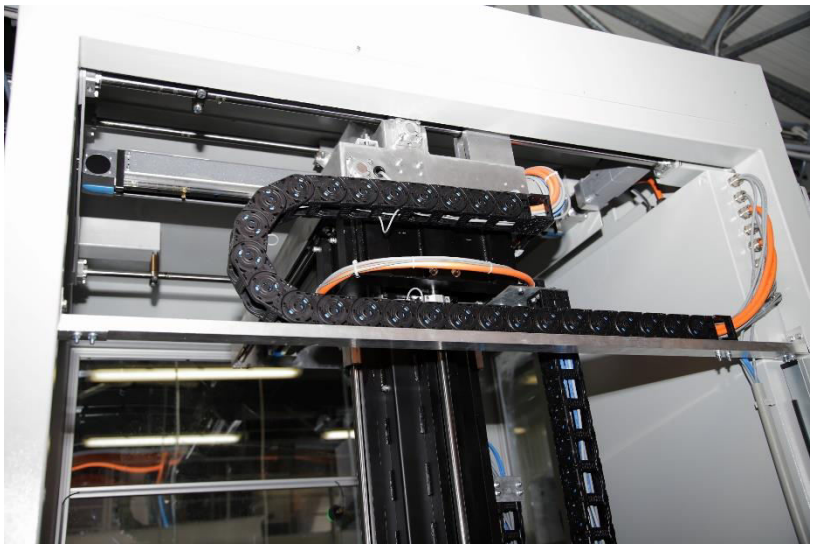

.*Figure 2* Trolley loaded with boxes

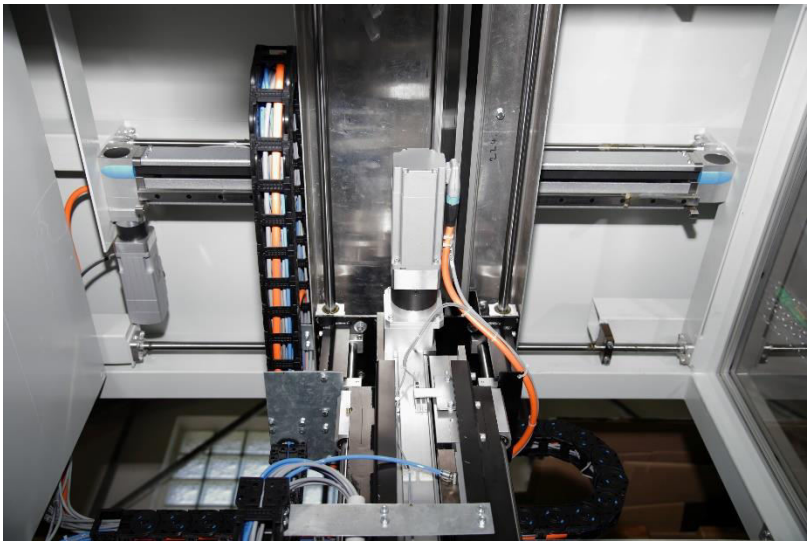

Figure 3 Trolley loaded with boxes

SIMULATION OF AN OPERATING MACHINE IN DUST CHAMBER

TOLLÁR Sándor, BOLLÓ Betti PhD
University of Miskolc
E-mail: aramts@uni-miskolc.hu, aramzb@uni-miskolc.hu

Keywords: dust chamber, simulation,

Auxiliary equipment used in the automotive industry, such as generator, air conditioner, or starter, is often exposed to harsh conditions, for example splash water, frost, or serious dust load. Therefore, these auxiliary devices are intended to be prepared by the manufacturers to this conditions. The topic of this paper is a part of the analysis of the dust control of generators, which in principle is no different from the examination of other equipment.
The essence of the dust test is to create an environment around the equipment to be tested, which can access the built-in auxiliary equipment in a critical area of use. The dusty environment is shaped by the chamber so that a predetermined particle size and amount of dust blows at the prescribed intervals into the chamber space, where the desired dust distribution is formed due to the formation of the chamber, where the dust then settles down.
Built into this environment, the working auxiliary equipment can be used to examine the effects of dust on the operation of the equipment. It is possible to find out where can the dust penetrate the interior of the equipment, or lock off important cooling apertures or cause unwanted wear on the working surfaces.
If the equipment to be tested creates an airflow during operation, the equipment must be installed in the dust chamber in operating situation. This is also the case for generators as the generators are equipped with their own cooling fan. For the installation a mounting frame is required that meets the following requirements:

- properly positioned and fixed in the dust chamber.
- attach to the equipment to be tested (if you want to examine several types, you have the option of using different fixing points)
- allows the machine to drive (in our case: it does not hinder the belt drive)
- preferably does not affect the flow around the equipment under examination and does not cover surfaces from the settling dust.

Planning the mounting frame therefore requires great care. We are working to make sure that our design of the built-in frame complies with our expectations before sharp industrial inspections. We must know that the result of the experiments on the dust chamber is not due to the effect of the mounting frame.
This is why a simulation model is needed to determine the way the design of the mounting frame. So our goal is to create this simulation model. This article describes the phases of this model building.
The simulation test consists of the following main steps:
First of all we need a 3D model of the dust chamber, which contains all the important details of the inside of the dust chamber, including the grid for placing the equipment to be tested. This 3D model is the space where we want to test the settling of the dust.
There is need for the 3D model of the generator to be placed in the initial position in the dust chamber, ensuring its operation. This practically means that the drive shaft must be able to drive the generator and leave enough space around the walls so that the flow in the dust chamber can not be influenced by the walls.
We must design an initial model for fixing the equipment into the dust chamber. This model shall be designed to cover as little space as possible, but shall be joined on the generator's anchorages. Of course, it is also necessary to secure the mounting frame to the dust chamber grille.
If these models are available, the test space is virtually assembled.
The simulation serves firstly to map the flows in the chamber. The model will thus be a space delimited by the chamber walls, which must define the cross-section for the air supply, the outlet section, the airflow volume and the temperature of the air.
To run the simulation, we need data. We need to define the working point of the fan of the dust control. This was determined by the measurement of the colleagues in the absence of technical data. The fan working point can be described with the following values:

$$Q = 340\ \mathrm{m^3/h},$$
$$\Delta p_t = 920\ \mathrm{Pa},$$
$$\Delta p_{st} = 850\ \mathrm{Pa}.$$

For accurate simulation, however, it is essential to take into account the flows from the generator's operation. The generator has its own cooling fan witch rotating at the generator speed. As a consequence, in different operating states means different degrees of flow around the generator. We have been selected two characteristic speeds for the tests: RPM 3000 and RPM 6000.
In itself, the simulation of the flow generated by the generator's own fans is a more complex task than the simulation of the dust chamber, so we needed to find a suitable solution for taking into account the flows generated by the generator fans.
Our chosen solution was to measure the flows formed by the rotating generator around the characteristic rotation of the generator by CTA flow measurement, and then it was shown as a source data for the simulation of the dust chamber. In this way we can gain a simulation result that is close to the reality.
Some of the results of the CTA measurements of the typical speeds at RPM 3000 are in Table 1.

Table 1 Data for the measured velocity around of the generator (samples)

RPM 3000	X pos.	Y pos.	Z pos.	U Mean	U RMS	V Mean	V RMS	C
	[mm]			[m/s]				
inlet	**0**	**22**	**41**	4,154	0,492	1,058	0,47	**4,287**
	41	**22**	**0**	3,378	0,788	-1,212	0,457	**3,589**
outlet	**7**	**44**	**67**	2,954	1,193	-0,536	0,708	**3,002**
	7	**39**	**65**	3,631	1,442	-0,205	0,814	**3,637**

The simulation space is complete. Input data are also available. So we can start to make the simulation model. We are currently in the meshing phase. We would like to report on the results of the flow simulation in a subsequent communication.

PROPERTIES OF CELLULOSE SHEETS MODIFIED WITH POTASSIUM-HUMATE AND COPPER (II)-SULFATE

TÓTH Annamária, HALÁSZ Katalin PhD, PAPP Éva Annamária PhD
Simonyi Károly Faculty, Institute of Wood Based Products and Technologies, University of Sopron
E-mail: toth.annamaria@phd.uni-sopron.hu, halasz.kata@uni-sopron.hu, papp.eva.annamaria@uni-sopron.hu

Keywords: cellulose, copper(II)-sulfate, humate, tensile properties, surface energy

Humic substances like humic acids advanced during the geological periods, where the long polymer chains of the humic acids were created by microbial transformations and slow geological effects mostly from former plant components (Dogan et al. 2015, Erdogan et al. 2007, Kumar et al. 2013). Presences of humic acids and its water-soluble salts, the humates determine the soil quality and plant nutrition efficiency. Beside their impact on the soil fertility, humates are biologically active substances and used in the human medicine as well (Kumar et al. 2013, Stepchenko et al.1991, Tunc et al. 2017). In our study we produced alkali humic acid from Dudar coal than made test sheets with Linter cellulose basis. During the preparation of test sheets we added potassium-humate and copper(II)-sulphate to the cellulose fibres in a different proportion. Table 1 shows the different contents of test sheets. Tensile properties, bending resistance, short span compressive strength, surface energy and the colour (CIE Lab) were examined of the produced sheets of paper.

Table 1 Different test sheets compositions and grammages

	Content (%)	Grammage (g/m^2)
Test sheet 1	Control	142,26
Test sheet 2	90% Copper-cellulose with 10% potassium-humate	149,23
Test sheet 3	75% Copper-cellulose with 25 % potassium-humate	153,07
Test sheet 4	66,67% Copper-cellulose 33,33%with potassium-humate	249,22
Test sheet 5	100% Copper-cellulose	169,55

RESULTS

The potassium-humate effectively adsorbed onto the cellulose fibers which was shown by the color difference of the sheets as well. Test sheets containing potassium-humate showed higher tensile strength and bending resistance than samples without potassium-humate. Compared to cellulose sheets without humate, test sheets with 10% potassium-humate had 25% higher, test sheets with 25% potassium-humate has 86% higher bending resistance. In contrast, the compression strength measurement indicated lower values in sheets containing potassium-humate. According to the content angle measurement, the surface energy of the sheets were not affected by the humates.

CONCLUSIONS

Based on the results, test sheets content humate has higher bending resistance than control sheets except for tensile strength measurement results. Although the copper release and the antibacterial properties needs further investigations, sheets humate could be suitable for the production of active packaging which contain and periodically give off copper ions which support the prolongation of the shelf life of food.

REFERENCES

[1] H. Dogan, M. Koral, A. Vatansever, T. Inan, M. Ziypak, Z. Olgun, Ü. Beker: *New Method for the Production of Barium Humate from Turkish Coal.* Advances in Chemical Engineering and Science, 5.03: 290, 2015.

[2] S. Erdogan, A. Baysal, O. Akba, C. Hamamci: *Interaction of Metals with Humic Acid Isolated from Oxidized Coal.* Polish Journal of Environmental Studies. 16, 671-675, 2007.

[3] D. Kumar, A. P. Singh, P. Raha, A. Rakshit, P. Kishor, C. M. Singh: *Potassium humate: A potential soil conditioner and plant growth promoter.* International Journal of Agriculture Environment and Biotechnology, 6(3), 441-46, 2013.

[4] L. M. Stepchenko, L. V. Zhorina, L. V. Kravtsova: *The effect of sodium humate on metabolism and resistance in highly productive poultry.* In Nauchnye doklady vysshei shkoly. Biologicheskie nauki (No. 10, pp. 90-95). 1991.

[5] M. A. Tunc, M. A. Yoruk: *Effects of Humate and Probiotic on the Number of Escherichia coli, Blood and Antioxidant Parameters in Suckling Period of Calves.* Asian Journal of Animal and Veterinary Advances, 12, 169-176. 2017.

THE EFFECTS OF QUENCHING AND TEMPERING TREATMENT ON THE HARDNESS AND MICROSTRUCTURES OF A COLD WORK TOOL STEEL

TÓTH László PhD, FÁBIÁN Enikő Réka PhD
Bánki Donát Faculty of Mechanical and Safety Engineering, Óbuda University
E-Mail: toth.laszlo@bgk.uni-obuda.hu, fabian.reka@bgk.uni-obuda.hu

Keywords: *heat treatment, hardness, microstructures, tool steel, cryogenic treatment*

The 12% ledeburitic chromium steel K110 characteristically have a particularly high abrasive wear resistance, due to their high carbon and high chromium contents with a large volume of carbides in the microstructure. This steel quality has high compression strength, excellent deep hardenability and toughness properties, dimensional stability during heat treatment, high resistance to softening at elevated temperatures. Studies on cryogenically treated tool steels show microstructural changes in the material that can influence tool service lives, material properties and productivity significantly. In this work the hardness and microstructure evolution of a K110 Böhler cold work tool steel quenched conventionally and cryogenically (-80°C) and tempered on different temperatures were investigated.
The chemical composition of studied K110 Böhler cold work steel (EN 1.2379) is given in Table 1. The microstructure of samples in delivered condition consisted from primary carbide net (Fig.1. a) and spheroid perlite (Fig 2.a). The hardness of studied material was 246HV1 before hat treatments.

Table 1 Chemical composition of the steel in this investigation

1.2379	C(%)	Si(%)	Mn(%)	P(%)	S(%)	Cr(%)	Mo(%)	V(%)
	1.6	0.37	0.41	0.02	0.02	11.3	0.84	1.2

There were studied the effect of different heat treatment processes on microstructure and on the hardness. Each of the studied sample was austenitized at 1070°C, for 55 minutes. Three of the samples were quenched conventional to room temperature, they were tempered at different temperatures. The hardness of the sample tempered at 200°C for 1 hour was 641HV, after tempering at 510°C was 663HV and after triple tempering at 510°C+480°C+480°C was 695HV. The average hardness of cryogenic treated sample tempered at 510°C has become 746HV and after triple tempered at 510°C+480°C+480°C has become 738HV1. The higher hardness of cryogenic treated samples in comparison with conventional quenched samples mean lower quantity of rest austenite as at samples quenched to room temperature and tempered in similar condition. This measurement is in good correlation with the microstructure studied in relative high resolution (Figure2).
Studying the microstructure of samples there were observed that the primary carbide net has not been changed during to austenitization, the primary carbide did not dissolve at 1070°C in 1 hour. The distributions of primary carbides appear approximative identical indifferent of the type of heat treatment (Figure 1); which was expected at heat because the characteristics of the primary carbides are controlled only by the time and temperature of austenitization [1,2], which were constant for the present study. During to tempering at high temperature the primary carbides have become more and more rounded (Figure 1). After low tempering temperature in martensite were observed some small rounded carbides also, increasing the tempering temperature the quantity of fineli dispersed carbides increased, which result higher hardness. Triple tempering result more fine carbides in the matrix than simple tempering at high temperature (Figure 2).

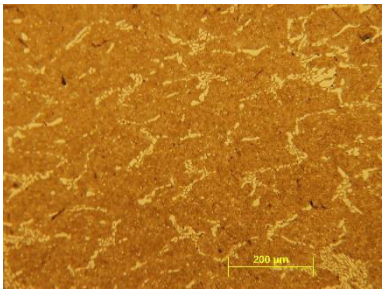

a)
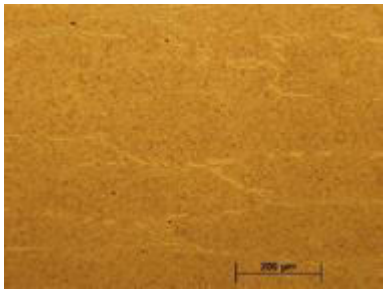
b)
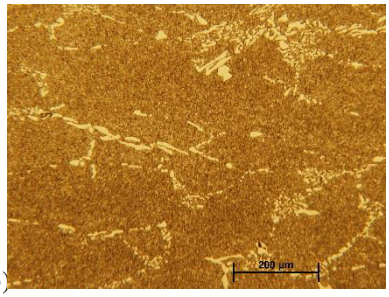

c)

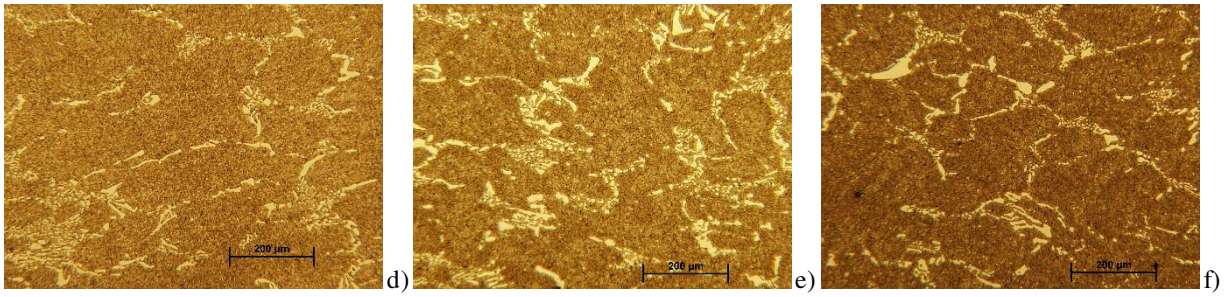

Figure 1 The appearence of primary carbide net a) delivery condition, (b) quenched to RT and tempered at 200°C, (c) quenched and tempered at 510°C (d) quenched and triple tempered (510°C+480°C+480°C), (e) quenched, cryorgenically treated and tempered at 510°C (e) quenched, cryorgenically treated and triple tempered (510°C+480°C+480°C). $N_{original}$=100x. Nital 2%.

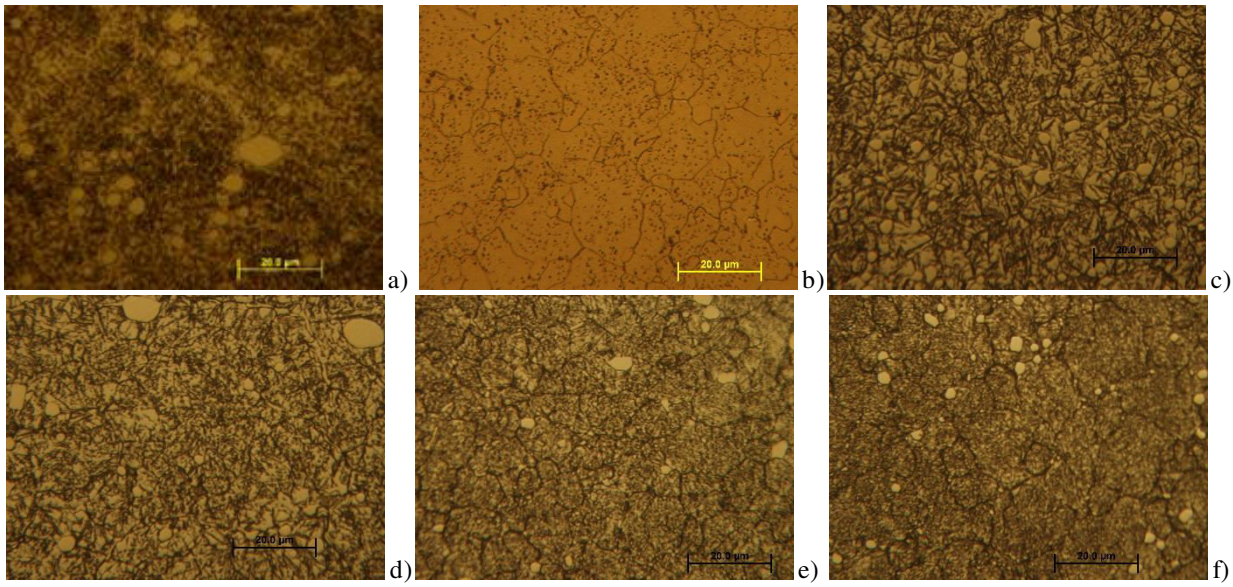

Figure 2 Representative microstructures of samples in (a) delivery condition, (b) quenched and tempered at 200°C, (c) quenched and tempered at 510°C (d) quenched and triple tempered (510°C+480°C+480°C), (e) quenched, cryorgenically treated and tempered at 510°C (e) quenched, cryorgenically treated and triple tempered (510°C+480°C+480°C) after etching with nital 2%. $N_{original}$=1000x

ACKNOWLEDGMENTS
The authors acknowledge the financial support of this work by the Hungarian State and the European Union under the EFOP-3.6.1-16-2016-00010 project.

REFFERENCE

[1] D. Das, A. K Dutta, K.K. Rax: *On the refinement of carbide precipitates by cryotreatment in AISI D2*. Philosofical Magazine 89, 55-76, 2009.
[2] Simranpreet Sing Gill, Jagdev Singh, Rupinder Singh, Harpreet Singh: *Effect of cryogenic treatment onAISI M2 high speed steel : Metallurgical and Mechanical characterization*: Jurnal of Materials Engineering and Performance 21, 1320-1326, 2012.

DEVELOPMENT OF AN UNIVERSAL DEVICE HOLDER SYSTEM FOR DUST-TEST CHAMBER EQUIPMENT

TÓTH Sándor Gergő, TAKÁCS György PhD
Institute of Machine Tools and Mechatronics, University of Miskolc
E-mail: szgttosg@uni-miskolc.hu, takacs.gyorgy@uni-miskolc.hu

Keywords: modular device system, dust-testing, parametric modelling, function analysis.

INTRODUCTION

In connection with several life-test equipment, there has been a need to develop a device systemthat can be an economical solution for testing a large number of generators. The concept of modular device system (MDDT) designed for carrying out the steady-pressurized dust test (Figure 1). A design method was used for generating conception, which is based on the function analysis, and the elemental functions, derived from the requirements system, were expose. From the elemental functions device structures were created, the elements of the set that were taken into consideration in the variation were recorded. Creating the possible concept variants was done by generating subgraphs. The chosen device plan was set out and manufactured.

THE MODULAR DEVICE FOR DUST TEST CONCEPT

During the constitution of the Modular Device for Dust Test (MDDT) concept, a design method was applied [1-3], wherein the main and side functions is derived from the exposed requirement- and environmental system. Elementary functions can be linked in a variety of ways to a function structure that fulfils the MDDT systemdesign requirements. From the elemental functions devices structures were derived and the elements of the set, which were taken into consideration in the variation were recorded.

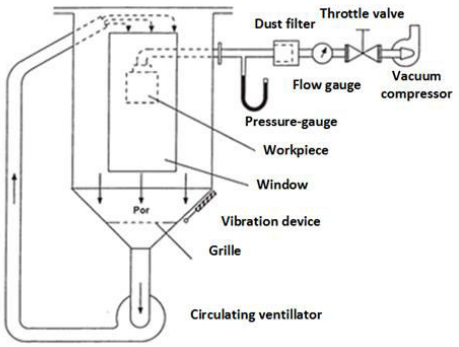

Figure 1 Steady pressured dust test chamber

Creating the possible concept variants was done by generating subgraphs (Figure 2.). Determining the number of variants means solving the problem of how many graphs of subgraphs in the full graph are capable of satisfy ing the condition of the generator to be tested as independent apparatus variants.

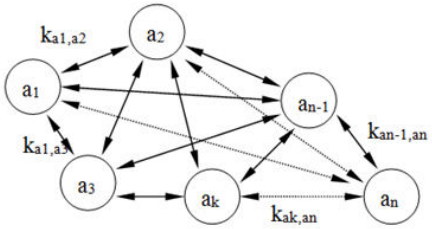

Figure 2 The graph of the elemental functions

The base of the selected device variant is the attachment on a wheelbase, where the generators can be mounted at any position. The fixing tabs are modular, even the attachment of a whole product line can be solved. The device is designed

for multi-directional adjustment, the mounting tabs can be generated with parametric modelling. During the development, new requirements also had to be taken into consideration (transverse flow, adjusting belt tension), the device concept without transforming the basic structure.

FINAL DEVICE PLAN

Flow conditions must be ensured horizontally, belt tensioning must be adjustable and weight reduction must be achieved so that the device can be installed without an external lifting device.

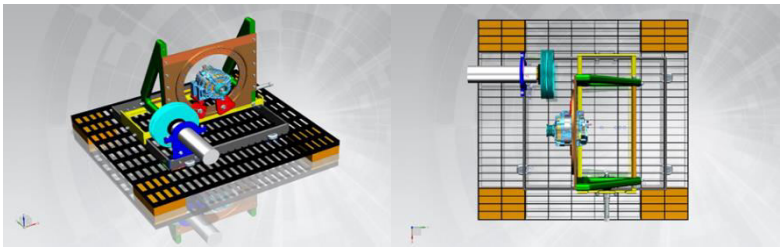

Figure 3 3D assembly model of the final MDDT

The final design is shown in the Figure 3 [4]. In the assembly model, the position of the device within the MDDT can be accurately determined .With the help of several 3D generator model borrowed from the industrial partner, different types of mounting tabs were designed to fasten all current and new generators at the fix points, perpendicular or parallel to the generator's axis line. In view of known fix points and the postition of the generator in the MDDT, mountings tabs can be generated by parametric modeling.

The external components exposed to the dust is polished on the device. The openings on the machine concept are wrapped around the dust, the threads are covered in full length by protection bellows and closed nuts. At the belt tensioning an informative measurement is possible with torque wrench. The shelf was split into two, the top sheet can be removed when the mounting tabs are not attached to this sheet so that the dust can flow from the top of the screen almost unhindered. The outer frame is fastened at several points in the dust chamber. The device is also mounted with a binder to the drive shaft drive shaft housing.

CONCLUSION

During the development of the concept of a modular device system(MDDT) designed for carrying out dust sample tests, the design method used in the developing based on the function analysis was selected. With the help of the requirement list set up by the dust chamber, elementary functions were defined, from which a graph can be set up. Among the equipment variables deriving from the graph, a device concept was selected along with the industrial members. The final MDDT were elaborated in the spirit of parametric modelling.

ACKNOWLEDGMENTS

This research was supported by the European Union and the Hungarian State, co-financed by the European Regional Development Fund in the framework of the GINOP-2.3.4-15-2016-00004 project, aimed to promote the cooperation between the higher education and the industry.

REFERENCES

[1] J. Tajnafői: *Szerszámgéptervezés II., (Struktúraképzések)*. Tankönyvkiadó, Budapest, 1990.
[2] W. E. Eder: *Designing as an Educational Discipline, Engineering Education*, Vol. 15., Nr. 1., 1999.
[3] T. Bercsey, S. Lőrincz: *A terméktervezés megújulás: az új alapelvek és integrált módszerek*, Gyártástech., No 7-8.
[4] Sándor Gergő Tóth, Dr. György Takács, Dániel Tóth: *Új generációs termékek élettartam tesztelő berendezésének kifejlesztése. Hazai és külföldi modellek a projektoktatásban tanulmánykötete*. Budapest: Óbudai Egyetem Rejtő Sándor Könnyűipari és Környezetmérnöki Kar, pp. 29-44., ISBN:978-963-449-074-6, 2018.

INVESTIGATION OF ALUMINUM DROSS AS A POTENTIAL ASPHALT FILLER

UDVARDI Bella, GÉBER Róbert PhD, KOCSERHA István PhD
Institute of Ceramics and Polymer Engineering, Institute University of Miskolc
E-mail: fembella@uni-miskolc.hu, robert.geber@uni-miskolc.hu, istvan.kocserha@uni-miskolc.hu

Keywords: aluminum dross, filler, utilization

There is a great concern about utilizing different waste materials all over the world. Stockpiling in landfills is not a final solution, therefore researchers try to find alternative methods to utilize these materials [1-5]. One potential area may be road construction. Fillers are one of the most important components of asphalt pavements. It has a dual role. First of all, these fine grained mineral materials (d<0.063 mm) enhance the cohesion with bitumen. Second is to fill the gaps between the particles to produce more compact mixture [6]. The aim of this research is to reveal the possibility of utilization of aluminum dross as a potential asphalt filler. This material, which is a by-product of aluminum casting process, is produced in large quantities year by year and its storage in landfills is not a proper solution. Therefore, there is an increasing demand to utilize this material.
There are two types of aluminum dross. One forms of the dross is a white dross or non-salt containing and the other forms is a black dross or salt containing. White dross is formed from the primary Al refining process, which has higher metallic aluminum content. Black dross is produced during the secondary aluminum casting and this material has a lower metallic aluminum content [7,8]. During the research the Authors try to utilize black dross.
In this research different material structural tests were made, which can characterize the samples and the cohesion between bitumen and filler can also reveal. During the tests limestone was used as a reference material. Chemical element composition was determined on the fillers by energy dispersive X-ray spectroscopy, which are shown in Table 1.

Table 1 Chemical composition of the fillers

Chemical element	Limestone [wt%]	Aluminum dross [wt%]
C	9.20	0.00
O	37.34	18.13
Mg	0.49	2.90
Al	0.87	31.8
Si	2.08	1.31
Ca	49.59	3.32
Na	0.00	10.39
Cl	0.00	25.82
K	0.45	5.79
Total	100.02	99.46

Both fillers contained O, Mg, Al, Si, Ca, K elements, but these are in different quantities. It can be observed that the dross is contained aluminum metal in significant amount. It can be stated that the dross still contains aluminum obtained from other methods. In addition aluminum dross contains Na, Cl and K elements in high amount, which indicates the presence of slag-forming agents.
Particle size distribution were determined by Malvern Mastersizer X type particle size analyzer. According to the results, there is no significant difference between the particle size of fillers. However, limestone contains finer particles, dross contains coarser particles in higher amount. Both fillers have a significant amount of fine particles under the size of 10 μm.
During the research scanning electron micrographs were taken to observe the microstructure and surface features of fillers. It is important that the raw materials are sufficient geometrical properties, because it affects the friction of mineral skeleton and bearing capacity of the asphalt pavement.
BET specific surface area were investigated by N_2 adsorption method. The test is important because the mineral materials with high specific surface area require bitumen surpluses, which can reduce the strength and stiffness of the asphalt pavement over a certain limit. The bitumen surplus is economically disadvantageous. According to the results, BET specific surface area of fillers are similar. Using N_2 adsorption pore size distributions can be determined using Barett-Joyner-Halenda (BJH) method in a nanometric scale (in the range of 1.7 to 300 nm). Porosity affects the physical adsorption between the bitumen and mineral materials. The pore size of the particles increases the specific surface area

of the filler, therefore it effects on the bitumen content. Pore size distribution was determined using the desorption isotherms. The results show that the average pore diameters are almost the same (limestone: 27.64 nm, dross: 30.05 nm), which is favourable for the utilization aspects. Pore size distribution in a micrometric scale (in the range of 0.004 µm and 100 µm) were determined by mercury intrusion porosimetry. The test results show that limestone has a lower average pore size, than in case of dross, but this difference is negligible.
German Filler Test [6] is a test method for the determination of the oil adsorption capacity of fillers. This test indicates the cohesion between bitumen and filler. During the test filler and hydraulic oil is mixed together in a certain amount. After mixing additional amount of dry material are added into the mix. When cohesion is lost between filler and oil, the amount of dry material is recorded. The measurement is not standardized but very useful in practice. Dross has a lower value than limestone, but this difference is not relevant. Table 2 show the results of tests.

Table 2 Test results

Parameter	Unit	Limestone	Aluminum dross
Specific gravity, ρ	g/cm^3	2.822	2.904
Average particle size, d_{50}	µm	13.77	15.62
Specific surface area, SSA	m^2/g	1,55	1,26
BJH Desorption average pore diameter	nm	27.64	30.05
BJH Desorption cumulative pore volume of pores	nm	0.006675	0.009535
BJH Desorption cumulative surface area of pores	m^2/g	0.9661	1.1017
Average pore size (mercury intrusion porosimetry)	µm	2.06	4.05
German Filler Test (amount of dry materials)	g	50	45

Test results show that dross is very similar to limestone powder. Average particle size and BET specific surface area are close to each other. According to the porosity and oil adsorption dross have favourable properties in the viewpoint of asphalt technology. It can be concluded, that dross may be a potential asphalt filler to substitute limestone powder. However, further investigations and standard asphalt tests are needed to determine the exact amount of dross in asphalt mixtures.

ACKNOWLEDGEMENTS
Present research is a part of GINOP -2.2.1-15-201600018 project.

REFERENCES
[1] Dhir LJC R.K., Dyer T.D., Smith G.W.: *Cleaned oil-drill cuttings for use as filler in bituminous mixtures. Construction and Building Materials.* 24:322-5. 2010.
[2] Gürer GŞS C.*: Investigation of Properties of Asphalt Concrete Containing Boron Waste as Mineral Filler.* Materials Science (Medziagotyra). 22(1):118-25. 2016.
[3] Reddy M. S., Neeraja D.: *Mechanical and durability aspects of concrete incorporating secondary aluminium slag:* Resource-Efficient Technologies, Vol. 2. pp. 225-232. 2016.
[4] Chen M., Lin J., Wu S., Liu C.: *Utilization of recycled brick powder as alternative filler in asphalt mixture.* Construction and Building Materials. 25:1532-6. 2011.
[5] Wu S., Zhu J., Zhong J., Wang D.*: Experimental investigation on related properties of asphalt mastic containing recycled red brick powder;* Construction and Building Materials, Vol. 25 pp. 2883–2887. 2011.
[6] S. Prithvi, Cynthia Kandhal, Lynn Y., Parker Frazier Jr: *Characterization tests for mineral fillers related to performance of asphalt paving mixtures.* NCAT Report No. 98-2 1998.
[7] Chen D.: *Development of aluminium dross-based material for engineering application*; A Thesis 2012.
[8] Petavratzi E., Wilson S.: *Residues from aluminium dross recycling in cement*, Case study 2007.

THE INFLUENCE OF CORE PRODUCTION PARAMETERS ON THE PROPERTIES OF WATER GLASS CORES USING NEW SAND AND MECHANICALLY RECLAIMED SAND

VARGA László PhD, DARGAI Viktória
Faculty of Materials Science and Engineering, Institute of Foundry, University of Miskolc
E-mail: ontvlaci@uni-miskolc.hu, dviki72@gmail.com

Keywords: water glass, core box temperature, gassing time, new sand, reclaimed sand

The bending strengths of new sand and mechanically reclaimed inorganic sand were investigated and compared using a common two-component inorganic core binder system. The investigation encompasses the influence of various production parameters. The immediate and final strength as well as the residual strengths after thermal stress were investigated.
First, new sand and mechanically reclaimed sand were compared with default test parameters. With the same amount of binder and additive, the bending strengths of the mechanically reclaimed sand increased on average by 50%.

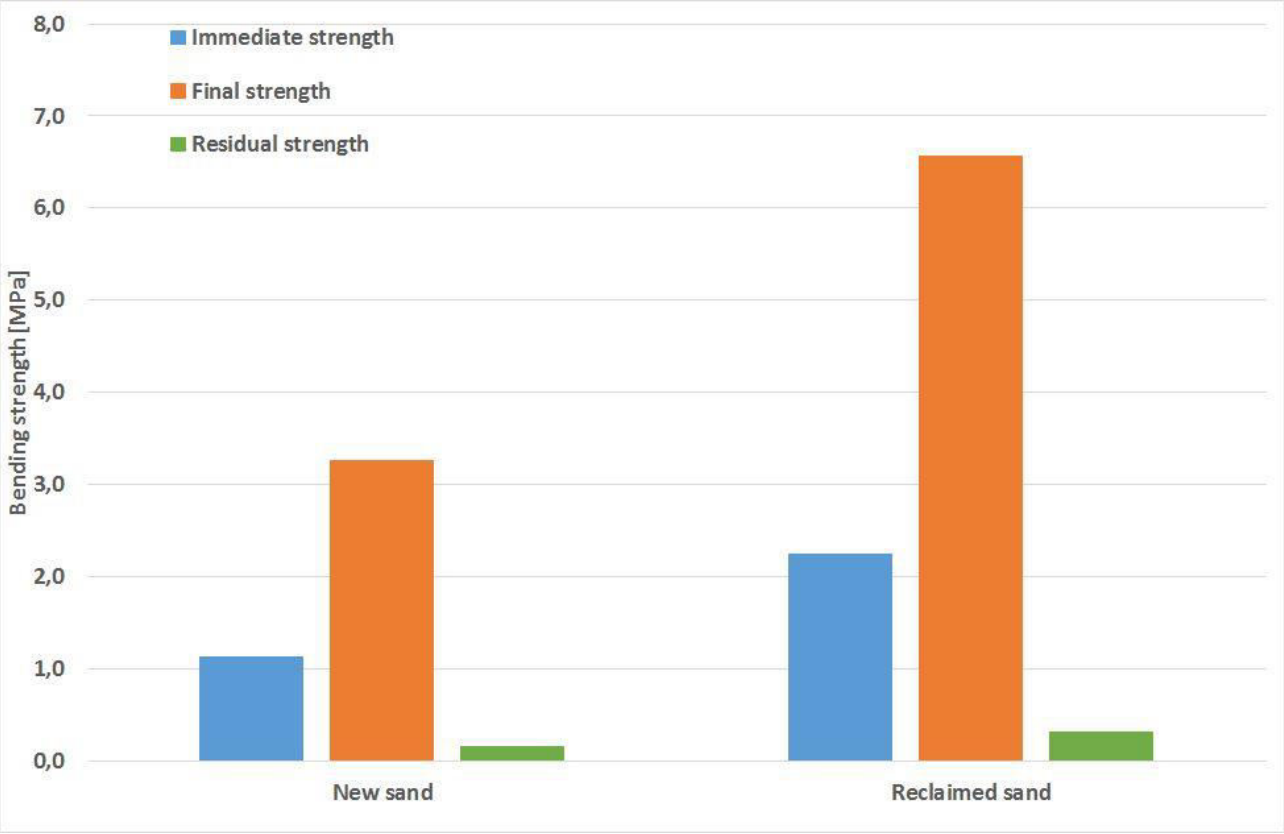

Figure 1 Bending strength of new sand and mechanically reclaimed sand

The default test parameters are defined as follows:

Table 1 Default test parameters for specimens

Blow pressure	3 bar
Gassing pressure	2 bar
Hardening time	15 s
Gassing time	15 s
Gassing temperature	100 °C
Core box temperature	180 °C

The influence of the core box temperatures was determined in the following temperature range: 100 °C - 220 °C. For new sand, it can be surmised that both the immediate strengths and the final strengths increase as a function of the core box temperature.

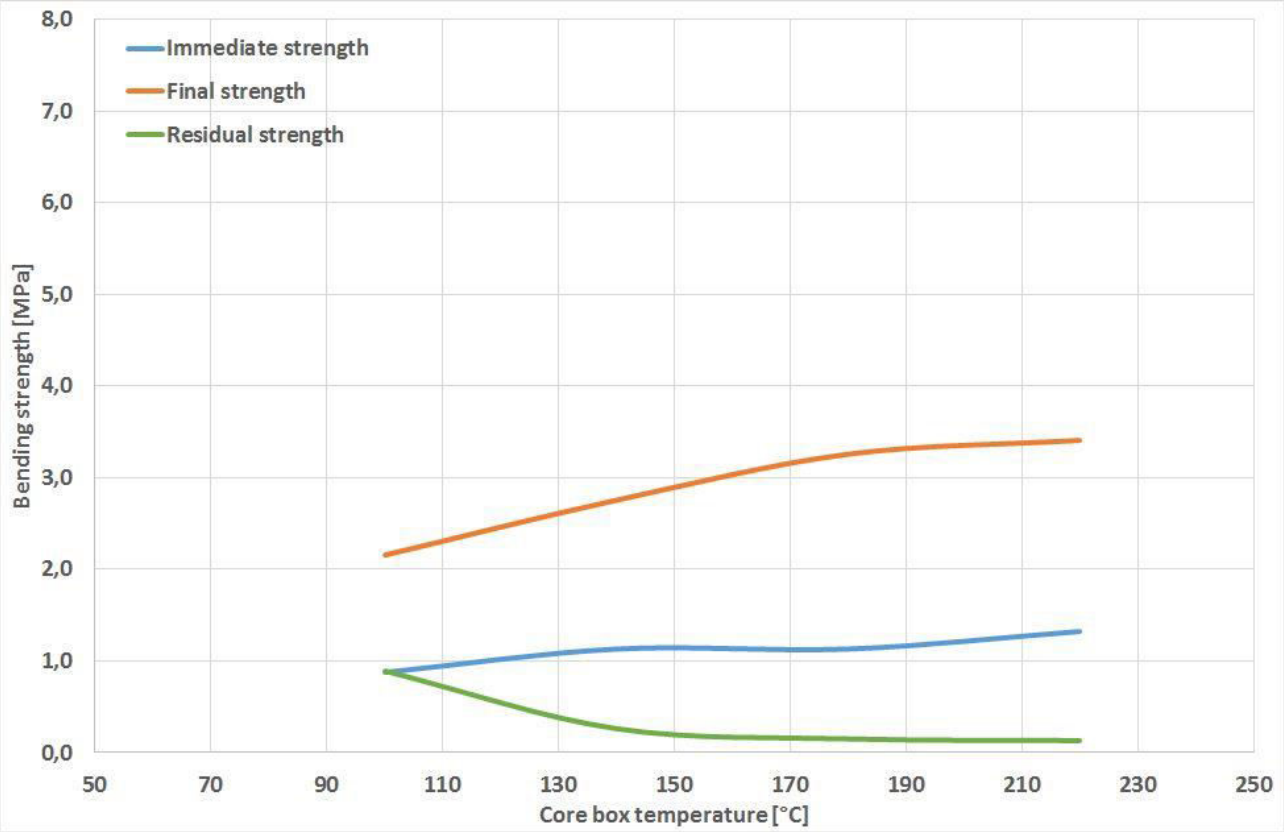

Figure 2 Bending strength of new sand and mechanically reclaimed sand

In the context of the described experimental series, it has been shown that with mechanically reclaimed sand at least 50% higher strength compared to new sand can be achieved. Of the core shooting parameters examined, the blow pressure and the gassing pressure have the least influence on the bending strengths. For new sand as well as for mechanically reclaimed sand, the main influencing factors are the core box temperature and the gassing time as well as the combination there of, i.e. parameters that influence the drying of the cores. In general, it can be summarised that with increasing core box temperature and gassing time the immediate strengths, the final strengths (1h) and in most cases the final strengths (24h) increase. The residual strengths show an opposite effect, in combination with the core box temperature and gassing time, the residual strength decreases, which means a better core extraction result is expected. The final strengths show that at high core box temperatures and long gassing times, the strength drops. This effect is already known from the waterglass-CO_2-process.

EXAMINATION OF INFRARED TOMATO DRYING

[1]VÁRKONYI Zsombor, [2]SEBESI Viktória
[1]Workplace: OT Industries Plc.
E-mail: zsombor.varkonyi@gmail.com
[2]Faculty of Mechanical Engineering, University of Technology and Economics
E-mail: sebesi.viki@gmail.com

Keywords: tomato, drying, infra-radiation, Handerson-Pabis.

The aim of this paper is to show a detailed insight into infra-radiation based drying process; as well to widen the possible usage range of a well-known approximation method for describing the temporal moisture variation in function of process parameters. The mass decrease of tomato slices was examined, in function of specific radiation power, heat source and sample distance, in forced and natural air flow. Based on the results dimensionless moisture ratio change over time was fitted as an exponential function, which may be applied in industrial drying process optimization.

Tomato is a highly perishable food, thus preservation is required to meet the continuous market demand compared to the unbalanced yearly production peak. Many experiments were conducted regarding the process parameters of infrared drying. In the paper of H. Kocabiyik the drying time, specific energy consumption, shrinking, color, vitamin C and lycopene content was represented at different radiation powers and ambient air speeds. He found that while at convective drying the increased velocity of drying gas results in better heat transfer, thus quicker drying; it is completely the opposite with radiation driven process. This is corresponding with the paper of G.P. Sharma, who IR dried onion slices and noted, that time is inversely proportional to the surface or core temperature of sample during the procedure. Ginzburg and Akanbi showed achievable dry matter based water content versus relative moisture of air at different process parameters. According to T. M. Afzal the humidity of air has almost no effect on the speed of infrared drying of potato slices, but only the final water content of product. Based on the wide range of available literature it can be stated that infrared drying of tomato and other vegetables is well examined and the effect of changing various parameters are approximately known based on the results. However the probe – radiation source distance is not inspected in details, which lack shall be partially filled with this paper.

Based on the theoretical description of radiation, the transferred heat is proportional to the surface of source, emission factor of both elements, geometric relations and the difference of the absolute temperature of the two objects on the power of four. The total radiated heat glows on a theoretical area and only a proportional part reaches the tomato itself, which effect shall also be taken into account. The received heat is spent on increasing the temperature of tomato (which duty is negligible due to the low value of heat capacity compared to the latent heat), heat losses and evaporation of water. Latter is interpretable as temporal mass decrease multiplied by latent heat. Supposing a generally accepted constant dry matter during the process the mass change can be expressed as pure evaporated water, which is a moisture content derivative. Furthermore moisture content can be expressed as a dimensionless number, to avoid conversion problems. The moisture ratio MR(t) is the moisture at given moment X(t), divided by the initial value X_0 (supposing the equilibrium X_e is significantly smaller than the before mentioned two). MR(t) function was given by many authors according to the collection of Ali Mohammadi. From those the $MR=a\cdot e^{-b\cdot t}$, know as Henderson-Pabis (H-P from now on) model is broadly used for radiational and convectional drying processes, as it is quite simple, usually fits the experimental results and the theoretical background can be easily seen from the differential equation. In the expression parameter a is a dimensionless number to describe the initial or permanently residual water content while factor b [1/s] defines the time dependent change.

Experiments were conducted with approximate 60-70g weight, round, slightly hard, evenly red color common hungarian tomato type (Lycopersicon lycopersicum) to realize the H-P model parameters for tomato. According to the literature 8 mm thick, 60±5mm diameter, round slices were dried to avoid quick burning, but also to achieve relative quick drying procedure. An infrared bulb was placed on a stand. Under it the tomato sits on a welded grid, while it is placed on a weighing scale. The surface temperature was measured by a pre-calibrated infra-thermometer. The data recorder saved the physical properties of ambient air, the surface temperature, core temperature and the mass every half minute during the drying procedure. The tomato slice - situated from a given height distance under the heat source – was blown from the side by a fan with given speed ambient air. The exact electric consumption of light bulb was measured at the electric socket. Instrumentation was assembled in a way that all required parameters can be measured to obtain as exact results as possible. The experiments were concluded with several different parameters. The probe to radiation source distance was set to 100, 125, 150, 175, 200 and 250 mm. From the height of the gap, the angle of the wall of light bulb the radiated surface can be calculated, which together with the measured 231±1 W power determines the surface specific heat duty as well. Besides this, at half of the cases the forced ambient air speed was 1 m/s from the

side, while at others it was 0 m/s, only natural flow happened, to see if this parameter has any significant advantage compared to the known heat loss detriment.
Results were evaluated until 42%wt water content (MR=0.05) to set similar comparison conditions. At the initial time moment MR = 1, thus the value of H-P model *a* parameter is 1. Parameter *b* can be obtained from the rearranged equation for each case. After calculating the parameter the theoretical and experimental MR decrease curves were compared and error square R^2 is bigger than 0.8 in any cases. During the evaluation the heat loss from the surface of the tomato and the heat required for increasing the temperature of the sample until the constant drying speed phase was neglected. The parameter *b* of H-P model contains all the collateral heat losses or increments, which shall be taken into consideration. It worth mentioning, that other – less commonly known - models may fit the results with smaller deviation, which could be a topic for further evaluation in an other paper. The *b* parameter of the H-P model was determined for 100-250 mm radiation source to probe distance (3000-18000 W/m^2 specific heat duty), for 0 m/s air flow speed, for the 1 to 0.05 moisture ratio range, which can be seen in Figure 1.

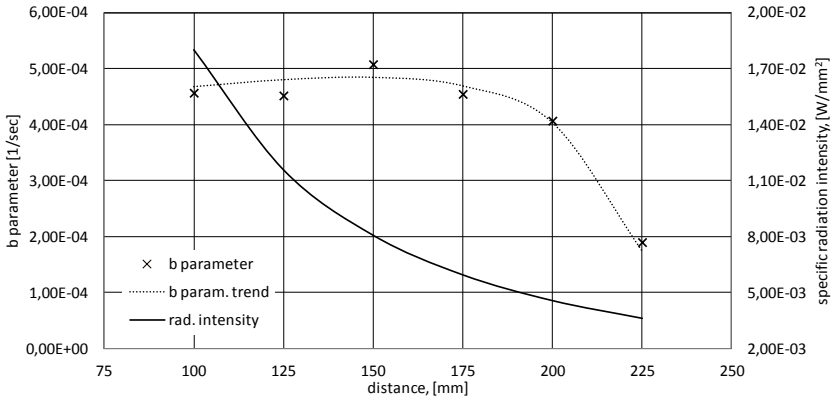

Figure 1 Parameter *b* of H-P model and radiation intensity in function of tomato – bulb distance

Moreover, other general outcomes can be defined. First, from the experimental results it can be concluded, that – when every process parameters were similar – it takes less time to reach the same moisture content in case of zero gas flow, so the drying process is quicker. At convectional drying the higher velocity means higher Reynolds number, so better, quicker heat transfer. This turns into a disadvantage at infrared drying, because here the conductive heat transfer is minimized and the generally cooler ambient air only causes heat loss. Second, the quicker, more energy efficient, but not so gentle procedure influenced the product quality a lot. For example the ratio of final versus initial slice area was about 0.58 when there was no air flow and about 0.65 in the other case, additionally independent from other process parameters. The bigger shrinkage generally means bigger deformation, thus more amorphous, less appealing endproduct. Third, putting too close the heat source affects the temperature in a disadvantageous way. At 100 mm between the vegetable and light bulb and no artificial air flow the surface reached average 80°C during the constant drying rate phase and more than 120°C later, over the 60°C decomposition limit temperature of lycopene or vitamin C, also resulting in burnt tomato.
Within the frames of this project an experimental method and measuring station was composed to examine infra red food drying process. The light bulb to tomato slice distance and natural versus low speed forced air flow were the two main parameters which were reviewed. Based on the experimental results a widely known mathematical expression was fitted to describe the moisture ratio in function of time. The drying process time until the 8 mm thick 60 mm diameter tomato slices reach MR=0.05 value with 231 W infrared light bulb, in function of radiation source to product distance, in case of no forced ambient air flow can be estimated applying the given equation. If the parameters of the H-P model of a vegetable drying process is known, then the time dependent moisture ratio and water content is known, thus the temporal weight variation as well the approximate heat requirement can be obtained. This calculation method may be benefited in simulation, optimization or process time determination in lab-, pilot- or industrial scale dying procedures.

ACKNOWLEDGMENTS
The research reported in this paper was supported by the Higher Education Excellence Program of the Ministry of Human Capacities in the frame of Water science & Disaster Prevention research area of Budapest University of Technology and Economics (BME FIKP-VÍZ).

INTRODUCTION TO DESIGN AND ANALYSIS OF TORSIONAL VIBRATION DAMPERS IN VEHICLE INDUSTRY

VENCZEL Márk, VERESS Árpád PhD
Department of Aeronautics, Naval Architectures and Railway Vehicles, Budapest University of Technology and Economics
E-mail: averess@vrht.bme.hu, mvenczel@vrht.bme.hu

Keywords: torsional vibration damper, stress and fatigue analysis, parametric optimization, CFD

The crankshaft of today's internal combustion engines with high performance output are exposed to harmful torsional oscillations originated from the unbalanced gas and inertial forces. These oscillations can lead to the fatigue damage of engine components. To avoid this, a torsional vibration damper can be mounted onto the free-end of the crankshaft (see left side of *Figure 1*) or integrated into the flywheel.
Visco-dampers are one type of the torsional vibration dampers and their operational fluid is silicone oil. The structure (see right side of *Figure 1*) consists of an annular space (called housing) including the inertia ring, guided by slide bearings and the silicone fluid. A plate (called cover) is welded to the housing to make the annular space closed.
Since torsional vibration dampers are highly important vehicle structures from the operation and safety point of view, targeted and profound investigations must be carried out before production by means of stress, fatigue, fluid dynamic and thermal analyses. Nowadays, cost effective R&D activities are the key factors for increasing market sharing and profit in the vehicle industry. Due to this demanding market situation and the complexity of the model, it is impossible to handle the problem in analytical way. Finite element and finite volume numerical discretization methods based calculation techniques must be involved into the engineering work supported by the modern computer technology.
The aim of this paper is to provide an insight into the multidisciplinary design and development process of torsional vibration dampers in vehicle industry applications. Four different examples as structural, fatigue, CFD analyses and structural optimization have been introduced in the present work. The real operational conditions have been transformed into the settings of virtual reality for each numerical analysis. Particular care has been taken into consideration to create the correct numerical mesh, which is able to capture all relevant mechanical, fluid dynamic and thermal phenomena with acceptable accuracy.

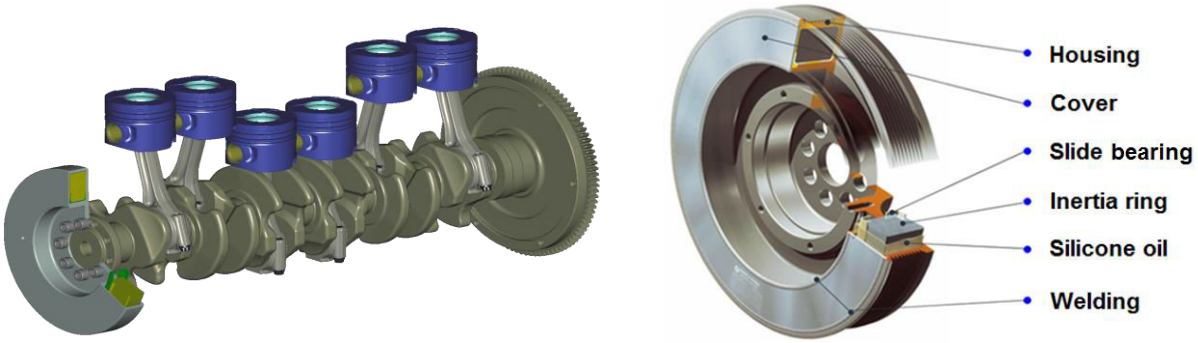

Figure 1 Torsional vibration damper mounted onto the crankshaft (left) and the structure of a visco-damper (right)

Static structural stress analysis has been carried out on the assembly of the selected visco-damper geometry in ANSYS environment, where the static loads (bolt pretension, centrifugal force and silicon fluid (internal) pressure) and dynamic loads (dynamic torque, accelerations in different directions, belt torque, belt force and gravity force) have been considered with help of different types of load steps. The software calculates the geometrical deformations and stress state belongs to the given load conditions by solving the set of constitutive and compatibility equations. The criterion for the correct operation is the yield limit including safety factor cannot be reached by the maximum equivalent stress at the nominated regions. Following the verification of the static structural integrity, the next step is the fatigue assessment by FEMFAT software considering the so called positive and negative load cases resulted by the dynamic loads. Safety factors related to fatigue limit have been visualized both in three-dimensional figures of the damper geometry (see left side of *Figure 2*) and in Haigh-diagrams in order to determine the most loaded points of the investigated damper structure.

While design and strength criteria, with help of the stress and fatigue analyses, are met, efforts must be made to minimize development and production costs by means of mass and volume reduction, which, consequently, decreases material consumption. Structural optimization has been performed in ANSYS DesignXplorer module on a simplified, three-dimensional visco-damper geometry with especial care for minimizing the mass at given allowable static stress limit over reasonable computational cost. The applied genetic algorithm approximates the desired geometry optimum through parameter sensitivity analyses, taking into account the predefined cost function. In the outcome of the structural optimization process, the achieved rate of mass reduction is 34.36%. Another structural analysis, performed on the newly optimized but not simplified damper geometry, showed higher (but allowable) equivalent stress values due to improved utilization of the damper geometry.

Special care must be taken into consideration also at the inside of the visco-damper, where the undesired vibrations will be damped and converted into certain amount of heat. The dissipated heat causes increasing temperature and influences the viscosity, damping characteristics and lifetime of the damping fluid. The fluid dynamic and heat transfer phenomena are described by the mass, momentum, and energy conservation laws. The applied software computes the solution of the discretized form of the governing equations through iteration steps. A three-dimensional damper segment has been numerically investigated by using ANSYS CFX, where the impact of cooling fin characteristics and the proximity of engine have been also considered. In the evaluation of the obtained results, the streamlines around the cooling fins and the temperature distribution along the geometry are then visualized in the post-processor. According to the streamline result, a turbulent region of air evolved between the engine and the damper (called engine-damper-gap) during the operation. Air is stuck in this region due to the lack of free stream. Because of this reason, the mounted cooling fins, working in the engine-damper-gap, show poor cooling efficiency, which can be proved by the heat transfer result as well (see right side of *Figure 2*). The intensity of heat transfer on the engine-damper-gap side is found to be significantly lower compared to the free-side surrounded by free stream. Consequently, it is advisable to mount the cooling fins onto the free-side of the damper, far away from the engine-damper-gap. As a next step, the effect of high temperatures, gap sizes and cooling fin geometries on the lifetime of damping fluid should be thoroughly investigated and built into the development process in form of a reliable lifetime calculation method.

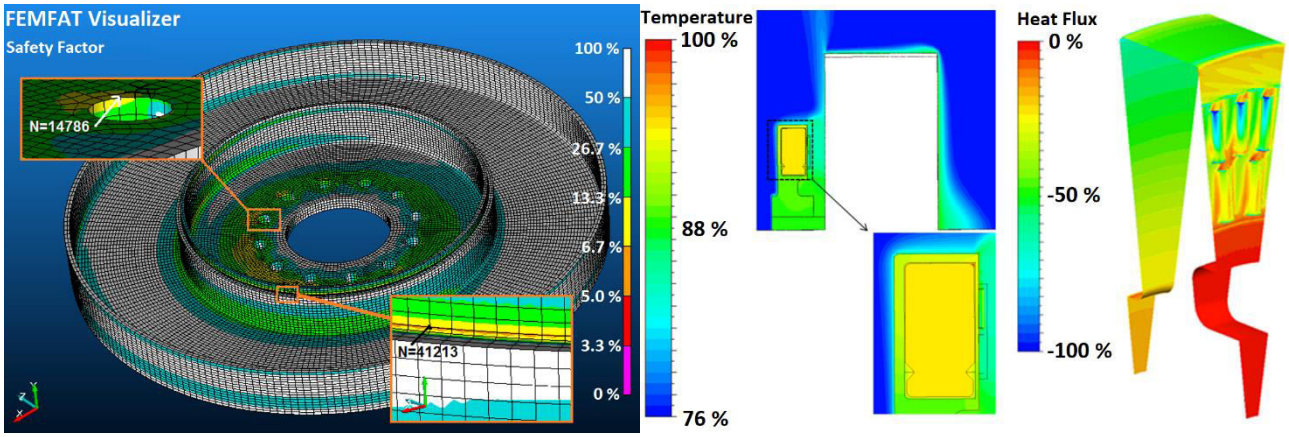

Figure 2 FEMFAT fatigue analysis result with critical points (left side) and heat transfer result (right side)

ACKNOWLEDGMENTS

The research is supported by the Hungarian Automotive Higher Education Foundation, and the ETDB at BME.

PERFORMANCE ANALYSIS OF MICRO-END MILLS BASED ON VIBRATION APPLYING COMPUTER AIDED DESIGN ANALYSIS

[1]YILMAZ Okan Deniz, [1]NADIMI BAVIL OLIAEI Samad, [2]DADVANDIPOUR Samad PhD
[1]Department of Manufacturing Engineering, ATILIM University
E-mail: okan.yilmaz@atilim.edu.tr, samad.nadimi@atilim.edu.tr
[2]Department of Applied Information Science, University of Miskolc
E-mail: aitsamad@uni-miskolc.hu

Keywords: Micromilling, Vibration analysis, Micro-end mill, Frequency response function, Transient response.

Micromilling is one of the most important and cost-effective methods of fabricating miniaturised components from different engineering materials. The efficiency of this process highly relies on micro-end mills with diameters less than 1 mm, which are exposed to harsh micromachining conditions during the material removal process. They are considered the most flexible part of the micro-milling process chain, and their performances directly dictate the accuracy and feasibility of the micro-milling process. Understanding the vibratory response of end-mills having different geometries can be considered as an efficient method towards designing micro-end mills tailored for specific applications regarding their vibrational characteristics. In this study, the vibratory response of two micro-end mills having different geometries has been analyzed by finite element method. The investigated cutting tool geometries include commercial micro-end mills with helical geometries and D-shaped straight micro-end mills, which are shown to be quite useful in the literature. Although models based on different beam theories such as Euler-Bernoulli, Timoshenko or unified beam theories are useful for predicting the dynamic response of beams and beam-like structures, however the complex geometry of micro end mills and their stepped geometry and size variations, makes it difficult to predict the dynamics of micro end mills by using beam theories. Therefore, numerical methods such as finite element method (FEM) can be used reliably to model the dynamic behaviour of micro end mills.
In this study, FEM has been used to study the vibrational characteristics of two different micro-end mills. The meshed model of the tools is shown in Figure 1.

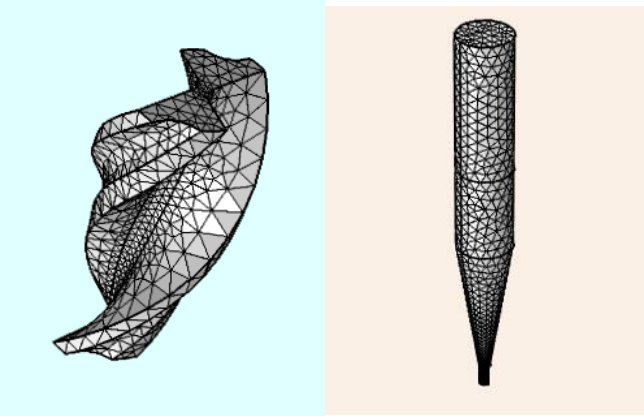

Figure 1 Meshed model of the micro-cutting tools

The cutting tools are assumed to have a diameter of 0.8 mm, a length of cutting part of 1.6 mm, a neck taper angle of 9° and a shank diameter of 4 mm. A clamping length of 10 mm has been considered for the modelling. Figure 2 and 3 illustrate the mode shapes of the D-shaped and commercial micro end mills, respectively. The material properties are shown in Table 1. A comparison between the natural frequency of the D-shaped and commercial micro end mill is illustrated in Table 2.

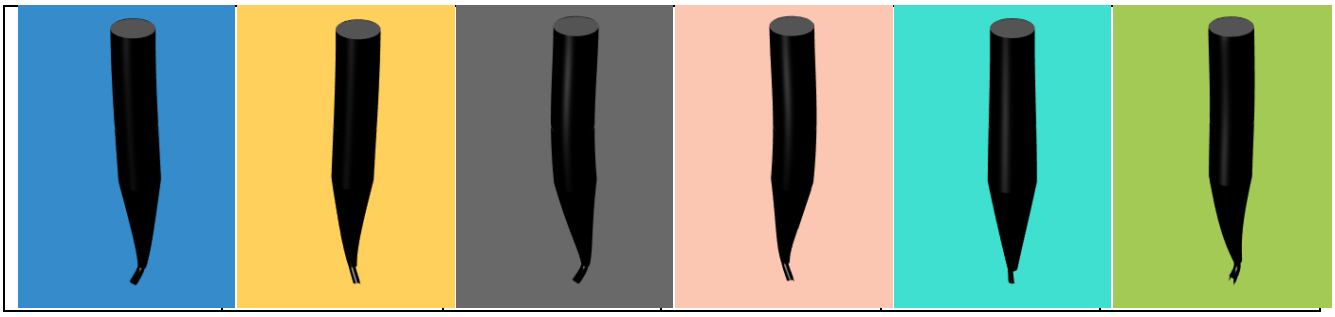

Figure 2 Mode shapes of the D-shaped micro end mill

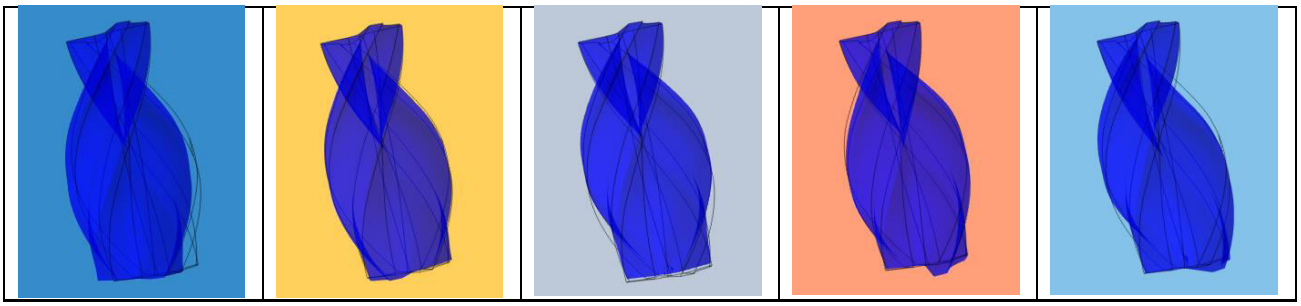

Figure 3 Mode shapes of the commercial micro end mill

Table 1 Material Properties of Tungsten Carbide

Properties	**Value**	**Unit**
Grain Size	0.5-1	μm
Density	14.6	$g.cm^{-3}$
Hardness	90.7-91.3	HRA
Young's Modulus	620	GPa
Poisson's Ratio	0.22	-
Transverse Rupture Strength	> 3.7	GPa
Compression Strength	5170	MPa

Table 2 Natural frequencies associated with each mode

MODES	NATURAL FREQUENCY (Helical) [Hz]	NATURAL FREQUENCY (D-shaped) [Hz]
1	3.86×10^5	10696
2	6.38×10^5	12341
3	1.25×10^6	43226
4	2.09×10^6	45426
5	2.82×10^6	56226
6	3.28×10^6	81242

It can be seen that the natural frequency of the helical geometry is much higher than that of the D-shaped micro end mill. Therefore, it can be used at high rotational speeds without encountering any resonance.

ACKNOWLEDGEMENTS
The described work was carried out as part of a project supported by ATILIM University BAP program under the project number of ATU-BAP-1617-05. The authors would like to appreciate ATILIM University and ATILIM ARGEDA-TTO for supporting this work. The help of Ms Sema HÜSEYİN is highly appreciated.

APPLICATION OF REXROTH CONTROLLING FOR INVERTED PENDULUM

RÓNAI László, SZABÓ Tamás PhD
Robert Bosch Department of Mechatronics, University of Miskolc
E-mail:ronai.laszlo@uni-miskolc.hu, szabo.tamas@uni-miskolc.hu

Keywords: inverted pendulum, LQR controlling, feedback

This research work deals with balancing of an inverted pendulum [1], which is controlled by Rexroth IndraDrive HCS02 axis controller. The inverted pendulum is mounted on a Rexroth Compact Module CKK 15-110.
Main goals of the research work is to create a system, which can automatically swing up the pendulum then control it in order to keep in inverted position. The model of the pendulum is shown in Figure 1 (a), (b), where L is the length of the rod, m denotes the mass, g is the gravitational acceleration, φ is the angle of the rod measured from the vertical position and $u(t)$ is the prescribed position of the carriage. The motion of the physical pendulum can be modelled with the mathematical counterpart.

(a)

(b)

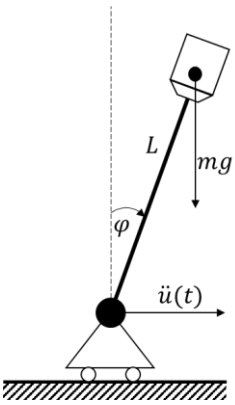

Figure 1 (a) Inverted pendulum, (b) mechanical model of the system

The linearized differential equation of the mathematical pendulum is given as:

$$\ddot{\varphi}(t) - \frac{g}{L}\varphi(t) = -\frac{1}{L}\ddot{u}(t),$$

which can be formulated also in state space representation:

$$\dot{\mathbf{x}} = \mathbf{A}\mathbf{x} + \mathbf{b}\ddot{u}, \qquad \mathbf{A} = \begin{bmatrix} 0 & 1 \\ \frac{g}{L} & 0 \end{bmatrix}, \mathbf{b} = \begin{bmatrix} 0 \\ -\frac{1}{L} \end{bmatrix}, \mathbf{x} = \begin{bmatrix} \varphi \\ \dot{\varphi} \end{bmatrix},$$

where $\mathbf{A}$ and $\mathbf{b}$ are the state matrices, $\mathbf{x}$ is the state space vector. The inverted pendulum is controlled by state feedback.

$$\ddot{u} = -\mathbf{k}^T\mathbf{x},$$

where $\mathbf{k}^T$ is the column vector of gains, which is determined by LQR (Linear Quadratic Regulator) controller. The problem is handled with *MC_MoveVelocity* function block, which needs the acceleration and deceleration of the carriage in addition to its velocity, i.e., $\dot{u} = -\mathbf{k}^T \int_{t_0}^{t} \mathbf{x}\, dt$.

Inventor 2016 software is used to create the 3D model of the system. It consists of an aluminium hollow section 60x40, shaft Ø 8 mm supported with two ball bearings and a rod diameter Ø 8 mm, the length is $L = 630\ mm$, the mass is $m = 0.35\ kg$. Thereafter it was manufactured (see in Figure 1 (b)).
The angle of the pendulum is measured by PMI360D_F130-IE8_V15 inductive sensor [2]. The analogue input of the PLC is voltage based. The output of the sensor is 4-20 mA, which covers the angle of 0-360°. Therefore two 1000 Ω resistors in parallel connection were wired to produce 2-10 V voltage input for the PLC.
The system was mounted onto a Rexroth compact module 16x10 with a MSK030C Bosch Rexroth servo motor and a Rexroth IndraDrive HCS02 axis controller. The maximum rotational speed of the motor is 9000 rpm [3], which can produce up to 1.5 m/s carriage speed. The Rexroth system can be programmed under the standard PLC programming languages and also with a Continuous Function Chart (CFC).

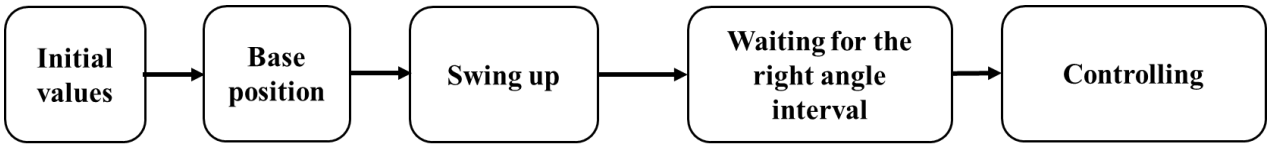

Figure 2 The flowchart of the pendulum controller

The initial values are given in the block of *Initial values* (see Figure 2), then the carriage is moved to its base position (*Base position*) using *MC_MoveAbsolute* function block. Thereafter the pendulum is swung up to the inverted position. In the next step the system is waiting for the rod to reach its inverted position, from which the balancing is started in the *Controlling* block.
The main program, which contains the steps has been written in SFC (Sequential Function Chart). The initial values are given in ST (Structured Text) programming language. The rest of the blocks are programed in CFC using the standard library functions, special purpose function blocks and user defined blocks.
The motion of the carriage is controlled by *MC_MoveVelocity* function block, which can produce relative movements during a Δt time increment.
The presentation will detail the 3D design of the test bench, theoretical formulation of the inverted pendulum, the determination of the gains and the numerical integration to determine the velocity of the carriage. Concluding remarks will be drawn from the tests.

ACKNOWLEDGMENTS
The described article/presentation was carried out as part of the EFOP-3.6.1-16-2016-00011 "Younger and Renewing University – Innovative Knowledge City – institutional development of the University of Miskolc aiming at intelligent specialisation" project implemented in the framework of the Szechenyi 2020 program. The realization of this project is supported by the European Union, co-financed by the European Social Fund.

REFERENCES
[1] J. Bokor, P. Gáspár: *Irányítástechnika járműdinamikai alkalmazásokkal*, Typotex, Budapest, 2008.
[2] Datasheet: *PMI360D_F130-IE8_V15 inductive positioning system*, Pepperl+Fuchs GmbH, 2007.
[3] Rexroth IndraDyn S MSK Synchronous Motors: *MSK030C-0900 technical data*, Bosch Rexroth AG, 2006.

SIMULATION ASPECTS OF THE HIGH PRESSURE DIE CASTING PROCESS

BUBENKÓ Marianna, MOLNÁR Dániel
Faculty of Material Science and Engineering, University of Miskolc
E-mail: ontbm@uni-miskolc.hu, daniel.molnar@uni-miskolc.hu

Keywords: Computer simulation, Control Volume Method, High pressure Die Casting.

Die casting is a manufacturing process for producing accurately dimensioned, sharply defined, smooth or textured surface metal parts. It is accomplished by injecting liquid metal at fast velocity and under high pressure into reusable steel dies. Compared to other casting processes, die casting is at the top end of both velocity and pressure. The high velocity translates into a very turbulent flow condition. The process is often described as the shortest distance between raw material and the finished product.

In high pressure die casting the liquid melt is charged into the shot sleeve according to the chamber fill ratio. The time of metal charging affects cycle time, productivity and profitability. The target of charging is the air displacement from the chamber through the casting cavity, so the piston moves forward with a controlled slow velocity and the melt accumulates on the frontal face of it. During the movement of the piston waves are developing in the melt and moves along the sleeve and displaces air. The first phase is over when the melt fills the whole shot sleeve cavity which indicates a switching sign. This switching sing starts the second phase when the movement of the piston is fast and the cavity fills totally until the piston abrupt stops and hit the liquid melt. At this moment the kinetic energy transforms into pressure energy and frictional thermal energy. In the third phase the entrapped air bubbles and the shrinkage cavities are compressed with a high pressure during solidification.

The solution of a technological problem can be seen in Fig.1.

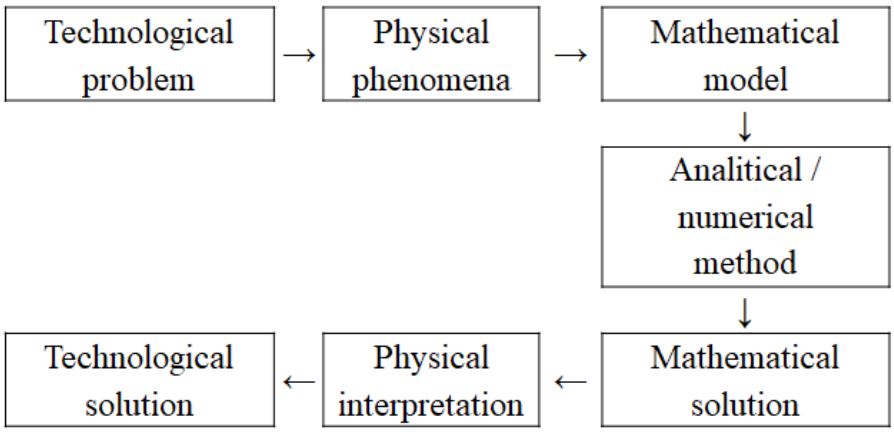

Figure 1 The solution of a technological problem

The first step in the modelling process is to define the geometry of the casting system. After the definition of the geometry of the casting system, this must be divided into a discrete number of segmented volume elements for the subsequent calculations. This is denoted the mesh or the grid. The critical point to keep in mind at this point is the influence of the fineness/coarseness of the mesh on the computations. The accuracy of the results increases with the fineness of the mesh, although the improvement in the accuracy becomes incrementally smaller as the fineness becomes increasingly larger. On the other hand, the computation time increases as the mesh becomes finer. In general, a balance needs to be found between the needed accuracy and the computational time.

Before the equations that govern the filling and solidification processes can be solved, the necessary thermophysical material data must be available. For the calculation of the temperature field in the casting system, information is

required about the densities, specific heat capacities, and thermal conductivities for all of the materials in the casting system (casting, mould, environment) In addition, the latent heat of fusion of the cast alloy is required.

Apart from the material data themselves, other relevant process parameters have to be defined. Other process relevant information also needs to be input, so that all the factors that affect the filling and solidification of the casting can be accounted for. It is important to realize that the results of a foundry process simulation can only be as good as the material and process parameters used in the simulation.
After the geometry has been defined and the mesh generation has been performed, the most demanding part of the numerical simulation follows in respect of both the algorithmic development and the requirements for computer capacity – the actual calculation, i.e. solution of the governing equations. The most usual approach here is to solve all the basic equations, this being a prerequisite for simulating all relevant casting problems of a technical nature. It is clear that these calculations, in which primitive fields such as temperatures, displacements, stresses, velocities, pressure, etc. are determined, require the solution of the governing differential equations.

After the computations, the resulting basic fields (temperatures, velocities, etc.) should be presented in an appropriate way. The results are often made more instructive by colour displays and curves. In the latter case a comparison with experimentally determined values, e.g. temperature-time curves based on thermocouple measurements will be straight-forward.

The simulation procedure can be seen in Fig.2.

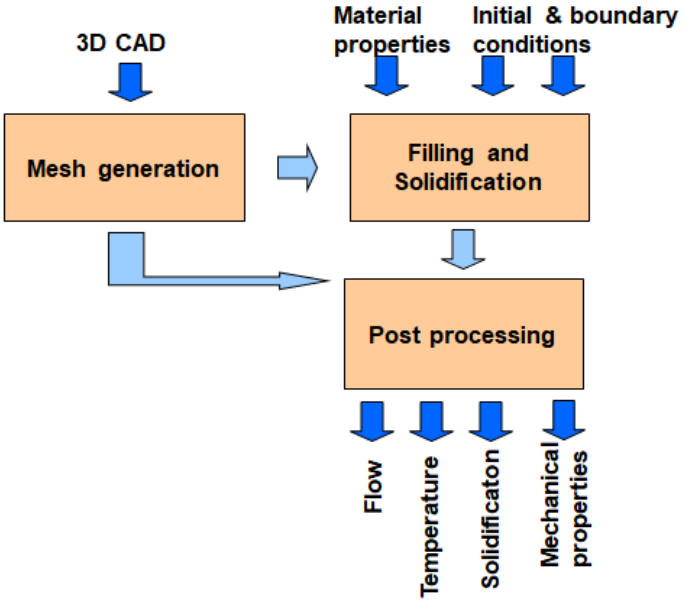

Figure 2 The simulation procedure

REFERENCES:

[1] M. Sirvio et al.: *Complete Simulation of High Pressure Die Casting Process*, VTT Industrial Systems, Finland, 2015.
[2] B. Andresen*: Die Casting Engineering*, Marcel Dekker, New York, 2005.
[3] *Forcasts Software Manual,* Arbeitsgemeinschaft Metallguss GmbH, Aalen, 2012.
[4] J. Hattel: *Fundamentals of Numerical Modelling of Casting Processes*, Polyteknisk, Lyngby, 2005.
[5] *NovaFlow&Solid User Guide,* Novacast Systems AB, Ronneby, 2016.

SUPPORTING COMPANIES

THE ISCAME 2018 CONFERENCE AND THE 6th MECHANICAL ENGINEERING INDUSTRIAL EXHIBITION, DEBRECEN

Company name	Website	Location
ALFRA Consulting Kft.	www.alfraconsulting.eu	Budapest
Aventics Hungary Kft.	www.aventics.hu	Eger
Coloplast Hungary Kft.	www.coloplast.hu	Nyírbátor
Continental Automotive Hungary Kft.	www.continental-corporation.com	Budapest
Diehl Aircabin Hungary Kft.	www.diehl-aerosystems.com	Nyírbátor
DKV Debreceni Közlekedési Zrt.	www.dkv.hu	Debrecen
eCon Engineering Kft.	www.econengineering.com	Budapest
Enterprise Communications Magyarország Kft.	www.enterprisegroup.hu	Budapest
EUROSOLID Kft.	www.eurosolid.hu	Budaörs
FAG Magyarország Ipari Kft.	www.schaeffler.hu	Debrecen
Flexiforce Hungary Kft.	www.flexiforce.com	Debrecen
HAAS Factory Outlet	www.haascnc.com	Leoben
Hoffmann Hungary Quality Tools Kft.	www.hoffmann-group.com	Budapest
HOYA Szemüveglencse Gyártó Magyarország Zrt.	www.hoya.com	Mátészalka
igm Robotrendszerek Kft.	www.igm-group.com	Győr
Joyson Safety Systems hungary Kft.	www.joysonsafety.com	Miskolc
Linamar Hungary Autóipari és Gépgyártó Zrt.	www.linamar.hu	Orosháza
Manz Hungary Gépgyártó Kft.	www.manz.com	Debrecen
MSK Hungary Gépgyártó Bt.	www.msk.hu	Nyírbátor
NAGÉV RÁCS Kft.	www.nagev.hu	Hajdúböszörmény
NCT Ipari Elektronikai Kft.	www.nct.hu	Budapest
Robert Bosch Automotive Steering Kft.	www.bosch.hu	Eger, Maklár
S&T Consulting Hungary Kft.	www.snt.hu	Budaörs
SPM Instrument Budapest Kft.	www.spminstrument.com	Budapest
Unilever Magyarország Kft.	www.unilever.hu	Nyírbátor
ZF Hungária Kft.	www.zf.com	Eger

CONTINENTAL HUNGARIA KFT.
Address: 2040 Budaörs, Távíró köz 2-4.
Phone: +36-23-511-711
Webpage: https://www.continental-corporation.com

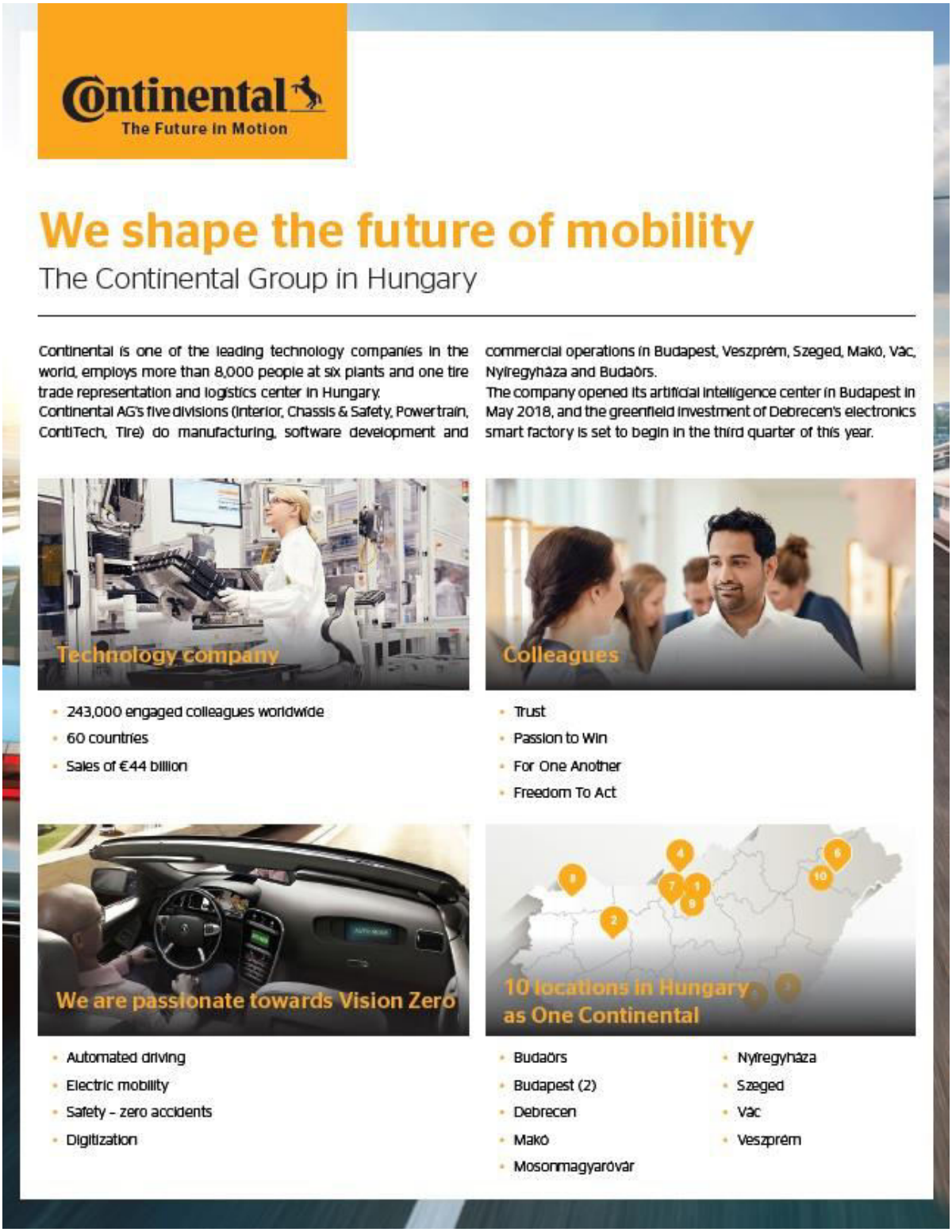

DIEHL AVIATION HUNGARY KFT.
Address: 4034 Debrecen, Vágóhíd u. 2.
Phone: +36-80-200-270
Webpage: http://www.diehl.com/en/diehl-aerosystems.html

Diehl Aviation - being part of Diehl Group which employs 17,000 people worldwide - is an aircraft part supplier for companies such as Airbus and Boeing. Under this flying brand, Diehl Aviation Hungary started its manufacturing operation in 2011 in Nyírbátor, and has become one of the region´s most remarkable employers with its nearly 650 employees. As a result of this continuous growth and success, in 2017 Diehl opened a new Engineering Center in Debrecen. Till the end of 2020, this service center will hire 150 pro- fessionals for the fields of engineering, finance, procurement, ordering and customer support.

The values of our colleagues are important for us, so we provide professional trainings, language learning opportunities, competitive benefit packages, and friendly work atmosphere for them. The basis of our corporate culture is the common development, in order to bring out the best of each other. The proof of that is the continous growth of the company, regarding the range of our products, our territorial size, and the number of our employees as well.

If we have raised your interest, do not hesitate contacting us! You can also check out our current job offers on Facebook and if one grabs your attention, send us your English or German CV to our e-mail address which can be found below!

facebook.com/diehlaviationhungary
Free Diehl-line: +36-80/200-270
dac-debrecen-jobs@diehl.com
4034 Debrecen, Vágóhíd utca 2.

ECON ENGINEERING KFT.
Address: 1116 Budapest, Kondorosi út 3.
Phone: +36-1-279-0320
Webpage: http://econengineering.com/

SOFTWARE SALES AND SUPPORT:

eCon Engineering Kft. was established in 2002. We emphasize our mission on the distribution of advanced engineering simulation technologies by representing such products as ANSYS, Moldex3D and Cast-Designer.

Beside the distribution of these software products we also provide solid mechanical-, fluid dynamical-, thermal- and electromagnetic analyses, injection moulding simulations, moulding optimisation and metal casting simulations during the product and design development of our customers.

The 46 years of experience and the thousands of developers worldwide are the guarantees for the market leader position of ANSYS, which was earned by its wide variety of solvers, easy operability and reliability of engineering simulations in the fields of solid mechanics, thermodynamics, fluid dynamics and electromagnetics. The ANSYS software family offers outstanding possibilities for Simulation Driven Product Development, which is indispensable in today's modern and cost-effective engineering.

The leading injection moulding simulation software provides product designers, designers/producers of moulding tools and manufacturers with the capability of predicting the outcome of their work. This way the injection moulding technology and the quality of the final product becomes much more reliable.

A practical cast designer and simulation software that enables the investigation of the cast parameters and eliminates the possible failures of the casting process during the design phase. It's a reliable tool for product and casting tool designers for cost- and time-effective cast design and production.

CAE SOLUTIONS:

Finite Element Method Analysis based development fits into the profile of eCon. With valuable experiences in the field of FEM development we offer engineering solutions for our partners.

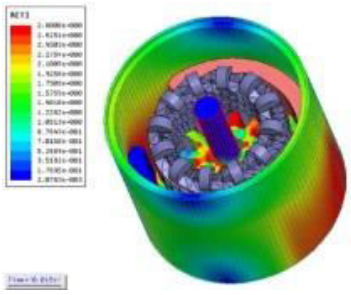

A skilled team of 50 engineers with a wide spectrum of knowledge in the fields of mechanics, optimisation, durability and fatigue analysis, analysis of composite frames, hydrodynamics, thermodynamics, correlation analysis, dynamics, vehicle construction, medical technology and turbine physics. It's very important for us to provide our customers with a complex solution on the most professional level. We don't only focus on just a single problem, we aim analyse the whole spectrum of possible problems and provide a comprehensive solution.

SINGLE-PURPOSE MACHINES:

Our company also produces special single-purpose machines, assembly lines, testers for the car and the IT industry, according to the customer's needs.

Projects include the whole production process, from the development of technology to the executionprocedure, concluding with onsite installation. Guarantee servicing and full-scale project management are also included.

Our quality policy is to use our experience, developments and knowledge to fulfil and to exceed our customer expectations.

ELECTROLUX LEHEL LTD.
Address: 4401, Nyíregyháza, Ipari Park
Phone: +36-42-594-856
Webpage: www.electrolux.hu

SHAPE LIVING FOR THE BETTER

Our future is determined by the way we all live our lives. That's why we strive to improve everyday life for millions of people and the world around us. It is embodied in everything we do. In every idea, every product and every human interaction.

WHO WE ARE

Electrolux is a global leader in home appliances and appliances for professional use. Our company Electrolux Lehel Ltd. is one of the subsidiaries of the Swedish AB Electrolux. At Electrolux Lehel Ltd., the manufacturing operations are located in Jászberény and Nyíregyháza, while the sales and marketing organization and the Global Logistics Centre of Small Appliances can be found in Budapest. The company's main profile is the production of refrigerators, freezers, chest freezers and vacuum cleaners. The Jaszbereny and Nyiregyhaza refrigerator plants together form the company group's largest refrigerator base, whereas the vacuum cleaner factory is the only Electrolux manufacturing base in Europe.
According to the TOP 200 survey comparing domestic companies, Electrolux Lehel Ltd. has become the 22nd largest export company. In 2017, Electrolux reached the total turnover of 250.2 billion Hungarian Forints in Hungary.

WE BELIEVE

We believe that outstanding taste experiences should be easy for everyone. That there is always a better way to care for our clothes to make them look and feel new longer. That the home should be a place for wellbeing, a place to care for ourselves and our loved ones. To succeed, we continuously rethink and improve our ways of working - internally, and together with our customers and partners. By creating desirable solutions and great experiences that enrich peoples' daily lives and the health of our planet, we want to be a driving force in defining enjoyable and sustainable living.

This is us – at Electrolux we shape living for the better.

EUROSOLID LTD.
Address: 1117 Budapest, Szerémi út 7/B.
Phone: +36-20-222-0454
Webpage: www.eurosolid.hu

EuroSolid Ltd. has been dealing with the introduction and installation of CAD/CAM/PLM/MDC systems, process optimization, education and support of technical, engineering and manufacturing softwares for 20 years in Hungary. Since its foundation, our company was driven by one goal which is to help companies in product development and manufacturing fields in the most efficient way and at the highest professional standards to tackle their technical challenges.

Today EuroSolid Ltd is one of the market leaders and has more than 800 partners with references such as Michelin, Aloca, Coloplast, GE or Linamar.

Our company is the sole and exclusive distributor of SOLIDWORKS softwares in Hungary plus the only qualified education and support centre in the country. As the representative of SOLIDWORKS, our activities include professional client support, data management system installation, delivering and solving engineering tasks and performing different simulation tests with our softwares.

SOLIDWORKS is the market leading and the most integrated software system available. In the past 25 years the CAD software has grown out to become the foundation of a wide ranged product portfolio which not only includes engineering design and simulation but also electrical design, data management, quality management for inter- and post production processes, sheet-less sketch creation, rendering, technical documentation modules and so much more.

Our goal is to deliver solutions with the excellent tools, quickly-to-adapt and easy-to-learn systems of SOLIDWORKS and with the new technologies supporting design and manufacturing that ensure profitable investment and increasing productivity with optimized workflow for our clients.

FAG MAGYARORSZÁG IPARI KFT.
Address: 4031 Debrecen, Határ Road/Street, 1/D.
Phone: +36-52-581-700
Webpage: http://www.schaeffler.hu

SCHAEFFLER

A leading global technology company

The Schaeffler Group is a global automotive and industrial supplier. Top quality, outstanding technology, and exceptionally innovative spirit form the basis for the continued success of the company. By delivering high-precision components and systems in engine, transmission, and chassis applications, as well as rolling and plain bearing solutions for a large number of industrial applications, the Schaeffler Group is already shaping "Mobility for tomorrow" to a significant degree. The technology company generated sales of approximately EUR 14 billion in 2017. With around 90,200 employees, Schaeffler is one of the world's largest family companies and, with approximately 170 locations in over 50 countries, has a worldwide network of manufacturing locations, research and development facilities, and sales companies.

Divisions and business divisions

Schaeffler develops and manufactures precision products for approximately 60 sectors around the world. Its technologically advanced components and systems are used in applications in vehicles, machinery, plants, as well as in aerospace applications. The group distributes its products and services to numerous auto- motive manufacturers and industrial customers.

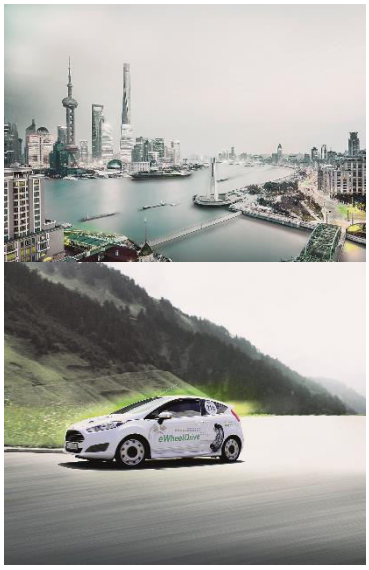

Mobility for tomorrow

Globalization, urbanization, digitalization, scarcity of resources, renewable energy, and the growing demand for affordable mobility are leading to changed, much more dynamic market requirements and business models. Based on these megatrends, the Schaeffler Group has developed its "Mobility for tomorrow" strategy concept, under which the company focuses on four areas across divisions and regions: eco-friendly drives, urban mobility, interurban mobility, and the energy chain.

Schaeffler plays an active part in shaping these focal areas through its own research and development activities and, as a leading expert in innovation and technology, offers an attractive product range to its customers and business partners.

The group's broad portfolio of products and services ranges from components and systems for automotive drive trains to products for high-speed trains and from rolling bearings for solar power plants to innovative solutions for aerospace applications.

HOFFMANN HUNGARY QUALITY TOOLS KFT.
Address: 1121 Budapest, Zugligeti út 41.
Phone: +36-1-392-0290
Webpage: www.hoffmann-group.com

The Hoffmann Group

As Europe's leading system partner for quality tools, the Hoffmann Group combines commercial expertise with both manufacturing and service competence. To more than 135,000 customers this combination guarantees reliability in supply, quality and productivity, in the tooling sector and also in the workstations and storage sector. Optimum and reliable advice, from individual needs analysis through to efficient use of products, is assured at all times. Alongside tools for machining, clamping, measuring, grinding and cutting, the portfolio also comprises hand tools, protective work-wear, workstations, and storage and workshop accessories.

Customers include major listed companies as well as medium-sized and small companies in more than 50 countries. In 2017, the Hoffmann Group generated a worldwide turnover of more than 1.2 billion Euros. Including GARANT, its own premium brand, the Hoffmann Group offers 80,000 quality tools from the world's leading manufacturers. With comprehensive customer service and delivery quality of over 99 percent as certified by the TÜV, the tools specialist, headquartered in Munich, is a reliable and efficient partner for its customers.

HOYA LENS MANUFACTURING HUNGARY PRIVATE CO.
Address: 4700 Mátészalka, Ipari út 18.
Phone: +36-44-502-831
Webpage: www.hoya.hu

HOYA Corporation is a diversified, multinational company and leading supplier of innovative and indispensable high-tech and healthcare products. HOYA is active in two main business segments: The Life Care segment encompasses health care areas such as eyeglass lenses and the operation of contact lens retail stores, as well as medical related areas such as intraocular lenses for cataract surgery, medical endoscopes, surgical equipment and artificial bones and implants. HOYA´s Information Technology segment focuses on electronics products for the semiconductor industry and LCD panels, glass disks for HDDs and optical lenses for digital cameras and smartphones. The HOYA Group comprises over 100 subsidiaries and affiliates and over 34,000 people worldwide.

Life Care

HOYA has diversified its business portfolio with its optical technologies providing indispensable products to people´s lives. We strongly believe that by providing enduring solutions that meet needs in areas closely connected to people's lives, such as endoscopes, eyeglass lenses and intraocular lenses, it will be able to bring about changes in the quality of those lives.

Life Care Segment, Health Care

HOYA provides products and services to care for that most important sensory organ- the eye. HOYA started manufacturing eyeglass lenses in 1962 and contact lenses in 1972. Based on the optical and material technologies acquired since 1941, HOYA continues to contribute quality high value-added vision products to people around the world.

Eyeglass lenses

As a global manufacturer of eyeglass lenses, HOYA has passionately driven optical technology innovation with the aim of finding only the best vision solutions.

HOYA´s unparalleled technology creates a profoundly clear vision experience for the progressive lens wearer.
Integrated Double Surface Design (iD), HOYA´s patented, award-winning design technology, separates the surface geometry of progressive lenses into two components: vertical and horizontal, positioned individually on each of the two lens surfaces. Thanks to this technology, HOYA´s premium progressive lenses can be individually designed; each patient´s unique visual and lifestyle requirements can be integrated in the lens design to provide them with the most comfortable and accurate vision, tailored to their individual needs.

HOYA Vision Care Company is a global organization covering 52 countries with a network of over 12,000 employees and over 64,000 active accounts globally.

HOYA Lens Manufacturing Hungary private Co., Mátészalka

HOYA Lens Manufacturing Hungary private Co. is the largest unit of Hoya group in Europe based on the headcount and production volume as well. The past of the company and the nearness of the European market give a geopolitical advantage and stabile future for the company. A Belgian investor bought 50% of Optikai Művek factory's unit in 1991. In 1994 with total ownership the enterprise with mass production has been called Buchmann Optical Művek for 8 years. Hoya has bought the Buchmann-group in 1994, so the plant in Mátészalka also became a member of the japan lens production company. By now the company do partial serving of all affiliated companies in Europe.

IGM ROBOTRENDSZEREK KFT.
Address: 9027 Győr Csörgőfa sor 1.
Phone: +36-1-279-0320, +36-96-513-910
Webpage: http://www.igm-group.com

igm was established in 1967 as a trading company for industrial devices and machine tools. In 1980, the world-wide first continuous path welding robot type was developed. As the inventor of the unique hollow shaft for welding robots, igm gained world-wide reputation for this design feature. This was the start of a successful development to one of the most important supplier of automated welding technology to the heavy machinery producers.

In 1990, there was the start of a joint venture in Győr regarding production of components for robot systems in Hungary. This successful cooperation lead to the establishment of igm Robotrendszerek Kft. and the shift of the complete manufacturing and assembly of all robot systems to the new work shop in the industrial park of Győr in 2002. With the ongoing further expansion and modernisation of this production site igm offers a high performance and up-to-date manufacturing facility.

Today igm is Austria's most prestigious manufacturer of robots specifically developed for arc welding. Now for 50 years igm Robotersysteme AG has been a market leader in the field of arc welding automation and has developed extensive and comprehensive expertise in many diversified applications for arc welding robot systems for MIG/MAG and TIG welding process. Beside of complex, sensor guided cutting and welding robot systems, igm's portfolio comprises robot based plasma or oxy-fuel cutting and bevelling solutions. The product variety is available for individual applications in robot welding and cutting technology is unique throughout the world.

igm robotic systems are exported worldwide to manufacturer of earthmoving machinery, construction machinery, heavy road transportation vehicles and cranes, railway coaches and wagons, boilers, machine tools and shipbuilding, representing the basis of production for many internationally well-known manufacturers. With subsidiaries and sales partners in more than 20 countries, igm is today the world's only manufacturer of automated welding and cutting systems with arc, laser and electron beam technology. The current igm group sales amounts to about 140 M€ with a total of 800 employees.

Welding robot system for track roller frames

Welding robot system for waste containers

igm bevelling system

Welding robot system for fork lift masts

MSK HUNGARY BT
Address: 4300 Nyírbátor, MSK tér 1.
Phone: +36-42-511-130
Webpage:www.msk.hu

MSK a global market leader – already set up for the future

The MSK Covertech Group is one of the leading international manufacturers of packaging machines and material-flow technology for pallet load units and large containers. The MSK headquarters are in Kleve, Germany, moreover, the MSK Covertech Group has subsidiaries in Hungary, France, USA and China. The biggest manufacturing site is located in Nyírbátor, the MSK Hungary, where - more than 400 employees are employed.

MSK is an independent, family-run business. Founded in 1975 by entrepreneur Reiner Hannen, who, from the very beginning, applied his courageous vision, relentless hard work and will to succeed, to build a company group with the support of his teams. Today the company group is run by Christina Hannen, Managing shareholder, and daughter Linda Hannen, Majority shareholder. For the future, MSK will carry forward and expand its strengths and traditions, continuing to create cutting edge technology. International teams in the MSK Group are working together on numerous projects to achieve this goal.

Excellent and responsible employer

At MSK you will find excellent working environment, modern work tools, appreciation of knowledge and work experience with the opportunity of building an international career. We offer an interesting workplace in an international and innovative team, as well as additional benefits, like healthy foods in the MSK Restaurant and complimentary fruit.

To strengthen our team in Hungary, we are looking continuous for top motivated employees both for the technical and for the commercial area. More information about our vacancies can be found here https://www.msk.hu/karrier/jobs/.

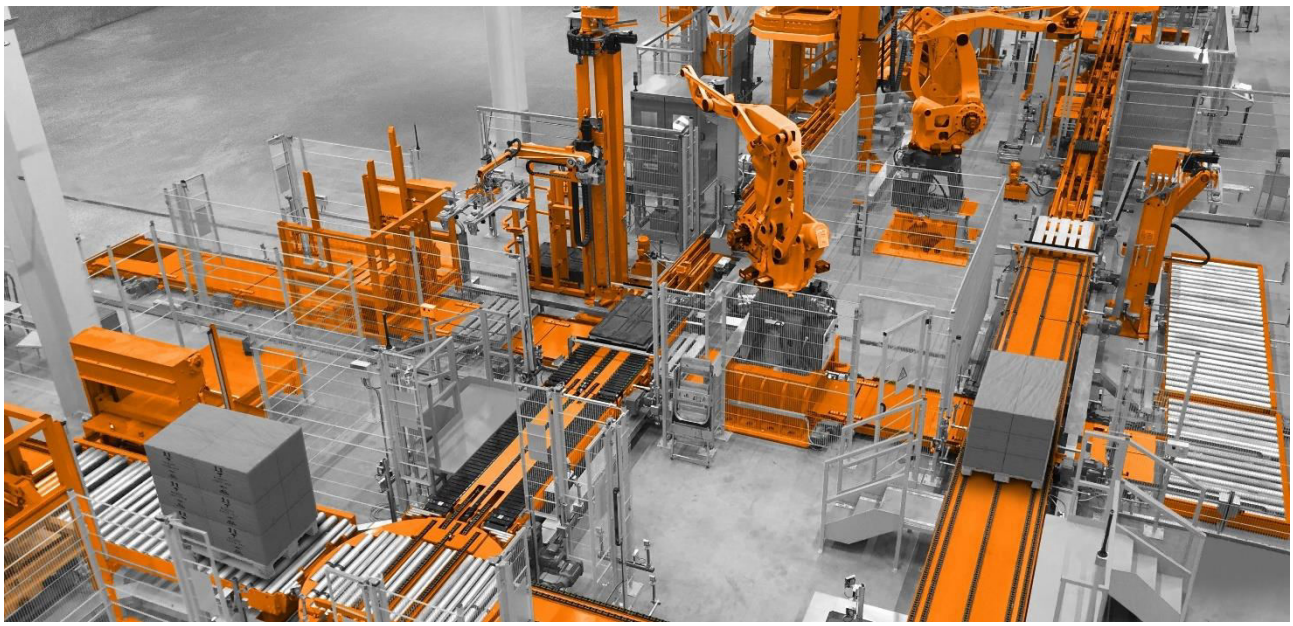

NAGÉV RÁCS KFT.
Address: 4220 Hajdúböszörmény, Kinizsi utca 7.
Phone: +36-52-563-113
Webpage: http://nagev.hu/

Gratings are of paramount importance among the products produced by the NAGÉV group. Actually, this is one of our first products but the demand for it remained high in Hungary and abroad.

According to definition, grating is a flat-surface structure between two supportive points, enclosed by an integrated frame, consisting of main ribs and secondary ribs that are perpendicular to each other, and is suitable for bearing the orthogonal forces reaching the load planes formed by the ribs and the frame.

They are produced with a smooth walking surface, however, if required – in order to increase adhesion – the main ribs and the ribs can be produced with a non-slip design, meaning a pattern below or above the level of the walking surface. We recommend fixing the grating to the supportive structure by using screw joints that can be loosened.

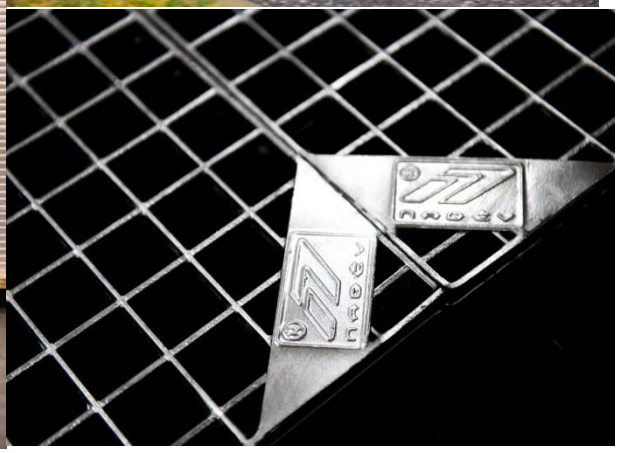

ROBERT BOSCH AUTOMOTIVE STEERING KFT.
Address: 3397 Maklár, Havasi László u. 2.
Phone: +36-36-510-930
Webpage: www.bosch.hu

BOSCH
Invented for life

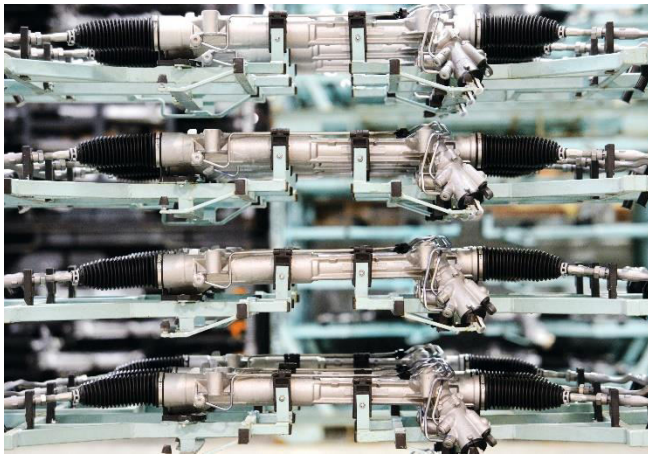

The Eger based company has been producing automotive components since 2003. The product portfolio includes hydraulic steering gears, steering columns and steering shafts, both for passenger cars and commercial vehicles. Since 2014 hightech electric steering systems have also been produced in Eger and Maklár. As an automotive supplier, we deliver parts to more than 100 vehicle manufacturers worldwide. As of 2015 Bosch has acquired the entire ownership of the previous 50-50 percent joint venture. The new affiliate with locations in Eger and in Maklár has become a full fledged Bosch family member and the name of the company has changed to Robert Bosch Automotive Steering Kft.

Our company belongs to the Mobility Solutions business
sector of the Bosch Group. In our vision statement, we explain that we intend to be the worldwide leading supplier of innovative steering systems and play a decisive role in shaping the future of mobility. We finance our growth through our benchmark profitability, securing our long-term market success.

We focus on the innovation and provide solutions to our customers, which make driving safer, more dynamic, sustainable and more comfortable. With our hightech products, we are pacemakers of autonomous driving. We deliver excellence in every function.

UNILEVER MAGYARORSZÁG KFT NYÍRBÁTOR HOMECARE FACTORY
Address: 4300 Nyírbátor, Táncsics Mihály str 2-4.
Phone: +36-80-180-144
Webpage: http://www.unilever.com

Unilever is one of the largest fast-moving consumer goods (FMCG) companies in the world. We take care of the whole supply chain of our products, from development and sourcing right through to production, marketing and distribution. Over 172 000 employees around the world bring this operation to life. Our brands are sold in 190 countries and are used by 2 billion people every day.
Our factory in Nyírbátor was established in the 19th century and was taken by Unilever in 1991. Our head office is in Budapest and the company runs three sourcing units: one in Veszprém (ice cream factory) and the other two in Röszke (food processing) and Nyírbátor (homecare products). Our factory in Nyírbátor is the biggest and fastest-growing homecare factory in Europe, producing the well-known brands like Coccolino, Surf, Domestos, Cif, Savo and Floraszept.
We produce an annual 260 ktons of cleansing products, fabric softeners and detergents creating an approximately 300m euros turnover a year. We employ more than 250 people, and we keep a special focus on hiring students in internship programmes co-operating with universities. For years we have been employing young people who turned to be successful in our engineering competition or at their internship programme.

ZF HUNGÁRIA KFT.
Address: 3300 Eger, Kistályai út 2.
Phone: +36-36-520-100
Webpage: www.zf.com/hu

The ZF Group

Our parent company, the German ZF Friedrichshafen AG is one of the largest automotive companies, stands on the first place of the global selling-list with more product family.
It is for example world's beater in producing and distribution of clutch units, hydraulic and electrical steering components, dampers, automated transmissions of commercial vehicles weighing more than 6 tones. In 2015 the ZF increased significantly its product range and production capacity with buying the TRW automotive company in the USA. Presently it operates 230 locations, which deal with development, production and service on five continents, in 40 countries, with around 134.000 employees.

The ZF Hungária Kft.

Manual and automatic gearboxes have been manufactured for commercial vehicles in the manufacturing unit since 1996.
Our most important customers are: IVECO, MAN, RENAULT, LEYLAND, VOLVO, NISSAN, DAF, KIA, HYUNDAI, BMC, GAZ, KAMAZ, IRISBUS IVECO, VDL, DAEWOO, VANHOOL, HINO, NEOPLAN, TEMSA, ISUZU, AUTOSAN, OTOKAR, SOLARIS, KING LONG, SOLBUS, VW

ZF invested nearly 100 million euros in expanding its Eger site, resulting in 770 new jobs being created. The ZF Drive Technology Unit, Car Powertrain Technology - "Car Division", is expanding in Eger. The determining factors of ZF's decision were the decades of experience in gearbox manufacturing, the best experts and excellent infrastructure.

ZF Hungaria almost doubles the number employees – currently 1000 people - with this investment by 2019.


The new plant

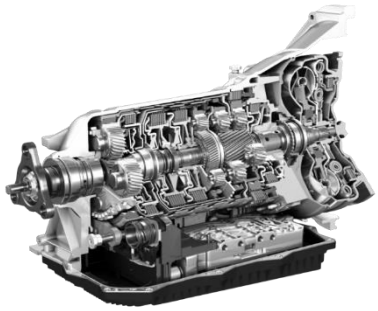
The new product: ZF 8HP transmission

Applying for job:
Continuously, sending CV in Hungarian and foreign language via e-mail: allaspalyazatzfh@zf.com
We are waiting for applying of Career starters, interns and also who prepare thesis.

The Department of Mechanical Engineering is responsible for the mechanical engineering education on bachelor (BSc) and master (MSc) levels. The research activity of the department covers the mechanical engineering scientific area starting from the materials science to the specific fields (diagnostics, material handling, etc.). From 2015 we have introduced the dual training. At the moment we cooperate with 19 industrial partners.

DEPARTMENT STAFF

Tamás MANKOVITS PhD associate professor head of department *mechanics* *finite element method* 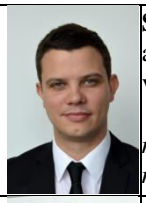	**Sándor BODZÁS PhD** associate professor vice head of department *manufacturing,* *machine elements* 	**Sándor HAJDU PhD** associate professor vice head of department *material handling,* *mechanics* 
Lajos FAZEKAS PhD college professor *logistics,* *machine repairing* 	**Zsolt TIBA PhD** college professor *machine elements* 	**Ágnes BATTÁNÉ GINDERT-KELE PhD** associate professor *manufacturing,* *machine elements* 
Levente CZÉGÉ PhD associate professor *process analysis,* *machine elements,* 	**György JUHÁSZ PhD** associate professor *machine elements,* *hydraulics and pneumatics* 	**Sándor PÁLINKÁS PhD** associate professor *materials science,* *manufacturing* 
József MENYHÁRT PhD assistant professor *process analysis,* *computer aided design* 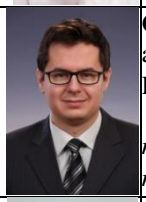	**Gábor BALOGH** assistant lecturer PhD student *materials science,* *manufacturing* 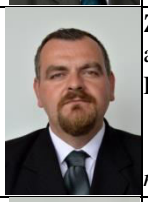	**Zsolt BÉKÉSI** assistant lecturer PhD student *machine elements* 
Krisztián DEÁK assistant lecturer PhD student *diagnostics,* *mechanics* 	**Dávid HURI** assistant lecturer PhD student *mechanics,* *finite element method* 	**András GÁBORA** department engineer PhD student *materials science,* *technology* 
Márton LÉVAI department teacher *materials science,* *technology* 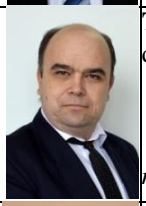	**Tibor PÁLFI** department teacher *machine elements* 	**Zoltán Gergő GÉRESI** CNC technologist *manufacturing* 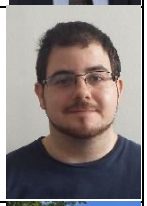
Lilla CSONKÁNÉ DÓRÓ administrative assistant 	**Szandra SITKU** administrative assistant 	**Department of Mechanical Engineering** **Faculty of Engineering,** **University of Debrecen** 4028 Hungary, Debrecen, 2-4 Ótemető Tel.: +36-52-512-900 E-mail: gepeszmernok@eng.unideb.hu Website: www.mecheng.unideb.hu 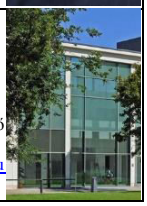

Mechanical Engineering BSc Program

Automotive Production Process Control Specialization

The aim of the teaching program includes preparing engineers to improve quality and use lean tools in the vehicle industry, enabling them to gain an understanding of the complete product development (from the supplier to the customer) and lead project teams. In cooperation with local vehicle suppliers students learn about completing cost estimation, utilizing computer software to solve manufacturing problems.

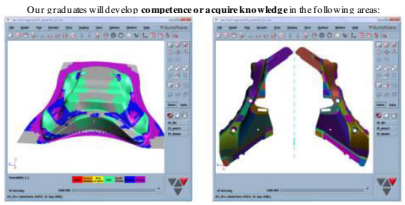

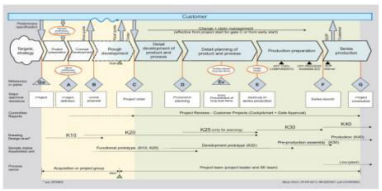

- introducing and applying modern technologies, computational engineering methods and systems (manufacturing technologies, CAE)
- operating and developing mechatronical systems (electrotechnics and electronics, measuring and automatics, hydraulics and pneumatics)
- designing and redesigning plant layouts, checking KPI systems robot technology, automation, etc.
- planning material handling and manufacturing processes
- analyzing, controlling and optimizing production processes
- applying modern manufacturing management philosophies (Lean management) in the vehicle industry

The **curriculum** contains the following **subject modules**:

Basic science subjects: 48 credits
- Mathematics, Technical Mechanics, Engineering Physics, Operation and Theory of Machines, Thermodynamics and Fluid Mechanics, Technical Chemistry

Economics and humanities subjects: 20 credits
- Economics for Engineers, Microeconomics, Basics of Quality Management, Management for Engineers, State Administration and Law, Introduction to Ethics

Professional subjects: 117 credits
- Informatics, Machine Elements, CAD and CAE, 3D Computer-Aided Design, Materials Science, Technology of Structural Materials, Electrotechnics and Electronics, Thermal and Fluid Machines, Manufacturing Processes, Logistics, Industrial Safety, Computational Engineering Methods and Systems, Measuring and Automatics, Hydraulics and Pneumatics, Mechanical System Engineering, Quality Management, Safety Engineering, Material Handling and Robotics, CAM, Manufacturing Planning, Maintenance Engineering, PLC.

Optional subjects: 10 credits
Thesis: 15 credits
Duration of studies: 7 semesters, Contact hours: 2.352
ECTS credits: 210, Internship: 6 weeks

Final exam:

- Defending the thesis (oral presentation and discussion)
- Exam in two subject areas chosen by the student
  - Production Process and Control, Production Optimization, Logistics
  - Assembling Technology, CAM, Quality Management

Mechanical Engineering BSc Program

Operation and Maintenance Specialization

The aim of the teaching program is to train mechanical engineers who are able to operate and maintain machines and mechanical devices, introduce engineering technologies and apply them, organize and control work phases, mechanical developments, solve the general problems of research and planning as expected by the labor market. Those having completed the specialization have in-depth theoretical knowledge to continue their studies in the second cycle.

Our graduates will develop **competence or acquire knowledge** in the following areas:

- introducing and applying modern technologies and computational engineering methods and systems (manufacturing technologies, CAE)
- operating and developing mechatronical systems (electrotechnics and electronics, measuring and automatics, hydraulics and pneumatics)
- operating and maintaining machines and mechanical devices (mechanical system engineering, heat and fluid machines)
- organizing and controlling operational processes, mechanical developments
- planning the construction and designing of the machine parts, devices and apparatus (machine element, CAD, finite element method)
- solving the general problems of research and planning as expected by the labor market (studies of administration and law, basics of quality assurance, management for engineers, safety engineering)
- carrying out diagnostic testing, assessing the reliability of machines and devices (fracture mechanics, non-destructive testing and diagnostics)

The **curriculum** contains the following **subject modules**:

Basic science subjects: 48 credits
- Mathematics, Technical Mechanics, Engineering Physics, Operation and Theory of Machines, Thermodynamics and Fluid Mechanics, Technical Chemistry

Economics and humanities subjects: 20 credits
- Economics for Engineers, Microeconomics, Basics of Quality Management, Management for Engineers, State Administration and Law, Introduction to Ethics

Professional subjects: 117 credits
- Informatics, Descriptive Geometry, Technical Drawing, Machine Elements, CAD and CAE, 3D Computer-Aided Design, Materials Science, Technology of Structural Materials, Electrotechnics and Electronics, Measurements and Automatics, Thermal and Fluid Machines, Manufacturing Processes, Logistics, Industrial Safety, Steel Constructions, Hydraulics and Pneumatic Machines, Fracture Mechanics, Manufacturing Planning, Diagnostics, FEM, PLC, Material Handling and Robotics, Drivetrain Optimization, Machine Repairing, Maintenance Engineering.

Optional subjects: 10 credits
Thesis: 15 credits
Duration of studies: 7 semesters, Contact hours: 2.352
ECTS credits: 210, Internship: 6 weeks

Final exam:
- Defending the thesis (oral presentation and discussion)
- Exam in two subjects chosen by the student
  - Machine Repairing,
  - and one subject chosen by the student:
    - Material Handling and Robotics
    - *or* Maintenance Engineering

Mechanical Engineering MSc Program

Production Engineering Specialization

The aim of the teaching program is to train engineers who are able to design and elaborate production processes and the conceptions of manufacturing technologies as well as can be responsible for modelling, designing, operating, maintaining, supervising and organizing production tasks. They are capable of providing the conditions of precise and up-to-date production and its processes (optimizing and developing production processes; designing and implementing devices and systems serving the production). The specialization considers the needs of the partner industrial companies.

Our graduates will develop **competence or acquire knowledge** in the following areas:

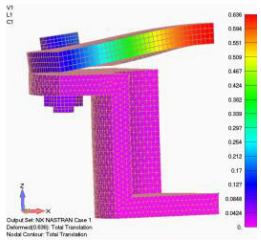

- applying modern computational engineering methods (CAD, CAM, CAE)
- supporting, optimizing and developing production systems and processes;
- designing of manufacturing and material handling systems,
- applying management methods and systems,
- supervising and organizing in production environment,
- applying expert systems (diagnostics and condition monitoring).

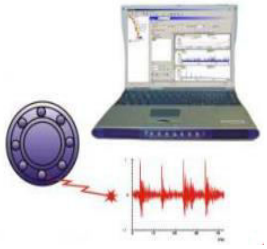

The **curriculum** contains the following **subject modules**:

Basic science subjects: 22 credits
- Mathematics, Applied Statistics, Modern Physics, Dynamics of Mechanical Systems, Thermodynamics and Fluid Mechanics, Advanced Material Science

Economics and humanities subjects: 16 credits
- Basics of Management, Quality Management, Financial and Advanced Economic Knowledge, Research Methodology

Professional subjects: 46 credits
- Measurement, Signal Processing and Electronics, Design of Engineering Structures, Engineering Modelling and Simulation, Manufacturing Equipments, Design and Quality Assurance of Manufacturing Processes, Assembly Automation, Design of Material Handling Systems, Production Logistics, Maintenance and Machine Repairing Technologies, Diagnostics and Condition Monitoring, Lean Production

Optional subjects: 6 credits
Thesis: 30 credits
Duration of studies: 4 semesters, Contact hours: 1.428
ECTS credits: 120, Internship: 4 weeks

Admission requirements for the Mechanical Engineering MSc program

Unconditional admission: Mechanical Engineering BSc:
Conditional admission by prescribing pre-master courses:
Materials Engineering BSc, Safety Engineering BSc, Energy Management BSc, Civil Engineering BSc, Industrial Design Engineering BSc, Vehicle Engineering BSc, Light Industrial Engineering BSc, Environmental Engineering BSc, Transportation Engineering BSc, Mechatronics Engineering BSc, Earth Science Engineering BSc, Technical Management BSc, Chemical Engineering BSc, Electrical Engineering BSc, Mechanical Engineering in Agriculture and Fodd Industry BSc
Final exam:

- Defending the thesis (oral presentation and discussion)
- Exam in two topics chosen by the student :
  - Production systems and processes (Design of Material Handling Systems, Production Logistics, Lean Production)
  - Manufacturing systems and processes (Manufacturing Equipments, Design and Quality Assurance of Manufacturing Processes)
  - Maintenance and operation (Maintenance and Machine Repairing Technologies, Diagnostics and Condition Monitoring)

Welcome in Debrecen for the

7^{th} International Scientific Conference on Advances in Mechanical Engineering (ISCAME 2019)

and

7^{th} Mechanical Engineering Exhibition

The Department of Mechanical Engineering
Faculty of Engineering, University of Debrecen